



ELECTRONIC EFFECTS GOVERNING THE REDOX PROPERTIES OF POLYOXOMETALATES.

Pablo Arturo Aparicio Sánchez

Dipòsit Legal: T 331-2016

ADVERTIMENT. L'accés als continguts d'aquesta tesi doctoral i la seva utilització ha de respectar els drets de la persona autora. Pot ser utilitzada per a consulta o estudi personal, així com en activitats o materials d'investigació i docència en els termes establerts a l'art. 32 del Text Refós de la Llei de Propietat Intel·lectual (RDL 1/1996). Per altres utilitzacions es requereix l'autorització prèvia i expressa de la persona autora. En qualsevol cas, en la utilització dels seus continguts caldrà indicar de forma clara el nom i cognoms de la persona autora i el títol de la tesi doctoral. No s'autoritza la seva reproducció o altres formes d'explotació efectuades amb finalitats de lucre ni la seva comunicació pública des d'un lloc aliè al servei TDX. Tampoc s'autoritza la presentació del seu contingut en una finestra o marc aliè a TDX (framing). Aquesta reserva de drets afecta tant als continguts de la tesi com als seus resums i índexs.

ADVERTENCIA. El acceso a los contenidos de esta tesis doctoral y su utilización debe respetar los derechos de la persona autora. Puede ser utilizada para consulta o estudio personal, así como en actividades o materiales de investigación y docencia en los términos establecidos en el art. 32 del Texto Refundido de la Ley de Propiedad Intelectual (RDL 1/1996). Para otros usos se requiere la autorización previa y expresa de la persona autora. En cualquier caso, en la utilización de sus contenidos se deberá indicar de forma clara el nombre y apellidos de la persona autora y el título de la tesis doctoral. No se autoriza su reproducción u otras formas de explotación efectuadas con fines lucrativos ni su comunicación pública desde un sitio ajeno al servicio TDR. Tampoco se autoriza la presentación de su contenido en una ventana o marco ajeno a TDR (framing). Esta reserva de derechos afecta tanto al contenido de la tesis como a sus resúmenes e índices.

WARNING. Access to the contents of this doctoral thesis and its use must respect the rights of the author. It can be used for reference or private study, as well as research and learning activities or materials in the terms established by the 32nd article of the Spanish Consolidated Copyright Act (RDL 1/1996). Express and previous authorization of the author is required for any other uses. In any case, when using its content, full name of the author and title of the thesis must be clearly indicated. Reproduction or other forms of for profit use or public communication from outside TDX service is not allowed. Presentation of its content in a window or frame external to TDX (framing) is not authorized either. These rights affect both the content of the thesis and its abstracts and indexes.

Pablo A. Aparicio Sánchez

Electronic Effects Governing the Redox Properties of Polyoxometalates

PhD Thesis

Supervised by:

Dr. Xavier López Fernández

Prof. Josep Maria Pobleat Rius

Quantum Chemistry Group

Departament de Química Física i Inorgànica



UNIVERSITAT ROVIRA I VIRGILI

Tarragona, September 2014

Departament de Química Física i Inorgànica

Xavier López Fernández, Professor Agregat del Departament de Química Física i Inorgànica de la Universitat Rovira i Virgili, i Josep Maria Poblet Rius, Catedràtic del Departament de Química Física i Inorgànica de la Universitat Rovira i Virgili,

Fem constar que la present memòria titulada:

“Electronic Effects Governing the Redox
Properties of Polyoxometalates”

Ha estat realitzada sota la nostra direcció al Departament de Química Física i Inorgànica de la Universitat Rovira i Virgili per Pablo A. Aparicio Sánchez per a l’obtenció del títol de Doctor, i que aconsegueix els requeriments per poder optar a la Menció Internacional.

Tarragona, 26 de Setembre de 2014.

Els directors de la tesis doctoral:

A mis hermanas Ana y Laura.

A mis abuelos Luis y Amparo.

Preface

This book collects my scientific research in the field of *polyoxometalates* (POMs). It was carried out during the last four years in the Quantum Chemistry Group of the Universitat Rovira i Virgili under the supervision of Dr. Xavier López and Prof. Josep M. Poblet. Technically, this is a thesis on chemical modeling. The main results arise from Density Functional Theory calculations—one of the most widely used modern Quantum Chemistry techniques working in computers—though the majority of the chapters present some background based on experimental work carried out by colleagues from the USA, France and Japan. The present thesis is, therefore, highly multidisciplinary and collaborative owing to the large amount of experimental-computational joint work. Certainly, modern research needs mixing the data from both worlds for a deeper analysis of chemical problems.

Despite that POMs are known since centuries ago, the use of computational power applied to the research on the field is quite recent. The Quantum Chemistry Group of the Universitat Rovira i Virgili joined the POM community in the late 1990s. Since, computer capabilities have hugely evolved to the point of computational work being widely accepted among researchers of the field. At present day, the fundamental knowledge of the physicochemical properties and technological innovation in the POM area is in perpetual progress thanks to the contributions of both experimentalists and theoreticians. This thesis is another step forward in that process.

The central goal of the present thesis is to shed new light in the rich properties of POMs, especially the processes of electron gain/release and the technologically interesting properties of highly-reduced systems. The chapters are ordered so that they show more fundamental aspects at the beginning and more complex and applied phenomena at the end of the book.

Welcome to the amazing world of POMs.

Tarragona, September 2014

Pablo A. Aparicio

Contents

List of abbreviations	xiii
------------------------------	------

Chapter 1. Introduction

1.1 A brief historical perspective of POMs	3
1.2 Structure and properties of POMs	5
1.2.1 Acidic properties	9
1.2.2 Redox properties	10
1.2.3 Electrochemistry	12
1.3 Reduced and mixed-valence POMs	13
1.3.1 Heteropoly blues	13
1.3.2 Heteropoly browns	13
1.4 Applications of POMs	14
1.5 Computational chemistry in POMs	16
1.6 Modeling of redox properties	19
1.7 Goals of the thesis	21
1.8 References	23

Chapter 2. Ability of DFT Calculations to Describe Redox Potentials and Electron (De)Localization

2.1 Introduction and objectives	29
2.2 Results and discussion	30
2.2.1 Atomic spin populations	31
2.2.2 Reduction energies	34
2.2.3 Calculation of the RE for P_2W_{18}	36
2.3 Conclusions	37

2.4	Computational details	38
2.5	References	40

Chapter 3. Tungsten Redox Waves in Keggin Compounds: Effect of Localized *versus* Delocalized Charges

3.1	Introduction and objectives	45
3.2	Results and discussion	46
3.3	Conclusions	56
3.4	Computational details	58
3.5	References	59

Chapter 4. Effect of Electron (De)Localization and Pairing in the Electrochemistry of Wells-Dawson Mo/W-Derivatives

4.1	Introduction and objectives	63
4.2	Experimental background	64
4.3	Results and discussion	68
4.3.1	Calculations on P_2W_{18} , α_2 - P_2W_{17} , α_2 - $P_2Mo_3W_{15}$ and α - $P_2Mo_6W_{12}$	69
4.3.2	Calculations on α_1 and α_2 - P_2MoW_{17}	70
4.4	Conclusions	77
4.5	Computational details	78
4.6	References	79

Chapter 5. Metal-substituted Wells-Dawson Tungstodiphosphates

5.1	Introduction and objectives	83
5.2	Tc and Re compounds	84
5.2.1	Experimental background	84
5.2.2	Results and discussion	88

5.2.2	Conclusions	93
5.3	Fe compounds	94
5.3.1	Experimental background	94
5.3.2	Results and discussion	95
5.3.2	Conclusions	100
5.4	Concluding remarks	101
5.5	Computational details	101
5.5.1	Tc and Re compounds	101
5.5.2	Fe compounds	102
5.6	References	103

Chapter 6. Mixed d Metal-Iron Containing Wells-Dawson Sandwich-type Complexes

6.1	Introduction and objectives	107
6.2	Experimental background	109
6.3	Results and discussion	113
6.4	Conclusions	119
6.5	Computational details	120
6.6	References	121

Chapter 7. ϵ -Keggin Polyoxomolybdate Capped with Lanthanide Groups

7.1	Introduction and objectives	125
7.2	Experimental background	126
7.3	Rotational isomers and electronic structure of Keggin polyoxoanions	127
7.4	Structural characterization of ϵ -La ₄ and ϵ -La ₃ Gd	130
7.5	Relative stability of ϵ -La ₄ and ϵ -La ₃ Gd	136

7.6	Conclusions	137
7.7	Computational details	137
7.8	References	139

Chapter 8. Polyoxometalates as Cathode-active Materials for Li-ion Batteries

8.1	Introduction and objectives	143
8.2	Results and discussion	145
8.2.1	Keggin compounds	145
8.2.2	Wells-Dawson compounds	147
8.2.3	Preyssler compound	149
8.2.4	Vanadate compounds	150
8.3	Conclusions	154
8.4	Computational details	154
8.5	Experimental methodology	154
8.6	References	156

Chapter 9. Concluding Remarks

List of publications	165
-----------------------------	-----

Acknowledgements	167
-------------------------	-----

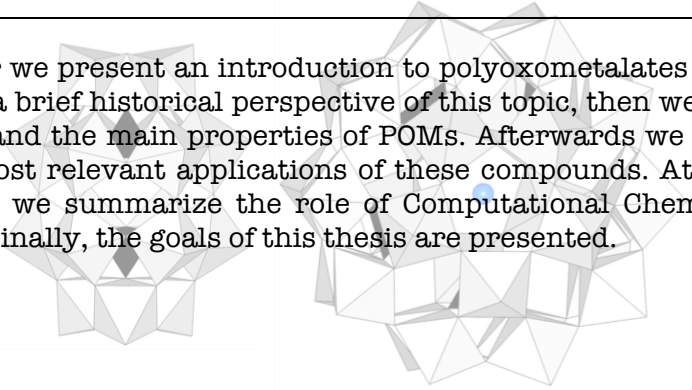
List of abbreviations

B3LYP	Becke 3-parameter, Lee, Yang and Parr functional
BP86	Becke-Perdew 86 functional
COSMO	Conductor-like Screening Model
DFT	Density Functional Theory
GGA	Generalized Gradient Approximation
HOMO	Highest Occupied Molecular Orbital
LANL	Los Alamos National Laboratory
LDA	Local Density Approximation
LUMO	Lowest Unoccupied Molecular Orbital
NHE	Normal Hydrogen Electrode
PCM	Polarizable Continuum Model
POM	Polyoxometalate
RE	Reduction Energy
SCE	Saturated Calomel Electrode
SMD	Solvation Model based on the Density
WD	Wells-Dawson
XM₁₂	[XM ₁₂ O ₄₀] ⁿ⁻
XMW₁₁	[XMW ₁₁ O ₄₀] ⁿ⁻
X₂M₁₈	[X ₂ M ₁₈ O ₆₂] ⁿ⁻
X₂MW₁₇	[X ₂ MW ₁₇ O ₆₂] ⁿ⁻
ZORA	Zeroth-order Regular Approximation



Chapter 1

Introduction



In this chapter we present an introduction to polyoxometalates (POMs). We start with a brief historical perspective of this topic, then we explain the structure and the main properties of POMs. Afterwards we describe some of the most relevant applications of these compounds. At the end of the chapter we summarize the role of Computational Chemistry in POM science. Finally, the goals of this thesis are presented.

1.1 A brief historical perspective of POMs

In 1778, the Swedish chemist C. W. Scheele published the first paper related to POMs. In this study, he characterized the blue water solutions of “molybdenum blue”, formed by oxidation of MoS_2 . It was observed in some springs located near Idaho Springs (Colorado) and in the Valley of Ten Thousand Smokes (Alaska). He described a reproducible experiment about this compound in his work named “Chemical Studies of the Molybdenum or Lead Water” (*Chemische Untersuchung über das Molybdänum oder Wasserbley*), and he realized that the compound was a reduced molybdenum oxide^[1]. This study was considered of great relevance and it was translated from Swedish to French under the title “*Sur la Mine de Plomb ou Molybdène*”, in the series of “*Observations sur la Physique, sur l’Histoire Naturelle et sur les Arts*” by M. L’Abbé Rozier and M. J. A. Mongez, which collected exciting and important scientific publications back then.

In the 19th century, around fifty years after Scheele discovery, Berzelius reported the synthesis of what we nowadays know as phosphomolybdic acid^[2], $\text{H}_3\text{PMo}_{12}\text{O}_{40}$. It is a yellow precipitate that appears after addition of an excess ammonium molybdate to a solution of phosphoric acid. In those days, the exact nature and structure of this compound was unknown. It was not until 1862 that C. Marignac carried out a systematic study about the composition of the silicotungstic acid^[3], $\text{H}_4\text{SiW}_{12}\text{O}_{40}$. He prepared and analyzed two different isomers of this acid, now known as α and β isomers, and various salts, and then their analytical composition were precisely determined. In the following years these phosphomolybdate and silicotungstate derivatives were used to determine the content of ammonium, phosphorus or silicon in different samples.

A. Miolati and P. Pizzighelli performed the first attempt to determine the structure of these metal oxides^[4] at the beginning of the 20th century, more than 40 years after the studies of Berzelius and Marignac. They explained that POMs were based on six-coordinate (6:1) heteroatoms with MO_4^{2-} or $\text{M}_2\text{O}_7^{2-}$ anions as ligands or bridging groups. The first criticism of this theory came from L. C. Pauling, in 1929, who noticed that Mo^{6+} and W^{6+} atoms had appropriate crystallographic radii for octahedral coordination by oxygen. He proposed that the structure of these polyoxoanions was based on a central PO_4 or SiO_4 tetrahedron surrounded by MO_6 octahedra (12:1)^[5]. Finally, in 1933, J.

F. Keggin performed the first X-ray analysis of phosphotungstic acid, $\text{H}_3[\text{PW}_{12}\text{O}_{40}] \cdot 5\text{H}_2\text{O}$ ^[6]. He showed that the anion was indeed based on WO_6 units as suggested by Pauling. The POM structure was afterwards confirmed by A. J. Bradley and J. W. Illingworth, who studied crystals of $\text{H}_3[\text{PW}_{12}\text{O}_{40}] \cdot 29\text{H}_2\text{O}$ ^[7]. Both structural determinations were significant achievements in the field of POMs, being based solely on powder photographs. Until 1971, only 25 new X-ray structures were reported by T. H. Evans^[8]. During the next years, improvements in crystallographic techniques increased the number of new published structures. Also, the development of new spectroscopic techniques combined with more accurate electrochemical and analytical determinations helped to get more precise characterizations of POM structures.

POM science rapidly exploded and rose in popularity during the last decades. An evidence of this is the review by M. T. Pope and A. Müller in 1991^[9]. A few years later, in 1998, a special issue on POMs, with C. L. Hill as guest editor, was published in *Chemical Reviews*, where the history, developments and applications of these compounds were discussed^[10]. More recently, in 2012, L. Cronin and A. Müller arranged the latest special issue on POM cluster science in *Chemical Society Reviews*^[11]. The number of publications involving POMs has dramatically increased in the last 20 years, as it is shown in Figure 1.1.

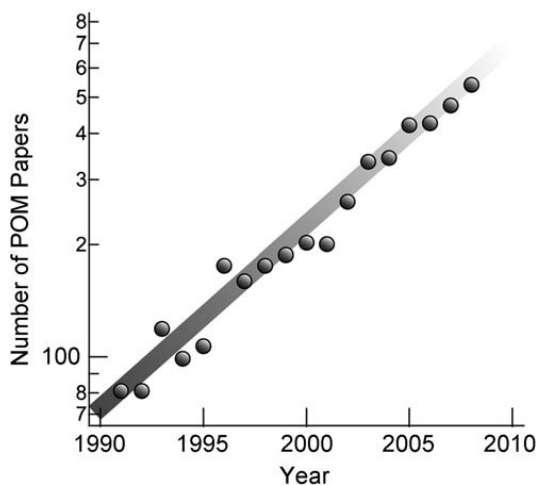


Figure 1.1. POM-related publications by year. The y-axis is plotted in logarithmic scale. (Figure obtained from Ref. [12])

1.2 Structure and properties of POMs

POMs are inorganic clusters made of oxygen and transition metal atoms usually in their highest oxidation states. These clusters feature an incomparable range of physical and chemical properties, acting as a set of building blocks that can be used in the formation of new materials. They also have the ability to form dynamic structures of different sizes, from the nano to the micro scale. POMs have the general formula $\{MO_x\}_n$, where M (*addendum atom*) is Mo^{6+} , W^{6+} or V^{5+} , and sometimes Nb^{5+} , and x goes from 4 to 7 normally, being 6 the most common value^[9]. POMs are typically built upon arrangements of edge and corner-sharing MO_6 octahedra (Figure 1.2). They can be classified according to their composition, oxidation state of the metals or due to structural aspects. Apart from M and O atoms, other elements can take part in POMs. They are the so-called central atoms or *heteroatoms* (labeled X in the above formulas). In general they are 4 or 6-fold coordinated and lie inside the metal oxide framework. The most representative POMs are shown in Figure 1.3. Depending on whether the heteroatom is present or not, we can classify POMs as:

(i) **Heteropolyanions** are metal oxide clusters with $[X_zM_nO_y]^{n-}$ formula that include heteroanions XO_4 , such as SO_4^{2-} or PO_4^{3-} , inside the metal oxide core. The most representative ones are the Keggin $[XM_{12}O_{40}]^{n-}$ and the Wells-Dawson $[X_2M_{18}O_{62}]^{n-}$ anions.

(ii) **Isopolyanions** are composed of a metal oxide framework without an internal heteroanion. They have a general formula $[M_nO_y]^{n-}$. The most popular structure in this family is the Lindqvist anion $[M_6O_{19}]^{n-}$.

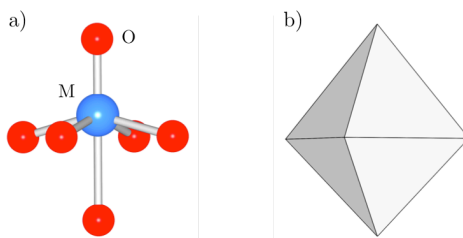


Figure 1.2. (a) Ball and stick (blue: metal atom, red: oxygen) and (b) polyhedral representations of the fundamental MO_6 unit. The M atom is displaced off the geometrical center of the octahedron towards one oxygen (commonly a terminal oxygen), thus giving rise to a distorted C_{4v} instead of O_h unit.

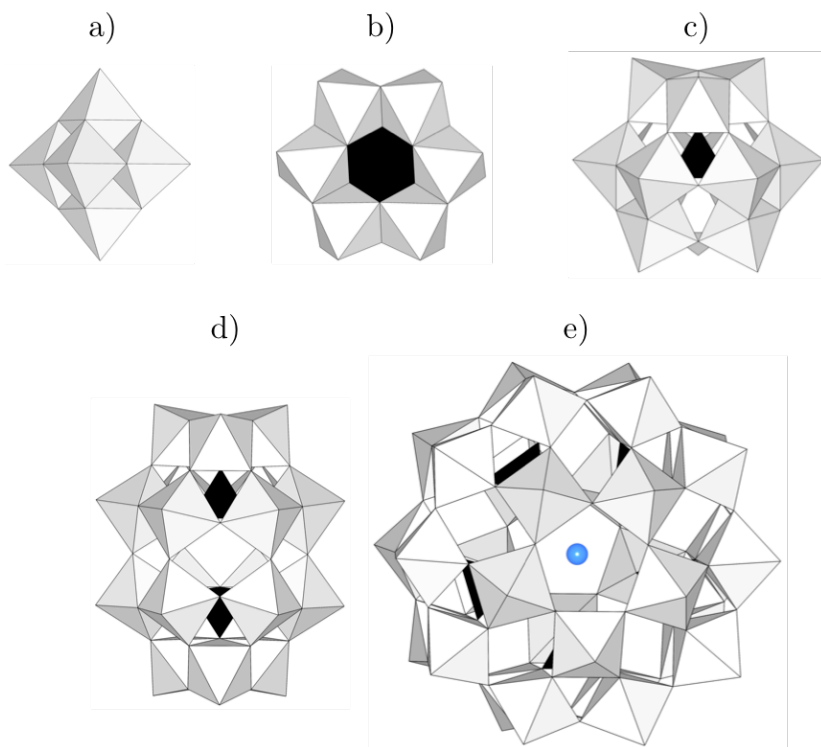


Figure 1.3. Polyhedral representation for the most typical POMs: (a) Lindqvist [M₆O₁₉]ⁿ⁻, (b) Anderson-Evans [X_M6O₂₄]ⁿ⁻, (c) Keggin [X_M12O₄₀]ⁿ⁻, (d) Wells-Dawson [X₂M₁₈O₆₂]ⁿ⁻ and (e) Preyssler [Z_X5M₃₀O₁₁₀]ⁿ⁻. Grey octahedral units are MO₆ octahedra and black tetrahedra contain the heteroatom XO₄.

Metal atoms in POMs usually occupy pseudo-octahedral sites with either one or two terminal oxygens and they are electronically analogous to mononuclear coordination complexes. In most structures, such as Keggin and Wells-Dawson compounds, metal atoms have only one terminal oxygen (Type I). In the idealized local C_{4v} symmetry of a metal atom, the d orbitals split into a_1 (z^2), b_1 (x^2-y^2), b_2 (xy) and e (xz, yz). A qualitative study of the orbitals yields that a_1 and b_1 are anti-bonding σ orbitals, e is the anti-bonding π component of the terminal oxo ligand and b_2 is formally non-bonding, or weakly anti-bonding if the equatorial ligands exhibit some π interactions with the metal. If one or two electrons occupy the b_2 orbital, no significant effect on the metal-ligand bond orders is observed. Indeed, many examples of POM compounds with d¹ or d² metal centers have been reported. Therefore, it is expected that polyoxoanions with this kind of structures can undergo reversible reduction processes easily, then giving isostructural compounds in which one or more metal centers have

a d^1 configuration (*heteropoly blues*). In POMs where the metal atoms have two terminal oxygens (Type II), there is no non-bonding d -like orbital and no example of stable d^1 complexes is known. For these reason, reductions of these POM anions is irreversible, leading to fragmentation or rearrangement to other structures.

The Keggin anion is the most deeply studied POM. It is formed by twelve MO_6 octahedra arranged in four edge-sharing M_3O_{13} groups surrounding a central XO_4 tetrahedron. It possesses five geometrical isomers, proposed by Baker and Figgis^[13], designated by the prefixes α , β , γ , δ and ϵ , the last four resulting from successive 60° rotations of the M_3O_{13} edge-sharing units about 3-fold symmetry axes of the α isomer (Figure 1.4). The α isomer has overall T_d symmetry, so the twelve octahedra are equivalent. The β isomer has C_{3v} symmetry and it arises from the 60° rotation of one of the M_3O_{13} triads. A rotation of another triad produces the γ isomer, which has C_{2v} symmetry. The δ isomer has C_{3v} , as the β isomer, and it results from a rotation of a third triad. Finally, when the four M_3O_{13} triads are rotated we obtain the ϵ isomer, which has T_d symmetry. In the γ isomer, after the rotation of the second triad, a short M-M contact appears. The α and β isomers do not present any of these M-M close contacts, whereas the δ and ϵ forms present two and three of these contacts, respectively.

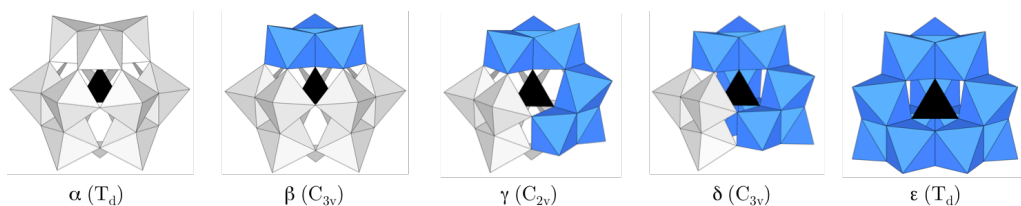


Figure 1.4. Polyhedral representation of the five rotational isomers of the Keggin anion. Each rotated M_3O_{13} unit is colored blue. The internal black tetrahedra contain the heteroatom.

The Wells-Dawson or simply Dawson structure,^[14] $\{\text{X}_2\text{M}_{18}\text{O}_{62}\}$, is another well-known POM. It is an ellipsoidal structure formed by two M_3 rings at the polar regions (caps) and two M_6 rings located at the equatorial region (belts). Inside this structure, two XO_4 anions are encapsulated. Each of the equatorial octahedra is connected to a polar octahedron by a single corner and it shares an edge with a neighbor of the same belt and a corner with the other belt. The Dawson anion may be seen as a derivative of the Keggin structure; the

removal of three neighboring corner-sharing octahedra produces a $\{XM_9O_{34}\}$ lacunary structure, which is prepared to link another equivalent moiety to produce the $\{X_2M_{18}O_{62}\}$ anion.

There are six rotational isomers of the $\{X_2M_{18}O_{62}\}$ polyoxoanion, named α , β , γ , α^* , β^* and γ^* . They were postulated in the 1970 by Baker and Figgis^[13]. The α isomer is built from two α - XM_9O_{34} units linked by 6 oxygen atoms and it belongs to the D_{3h} point group. The β anion derives from the α isomer by a 60° rotation of one cap M_3O_{13} group, and its symmetry is decreased to C_{3v} . The rotation of the second capping M_3O_{13} group by 60° produces the γ isomer, with a D_{3h} point symmetry. If one of the two α - XM_9O_{34} units is rotated by 60° with respect to the other half, the resulting structure is the α^* isomer and it belongs to the D_{3d} point group. The rotation of one or both cap M_3O_{13} groups of the α^* anion generates the other two isomers named β^* (C_{3v}) and γ^* (D_{3d}), respectively (Figure 1.5).

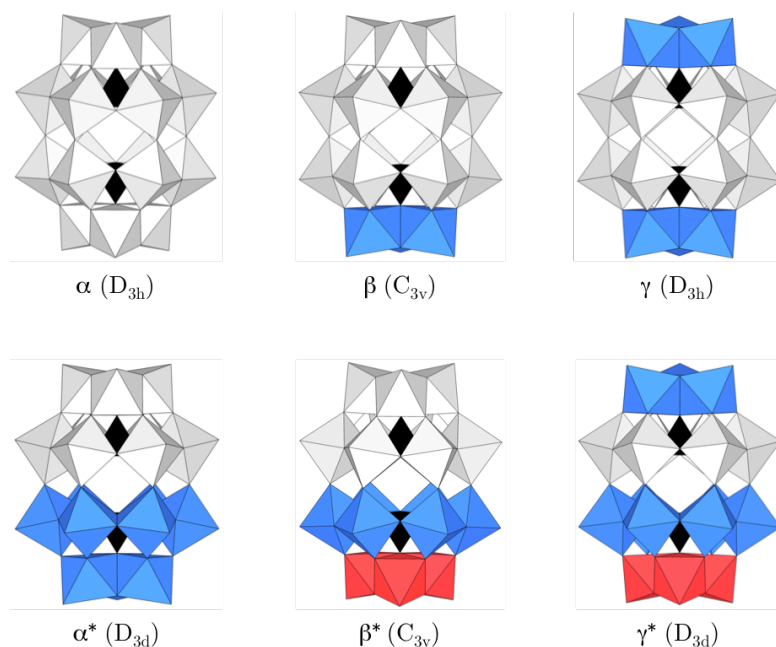


Figure 1.5. Polyhedral representation of the six rotational isomers of the Dawson structures. The grey octahedra represent the MO_6 , the black tetrahedra represent the internal XO_4^{2-} , the blue octahedra represent the first 60° rotation of the MO_6 and the red octahedra represent the second 60° rotation of the MO_6 units.

One of the abilities of the Dawson-type tungstodiphosphate is to generate lacunary species, and hence metal-substituted molecules. The mono-substituted heteropolyanions can be considered as the analogues of metallated porphyrins and can be used in catalytic processes^[15]. The location of the metal in the framework is one of the parameters that can modify the redox properties. The replacement of one metal from the α anion produces two different isomers named α_1 (belt) and α_2 (cap) (Figure 1.6). These two isomers are different at some effects despite being structurally so similar.

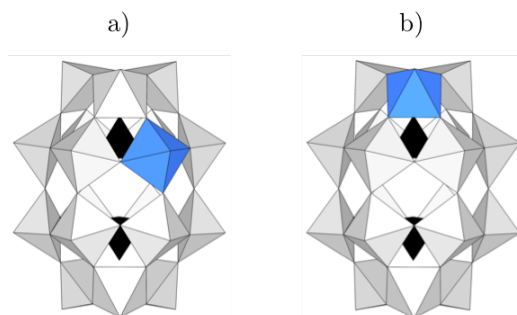


Figure 1.6. Polyhedral representation of addenda-substituted (a) α_1 and (b) α_2 - $\{P_2M'M_{17}O_{62}\}$ anions. Grey octahedra represent MO_6 groups, blue octahedra represent $M'O_6$ groups and black tetrahedra represent the internal anions.

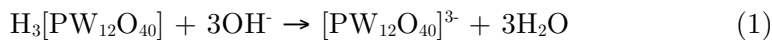
1.2.1 Acidic properties

POMs are very acidic compounds in aqueous solution despite carrying high negative charges. This is related to their low surface charge density. Some acid-base equilibria in solution have been reported, in which POMs act as polyacids^[16]. In many cases their pK_a is close to 1, sometimes even lower than 0, implying that all their protons can be released in water. Because of the chemical characteristics of the M atom, not all oxygen sites in a POM are identically acidic or basic. This depends on the covalency or ionicity of the M-O bond, the number of neighboring M atoms and the physical nature of M.

Heteropolyanions are considerably stronger Brønsted acids than common mineral acids^[17]. Therefore, the corresponding POM anions have very weak Brønsted basicity, and appear to be softer than simple nitrate and sulfate anions. According to Izumi *et al.*^[18] the order of softness is: $[SiW_{12}O_{40}]^{4-} > [PW_{12}O_{40}]^{3-} > [PMo_{12}O_{40}]^{3-} > [SiMo_{12}O_{40}]^{4-} > [NO_3]^-$.

Some methods for heteropolyacid characterization involve titration with base in order to establish or confirm the stoichiometry. In most of the cases, two

end points can be detected, the first corresponding to the neutralization of the acidic protons (1) and the second one being the complete degradation of the anion (2), for example:



Anion degradation does not usually begin before the neutralization is completed. It might be expected that the rates of both reactions would significantly differ, which is not always the case, especially with more labile atoms, such as Mo or V. Another controversial question about the acidity of POMs is where the protons are attached. POM surfaces contain terminal and bridging oxygen atoms susceptible to protonation. Many X-ray and neutron diffraction experiments have been performed in order to elucidate the location of the protons in POMs. In most of the cases the protonation sites were found to be the accessible *bridging* oxygens atoms^[19]. Protonation in terminal oxygens has been also observed but only in a few structures^[20].

The identification of protonation sites using the above-mentioned techniques might not necessarily reflect the solution behavior, because they are determined by anion packing and hydrogen-bonding considerations. A common method for inferring the protonation sites in solution has been the pH-dependency of ¹⁷O NMR chemical shifts^[21]. The conclusions reached from NMR experiments have generally been in accordance with those obtained based on crystallography.

1.2.2 Redox properties

Another property of POMs is that they are strong oxidizing agents. It can be understood analyzing their structure and composition. They are formed by metal atoms in a high oxidation state (V or VI), usually with d⁰ or d¹ electronic configuration, linked to O²⁻ atoms. The valence shell of metals is empty so they are capable to accept electrons without notable geometrical changes. When a POM is reduced, the added electrons can be partially or fully delocalized over the whole framework. The degree of delocalization depends on: (i) the local structure of the M-O-M linkage, and (ii) structural and chemical equivalency of the M sites.

The redox potentials of Type I polyoxoanions depend on the molecular structure and charge, and also on the nature of the metal atoms. M. T. Pope's

research focused on POM redox properties during decades. He rationalized most of the observations in this field, collecting a huge volume of electrochemical data for Keggin and Wells-Dawson anions. One of the most relevant measurements concerns Keggin reductions ($[XM_{12}O_{40}]^{n-} + e \rightarrow [XM_{12}O_{40}]^{(n+1)-}$). In the case of the tungsten derivatives with different heteroatoms, Pope's data show that the anion charge has the largest influence upon redox potentials and an increase by one charge unit varies the redox potential by about 180 mV^[22] (Figure 1.7). The isostructural molybdates have potentials that are *ca.* 400 mV more positive than the tungstate counterparts, and a similar trend is observed for the reduction of V in $[XVW_{11}O_{40}]^{n-}$ ($n = 4 - 7$)^[23]. The redox activity of POMs can also be centered on the heteroatom. In this case, the rather good correlation between the reduction potentials and the ionic charge shown in Figure 1.7 is no longer observed.

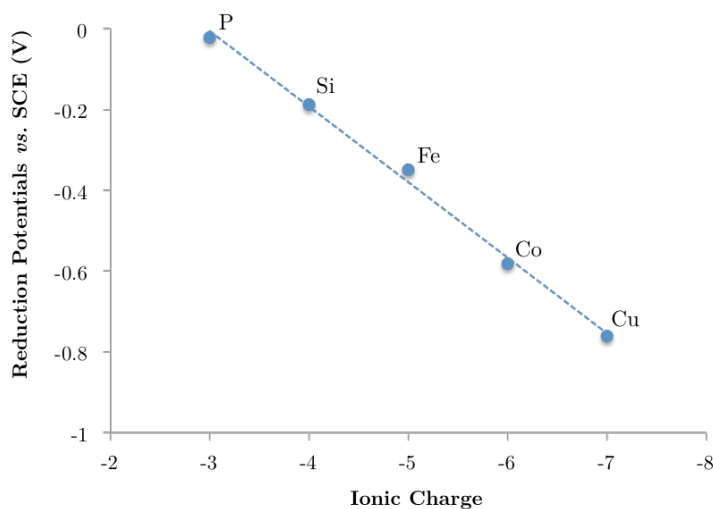


Figure 1.7. One-electron reduction potentials *vs.* SCE (in V) plotted against the ionic charge of $[XW_{12}O_{40}]^{n-}$ polyoxoanions. The heteroatom is indicated in each case.

Reduced POMs are strongly colored because of the intense d-d and charge transfer electronic transitions. Electron spin resonance (ESR) experiments show that the extra electron is *delocalized* over the twelve metal centers, in $[XM_{12}O_{40}]^{n-}$ compounds, by thermally activated intra-molecular electron hopping. The electron transfer rates between the oxidized and the reduced anions can be determined from NMR measurements^[24].

The ability to configure redox properties is one of the most important features of POMs. For example, the Wells-Dawson cluster can be readily 6-fold reduced without any change in the geometry. Furthermore, the redox properties of the same POM can be tuned by incorporating different heteroatoms or by replacement of one metal of the framework. Another example is the Preyssler anion, which is able to accept electrons at low potentials, to capture various metal cations and undergo acid-base reactions.

1.2.3 Electrochemistry

Souchay pioneered the application of electrochemistry to the study of POMs and it was related to polarography^[25]. More detailed investigations were done from his and others' groups during the latest 60's^[26]. Based on these studies, it was established that Keggin and Wells-Dawson derivatives experience a series of reversible one and two-electron reductions in aqueous media. It was shown that, in acidic conditions, these polyoxoanions can accept up to six electrons and six protons, usually in reversible two-electron steps. As the pH of the solution is increased, the reduction potentials become more negative (0.059 V/pH unit) until a pH is reached at which the reduced POM is no longer protonated. At this point, the two-electron wave splits into two one-electron waves and the reduction potentials are not pH-dependent anymore.

Under alkaline pH conditions, reduced POMs are kinetically more stable than their oxidized counterparts. Solutions of reduced POMs can be generated by controlled potential electrolysis under appropriate conditions of solvent and acidity. Electrochemical studies showed that the reduced anions could undergo irreversible isomerization, in the case of molybdate compounds, or intramolecular disproportionation, in the case of tungstate derivatives. Polarograms of reduced Keggin and Wells-Dawson anions in aqueous and organic solvents show that they gradually transform from α to β isomers. This behavior is the outcome of (i) the lability of polyoxomolybdates compared to polyoxotungstates and (ii) the more positive reduction potentials of the β isomers^[27]. Even though the reduced β isomers of tungstates should be favored thermodynamically according to the reduction potentials, an alternative reaction involving the formation of metal-metal bonds is also available^[28].

1.3 Reduced and mixed-valence POMs

Reduced POMs can be classified in two different groups: *heteropoly blues*, where the extra electron(s) are delocalized over the metal oxide framework, and *heteropoly browns*, which are mixed-valence species with well-defined valence states localized on a particular atom(s).

1.3.1 Heteropoly blues

As we have defined above, *heteropoly blues* are the reduced POMs where the extra electrons (metallic or *blue* electrons) are delocalized over the d-metal molecular orbitals. The term *blue* is related to the intense blue color that we can observe when a POM is reduced with few electrons. However, we will use the term *blue* regardless of the color of the reduced species. It solely indicates the presence of delocalized metal electrons.

The most deeply studied *heteropoly blues* have been the Lindqvist, Keggin and Wells-Dawson POMs, with emphasis on the one- and two-electron reduced forms. In the Keggin and Lindqvist anions all the metal centers are equivalent, but in the Wells-Dawson anion two types of metal atoms can be distinguished, those in *cap* and *belt* positions. ESR spectra of the one-electron reduced anions show very broad, even sometimes unobservable lines at room temperature. These observations can be interpreted according to a model of mixed-valence metal centers, i.e. a delocalized hopping electron at high temperatures that becomes *trapped* on a metal atom as the temperature is lowered.

1.3.2 Heteropoly browns

Contrarily to *heteropoly blues*, *heteropoly browns* are mixed-valence compounds where the extra electrons are localized on specific atoms. It has been demonstrated with vanadate and molybdate clusters described by A. Müller *et al.*^[29] that the reduced metal centers in these molecules show magnetic behavior.

Three examples of *heteropoly browns* with major attention in the latest years are the $[\text{XW}_9\text{O}_{37}\{\text{W}^{\text{IV}}(\text{OH}_2)_3\}]^{n-}$ structures (X = 2H, B, Si). Unlike the polyoxotungstate blues, they are stable to re-oxidation by air in aqueous solution. X-ray analysis and NMR spectroscopy confirm that W^{IV} atoms occupy a group of three edge-shared WO_6 octahedra in the Keggin structure^[30]. Each W^{IV} has a terminal aqua ligand instead of the oxo group in the oxidized

counterpart. It can be deprotonated to yield the tris-hydroxo anion. The deprotonation of the tris-hydroxo compound leads to the formation of the heteropolyblue solution. One of the most relevant features of the heteropoly browns in non-aqueous solutions is the possibility of acting as oxygen transfer reagents. In most of the cases, these reactions require high temperatures.

The $W^{IV}_3O_{13}$ group on the surface of the Keggin anion can act as a heterogroup for a larger POM framework. The reaction of $[BW_9O_{37}\{W^{IV}(OH)_2\}_3]^{5-}$ with tungstate leads to formation of the $[BW_{17}W^{IV}_3O_{66}OH_4]^{11-}$ anion^[31]. In general, the reactivity and electrochemistry of the *heteropoly browns* is an area of POM science that deserves further investigation.

1.4 Applications of POMs

POM clusters have a diverse range of electronic properties. This feature, combined with the ability to act as ligands in polynuclear transition metal clusters, make them good candidates for new molecular magnetic devices. For example, $[PMo_{12}O_{40}(VO_2)]^{n-}$ has been described by Coronado *et al.* as an important model compound of spin qubits. The redox core unit of the Keggin anion is capped on opposite positions by two V=O groups, each containing a localized $s=1/2$ spin. These two spins can be coupled through the central core electrons by electrical manipulation of the molecular redox potential owing to change of charge^[32] (Figure 1.8).

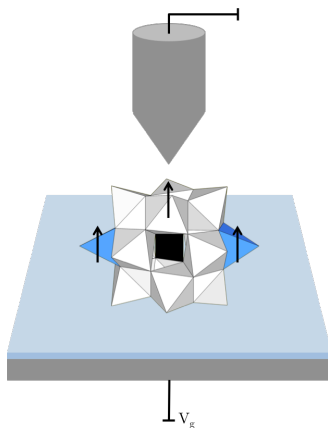


Figure 1.8. The $[PMo_{12}O_{40}(VO_2)]^{n-}$ compound connected to an electric circuit through a STM setup. It is a mixed-valence POM combining two localized electrons on the capping vanadyl groups with delocalized electrons in the Keggin core. The magnetic coupling between the two spins located at the V=O sites can be controlled by an electric tunneling current (V_g).

The use of POMs as catalysts is one of the most important applications, in particular for industrial processes. Some reviews show the development of green H_2O_2 -based epoxidation systems^[33], catalytic oxidation of organic substrates by molecular oxygen and hydrogen peroxide^[34], and catalytic strategies for sustainable oxidations in water^[35]. Efficient catalytic water splitting is another important area of research, and in particular for the utilization of solar energy. Studies have been carried out on many catalysts. For example, Prof. C. L. Hill and co-workers showed that the $[\{\text{Ru}_4\text{O}_4(\text{OH})_2(\text{H}_2\text{O})_4\}(\gamma\text{-SiW}_{10}\text{O}_{36})_2]^{10-}$ compound combined with some $[\text{Ru}(\text{bipy})_3]^{3+}$ salt catalyzes the oxidation of H_2O to O_2 in water at room temperature and with considerable activity^[36]. The same research group also studied $[\text{Co}_4(\text{H}_2\text{O})_2(\text{PW}_9\text{O}_{34})_2]^{10-}$ (Co_4), with applications in water oxidation catalysis^[37]. On the other hand, the investigations of Prof. R. G. Finke *et al.* showed that under different experimental conditions the CoO_x unit is the dominant catalyst^[38]. The group of Prof. J. R. Galán-Mascarós has recently shown that $[\text{Co}_9(\text{H}_2\text{O})_6(\text{OH})_3(\text{HPO}_4)_2(\text{PW}_9\text{O}_{34})_3]^{16-}$ (Co_9) is a robust homogeneous water oxidation catalyst^[39]. A representation of both Co compounds, Co_4 and Co_9 , is shown in Figure 1.9.

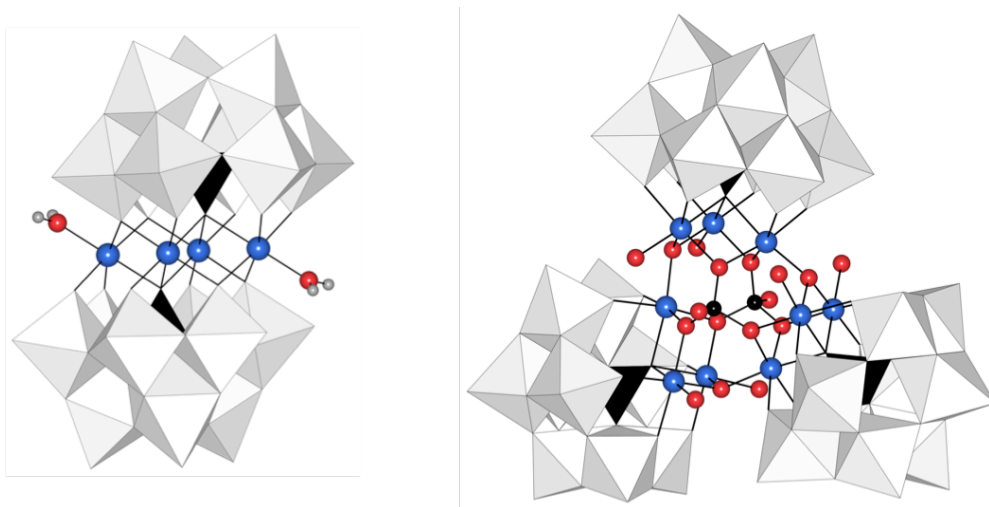


Figure 1.9. Combined polyhedral (grey: WO_6 groups and black: PO_4 groups) and ball and stick (blue: cobalt, red: oxygen, grey: hydrogen and black: phosphorus) representation of Co_4 (left) and Co_9 (right) clusters. In the case of the Co_9 compound, the H atoms are not shown for the sake of clarity.

The characteristics of POMs such as their well defined size, modulated charge and the ability to produce organic and inorganic compounds give them a great

potential to interact with biomolecules. Many studies have been done employing POMs as anticancer or anti-viral agents. The reduced POM $[\text{Me}_3\text{NH}_6][\text{H}_2\text{Mo}^{\text{V}}_{12}\text{O}_{28}(\text{OH})_{12}(\text{Mo}^{\text{VI}}\text{O}_3)_4]$ was reported by Yamase *et al.*^[40] as a compound with antitumoral activity. Some POMs have been tested for anti-RNA viral activity and they are promising candidates for therapeutics in respiratory diseases^[41]. The Keggin-type polyoxotungstate ($\text{K}_7[\text{PTi}_2\text{W}_{10}\text{O}_{40}]6\text{H}_2\text{O}:\text{PM}-19$) is a potent inhibitor of the replication of herpes simplex virus^[42].

POMs are very effective as components in multifunctional nanomaterials, such as carbon-based structures. It has been reported the $\{\text{U}_{60}\}$ cluster, $[\text{UO}_2(\text{O}_2)(\text{OH})]_{60}^{60-}$, a compound topologically identical to the C_{60} species, with uranium centers located in the corresponding positions of the carbon atoms^[43] (Figure 1.10). The use in nuclear waste treatment is a possible application of this type of clusters. It has also been shown the spontaneous and controllable formation of micrometer scale POM tubes, topologically very similar to carbon nanotubes. They are synthesized from crystals of a POM upon immersion in an aqueous solution containing a low concentration of an organic cation^[44].

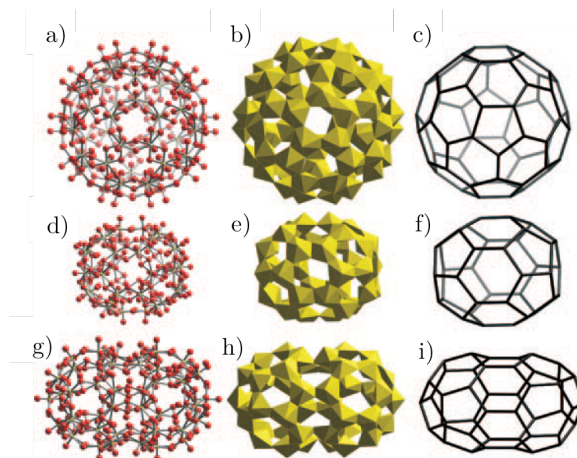


Figure 1.10. Uranyl peroxide structures of $\{\text{U}_{60}\}$ (a-c), $\{\text{U}_{36}\}$ (d-f) and $\{\text{U}_{44}\}$ (g-i). Ball and stick (left), polyhedral (center) and graphical (right) representations showing the cluster topologies. (Figure obtained from Ref. [43])

1.5 Computational chemistry in POMs

In the last years several groups have carried out computations to study POMs. The first calculation on POMs was performed using the model potential $X\alpha$ method in 1986 by N. Yamazoe and co-workers. They studied the electronic

structure and the redox mechanisms of the $[\text{PMo}_{12}\text{O}_{40}]^{3-}$ anion^[45], describing the properties of the most relevant molecular orbitals. During the following years, some works using semi-empirical methods were published. F. Ritschl and co-workers elucidated the POM structure containing Cu^{II} and V^{IV} cations using the SCF CNDO/2 approximation^[46].

In the early 90s, M. Bénard, M. M. Rohmer and co-workers did one of the first theoretical calculations on a POM compound using the more accurate Hartree-Fock Self-Consistent Field (HF-SCF) method. They carried out *ab initio* calculations on the relative basicities of the external oxygen sites in the $[\text{V}_{10}\text{O}_{28}]^{6-}$ anion^[47]. An interpretation of the structure of the inclusion complexes $[\text{RCN}\subset(\text{V}_{12}\text{O}_{34})^4]$ ($\text{R} = \text{CH}_3, \text{C}_6\text{H}_5$) from electrostatic potentials were done by this group^[48]. They also performed HF calculations on the octadecavanadate ion, $[\text{V}_{18}\text{O}_{42}]^{12-}$, and some related structures^[49].

For transition metals, the error made by using the HF-SCF method is usually too large. Part of this error can be solved with Density Functional Theory (DFT) methods, which are moderately time-consuming although providing sufficiently accurate information on the geometry and the electronic structure. The application of the DFT to the study of POMs started more than twenty years ago^[50]. Present DFT calculations allow introducing additional physical effects not taken into account originally, as for example relativistic and solvation effects, large atomic basis sets, hybrid functionals, etc. The solvent effects are included in an approximate way by continuum models as COSMO^[51], PCM^[52] or SMD^[53]. These effects have revealed fundamental for the right modeling of many POMs properties, such as electrochemistry or reactivity.

In most of the cases, pure GGA functionals and standard triple-zeta atomic basis sets should be enough to get good equilibrium geometries and electronic structures of most POMs. However, NMR calculations require very accurate geometries that can only be achieved with larger basis sets, tight numerical integration and stabilizing solvent effects^[54].

Correlated *ab initio* calculations as CASSCF and DDCI have also been applied to the study of systems with unpaired electrons. These accurate methods are much more expensive from a computational point of view and, thus, they are not routinely applied to POMs, unless these are small or in a fragment analysis^[55].

A very active group in the theoretical study of POMs is the one of J. M. Poblet and co-workers. Some years ago they investigated the structure and effects on the diffusion coefficient of the ion pairs between Keggin $[XW_{12}O_{40}]^{n-}$ anions ($X = P, Si, Al; n = 3, 4, 5$) and mono-valent alkali counterions (Li^+, Na^+, K^+) in water by molecular dynamics simulation^[56]. They also have studied the electronic and magnetic properties of the α -Keggin anion, the $[XW_{12}O_{40}]^{n-}$ where $M = W, Mo; X = Al^{III}, Si^{IV}, P^V, Fe^{III}, Co^{II}, Co^{III}$ and the $[SiM_{11}VO_{40}]^{n-}$ ($M = Mo$ and W)^[57]. A few years ago, F. Q. Zhang *et al.* performed a DFT study on the relative stability of α and β $[XW_{12}O_{40}]^{n-}$ ($X = Cr^{VI}, V^V, Ti^{IV}, Fe^{III}, Co^{III}, Ni^{III}, Co^{II},$ and Zn^{II}) Keggin anions. They confirmed the conventional trend of the higher stability of α over the β isomer^[58]. More recently they have carried out a DFT study on the five Keggin isomers. They have investigated the origin of the inverted stability order of the $[(MnO_4)(CH_3)_{12}Sb_{12}O_{24}]^{6-}$ anions^[59].

The DFT methodology is implemented in many programs, codes and packages. Although the computational details are described in each chapter of this thesis, a general description of the used software is presented here. *Gaussian* package^[60] is one of the most widely used programs. It can handle calculations of up to a few hundred atoms and it can predict the geometrical structures and electronic properties of large molecules with any type of atoms, including metals. It uses a linear combination of gaussian-type functions (GTOs) as atomic orbitals. A basis set is the mathematical ensemble of orbitals of a system used to perform theoretical calculations. *Gaussian* has different pre-defined basis sets, which are classified by the number and types of basis functions that they contain. Basis sets assign a group of basis functions to each atom within a molecule to approximate its orbitals. Basis sets for atoms beyond the 3rd row of the periodic table are computed differently. In these big atoms, internal electrons are treated in an approximate way, via effective core potentials (ECPs). This treatment includes part of the relativistic effects, which are important in heavy atoms. Los Alamos National Laboratory pseudopotential with the standard 2-double-zeta (LANL2DZ) is one of the best-known basis set. DFT methods calculate electron correlation using general *functionals* of the electron density. One of the advantages of *Gaussian* is that hybrid functionals can be very efficiently used.

Another well-known package is the *ADF* suite of programs^[61]. The main difference with the *Gaussian* code is that *ADF* uses basis sets built with

Slater-type orbital functions (STOs). Slater orbitals are more accurate than the same number of gaussian functions for molecular orbital computations. Although numerical integration is more computationally demanding with STOs. It is generally accepted that STOs allow the construction of high-quality basis sets with relatively small number of functions. *ADF* also incorporates relativistic effects with the *zeroth-order regular approximation* (ZORA)^[62]. Hybrid functionals are also implemented in *ADF*, but not in a very efficient way. Nowadays, geometrical optimization using these types of functionals is not suitable. *ADF* exploits optimally molecular symmetry for analysis purposes and to enhance the computational efficiency. It uses the full molecular symmetry in the calculations and it includes all point group symmetries. On the other hand, *Gaussian* is not always able to use the full symmetry since it restricts to abelian point groups. For example, a molecule with T_d as full point group is computed with the D_2 subgroup.

TURBOMOLE is another quantum chemical package^[63] and it consists of modules and tools to facilitate their use. It has the advantages of *Gaussian* and *ADF*, i.e., it is able to perform calculations using hybrid functionals and full symmetry. It also provides different possibilities for the treatment of relativistic effects: via effective core potentials (ECPs) or via all-electron approaches. One of the disadvantages of this code is that the analysis of the data is not as friendly as the other packages. However, it is considered one of the fastest programs of its kind.

1.6 Modeling of redox properties

As we have discussed before, one of the most relevant properties of POMs is their oxidizing power, which arises from the presence of many metal centers in high oxidation states. The reduction usually occurs in the metal-like molecular orbitals with non-bonding character^[57]. Dealing with POMs in anionic form, a reasonable treatment of the environment is fundamental. The solvent effects should be included by means of continuum models because it has revealed necessary for the correct modeling of POMs properties. These models, introduced to mimic the environment of the molecule, not only accounts for the solvent effects but also distributes the positive charge necessary to counterbalance the negative charge carried by POMs. Without solvent effects, there is no match between computed and experimental reduction potentials because the POM orbitals are too high in energy^[64].

The theoretical calculation of the redox potential requires the determination of the free energy associated to the process:



In an electrochemical process, the redox potential (E) and the Gibbs free energy (ΔG) are formally linked by the number of electrons exchanged in the process and the Faraday constant:

$$\Delta G = -nFE$$

Throughout this thesis, we present the reduction energies (RE) defined as the difference in energy of the reduced and oxidized POM, that is:

$$\text{RE} = E(\text{POM}_{\text{n-red}}) - E(\text{POM}_{\text{ox}})$$

For this purpose, we computed electronic energies for the n -fold reduced and oxidized forms with the energy of the free electron taken as zero. Assuming that the electronic energy change during the reduction process is practically equal to the Gibbs free energy change (neglecting the entropic change term, $\Delta S \approx 0$), $\text{RE} \approx \Delta G$, the computed REs may be seen as theoretical straightforward measurements of the experimental reduction potentials:

$$\text{RE} \approx -nFE$$

The last expression shows that a species with more negative RE than another will consequently have a more positive potential (E), and vice versa. We will discuss the computational results mostly as differences between REs (in eV) or E (in V).

As for electrochemical data, in which the normal hydrogen electrode (NHE) is usually taken as zero on the relative scale, the theoretical values should be referred to an *absolute theoretical zero*. Cramer *et al.*^[65] computed this absolute zero to be -4.28 eV for the free energy change in the NHE reaction: $\text{H}^+ + e \rightarrow \frac{1}{2}\text{H}_2$. In general, computed absolute REs for POMs are in some discrepancy with the experimental ones. However, relative reduction energies behave much better.

M. T. Pope introduced the anion charge effect studying the electrochemical behavior of differently charged structures. As we have explained in section 1.2.2, he focused on a family of isostructural $[\text{XM}_{12}\text{O}_{40}]^{n-}$ Keggin anions, showing dependence in the reduction potential of -0.18 V per each additional negative charge. The group of J. M. Poblet demonstrated that the anion

charge effect can be generalized to POMs of any size and charge by explicitly considering the overall negative charge, q , and the number of metal atoms, m , present in a structure. Also, the oxidizing power of a POM shows a mathematical relationship with the q/m ratio (a sort of molecular charge density)^[66], a parameter previously introduced by the same group to discuss the importance of solvent effects in the modeling of POMs^[67] (Figure 1.11).

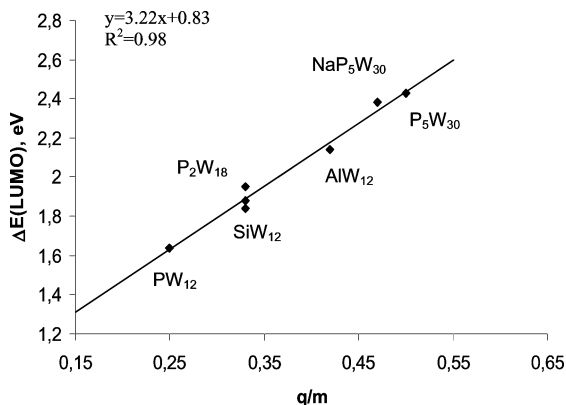


Figure 1.11. Variation of the computed E(LUMO) after encapsulating the anion in the neutral cage, calculated as $\Delta E(\text{LUMO})$, vs. q/m of the anion (Figure obtained from Ref. [66]).

One of the main facts is that POMs with a large q/m value (as for example the $\text{Nb}_6\text{O}_{19}^{8-}$ anion) have to be described with an external field (solvent) to avoid the wrong description of interatomic distances and molecular orbital energies. This study also concludes that POMs with moderate and low q/m values (as Keggin and Wells-Dawson compounds) are well described without solvent effects. However, the right description of geometrical parameters is always well accomplished when solvation effects are introduced.

1.7 Goals of the thesis

The theoretical modeling of redox processes in systems with several metal atoms, as POMs, is still a challenge, especially when the experimental reduction potentials are to be quantitatively reproduced. This thesis does not intend to be a definitive work on this topic, but a new step forward on a better understanding of the subject. From the computational point of view, DFT methods are the most suitable for the study of these polymetallic systems, as we have explained in section 1.5. The main goals of this work are: (i) to optimize the theoretical description of the redox properties of POMs,

notably reduction energies; (ii) to find general rules to explain the redox properties of POMs; (iii) to understand which are the main electronic phenomena capable of varying the redox behavior of a system; (iv) to study processes and compounds where multiple reductions are involved, and (v) giving new, valuable and general information to experimentalists working in the field.

In the first part of the thesis we will discuss which is the best functional to estimate the reduction energies of different model compounds and to describe the correct localization/delocalization of the extra electrons (Chapter 2). After this, we will study some relevant aspects related to the redox chemistry of mono-substituted Keggin derivatives. Three different cases will be analyzed: internal charge effect, external localized charge effect and external delocalized charge effect (Chapter 3). After studying these phenomena in Keggin compounds, we will try to reproduce the same work in larger systems, namely the substituted Wells-Dawson anions. Only two of the effects will be studied in these compounds, the external localized and delocalized charge effect (Chapter 4). The redox chemistry of some systems needs the explicit incorporation of protonation. This is the case of the mono-substituted Wells-Dawson anions with Fe, Tc and Re (Chapter 5). Later, we will study the electrochemical behavior of mixed d metal-iron containing Wells-Dawson sandwich-type complexes (Chapter 6).

At the end of the thesis we will discuss two different works that move away a little bit from the main topic. The first one is related to the ϵ isomer of the Keggin anion, which is synthesized with eight metal electrons as the most stable form. This compound presents unique electronic and geometrical features. It is possible to add metal cations or complexes to the surface of the Keggin framework as capping groups (Chapter 7). Finally, the last work is a collaborative study between Prof. Irle and Assist. Prof. Yoshikawa at Nagoya University, and our group. We study different POMs as cathode-active materials for Li-ion batteries from a computational and experimental point of view (Chapter 8).

1.8 References

- [1] C. W. Scheele, in *Sämtliche Physische und Chemische Werke* (Ed.: D. S. F. Hermbstädt), Niederwaluf/Wiesbaden, **1971 (Original: 1793)**.
- [2] J. J. Berzelius, *Pogg. Ann. Phys. Chem.* **1826**, 6, 369.
- [3] C. Marignac, *C. R. Acad. Sci.* **1862**, 55, 888.
- [4] A. Miolati, P. Pizzighelli, *J. Prakt. Chem.* **1908**, 77, 417.
- [5] L. C. Pauling, *J. Am. Chem. Soc.* **1929**, 51, 2868.
- [6] J. F. Keggin, *Nature* **1933**, 131, 908.
- [7] A. J. Bradley, J. W. Illingworth, *Proc. Roy. Soc.* **1936**, 157, 113.
- [8] H. T. Evans, *Perspect. Struct. Chem.* **1971**, 4, 1.
- [9] M. T. Pope, A. Müller, *Angew. Chem.* **1991**, 103, 56.
- [10] C. L. Hill, *Chem. Rev.* **1998**, 98, 1.
- [11] L. Cronin, A. Muller, *Chem. Soc. Rev.* **2012**, 41, 7333.
- [12] D.-L. Long, R. Tsunashima, L. Cronin, *Angew. Chem., Int. Ed.* **2010**, 49, 1736.
- [13] L. C. W. Baker, J. S. Figgis, *J. Am. Chem. Soc.* **1970**, 92, 3794.
- [14] B. Dawson, *Acta Crystallogr. B* **1953**, 6, 113.
- [15] L. C. W. Baker, *Plenary Lecture Proc. XV Int. Conf. Coord. Chem.* **1973**, Moscow.
- [16] C. Aubry, G. Chottard, N. Platzer, J. M. Brégeault, R. Thouvenot, F. Chauveau, C. Huet, H. Ledon, *Inorg. Chem.* **1991**, 23, 4409.
- [17] I. V. Kozhevnikov, *Chem. Rev.* **1998**, 98, 171.
- [18] a) Y. Izumi, K. Matsuo, K. Urabe, *J. Mol. Catal.* **1983**, 18, 299; b) Y. Izumi, K. Urabe, M. Onaka, *Zeolite, Clay, and Heteropoly Acid in Organic Reactions*, VCH, Weinheim, New York, 1992.
- [19] a) K. M. Barkigia, L. M. Rajkovic-Blazer, M. T. Pope, E. Prince, C. O. Quicksall, *Inorg. Chem.* **1980**, 19, 2531; b) H. T. Evans, E. Prince, *J. Am. Chem. Soc.* **1983**, 105, 4838; c) M. I. Khan, J. Zubieta, P. Toscano, *Inorg. Chim. Acta* **1992**, 193, 17.
- [20] M. Isobe, F. Marumo, T. Yamase, T. Ikawa, *Acta Crystallogr.* **1978**, B34, 2728.
- [21] a) W. G. Kempler, W. Shum, *J. Am. Chem. Soc.* **1977**, 99, 3544; b) A. T. Harrison, O. W. Howarth, *J. Chem. Soc., Dalton Trans.* **1985**, 1953.
- [22] M. T. Pope, G. M. Varga, *Inorg. Chem.* **1966**, 5, 1249.
- [23] J. J. Altenau, M. T. Pope, R. A. Prados, H. So, *Inorg. Chem.* **1975**, 14, 417.
- [24] M. Kozik, C. F. Hammer, L. C. W. Baker, *J. Am. Chem. Soc.* **1986**, 108, 7627.
- [25] a) P. Souchay, *Ann. Chim., Sér. II* **1943**, 18, 61; b) P. Souchay, *Ann. Chim., Sér. II* **1944**, 19, 102.

- [26] a) R. Massart, *Ann. Chim.* **1969**, *4*, 285; b) G. Hervé, *Ann. Chim.* **1971**, *6*, 219.
- [27] X. López, J. M. Maestre, C. Bo, J.-M. Poblet, *J. Am. Chem. Soc.* **2001**, *123*, 9571.
- [28] J. P. Launay, M. Boyer, F. Chauveau, *J. Inorg. Nucl. Chem.* **1976**, *38*, 243.
- [29] a) D. Gatteschi, B. Tsukerblatt, A. L. Barra, L. C. Brunel, A. Müller, J. Döring, *Inorg. Chem.* **1993**, *32*, 2114; b) A. Müller, W. Plass, E. Krickemeyer, S. Dillinger, H. Bögge, A. Armatage, A. Proust, C. Beugholt, U. Bergmann, *Angew. Chem., Int. Ed. Engl.* **1994**, *33*, 849; c) A. Müller, S. Q. N. Shah, H. Bögge, M. Schmidtman, P. Kögerler, B. Hauptfleisch, S. Leiding, K. Wittler, *Angew. Chem., Int. Ed.* **2000**, *39*, 1614.
- [30] a) Y. Jeannin, J. P. Launay, M. A. Said Sedjadi, *Inorg. Chem.* **1980**, *19*, 2933; b) K. Pieprgrass, M. T. Pope, *J. Am. Chem. Soc.* **1987**, *109*, 1586; c) T. Yamase, E. Ishikawa, *J. Chem. Soc., Dalton Trans.* **1996**, 1619.
- [31] M. H. Dickman, T. Ozeki, H. T. Evans, C. Rong, G. B. Jameson, M. T. Pope, *J. Chem. Soc., Dalton Trans.* **2000**, 149.
- [32] J. Lehmann, A. Gaita-Arino, E. Coronado, D. Loss, *Nature Nanotech.* **2007**, *2*, 312.
- [33] N. Mizuno, K. Yamaguchi, *Chem. Rec.* **2006**, *6*, 12.
- [34] J. Piera, J. E. Bäckvall, *Angew. Chem., Int. Ed.* **2008**, *47*, 3506.
- [35] M. Carraro, A. Sartorel, G. Scorrano, T. Carofiglio, M. Bonchio, *Synthesis* **2008**, 1971.
- [36] Y. V. Geletii, B. Botar, P. Kögerler, D. A. Hilesheim, D. G. Musaev, C. L. Hill, *Angew. Chem., Int. Ed.* **2008**, *47*, 3896.
- [37] a) J. W. Vickers, H. Lv, J. M. Sumliner, G. Zhu, Z. Luo, D. G. Musaev, Y. V. Geletii, C. L. Hill, *J. Am. Chem. Soc.* **2013**, *135*, 14110; b) Q. Yin, J. Tan, C. Besson, Y. Geletii, D. Musaev, A. Kuznetsov, Z. Luo, K. Hardcastle, C. Hill, *Science* **2010**, *328*, 342.
- [38] J. J. Stracke, R. G. Finke, *J. Am. Chem. Soc.* **2011**, *133*, 14872.
- [39] a) S. Goberna-Ferrón, L. Vigarà, J. Soriano-López, J. R. Galán-Mascarós, *Inorg. Chem.* **2012**, *51*, 11707; b) J. Soriano-López, S. Goberna-Ferrón, L. Vigarà, J. J. Carbó, J. M. Poblet, J. R. Galán-Mascarós, *Inorg. Chem.* **2013**, *52*, 4753.
- [40] A. Ogata, H. Yanagie, T. Yamase, M. Eriguchi, *Br. J. Cancer* **2008**, *98*, 399.
- [41] S. Shigeta, S. Mori, T. Yamase, N. Yamamoto, *Biomed. Pharmacother.* **2006**, *60*, 211.
- [42] K. Dan, T. Yamase, *Biomed. Pharmacother.* **2006**, *60*, 169.
- [43] G. E. Sigmon, D. K. Unruh, J. Ling, B. Weaver, M. Ward, L. Pressprich, *Angew. Chem., Int. Ed.* **2009**, *48*, 2737.
- [44] C. Ritchie, G. J. T. Cooper, L. Cronin, Y. F. Song, C. Streb, *Nature Chem.* **2009**, *1*, 47.
- [45] H. Taketa, S. Katsuki, K. Eguchi, T. Seiyama, N. Yamazoe, *J. Phys. Chem.* **1986**, *90*, 2959.

- [46] a) F. Ritschl, R. Fricke, *J. Chem. Soc., Faraday Trans. 1* **1987**, 83, 1041; b) G. Scholz, R. Luck, R. Stosser, H. J. Lunk, F. Ritschl, *J. Chem. Soc., Faraday Trans.* **1991**, 87, 717.
- [47] J. Y. Kempf, M.-M. Rohmer, J. M. Poblet, C. Bo, M. Bénard, *J. Am. Chem. Soc* **1992**, 114, 1136.
- [48] M. M. Rohmer, M. Bénard, *J. Am. Chem. Soc* **1994**, 116, 6959.
- [49] J. P. Biauudeau, M.-M. Rohmer, M. Bénard, N. E. Ghermani, *C. R. Chimie* **1998**, 1, 319.
- [50] J. M. Poblet, X. López, C. Bo, *Chem. Soc. Rev.* **2003**, 32, 297.
- [51] a) J. Andzelm, C. Kölmel, A. Klamt, *J. Chem. Phys.* **1995**, 103, 9312; b) A. Klamt, *J. Chem. Phys.* **1995**, 102-103, 2224; c) A. Klamt, G. Schüürmann, *J. Chem. Soc., Perkin Trans. 2* **1993**, 799; d) C. C. Pye, T. Ziegler, *Theor. Chem. Acc.* **1999**, 101, 396.
- [52] S. Miertus, E. Scrocco, J. Tomasi, *Chem. Phys.* **1981**, 55, 117.
- [53] A. V. Marenich, C. J. Cramer, D. G. Truhlar, *J. Phys. Chem. B* **2009**, 113, 6378.
- [54] M. Pascual-Borràs, X. López, A. Rodríguez-Forteza, R. J. Errington, J. M. Poblet, *Chem. Sci.* **2014**, 5, 2031.
- [55] X. Lopez, C. Bo, J. M. Poblet, J. J. Carbó, P. Miró, *Theor. Chem. Acc.* **2011**, 128, 393.
- [56] F. Leroy, C. Bo, J. M. Poblet, P. Miró, J. B. Bonet-Ávalos, *J. Phys. Chem. B.* **2008**, 112, 8591.
- [57] J. M. Maestre, X. López, C. Bo, J. M. Poblet, N. Casañ-Pastor, *J. Am. Chem. Soc.* **2001**, 123, 3749.
- [58] F. Q. Zhang, X. M. Zhang, H. S. Wu, H. Jiao, *J. Phys. Chem. A* **2007**, 111, 159.
- [59] F. Q. Zhang, W. Guan, Y. T. Zhang, M. T. Xu, J. Li, Z. M. Su, *Inorg. Chem.* **2010**, 49, 5472.
- [60] Gaussian 09, Revision A.02, M. J. Frisch, G. W. Trucks, H. B. Schlegel, G. E. Scuseria, M. A. Robb, J. R. Cheeseman, G. Scalmani, V. Barone, B. Mennucci, G. A. Petersson, H. Nakatsuji, M. Caricato, X. Li, H. P. Hratchian, A. F. Izmaylov, J. Bloino, G. Zheng, J. L. Sonnenberg, M. Hada, M. Ehara, K. Toyota, R. Fukuda, J. Hasegawa, M. Ishida, T. Nakajima, Y. Honda, O. Kitao, H. Nakai, T. Vreven, J. Montgomery, J. A., J. E. Peralta, F. Ogliaro, M. Bearpark, J. J. Heyd, E. Brothers, K. N. Kudin, V. N. Staroverov, R. Kobayashi, J. Normand, K. Raghavachari, A. Rendell, J. C. Burant, S. S. Iyengar, J. Tomasi, M. Cossi, N. Rega, N. J. Millam, M. Klene, J. E. Knox, J. B. Cross, V. Bakken, C. Adamo, J. Jaramillo, R. Gomperts, R. E. Stratmann, O. Yazyev, A. J. Austin, R. Cammi, C. Pomelli, J. W. Ochterski, R. L. Martin, K. Morokuma, V. G. Zakrzewski, G. A. Voth, P. Salvador, J. J. Dannenberg, S. Dapprich, A. D. Daniels, Ö. Farkas, J. B. Foresman, J. V. Ortiz, J. Cioslowski, D. J. Fox, Gaussian, Inc., Wallingford CT, 2009.
- [61] a) G. te Velde, F. M. Bickelhaupt, E. J. Baerends, C. Fonseca Guerra, S. J. A. van Gisbergen, J. G. Snijders, T. Ziegler, *J. Comput. Chem.* **2001**, 22, 931; b) C. Fonseca Guerra, J. G. Snijders, G. te Velde, E. J. Baerends, *Theor. Chem. Acc.* **1998**, 99, 391;

- c) ADF2011.01, SCM, Vrije Universiteit, Amsterdam, The Netherlands, <http://www.scm.com>, 2011.
- [62] a) E. van Lenthe, E. J. Baerends, J. G. Snijders, *J. Chem. Phys.* **1993**, *99*, 4597; b) E. van Lenthe, E. J. Baerends, J. G. Snijders, *J. Chem. Phys.* **1994**, *101*, 9783; c) E. van Lenthe, A. E. Ehlers, E. J. Baerends, *J. Chem. Phys.* **1999**, *110*, 8943; d) E. van Lenthe, R. van Leeuwen, E. J. Baerends, J. G. Snijders, *Int. J. Quantum Chem.* **1996**, *57*, 281.
- [63] TURBOMOLE V6.5 2013, a development by the University of Karlsruhe and Forschungszentrum Karlsruhe GmbH, 1989-2007, TURBOMOLE GmbH, since 2007; available from <http://www.turbomole.com>, 2013.
- [64] X. López, P. Miró, J. J. Carbó, A. Rodríguez-Fortea, C. Bo, J. M. Poblet, *Theor. Chem. Acc.* **2011**, *128*, 393.
- [65] a) A. Lewis, J. A. Bumpus, D. G. Truhlar, C. J. Cramer, *J. Chem. Educ.* **2004**, *81*, 596; b) A. Lewis, J. A. Bumpus, D. G. Truhlar, C. J. Cramer, *J. Chem. Educ.* **2007**, *84*, 934.
- [66] X. López, J. A. Fernández, J. M. Poblet, *Dalton Trans.* **2006**, 1162.
- [67] X. López, J. A. Fernández, S. Romo, J. F. Paul, L. Kazansky, J. M. Poblet, *J. Comput. Chem.* **2004**, *25*, 1542.

Chapter 2

Ability of DFT Calculations to Describe Redox Potentials and Electron (De)Localization

In this chapter, we aim to study how DFT calculations can describe redox potentials and electron (de)localization in different Wells-Dawson polyoxotungstates. We performed DFT calculations on fully oxidized $[\text{P}_2\text{W}_{18}\text{O}_{62}]^{6-}$ and $\alpha_1/\alpha_2\text{-}[\text{P}_2\text{MW}_{17}\text{O}_{62}]^{2-}$ ($M = \text{V}, \text{Mo}$) anions, and their one-electron reduced partners.

Related publication:

P. A. Aparicio, X. López, J. M. Poblet, *J. Mol. Eng. Mater.* **2014**, *2*, 1440004.

2.1 Introduction and objectives

Many interesting properties of polyoxometalates are related to their ability to reversibly accept and release electrons. The correct computational description of metal electrons in POMs is central to fully understand the implications and mechanisms related to reduced structures. Computational studies of molecules of the *nano* size like POMs^[1] are becoming of increasing relevance as the research focus moves toward larger systems. The success of computational methods describing physicochemical properties of compounds of any nature is nowadays well known. In this framework, DFT plays an important role since it is the only computational method capable of tackling, at a reasonable cost, challenging electronic properties of medium to large molecular systems containing many transition metal atoms. Different computational approaches have been applied to the POM family, although DFT has been massively utilized to study electronic and magnetic properties of POMs, as well as reaction mechanisms or redox processes, among others^[1b]. However, still some fundamental features are difficult to describe correctly at the DFT level, namely, the (de)localization of d metal electrons in some POMs. This subject has implications in the understanding of redox properties^[2], redox-mediated reactions and magnetic properties, for example.

Many classical POM structures with d valence metal electrons have been correctly described with standard DFT methods^[3]. However, others can be problematic due to their more intricate electronic properties. A representative example of this issue can be found in metal-substituted Wells–Dawson (WD) anions with formula α_1 or α_2 -[P₂MW₁₇O₆₂]ⁿ⁻, the nomenclature α_1 and α_2 designating the M center placed at the belt or at the cap region, respectively. Compounds of mixed-metal nature have shown an improvement in their catalytic activity with respect to the non-substituted ones^[4]. In the fully oxidized [P₂W₁₈O₆₂]⁶⁻ structure (P₂W₁₈ in short) all the W centers are in the oxidation state VI, and the lowest unoccupied orbitals are W-like in nature. The first three of these orbitals correspond to atoms located in the belt regions and the next two empty orbitals to W atoms in cap regions^[5]. If we use the ideal maximal D_{3h} symmetry of the P₂W₁₈ anion, the structure and molecular orbital energies can be represented as in Figure 2.1. The replacement of one W atom by another metal to give the P₂MW₁₇O₆₂ structure changes the electronic properties of the Wells-Dawson compounds and decreases the molecular

symmetry to C_1 (α_1 isomer) or C_s (α_2 isomer). In some cases, the first extra electron can be localized in the substituted metal atom (M), as is the case of the one-electron reduced P_2MoW_{17} species, independently of its position (cap or belt). In the case of V compounds, we observe the same electrochemical behavior. In this chapter, we focus the calculations on two main issues: (i) obtaining the best estimates for the reduction energies (REs) of the different compounds and, linked to this, (ii) describing correctly the (de)localization of the extra electron.

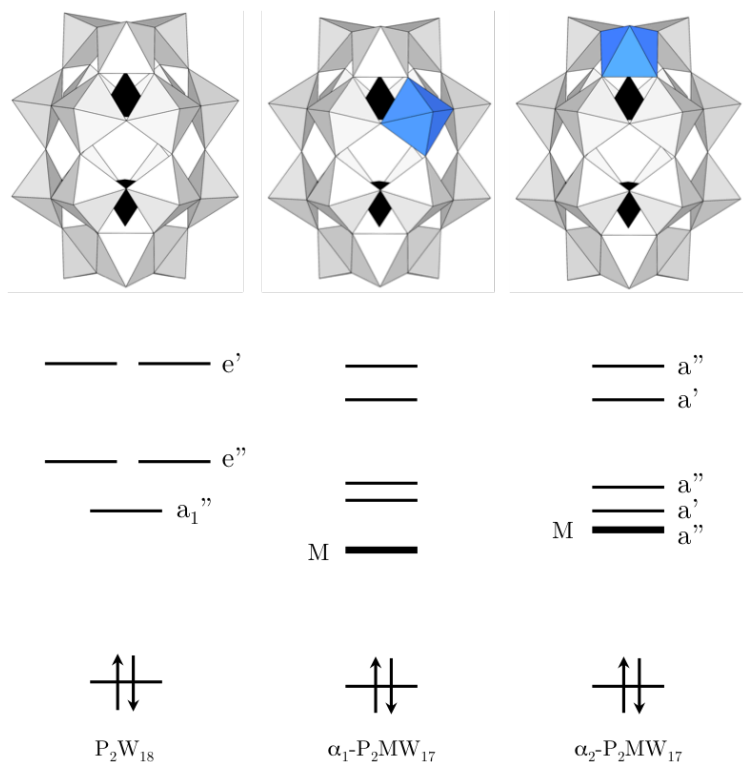


Figure 2.1. Highest occupied and lowest unoccupied molecular orbitals of the fully oxidized P_2W_{18} and α_1/α_2 - P_2MW_{17} ($M = Mo$ and V) anions, represented with substituted positions in blue. Thicker lines correspond to a predominant M character. Symmetry labels are shown except for the α_1 isomer, where all orbitals are of type a.

2.2 Results and discussion

For mixed-metal P_2MW_{17} compounds, experimental evidences show (structural determinations, electron spin resonance, etc.) that after the first one-electron reduction the oxidation states of Mo(VI) or V(V) decrease^[6], in line with the

well-known higher electronegativity of V^V and Mo^{VI} with respect to W^{VI}. This also implies that the half-wave potentials ($E_{1/2}$) for their respective first redox processes are more positive for P₂MW₁₇ (M = Mo, V) than for P₂W₁₈ (Table 2.1).

Consequently, the frontier orbital region of the original P₂W₁₈ structure changes upon metal replacement, notably the lowest unoccupied orbitals. The LUMO belongs to the substituting metal atom, whereas the orbitals related to W lie higher in energy as shown in Figure 2.1, a fact also demonstrated by means of Extended-Hückel calculations^[5a]. However, the lowest unoccupied orbitals belonging to M and W are quite close in energy and, especially for the α_2 isomer, their exact ordering may be difficult to reproduce by DFT. The worst case occurs when the extra electron (from reduction) delocalizes over the W sites instead of being localized in M, in contradiction with experimental evidence, with the associated wrong description of electronic properties. This is the case of the one-electron reduced form of α_2 -P₂MoW₁₇. Our goal is to study the mentioned α_1 and α_2 -P₂MW₁₇ structures with several GGA and hybrid density functionals in order to find which methodology correctly describes the reduction potentials and electron (de)localization in the reduced structures, with special emphasis on the problematic α_2 -P₂MoW₁₇ case.

Table 2.1. Half-wave potentials $E_{1/2}$ (V *vs.* SCE) for [P₂W₁₈O₆₂]⁶⁻ and α_1/α_2 -[P₂MW₁₇O₆₂]⁶⁻ derivatives and their difference $\Delta E_{1/2}$ (V *vs.* SCE).

	$E_{1/2}$		$\Delta E_{1/2}$	Ref.
	α_1	α_2		
P ₂ W ₁₈	+0.04		-	[6]
P ₂ VW ₁₇	+0.48	+0.39	0.090	[7]
P ₂ MoW ₁₇	+0.39	+0.23	0.160	[6]

2.2.1 Atomic spin populations

We computed the one-electron reduced states of α_1/α_2 -P₂MW₁₇ (M = Mo, V) anions with different density functionals and analyzed which of these can describe the electron (de)localization pattern correctly. We should expect that the atomic spin populations of V and Mo in the reduced α_1/α_2 -P₂MW₁₇ compounds are close to 0.8–1.0, depending on the functional chosen and the metal. The spin population values in Table 2.2 for BP86 (~0.7) and

B3LYP/M05 (~ 1.0) functionals show that, when it comes to describe the P_2VW_{17} compound, both GGA and hybrid functionals are capable of placing the extra electron in the V atom irrespective of the isomer. This is a consequence of the highly oxidant nature of V^V in front of W^{VI} . The numerical difference in the average spin populations per V atom depending on the functional (pure or hybrid) is as expected, since each of these have a different tendency to polarize the electron density towards the oxygen ligands. Hybrid functionals delocalize less the electrons compared with pure functionals.

When V is placed in the cap (α_2 - P_2MW_{17}), more competition between V and W for the incoming electron might be expected because the cap position is in disadvantage *vs.* the belt-tungstens region (see the molecular orbital scheme in Figure 2.1). Despite that, the polar vanadium atom traps the electron. The functionals tested for the $M = V$ case, standards for the pure and hybrid families, behave similarly and, therefore, it is not necessary to test other functionals since we expect the same behavior. If the replacing atom is Mo^{VI} , a proper description of electron localization turns problematic because it is less oxidant than V^V . The first unoccupied Mo-like orbital is rather close in energy to the low-lying belt-tungsten orbitals and competition for the incoming electron occurs. The spin populations on Mo and W in Table 2.2 reveal that, essentially, the pure density functionals (the tested BP86 and PBE) fail to reproduce the observed electron localization in the molybdotungstate compound studied. The disagreement with experiments is severe for the α_2 - P_2MoW_{17} isomer. Such computational problem, observed with some functionals and based in their mathematical formulation, consists in assigning too low energies to the more delocalized molecular orbitals compared with relatively localized ones of similar energy, which are unrealistically placed as more unstable.

Table 2.2. Mulliken Spin Populations on M atoms in α_1 and α_2 -P₂MW₁₇ anions.

	Functional	%HFX	α_1	α_2
M = V	BP86	0	0.692	0.771
	B3LYP	20	1.051	1.064
	M05	28	0.953	0.964
M = Mo	BP86	0	0.433	0.060
	PBE	0	0.442	0.068
	B3LYP	20	0.776	0.824
	PBE0	25	0.780	0.043
	M05	28	0.763	0.794
	LC- ω PBE	<i>varying</i>	0.012	0.064

The results listed in Table 2.2 has served as a filter to consider, in the following, only the functionals herein tested that perform well in the description of the localization of an extra electron in mixed-metal WD anions, namely B3LYP and M05. The general conclusion is that hybrid functionals perform better, in general, than GGA ones. The exceptions are LC- ω PBE and PBE0, which in the present study failed to place the metal electron on Mo at least in one isomer.

A molecular orbital analysis was done in order to elucidate the electronic structure of the reduced species when the wrong and right results are obtained. Figure 2.2 shows the singly occupied molecular orbital of the reduced form α_2 -[P₂MoW₁₇O₆₂]⁷⁻ obtained with the BP86 functional (left), where the electron appears to be delocalized over a part of the belt-tungstens predominantly even if the Mo atom is in the cap region of the molecule. On the other hand, with the B3LYP and M05 hybrid functionals (right) the electron is correctly localized in the cap-Mo atom. The same analysis was performed for the α_1 and α_2 -[P₂VW₁₇O₆₂]⁷⁻ anions and we observed that both GGA and hybrid functionals are able to localize the extra electron in the right site. The V orbitals are lower in energy than the Mo ones, so the electron goes inevitably to the right orbital, inline with the data from Table 2.2.

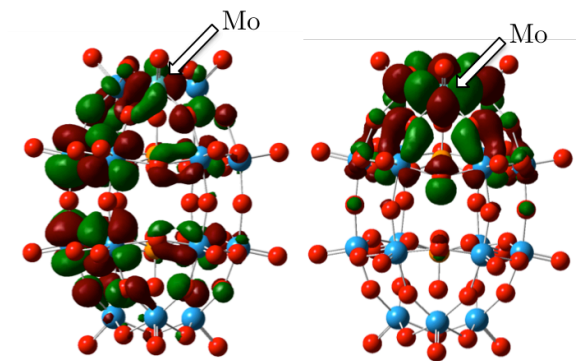


Figure 2.2. Singly occupied molecular orbital for the reduced α_2 - P_2MoW_{17} anion, with BP86 (left) and B3LYP (right) functionals.

2.2.2 Reduction energies

The REs for the P_2W_{18} and α_1/α_2 - P_2MW_{17} anions obtained with the B3LYP and M05 functionals are listed in Table 2.3, along with the experimental values obtained from the reduction free energy of the SCE electrode (-4.524 eV)^[8]. In this section we put the emphasis on accurately computing the *relative* oxidizing power of α_1/α_2 - P_2MW_{17} anions, and relative to $[P_2W_{18}O_{62}]^{6-}$. The error in the computed absolute REs with respect to the experimental ones is discussed afterwards.

The computed REs show large negative values, in agreement with the low-lying unoccupied orbitals of most POMs in solution despite their molecular negative charge. Besides that, our calculations reproduce the fact that the mixed-metal WD anions with Mo and V feature more negative REs than P_2W_{18} , a fact that from the electrochemical side consists in more positive reduction potentials for the P_2MW_{17} systems.

Comparison of the B3LYP and the experimental Δ REs (rightmost column of Table 2.3) shows an excellent agreement, with differences between isomers of the same order. For P_2VW_{17} , the computed Δ RE is 0.089 eV at the B3LYP level, which is in excellent agreement with the experiment ($\Delta E_{1/2} = 0.090$ V). Taking P_2MoW_{17} , we also observe a good match between B3LYP and experiment, with Δ RE = 0.145 and 0.160 eV, respectively. The M05 functional, on the other hand, performs poorly despite its good behavior in what concerns the atomic spin populations. It does not reproduce the correct order in oxidizing power for α_1/α_2 - P_2VW_{17} . In addition, it overestimates the Δ RE in the molybdate derivative up to 0.241 eV.

Table 2.3. Experimental (Exp.) and computed reduction energies (RE) and their difference (Δ RE) in eV.

		RE		
P ₂ W ₁₈	Exp. ^a	-4.564		
	B3LYP	-4.234		
	M05	-4.124		
		α_1	α_2	Δ RE
P ₂ VW ₁₇	Exp. ^a	-5.004	-4.914	0.090
	B3LYP	-4.673	-4.576	0.097
	M05	-4.232	-4.259	-0.026
P ₂ MoW ₁₇	Exp. ^a	-4.914	-4.754	0.160
	B3LYP	-4.594	-4.426	0.168
	M05	-4.396	-4.156	0.241

^a Experimental values obtained taking -4.524 eV as the reduction energy of the SCE electrode (see Ref. [8-9]).

The comparison of the computed absolute REs (respectively half-wave potentials, $E_{1/2}$) between the three anions is also important since it determines how chemical changes are tracked by DFT. The experimental gaps in $E_{1/2}$ between P₂W₁₈ and the mixed-metal systems are large: 0.19–0.35 V with P₂MoW₁₇ and 0.35–0.44 V with P₂VW₁₇ (Table 2.1). Our present B3LYP calculations are fully satisfactory in that point as they were for the Δ REs between isomers of the same compound. As pictorially represented in Figure 2.3, the B3LYP functional is perfectly capable of discerning the metal-substituted compounds from the single-addenda P₂W₁₈ anion. Furthermore, the relative REs for the P₂MW₁₇ systems are placed at the correct energies, something that does not occur with the M05 functional.

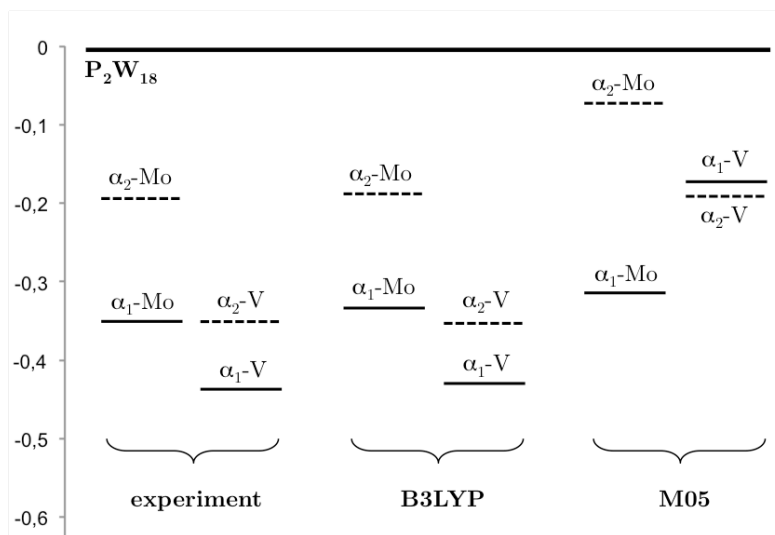


Figure 2.3. Graphical view of the REs computed with the B3LYP and M05 functionals for the single and mixed metal compounds, taking the RE of P_2W_{18} as zero. The vertical scale is in eV.

2.2.3 Calculation of the RE for P_2W_{18}

The appropriate use of molecular symmetry is fundamental for the correct calculation of REs. In the field of POMs this point is particularly determinant since they often present high symmetries. From the computational view, one has to be aware of the available point groups within Quantum Chemistry programs. Some of these codes are not designed to apply the full point group symmetries in all cases. Instead, a subgroup is applied for reasons of internal use of Group Theory. In such cases, some calculations may result in modestly accurate or unrealistic properties.

Electron delocalization in POMs is a very relevant property with energetic implications. Not using the full symmetry may entail an artificial electron localization that rises up the energy by a significant amount. The mono-substituted P_2MW_{17} compounds, with C_1 (α_1 isomer) and C_s (α_2 isomer), are computed with their full point group symmetry and thus their reduction energies are formally correct. On the other hand, care must be taken with P_2W_{18} , with ideal D_{3h} symmetry. Using two programs that make a different use of symmetry we estimated that the energy difference between a correct electron-delocalized solution (the 12 belt-W atoms sharing the unpaired electron under the D_{3h} symmetry; Figure 2.4, left) and a partially localized one (electron shared by four belt-W atoms only under the C_{2v} symmetry; Figure 2.4, right) can be around 265 meV. In other words, this is the energy

stabilization upon increasing the delocalization from 4 to 12 W atoms. In other POM structures, with a different number of equivalent metal atoms, this energy value associated to electron delocalization can change. We want to stress that the values discussed in Table 2.3 are based on the right (de)localized solutions.

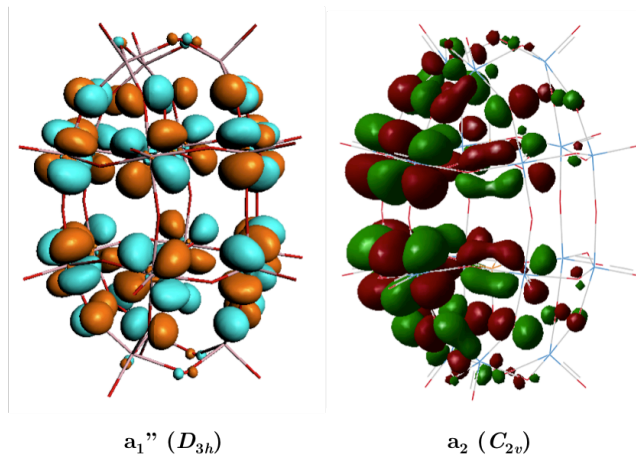


Figure 2.4. Singly occupied molecular orbital for the one-electron reduced P_2W_{18} anion obtained with the maximal symmetries assigned with two Quantum Chemistry programs: ADF full D_{3h} (right) and Gaussian C_{2v} (left) point groups.

2.3 Conclusions

DFT is the most widely used computational method to describe the electronic structure of polyoxometalates due to its relatively accurate results at moderate cost. Despite that, it is well known that the BP86 functional and other GGA-type ones tend to over-delocalize the electron density. This fact can become critical in some reduced polyoxometalates, such as the monoreduced α_2 - $[P_2MoW_{17}O_{62}]^{7-}$, for which GGA functionals put a delocalized electron over the belt tungstens instead of correctly localizing it in the cap-Mo. This fact entails that the computed reduction energies are far from reproducing the experimental data. To fix this issue, we tested a family of density functionals on one-electron reduced Wells-Dawson derivatives, namely BP86, B3LYP, PBE, PBE0, LC- ω PBE and M05. We found that the B3LYP hybrid functional (20% exact exchange) gives the best results in comparison to the electrochemical data, giving electron-localized solutions when expected, even in clusters containing different sites or regions with similar electron affinity. In our opinion, the fact that it also reproduces the difference in reduction

potentials between the α_1 and α_2 isomers of $[\text{P}_2\text{MoW}_{17}\text{O}_{62}]^{7-}$ is associated to the correct electron localization. If a larger percentage of exact exchange is added to the functional (25–28%), the electron-localized solution is reinforced as expected, but the reduction energies of the two isomers are less accurate. The analysis of the reduction energies of α_1 and α_2 - $[\text{P}_2\text{MW}_{17}\text{O}_{62}]^{7-}$ with $M = \text{Mo}, \text{V}$ or W could, a priori, be generalized to any compound of this family, thus concluding that the best functional for the computation of redox properties of POM compounds is, at present, B3LYP.

One last point that deserves comment is the *absolute* deviation that the computed REs present with respect to the reduction free energies obtained from the measured potentials (Table 2.3). It is evident that the reduction processes obtained with DFT are somewhat less exothermic than they should, being shifted by +0.330 eV on average with B3LYP. This is a general feature of DFT calculations applied to reduction of POMs. The origin of such discrepancies may arise from the *oversimplified* description of the real environment of the molecules, namely an approximate consideration of the effects of the solvent, counterions and ion pairing, and also not including the entropic term of the free energy that, in some cases, might be notable. In spite of the considerable absolute error in the REs, the *relative* values within this family are very well described with B3LYP since the five compounds present very similar errors ranging from 0.327 to 0.342 eV. This amount of energy represents less than ~8% of the total REs computed.

Atomic spin populations of the reduced forms reveal that pure GGA functionals, which over-delocalize the electron density by nature, cannot correctly describe the extra electron especially when competition between the localized and delocalized situations is very close in energy, namely for α_2 - $[\text{P}_2\text{MoW}_{17}\text{O}_{62}]^{7-}$. On the other hand, hybrid functionals like B3LYP or M05 can localize the electron at the correct site. Within these *well-behaved* density functionals, only B3LYP gives the correct ordering and relative reduction energies with respect to electrochemical measurements, although the absolute values are always less exothermic than expected. At present, this is the best density functional for computing redox properties of POMs.

2.4 Computational details

DFT calculations have been carried out using the Gaussian 09 suite of programs^[10] for the main results. The geometries of all the structures were fully

optimized in both the oxidized and reduced states for the sake of accuracy. We applied the pure GGA-type functionals BP86^[11], PBE^[12], and the hybrid B3LYP^[13], PBE0^[14], LC- ω PBE^[15] and the meta-hybrid M05 functional^[16]. The main difference between both sets is that, in the latter, a certain amount of exact Hartree-Fock exchange (HFx) is introduced to the electron exchange part of the density functional with the aim of somehow improving their performance. The basis sets are of double- ζ type supplemented by polarization functions: 6-31G(d,p) for O atoms and Hay-Wadt with LANL pseudopotentials for P, V, Mo and W atoms. The calculations include PCM^[17] to account for the solvent effects of water ($\epsilon = 78.4$) to stabilize highly charged anions and, more importantly, to give unbiased reduction energies. Not including the solvent effects in both the oxidized and reduced forms would unrealistically over-stabilize the former^[5b]. The solute cavity was created using a scaled Van der Waals surface and a grid of 5 points per \AA^2 . The atomic radii correspond to the Universal Force Field parameters. We applied the spin-unrestricted formalism to electronically open-shell molecules. Atomic spin densities were obtained by means of the Mulliken formula.

The discussion about the use of symmetry is aided by calculations performed with the ADF2011 program^[18]. The electrons are described by Slater-type functionals of TZP quality with the frozen core approximation for the internal shells of atoms (1s for O, 1s-2p for P, 1s-4f for W). We applied scalar relativistic corrections to the core electrons by means of ZORA^[19] with the core potentials generated using the DIRAC program. We applied the spin-unrestricted formalism to open shell species. We included COSMO^[20] to account for solvent effects of water. The solvent cavity surrounding the anions was created using the solvent-excluding method with fine tesserae. The ionic radii chosen for the atoms located in the metal oxide cage of the systems herein studied, and that actually define the size of the solvent cavity due to their peripheral positions, are the following: 1.26 \AA (W), 1.85 \AA (P) and 1.52 \AA (O).

2.5 References

- [1] a) D.-L. Long, R. Tsunashima, L. Cronin, *Angew. Chem. Int. Ed.* **2010**, *49*, 1736; b) X. López, P. Miró, J. J. Carbó, A. Rodríguez-Forteza, C. Bo, J. M. Poblet, *Theor. Chem. Acc.* **2011**, *128*, 393; c) X. López, J. J. Carbó, C. Bo, J. M. Poblet, *Chem. Soc. Rev.* **2012**, *41*, 7537.
- [2] D. E. Katsoulis, *Chem. Rev.* **1998**, *98*, 359.
- [3] P. A. Aparicio, J. M. Poblet, X. López, *Eur. J. Inorg. Chem.* **2013**, *2013*, 1910.
- [4] a) O. A. Kholdeeva, G. M. Maksimov, R. I. Maksimovskaya, L. A. Kovaleva, M. A. Fedotov, V. A. Grigoriev, C. L. Hill, *Inorg. Chem.* **2000**, *39*, 3828; b) C. Tourné, G. Tourné, *Bull. Soc. Chim. Fr.* **1969**, 1124; c) D. C. Duncan, R. C. Chambers, E. Hecht, C. L. Hill, *J. Am. Chem. Soc.* **1995**, *117*, 681; d) F. Cavani, M. Koutyrev, F. Trifirò, *Catal. Today* **1996**, *28*, 319; e) V. Kogan, Z. Aizenshtat, R. Neumann, *Angew. Chem., Int. Ed.* **1999**, *38*, 3331; f) A. Bagno, M. Bonchio, A. Sartorel, G. Scorrano, *Eur. J. Inorg. Chem.* **2000**, *2000*, 17; g) H. Zeng, G. R. Newkome, C. L. Hill, *Angew. Chem., Int. Ed.* **2000**, *39*, 1771; h) A. M. Khenkin, L. J. Shimon, R. Neumann, *Eur. J. Inorg. Chem.* **2001**, *2001*, 789; i) Y. Nishiyama, Y. Nakagawa, N. Mizuno, *Angew. Chem. Int. Ed.* **2001**, *40*, 3639.
- [5] a) B. Keita, B. Levy, L. Nadjo, R. Contant, *New. J. Chem.* **2002**, *26*, 1314; b) X. López, C. Bo, J. M. Poblet, *J. Am. Chem. Soc.* **2002**, *124*, 12574.
- [6] a) M. Abbessi, R. Contant, R. Thouvenot, G. Hervé, *Inorg. Chem.* **1991**, *30*, 1695; b) J. P. Ciabrini, R. Contant, J. M. Fruchart, *Polyhedron* **1983**, *2*, 1229; c) B. Keita, Y. W. Lu, L. Nadjo, R. Contant, M. Abbessi, J. Canny, M. Richet, *J. Electroanal. Chem.* **1999**, *477*, 146.
- [7] S. P. Harmalker, M. A. Leparulo, M. T. Pope, *J. Am. Chem. Soc.* **1983**, *105*, 4286.
- [8] A. Lewis, J. A. Bumpus, D. G. Truhlar, C. J. Cramer, *J. Chem. Educ.* **2007**, *84*, 934.
- [9] A. Lewis, J. A. Bumpus, D. G. Truhlar, C. J. Cramer, *J. Chem. Educ.* **2004**, *81*, 596.
- [10] Gaussian 09, Revision A.02, M. J. Frisch, G. W. Trucks, H. B. Schlegel, G. E. Scuseria, M. A. Robb, J. R. Cheeseman, G. Scalmani, V. Barone, B. Mennucci, G. A. Petersson, H. Nakatsuji, M. Caricato, X. Li, H. P. Hratchian, A. F. Izmaylov, J. Bloino, G. Zheng, J. L. Sonnenberg, M. Hada, M. Ehara, K. Toyota, R. Fukuda, J. Hasegawa, M. Ishida, T. Nakajima, Y. Honda, O. Kitao, H. Nakai, T. Vreven, J. Montgomery, J. A., J. E. Peralta, F. Ogliaro, M. Bearpark, J. J. Heyd, E. Brothers, K. N. Kudin, V. N. Staroverov, R. Kobayashi, J. Normand, K. Raghavachari, A. Rendell, J. C. Burant, S. S. Iyengar, J. Tomasi, M. Cossi, N. Rega, N. J. Millam, M. Klene, J. E. Knox, J. B. Cross, V. Bakken, C. Adamo, J. Jaramillo, R. Gomperts, R. E. Stratmann, O. Yazyev, A. J. Austin, R. Cammi, C. Pomelli, J. W. Ochterski, R. L. Martin, K. Morokuma, V. G. Zakrzewski, G. A. Voth, P. Salvador, J. J. Dannenberg, S. Dapprich, A. D. Daniels, Ö. Farkas, J. B. Foresman, J. V. Ortiz, J. Cioslowski, D. J. Fox, Gaussian, Inc., Wallingford CT, 2009.
- [11] a) A. D. Becke, *Phys. Rev. A* **1988**, *38*, 3098; b) J. P. Perdew, *Phys. Rev. B* **1986**, *34*, 7406; c) S. H. Vosko, L. Wilk, M. Nusair, *Can. J. Phys.* **1980**, *58*, 1200.

- [12] a) J. P. Perdew, K. Burke, M. Ernzerhof, *Phys. Rev. Lett.* **1996**, 77, 3865; b) J. P. Perdew, K. Burke, M. Ernzerhof, *Phys. Rev. Lett.* **1996**, 78, 1396.
- [13] a) C. T. Lee, W. T. Yang, R. G. Parr, *Phys. Rev. B* **1988**, 37, 785; b) P. J. Stephens, F. J. Devlin, C. F. Chabalowski, M. J. Frisch, *J. Phys. Chem.* **1994**, 98, 11623.
- [14] C. Adamo, V. Barone, *J. Chem. Phys.* **1999**, 110, 6158.
- [15] a) O. A. Vydrov, J. Heyd, A. Krukau, G. E. Scuseria, *J. Chem. Phys.* **2006**, 125, 074106; b) O. A. Vydrov, G. E. Scuseria, *J. Chem. Phys.* **2006**, 125, 234109; c) O. A. Vydrov, G. E. Scuseria, J. P. Perdew, *J. Chem. Phys.* **2007**, 126, 154109.
- [16] Y. Zhao, N. E. Schultz, D. G. Truhlar, *J. Chem. Phys.* **2005**, 123, 161103.
- [17] S. Miertus, E. Scrocco, J. Tomasi, *Chem. Phys.* **1981**, 55, 117.
- [18] ADF2011.01, SCM, Vrije Universiteit, Amsterdam, The Netherlands, <http://www.scm.com>, 2011.
- [19] a) E. van Lenthe, E. J. Baerends, J. G. Snijders, *J. Chem. Phys.* **1993**, 99, 4597; b) E. van Lenthe, E. J. Baerends, J. G. Snijders, *J. Chem. Phys.* **1994**, 101, 9783; c) E. van Lenthe, A. E. Ehlers, E. J. Baerends, *J. Chem. Phys.* **1999**, 110, 8943; d) E. van Lenthe, R. van Leeuwen, E. J. Baerends, J. G. Snijders, *Int. J. Quantum Chem.* **1996**, 57, 281.
- [20] a) J. Andzelm, C. Kölmel, A. Klamt, *J. Chem. Phys.* **1995**, 103, 9312; b) A. Klamt, *J. Chem. Phys.* **1995**, 102-103, 2224; c) A. Klamt, G. Schüürmann, *J. Chem. Soc., Perkin Trans. 2* **1993**, 799; d) C. C. Pye, T. Ziegler, *Theor. Chem. Acc.* **1999**, 101, 396.

Chapter 3

Tungsten Redox Waves in Keggin Compounds: Effect of Localized *versus* Delocalized Charges

In this chapter, we study theoretically the electrochemistry of a set of $[\alpha\text{-XMW}_{11}\text{O}_{40}]^n$ Keggin derivatives ($X = \text{P, Si, Al}$ and $M = \text{W, Mo, V, Nb, Ti}$). The redox W waves in these compounds can be modified upon changes in their negative charge. Three cases will be analyzed: internal charge effect, external localized charge effect and external delocalized charge effect.

Related publication:

P. A. Aparicio, J. M. Poblet, X. López, *Eur. J. Inorg. Chem.* **2013**, 1910.

3.1 Introduction and objectives

In a previous work, it has been reported a generalization of the *anion charge effect*^[1], a concept originally introduced by M. T. Pope^[2]. This empirical rule relates the shift towards negative/positive potentials of reduction-oxidation waves as we increase/decrease the total negative charge of a family of isostructural $[\alpha\text{-XW}_{12}\text{O}_{40}]^{n-}$ Keggin anions (Figure 3.1a). A slope of -0.180 V per negative unit charge was found^[2-3] and that finding was restricted to variations in the internal atom, or *heteroatom*, of the molecule ($X = \text{P}^{\text{V}}$, Si^{IV} , Al^{III} , etc). Also, it was recently shown that heteroatoms of the same group of the periodic table could moderately change the reduction potentials of Keggin anions despite carrying the same charge^[4]. However, other ways to change the charge of Keggin anions are commonplace, such as previous reduction processes or chemical changes in the external positions of the $\text{W}_{12}\text{O}_{36}$ cage, also leading to variations in their capacity to gain electrons. In the present chapter the oxidizing power will be analyzed, computed as reduction energies, for a family of differently charged $[\alpha\text{-XMW}_{11}\text{O}_{40}]^{n-}$ Keggin derivatives ($X = \text{P}^{\text{V}}$, Si^{IV} , Al^{III} and $M = \text{W}^{\text{VI}}$, Mo^{VI} , V^{V} , Nb^{V} , Ti^{IV}).

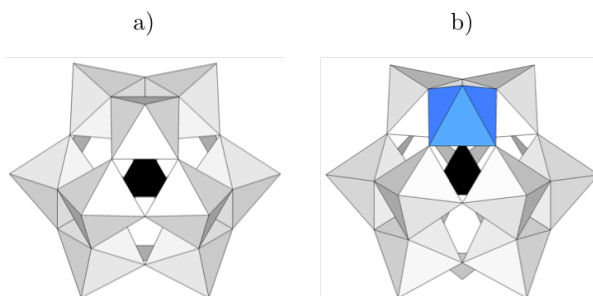


Figure 3.1. Polyhedral representation of a) the $[\alpha\text{-XW}_{12}\text{O}_{40}]^{n-}$ Keggin anion showing the twelve equivalent octahedra, WO_6 . The peripheral, or addenda, W metals can be replaced by other metals (indicated as a blue octahedron), such as Mo^{VI} , V^{V} , Nb^{V} or Ti^{IV} , among many others, to give b) $[\alpha\text{-XMW}_{11}\text{O}_{40}]^{n-}$. Black tetrahedra represent the internal XO_4^{n-} group ($X = \text{P}^{\text{V}}$, Si^{IV} , Al^{III}).

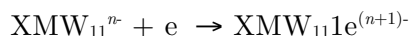
With a simple electrostatic model, a link between the electrostatic potential of a sphere of radius r , $ne/\epsilon r$ (where n is the molecular charge, e is the unit charge and ϵ is the dielectric constant of the solution), and its electron affinity, the difference in oxidizing power between two differently charged Keggin anions could be explained. From such an idealized picture, the trend in reduction potentials for cases with molecular charges in the range 3-7 was

justified. In a more generalized view, the combination of molecular charge and number of metal atoms (q and $m^{[1]}$) or molecular charge and volume (q and $V^{[5]}$) are good descriptors of the oxidizing power of polyoxotungstates, irrespective of their shape. Thus, it was evidenced that the anion charge effect can be generalized to POM compounds with shapes other than the Keggin, as long as the size parameter is accounted for.

The present work tackles a fundamental though relevant aspect related to the redox chemistry of POMs that may need further discussion. Namely, how the redox W waves in $[\alpha\text{-XMW}_{11}\text{O}_{40}]^n$ Keggin derivatives can be tuned upon changes in their negative charge and what originates the different reduction potential alterations observed. We herein take the *anion charge effect* concept to enter into more detail relating the potential shifts with all the possible ways of changing the molecular charge of Keggin compounds (internal or external, localized or delocalized).

3.2 Results and discussion

The α isomer of the Keggin tungstate is one of the most deeply studied structures of the POM family, with general formula $[\alpha\text{-XW}_{12}\text{O}_{40}]^n$ and formal T_d symmetry (Figure 3.1a) featuring twelve equivalent W centers at peripheral or external positions, also named *addenda* (located at the centers of octahedra in Figure 3.1). In suitable conditions, one or several electrons can reduce this system. If one extra electron is added, it usually delocalizes by thermal hopping over the whole molecule^[6] formally residing at the 12 tungsten atoms equally^[7], although the trapping time per W site is much dependent on temperature. On the other hand, chemical change can allow an extra electron to be localized in a single atom (i.e. $\text{PMo}^{\text{VI}}\text{W}_{11}\text{O}_{40} + e \rightarrow \text{PMo}^{\text{V}}\text{W}_{11}\text{O}_{40}$) if it is more active electrochemically, namely more oxidant, than W^{VI} (we call it *electroactive* in this particular context). Figure 3.1b shows a mono-substituted system, $[\alpha\text{-XMW}_{11}\text{O}_{40}]^n$. Computed reduction energies (REs) give the reaction energy for the one-electron reduction process:



and are defined as $\text{RE} = E(\text{POM}_{\text{red}}) - E(\text{POM}_{\text{ox}})$. REs are related with experimental reduction potentials such that E_c are proportional to $-\text{RE}$. The reduction energy of -4.28 eV, accurately computed for the process $\text{H}^+ + e \rightarrow 1/2\text{H}_2$ (normal hydrogen electrode, NHE), can be used to convert RE into E_c ^[8].

The present RE values were obtained from DFT calculations carried out for a set of $[\alpha\text{-XMW}_{11}\text{O}_{40}]^{n-}$ Keggin derivatives with $X = \text{P, Si, Al}$ and $M = \text{W, Mo, V, Nb, Ti}$. Taking PW_{12}^{3-} as *reference* compound, and its corresponding RE as zero, we can formally obtain all the compounds studied here by successive atom replacement or electron addition, and refer the computed REs to the former molecule.

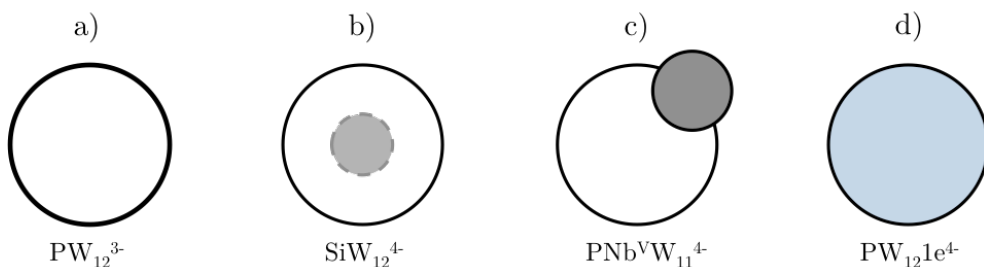


Figure 3.2. The three cases of negative charge addition discussed: from a) the reference compound, PW_{12}^{3-} , b) localized inside the cage by heteroatom substitution, c) localized in the external cage by addenda substitution, and d) delocalized over the external cage by a *blue* electron. The differently shaded areas represent the regions of (de)localization of the extra negative charge and to what extent it is concentrated/exposed to an incoming electron.

Replacing the internal atom X is one, but not the only, way of varying the molecular charge of Keggin anions (Figure 3.2b). It is well-known that addenda atoms (W^{VI} in polyoxotungstates) can be replaced by others (Figure 3.2c), generally with a lower oxidation state, such as Mo^{V} , Nb^{V} , $\text{V}^{\text{V,IV}}$ or Ti^{IV} . From the electrochemical point of view, this implies a couple of redox waves appearing at more negative potentials compared to the parent all- W^{VI} compound, even if the substituting metal atom is not electroactive. In the family of XMW_{11}^{n-} compounds, other metals than W can compete for the incoming electrons, such as V^{V} and Mo^{VI} , but their REs are not relevant here. On the other hand, the cases where V^{IV} or Mo^{V} (d^1 atoms) and also Nb^{V} or Ti^{IV} are present are important since they provide situations in which the reduced metal is W . Another way of shifting redox waves towards more negative potential values can be achieved without chemical change by previous reduction of the system (Figure 3.2d). This case produces the so-called *blue* species, characterized by the presence of one delocalized electron that hops from one peripheral metal to another (the delocalized nature of the *blue* electron is noted as XM_{12}e throughout the text).

Summarizing, if one negative charge is added to a system the next electron will enter, obviously, at a more negative potential than the first. But the

important point here is that the three ways of adding a negative charge to a Keggin anion affect *differently* the potential at which the reduction of W atoms occur. Our goal is to understand the observed trends through electronic structure calculations with quantum chemistry tools. We have restricted our study to simulate neutral to basic pH conditions, that is, reductions are assumed to occur without associated protonation of the POM. This is an important point since protonation is rather common in combination with redox processes.

Table 3.1. First and second one-electron reduction potentials (in Volts) relative to SCE.

	$E_{\text{red},1}^{\text{a}}$	$E_{\text{red},2}^{\text{a}}$	Experimental conditions	Ref.
PW ₁₂ ³⁻	-0.023	-0.280	pH 1, 1.0 M H ₂ SO ₄	[2]
	-0.01	-0.26	pH 1, NaCl electrolyte buffer	[9]
SiW ₁₂ ⁴⁻	-0.228	-0.433	pH 1, 1.0 M H ₂ SO ₄	[2]
	-0.189	-0.449	pH 1.0–4.5, NaCl electrolyte buffer	[9]
AlW ₁₂ ⁵⁻	-0.374	-0.604	pH 1.8–7.5, NaCl electrolyte buffer	[9]
	-0.410	-	pH 5, 0.4 M ac. buffer	[4]
PV ^V W ₁₁ ⁴⁻	+0.58 (V)	-0.6	pH 2.3, 0.8 M NaClO ₄ + 0.2 M ac. buffer	[10]
PMo ^{VI} W ₁₁ ³⁻	+0.492 (Mo)	-0.056 ^b	pH 1.5, 0.2 M Na ₂ SO ₄ + H ₂ SO ₄	[11]
SiMo ^{VI} W ₁₁ ⁴⁻	+0.320 (Mo)	-0.210 ^b	pH 2.7, 0.2 M Na ₂ SO ₄ + H ₂ SO ₄	[11]
PTi ^{IV} W ₁₁ ⁵⁻	-1.82	-	Non-aqueous medium (MeCN)	[12]

^a Values correspond to W reductions except otherwise indicated (in parenthesis). ^b Protonation process could be associated to this redox wave.

Table 3.1 contains the first ($E_{\text{red},1}$) and second ($E_{\text{red},2}$) reduction potentials taken from the literature for a set of Keggin compounds which illustrate the phenomena introduced above, with the experimental conditions of

measurement indicated. The different cases we want to discuss are shown to note how W reduction waves depend on the presence of *blue* electrons, heterometals or internal heteroatoms with different oxidation states. The dependence of W-waves on all these variables is not so clear at first glance although some facts are worth being enumerated. First, the reduction of *blue* Keggin anions ($XW_{12}1e$) requires an extra potential of about 240–260 mV with respect to their fully oxidized counterparts. On the other hand, heteroatom replacement (P, Si, Al, etc) requires about 180 mV of extra potential per unit charge, only. Concerning addenda replacement, systematization of the data for different compounds is much less intuitive, plus the possibility of protonation processes that shift potential values by a large extent and thus become not comparable with each other. The computational results presented below are aimed at unifying and rationalizing the bunch of experimental information obtained at conditions that make difficult a global comprehension and comparison.

The computational results obtained in the present work are listed in Table 3.2 with the first and second REs obtained for the compounds listed. The main results for our discussion are obtained at the BP86 level, and additional data were obtained with the B3LYP functional. It is well-known that these two functionals are rather different in how they treat electron-electron interactions, although the main conclusions are in accord.

Let us start with the *internal charge effect* represented in Figure 3.2b. This is the basis for the well-known slope obtained by Pope and co-workers^[2, 11]. Our theoretical data reveal very similar trends compared to the experiments, although somewhat larger than the 180 mV obtained from electrochemical techniques. If we compare the REs for PW_{12}^{3-} and SiW_{12}^{4-} , the difference is 222 meV, the tungstosilicate being less easily reduced due to its larger negative charge, and from SiW_{12}^{4-} to AlW_{12}^{5-} ca. 200 meV more are necessary. The same exercise of heteroatom replacement can be done if we compare the REs of $PNb^VW_{11}^{4-}$ and $SiNb^VW_{11}^{5-}$ (199 meV difference), and $PTi^{IV}W_{11}^{5-}$ with $SiTi^{IV}W_{11}^{6-}$ (175 meV). Finally, from $PW_{12}1e^{4-}$ to $SiW_{12}1e^{5-}$, the increment is 194 meV. On average, an increase of a unit charge inside the Keggin cage causes a negative potential shift (more positive REs) of 198 meV at the BP86 level. All the values are close to the average, and the trend observed from DFT calculations is in full agreement with Pope’s observations.

Regarding to the B3LYP results, similar trends are found. For PW_{12}^{3-} and SiW_{12}^{4-} , the REs difference is 224 meV, which is similar to the BP86 result (222 meV). In the case of the $\text{PMo}^{\text{VI}}\text{W}_{11}^{3-}$ and $\text{SiMo}^{\text{VI}}\text{W}_{11}^{4-}$, the difference of REs is 181 meV, a value very close to the Pope’s slope. In general, a negative potential shift of 213 meV, larger than the BP86 value, is observed at B3LYP level for increasing a unit charge in the Keggin anion.

Table 3.2. Computed first and second reduction energies (RE_1 and RE_2 , in eV) with the BP86 and B3LYP functionals. Values correspond to W reductions except otherwise indicated (in parenthesis).

	RE_1		RE_2	
	BP86	B3LYP	BP86	B3LYP
PW_{12}^{3-}	-4.074	-3.646	-3.679	-3.229
SiW_{12}^{4-}	-3.852	-3.422	-3.485	-3.044
AlW_{12}^{5-}	-3.654	-3.216	-3.282	-2.829
$\text{PMo}^{\text{VI}}\text{W}_{11}^{3-}$	-4.476 (Mo)	-4.577 (Mo)	-3.741	-3.491
$\text{PNb}^{\text{V}}\text{W}_{11}^{4-}$	-3.786	-3.632	-3.445	-3.240
$\text{PTi}^{\text{IV}}\text{W}_{11}^{5-}$	-3.460	-3.294	-3.200	-2.908
$\text{PV}^{\text{V}}\text{W}_{11}^{4-}$	-4.481 (V)	-4.820 (V)	-3.388	-3.150
$\text{SiMo}^{\text{VI}}\text{W}_{11}^{4-}$	-4.276 (Mo)	-4.396 (Mo)	-3.521	-3.474
$\text{SiNb}^{\text{V}}\text{W}_{11}^{5-}$	-3.587	-3.419	-3.227	-3.031
$\text{SiTi}^{\text{IV}}\text{W}_{11}^{6-}$	-3.285	-3.053	-2.938	-2.689

Variations in the external metal oxide cage (Figure 3.2c) by addenda substitution lead to the *external localized charge effect*. If the replacing metal atom carries a lower oxidation state than VI, a net increase of the molecular charge occurs. However, as Figure 3.3 shows, the redox properties are differently affected compared with heteroatom substitution. Some examples are listed in Table 3.3. The case of $\text{PNb}^{\text{V}}\text{W}_{11}^{4-}$ is self-explanatory. Its one-electron reduction is 288 meV more difficult than PW_{12}^{3-} , whereas SiW_{12}^{4-} is only 222 meV. So, introducing a negative charge in the external region of the POM by addenda replacement produces a larger positive shift in the next REs than in the case of heteroatom replacement. Figure 3.3 summarizes the main

results obtained from the calculations. The RE values, in meV, are referred to the case of PW_{12}^{3-} , to which an arbitrary RE = 0.0 is assigned. Thus, we are interested in the trend in REs more than in their absolute values. In the notation of Figure 3.3, more positive values denote less negative REs or more negative redox potentials with respect to PW_{12}^{3-} .

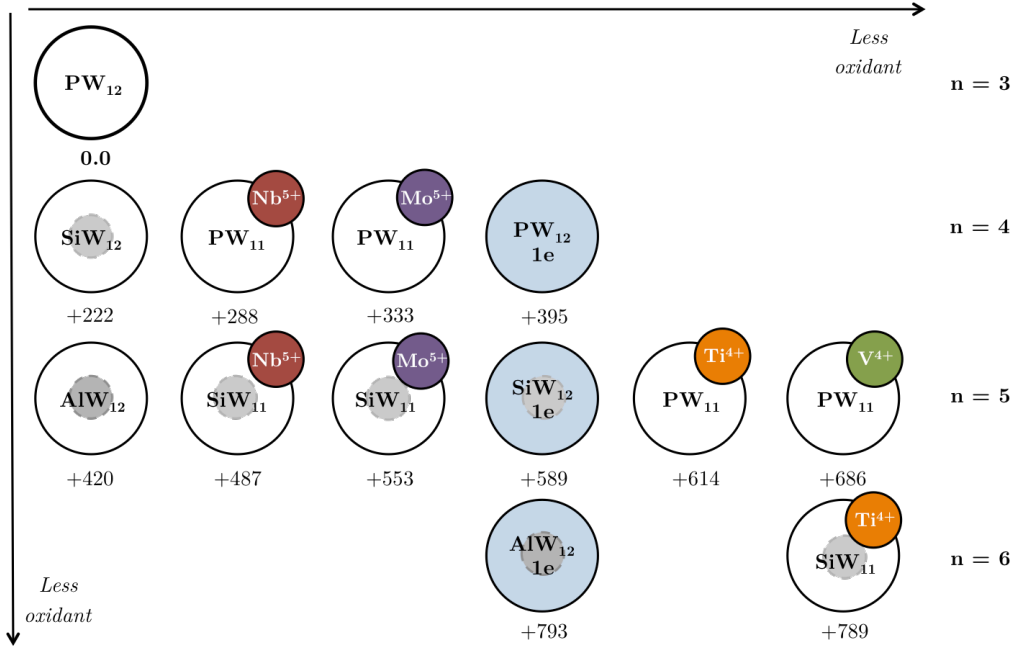


Figure 3.3. Dependence of the computed REs (in meV, BP86 data) with the substitution of the internal (X) or external (M) positions, and the addition of a *blue* electron. All values are referred to the RE for the process $\text{PW}_{12}^{3-} + e \rightarrow \text{PW}_{12}^{\text{1e}^{4-}}$, taken arbitrarily as zero. The n values indicate the total initial charge. Values also represent the reduction potentials (-RE, in mV) with respect to the reduction of PW_{12}^{3-} .

Notably, within the *external localized charge effect* we find some differences. From calculations, it can be deduced that adding a localized external charge to a system containing already one (i.e. $\text{PNb}^{\text{V}}\text{W}_{11}^{4-} \rightarrow \text{PTi}^{\text{IV}}\text{W}_{11}^{4-}$ or $\text{PMo}^{\text{V}}\text{W}_{11}^{4-} \rightarrow \text{PV}^{\text{IV}}\text{W}_{11}^{5-}$) leads to larger shifts in reduction waves than replacing W by M^{V} . Another example consists in adding two negative charges at once (i.e. $\text{PW}_{12}^{3-} \rightarrow \text{PTi}^{\text{IV}}\text{W}_{11}^{5-}$). The decrease in reduction energy is 614 meV, with a $\Delta\text{RE} = 307$ meV/unit charge. In the case of the silicate, the change per unit charge is 284 meV. From our calculations, we extracted an average ΔRE for changes in the external cage of 304 meV. Thus, localization of an extra negative charge in the external cage plays the same role than adding a negative charge in the heteroatom region, but the effect is more accentuated.

Table 3.3. REs (in eV) and Δ REs computed (BP86 functional) for pairs of compounds differing in one localized negative charge in the external cage. In all cases, the reduction occurs at the W sites.

	RE	Δ RE ^a
PW ₁₂ ³⁻	-4.074	
PNb ^V W ₁₁ ⁴⁻	-3.786	+288 meV
SiW ₁₂ ⁴⁻	-3.852	
SiNb ^V W ₁₁ ⁵⁻	-3.587	+265 meV
PNb ^V W ₁₁ ⁴⁻	-3.786	
PTi ^{IV} W ₁₁ ⁵⁻	-3.460	+326 meV
PW ₁₂ ³⁻	-4.074	
PMo ^V W ₁₁ ⁴⁻	-3.741	+333 meV
SiW ₁₂ ⁴⁻	-3.852	
SiMo ^V W ₁₁ ⁵⁻	-3.521	+331 meV
PMo ^V W ₁₁ ⁴⁻	-3.741	
PV ^{IV} W ₁₁ ⁵⁻	-3.388	+353 meV

^a The differences between experimental reduction potentials (in mV) are proportional to $-\Delta$ RE.

The trends observed can be clarified by close analysis of the degree of (de)localization of the extra electrons involved in W reduction processes. The addition of a localized extra negative charge in the external framework produces a less delocalized W-like molecular orbital of higher energy that is pushed away from the region where a metal atom has been substituted, as can be seen in Figure 3.4b-c. The spin population analysis of Table 3.4 gives numerical evidence for that fact, showing that the systems having one addenda atom with lower oxidation state than W^{VI} (Nb^V, Ti^{IV}, etc.) will delocalize the extra electron in a smaller region of the external framework. The differences encountered between the BP86 and B3LYP functionals are just accidental, leading to the same conclusions. Indeed, the B3LYP calculations furnish more localized *blue* electrons in the examples shown, as expected. The reduction of PMo^VW₁₁1e⁵⁻ compared to PNb^VW₁₁1e⁵⁻ deserves an additional comment.

Despite being two molecules with the same charge localized in the external cage, the RE computed for the niobium-substituted case is more negative by 45 meV. We attribute this to the presence of a valence electron in Mo^{V} , not in Nb^{V} , and maybe to the partial delocalization of the valence Mo^{V} electron over vicinal W atoms. When the next extra electron arrives to occupy the first empty W-like orbital, it experiences some repulsion with the Mo electron. We can deduce that an addenda metal with a lower oxidation state than VI can be of two types with regard to W-reduction: fully oxidized (d^0 , case of Nb^{V}) or partially reduced (d^1 , case of Mo^{V}). If we extend this discussion to the cases $\text{PTi}^{\text{IV}}\text{W}_{11}^{5-}$ and $\text{PV}^{\text{IV}}\text{W}_{11}^{5-}$ we arrive at the same conclusion. The presence of vanadium (V^{IV}) shifts the RE by 72 meV compared with the homologous Ti^{IV} system. From the data we have obtained, the cases with d^1 peripheral metals (Mo^{V} , V^{IV}) produce first W waves to be shifted to more negative potentials than the d^0 counterparts (Nb^{V} , Ti^{IV}).

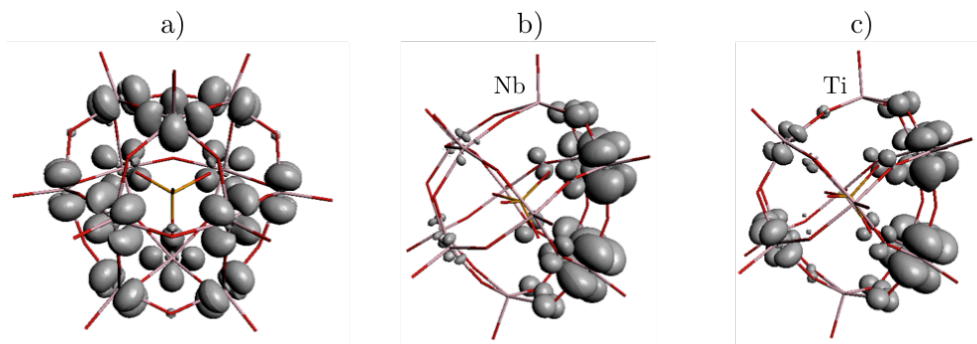


Figure 3.4. Spin density representation (isosurface for $\rho = 0.015 e$) for a) the single-addenda PW_{12}e^4 , and the metal-substituted compounds b) $\text{PNb}^{\text{V}}\text{W}_{11}\text{e}^4$ and c) $\text{PTi}^{\text{IV}}\text{W}_{11}\text{e}^5$. Numerical values of the atomic spin densities for cases b) and c) are listed in Table 3.4.

Finally, the *external delocalized charge effect* can be analyzed by adding a *blue* electron to the W_x core (Figure 3.2d) and observing what is the effect upon the next redox process, for instance comparing the REs for PW_{12}^{3-} and PW_{12}e^4 . From DFT calculations, the former compound reduces 395 meV before the latter due to the presence of a *blue* electron in the second case, corresponding to a value of 260mV from experiments^[2, 9]. In a similar fashion, the homologous $\text{SiW}_{12}^4/\text{SiW}_{12}\text{e}^5$ couple (and also $\text{AlW}_{12}^5/\text{AlW}_{12}\text{e}^6$) has REs differing by around 370 meV. Finally, for mixed-addenda compounds like $\text{PNb}^{\text{V}}\text{W}_{11}^4$ and its *blue* counterpart $\text{PNb}^{\text{V}}\text{W}_{11}^{5-}$, $\Delta\text{RE} = 341$ meV. On average, the RE shifts per unit charge added in a delocalized fashion are 369 meV, a rather large energy difference for systems differing by one charge unit, compared to the

computed values in the cases of heteroatom and addenda substitution. The computed values are somewhat larger than the experimental ones, although the trend is the same, that is, an external delocalized charge shifts the most the next reduction potential.

Purely electrostatic reasons are expected to be at the origin of the differences encountered, that is, the mutual interaction between the negative charge(s) of the Keggin anion previous to reduction (cases a-c in Figure 3.2) and the entering electron to which we are interested in. We can follow up this behavior from molecular orbital energies. From our experience in the theoretical treatment of POMs, this is a very good and simple way to follow the trends of some physicochemical properties, such as the redox behavior.

Table 3.4. Comparison of the atomic spin populations (larger than 0.05)^a computed at the BP86 and B3LYP levels for various systems containing one W-like electron.

	SiW ₁₂ 1e ⁵⁻	PNb ^V W ₁₁ 1e ⁵⁻	PMo ^V W ₁₁ 1e ⁵⁻	PV ^{IV} W ₁₁ 1e ⁶⁻	PTi ^{IV} W ₁₁ 1e ⁶⁻
BP86	0.087 (12)	0.230 (2)	0.194 (2)	0.175 (2)	0.263 (2)
		0.180 (2)	0.173 (2)	0.165 (2)	0.125 (2)
		0.056 (2)	0.129 (4)	0.126 (2)	0.073 (2)
			0.052 (2)	0.113 (2)	
> 0.05 ^b	12	6	10	8	6
B3LYP	0.090 (12)	0.280 (2)	0.188 (2)	0.205 (2)	0.342 (2)
		0.200 (2)	0.153 (2)	0.175 (2)	0.121 (2)
			0.138 (2)	0.085 (4)	
			0.123 (2)		
> 0.05 ^b	12	4	8	8	4

^a In parenthesis, the number of appearances of each value. ^b For each method, the last row indicates the total number of W atoms with spin population > 0.05.

The evolution of the computed highest oxo and first W-like orbitals, illustrated in Figure 3.5, shows how the different ways of molecular charge increase lead to the tuning of redox properties. In the first block shown, starting from the mono-reduced PW₁₂⁴⁻ system, an increase of one internal negative charge produces a positive shift of the singly-occupied W orbital of

235 meV, explaining a $\Delta\text{RE} = 222$ meV. If W by Mo^{V} addenda replacement occurs, the vertical shifts reaches 301 meV at the BP86 level, and even more (392 meV) when two *blue* electrons are present. In the second block, similar results are encountered starting from SiW_{12}^{5-} . The energy of the W-reduced orbital compiles all the effects and it best represents how favorable the reduction process is. The cases of $\text{PW}_{12}2\text{e}^{5-}$ and $\text{PMo}^{\text{V}}\text{W}_{11}1\text{e}^{5-}$ evidence that the addenda-substituted system has a lower W orbital after 2nd reduction since it has more freedom to move away from Mo^{V} than in $\text{PW}_{12}2\text{e}^{5-}$. In this latter case, the two *blue* electrons are forced to share the same region conferring more instability to this compound and, thus, a less negative RE (more positive reduction potential).

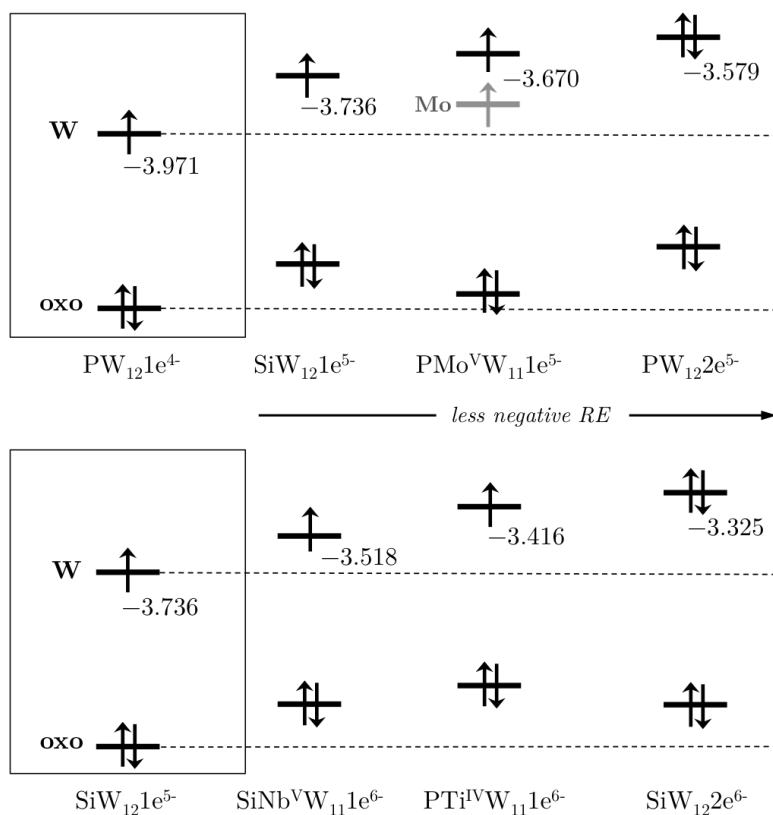


Figure 3.5. Evolution of the frontier molecular orbitals (energy values computed, in eV) upon addition of an additional negative charge in three different ways. From left to right, the oxidant power decreases (less negative RE).

It is also worth mentioning that heteroatom replacement (P^V to Si^{IV}) has the lowest influence on the next reduction process thanks to the fact that the new incoming electron occupies a large metal-electron-free region and can remain far away from the internal negative charge. In general, the differences observed in W-like molecular orbital energies are in good agreement with the RE variations calculated.

3.3 Conclusions

DFT calculations performed on a family of $[XW_{12}O_{40}]^{n-}$ and $[XMW_{11}O_{40}]^{n-}$ Keggin POMs show that the oxidizing power of these systems do not decrease in a *uniform* way with the addition of negative charge. Contrarily, they depend on the nature of such charge. Three cases are analyzed: internal charge effect (heteroatom replacement), external localized charge effect (addenda replacement) and external delocalized charge effect (presence of one *blue* electron). It arises that the nature of a unitary charge increment affects differently the reduction energy, the mildest change occurring upon variations in the internal position (heteroatom substitution), and the strongest, by a factor of ~ 1.85 by an additional charge unit compared to the previous one, the presence of a delocalized (or *blue*) electron. In between, replacement of a metal atom from an external position by another one with different oxidation state.

The results reveal that the oxidizing power decreases more if one charge is added as a *blue* electron (shifted by 370 meV on average at the BP86 level) than if it is added as an addenda metal with a lower oxidation state than W^{VI} (310 meV on average), and also than if it is added as an internal charge by heteroatom replacement (~ 200 meV). Clearly, these different shifts depend on how the incoming electron feels the negative charge of the Keggin molecule. The most exposed negative charges (external) produce systems less predisposed to reduction and, within this group, a delocalized charge makes the system more stable *vs.* further reduction than if the charge is localized. It is worth noting, for instance, that $PMo^VW_{11}^{4-}$ is reduced 275 mV more easily than PW_{12}^{4-} , a fact that is qualitatively reproduced at the DFT level. One interesting consequence derived from the facts stated above is the possibility to shift W redox waves towards positive potentials in a selected system equally charged than another. This is the case of the *second* reduction in $PMo^{VI}W_{11}^{3-}$ or $Mo^{VI}W_5^{2-}$ compared to, respectively, their single-addenda counterparts

PW_{12}^{3-} and W_6^{2-} . For the Lindqvist anions, we computed that the second REs differ by 86 meV at the BP86 level, and by 359 meV with the B3LYP functional, in favor of the Mo-substituted compound. In Figure 3.6 we illustrate this effect. Then, it is clear that a new incoming electron can feel charge variations quite differently and that the redox potentials can account for that. It is likely that the effects presented here can help the full understanding and tailoring of the redox properties of known and new Keggin-type and other POM compounds.

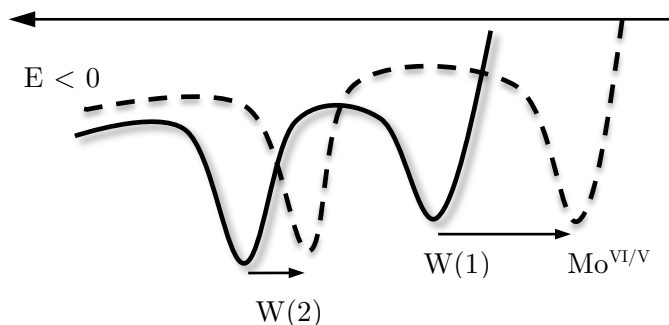


Figure 3.6. Simplified representation of the positive shift experienced by the second reduction wave, indicated as W(2), upon W^{VI} to Mo^{VI} substitution in PW_{12}^{3-} and W_6^{2-} . The solid line represents the two reduction waves for a single-addenda tungstate, and the dashed line the two reduction waves for the mono-substituted MoW_x counterpart. The shift in the first reduction wave is due to the larger electronegativity of Mo^{VI} . The second wave, W(2), shifts as consequence of the diminished repulsion produced by Mo^{V} with respect to the first *blue* electron.

3.4 Computational details

The present calculations were carried out using the DFT methodology as implemented in the ADF 2011 program^[13]. We applied the following functionals to obtain the molecular energies: (i) the GGA functional BP86^[14] and (ii) the hybrid functional B3LYP, with 20% of exact Hartree-Fock exchange^[15]. Full geometry optimizations under the constraints of the maximal point group symmetries of each molecule (T_d for $[\alpha\text{-XW}_{12}\text{O}_{40}]^{n-}$ and C_s for $\alpha\text{-[XMW}_{11}\text{O}_{40}]^{n-}$) were carried out for all systems in every reduction state with the BP86 functional, whereas the B3LYP energies were obtained after single point calculations. It is worth to say that the reduction energies computed with either functional may not be compared with each other since they present important differences due to their very nature. Instead, the trends computed with a given functional will furnish relevant conclusions. The electrons were described by Slater-type functions with basis sets of TZ2P quality for the

valence electrons of all atoms. *Core* electrons were kept frozen and described by single Slater functions (core shells by atom: O: 1s; Si, P: 1s-2p; W: 1s-4d; Nb, Mo: 1s-3d; Ti, V: 1s-3p). We applied scalar relativistic corrections to the core electrons by means of ZORA^[16] with the core potentials generated using the DIRAC program^[13]. We applied the spin-unrestricted formalism to open shell species. We included COSMO^[17] to account for solvent effects of water ($\epsilon = 78.4$) to all the calculations. The solvent cavity surrounding the anions was created using the solvent-excluding method with fine tesserae. The ionic radii chosen for the atoms located in the metal oxide cage of the systems herein studied, and that actually define the size of the solvent cavity due to their peripheral positions, are the following: 1.26 Å (W), 0.64 Å (Mo), 0.90 Å (Nb), 0.75 Å (Ti), 0.70 Å (V) and 1.52 Å (O).

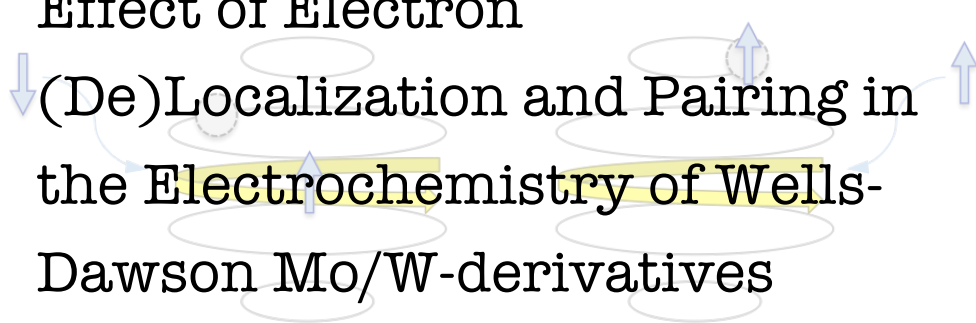
3.5 References

- [1] X. López, J. A. Fernández, J. M. Poblet, *Dalton Trans.* **2006**, 1162.
- [2] M. T. Pope, G. M. Varga, *Inorg. Chem.* **1966**, 5, 1249.
- [3] M. T. Pope, *Heteropoly and Isopoly Oxometalates*, Springer-Verlag, Berlin, 1983.
- [4] I. M. Mbomekallé, X. López, J. M. Poblet, F. Sécheresse, B. Keita, L. Nadjo, *Inorg. Chem.* **2010**, 49, 7001.
- [5] A. Bagno, M. Bonchio, J. Autschbach, *Chem. Eur. J.* **2006**, 12, 8460.
- [6] a) R. A. Prados, P. T. Meiklejohn, M. T. Pope, *J. Am. Chem. Soc.* **1974**, 96, 1261; b) G. M. Varga, E. Papaconstantinou, M. T. Pope, *Inorg. Chem.* **1970**, 9, 662.
- [7] J. M. Maestre, X. López, C. Bo, J. M. Poblet, N. Casañ-Pastor, *J. Am. Chem. Soc.* **2001**, 123, 3749.
- [8] a) A. Lewis, J. A. Bumpus, D. G. Truhlar, C. J. Cramer, *J. Chem. Educ.* **2004**, 81, 596; b) A. Lewis, J. A. Bumpus, D. G. Truhlar, C. J. Cramer, *J. Chem. Educ.* **2007**, 84, 934.
- [9] Y. V. Geletii, C. L. Hill, A. J. Bailey, K. I. Hardcastle, R. H. Atalla, I. A. Weinstock, *Inorg. Chem.* **2005**, 44, 8955.
- [10] D. P. Smith, M. T. Pope, *Inorg. Chem.* **1973**, 12, 331.
- [11] Y. Cui, L. Xu, W. J. Wang, G. G. Gao, E. B. Wang, *Chin. J. Chem.* **2006**, 24, 316.
- [12] O. A. Kholdeeva, G. M. Maksimov, R. I. Maksimovskaya, L. A. Kovaleva, M. A. Fedotov, V. A. Grigoriev, C. L. Hill, *Inorg. Chem.* **2000**, 39, 3828.
- [13] ADF2011.01, SCM, Vrije Universiteit, Amsterdam, The Netherlands, <http://www.scm.com>, 2011.
- [14] a) A. D. Becke, *Phys. Rev. A* **1988**, 38, 3098; b) J. P. Perdew, *Phys. Rev. B* **1986**, 33, 8822; c) S. H. Vosko, L. Wilk, M. Nusair, *Can. J. Phys.* **1980**, 58, 1200.
- [15] a) C. T. Lee, W. T. Yang, R. G. Parr, *Phys. Rev. B* **1988**, 37, 785; b) P. J. Stephens, F. J. Devlin, C. F. Chabalowski, M. J. Frisch, *J. Phys. Chem.* **1994**, 98, 11623.
- [16] a) E. van Lenthe, E. J. Baerends, J. G. Snijders, *J. Chem. Phys.* **1993**, 99, 4597; b) E. van Lenthe, E. J. Baerends, J. G. Snijders, *J. Chem. Phys.* **1994**, 101, 9783; c) E. van Lenthe, A. E. Ehlers, E. J. Baerends, *J. Chem. Phys.* **1999**, 110, 8943; d) E. van Lenthe, R. van Leeuwen, E. J. Baerends, J. G. Snijders, *Int. J. Quantum Chem.* **1996**, 57, 281.
- [17] a) J. Andzelm, C. Kölmel, A. Klamt, *J. Chem. Phys.* **1995**, 103, 9312; b) A. Klamt, *J. Chem. Phys.* **1995**, 102-103, 2224; c) A. Klamt, G. Schüürmann, *J. Chem. Soc., Perkin Trans. 2* **1993**, 799; d) C. C. Pye, T. Ziegler, *Theor. Chem. Acc.* **1999**, 101, 396.

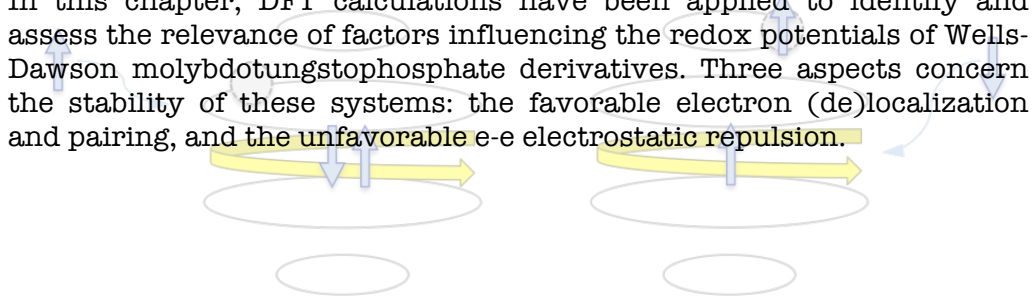
Chapter 4

Effect of Electron

↓ (De)Localization and Pairing in the Electrochemistry of Wells- Dawson Mo/W-derivatives



In this chapter, DFT calculations have been applied to identify and assess the relevance of factors influencing the redox potentials of Wells-Dawson molybdotungstophosphate derivatives. Three aspects concern the stability of these systems: the favorable electron (de)localization and pairing, and the unfavorable e-e electrostatic repulsion.



Related publication:

L. Parent, P. A. Aparicio, P. De Oliveira, A.-L. Teillout, J. M. Poblet, X. López, I. M. Mbomekallé, *Inorg. Chem.* **2014**, 53, 5941.

4.1 Introduction and objectives

In the family of tungsten-containing Wells-Dawson-type POMs, Contant *et al.* have shown that through stereo-selective multi-step syntheses, it is possible to replace 1 up to 6 W^{VI} centers by either Mo^{VI} or V^V atoms in a controlled way^[1]. By and large, POMs are seen as electron sponges, and are often implicated in reversible electron transfer processes, either at an electrode/solution interface or between species in solution, which makes them excellent models to study reaction mechanisms in electrochemistry^[2]. The above mentioned molybdenum-containing Wells-Dawson-type POMs, and in particular the behavior of electrons transferred to them, have attracted the attention of several authors. The aim of their studies is to determine, in a first step, if the electrons are preferentially transferred into a defined site (atom or group of atoms), and in a second step to check if the electrons remain located in that site or delocalized over neighboring sites or over the whole molecule, as is the case for tungsten-containing Keggin-type POMs. Other works may be cited, like the seminal papers by Livage and Launay^[3], Contant *et al.*^[4], and Baker *et al.*^[5]. These authors used either spectroscopic methods (NMR, EPR) or magnetic susceptibility measurement approaches on samples containing reduced POMs. Electrochemical results have seldom been compared to theoretical calculations, and in the majority of cases experimenters do not go beyond the description of the electrochemical features of the compounds.

In this chapter, experimental, standard electrochemical techniques as cyclic voltammetry (CV) and controlled potential coulometry (CPC), and theoretical (DFT calculations) data are combined to unravel the mechanisms ruling electron transfer and electron distribution within molybdo-tungstic Wells-Dawson-type POMs. The structures selected for the present study are shown in Figure 4.1: α_1 - $[P_2MoW_{17}O_{62}]^{6-}$ (α_1 - P_2MoW_{17}), α_2 - $[P_2MoW_{17}O_{62}]^{6-}$ (α_2 - P_2MoW_{17}), α - $[P_2Mo_3W_{15}O_{62}]^{6-}$ (α - $P_2Mo_3W_{15}$) and α - $[P_2Mo_6W_{12}O_{62}]^{6-}$ (α - $P_2Mo_6W_{12}$). They contain one Mo^{VI} center, three equivalent Mo^{VI} centers and six Mo^{VI} centers, equivalent in a 2(cap):4(belt) fashion, respectively. We resort both to experimental and theoretical methods in an effort to understand and rationalize the electron distribution between the molybdenum and the tungsten orbitals within these species.

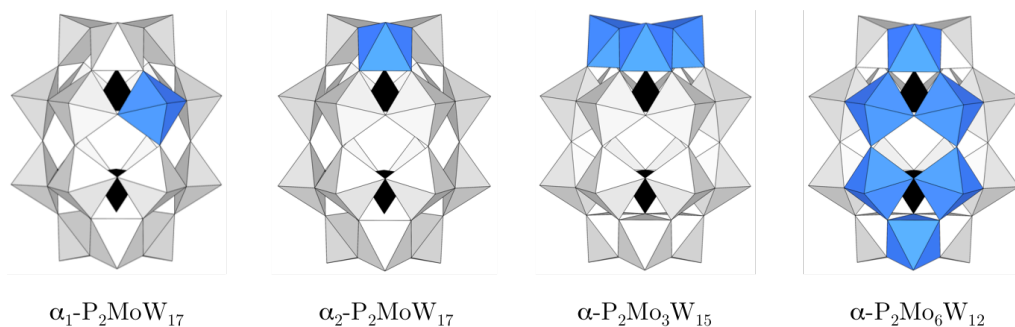


Figure 4.1 Idealized polyhedral representation of the molybdotungstate species discussed in this chapter. Grey and blue octahedra contain W and Mo atoms in the center, respectively. The black tetrahedra represent the internal PO_4^{3-} units.

4.2 Experimental background

Dr. I. M. Mbomekallé (Institut Lavoisier, Université de Versailles) has studied the electrochemistry of different molybdotungstophosphates: $\alpha_1\text{-P}_2\text{MoW}_{17}$, $\alpha_2\text{-P}_2\text{MoW}_{17}$, $\alpha\text{-P}_2\text{Mo}_3\text{W}_{15}$ and $\alpha\text{-P}_2\text{Mo}_6\text{W}_{12}$. Firstly, his research group compared the redox behavior of $\alpha_2\text{-P}_2\text{MoW}_{17}$ with the parent compound $[\text{P}_2\text{W}_{18}\text{O}_{62}]^{6-}$ (P_2W_{18}) and the mono-lacunary $\alpha_2\text{-}[\text{P}_2\text{W}_{17}\text{O}_{61}]^{10-}$ ($\alpha_2\text{-P}_2\text{W}_{17}$). Starting from P_2W_{18} , the loss of a WO^{4+} moiety during the formation of $\alpha_2\text{-P}_2\text{W}_{17}$ is accompanied by the increase of the overall charge of the polyanion from -6 to -10, and a concomitant strengthening of its basicity. Several changes are therefore observed when the CVs of both compounds are compared. The first two one-electron waves of the plenary structure P_2W_{18} merge into a first single two-electron wave in the case of the lacunary structure $\alpha_2\text{-P}_2\text{W}_{17}$. The latter is located at more negative potentials and is pH dependent, revealing the influence of a more pronounced alkaline character.

Results gathered from different pertinent articles show that, upon replacing the missing W atom by a d metal cation, the redox behavior of P_2W_{18} is not regenerated, i.e. the observation of two one-electron redox processes that are pH independent is not recovered^[6]. Indeed, it appears that, in terms of the redox behavior of the tungstic framework, the new substituted compound $\alpha_2\text{-P}_2\text{MW}_{17}$ (with $\text{M} = \text{Mn}^{\text{II}}, \text{Fe}^{\text{III}}, \text{Co}^{\text{II}}, \text{Ni}^{\text{II}}, \text{Cu}^{\text{II}}$ or Zn^{II}) is closer to its lacunary $\alpha_2\text{-P}_2\text{W}_{17}$ parent than to the plenary P_2W_{18} structure. The first three redox processes attributed to the tungsten framework remain bi-electronic and pH dependent. Even in the case of $\alpha_2\text{-P}_2\text{VW}_{17}$ where the substituent V^{IV} cation is in the same coordination environment as W, i.e. with a terminal oxo group,

$V=O$, the redox signature of $\alpha_2\text{-P}_2\text{W}_{17}$ remains, that is, three successive pH dependent two-electron reversible processes^[7]. Reduction waves associated to W usually stand clearly apart from the redox wave of the substituent cation M when the latter is easier to reduce than W. The first redox process, which is mono-electronic and pH independent, is easily attributed to the reduction of the V^V center, the following redox processes which may be assigned to the reduction of the W framework being almost the same as the ones observed on the CV of $\alpha_2\text{-P}_2\text{W}_{17}$ (Figure 4.2).

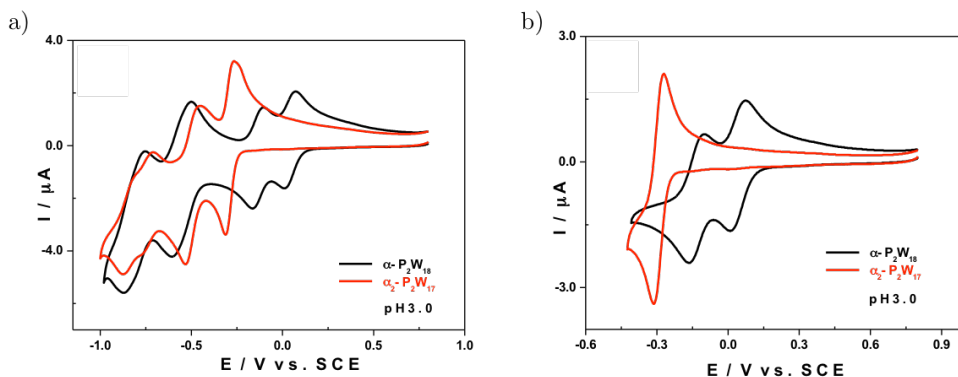


Figure 4.2. CVs of $\alpha\text{-[P}_2\text{W}_{18}\text{O}_{62}]^{6-}$ (black line) and $\alpha_2\text{-[P}_2\text{W}_{17}\text{O}_{61}]^{10-}$ (red line) in 0.5M $\text{Na}_2\text{SO}_4 + \text{H}_2\text{SO}_4$, pH = 3.0. Polyoxometalate concentration 0.5 mM; scan rate 10 $\text{mV}\cdot\text{s}^{-1}$; working electrode: glassy carbon; reference electrode: SCE. (a) All the reversible waves. (b) The processes corresponding to the transfer of the first two electrons.

Observations made on the CV of $\alpha_2\text{-P}_2\text{Mo}^{\text{VI}}\text{W}_{17}$ have clearly shown a different behavior, thus suggesting another interpretation. The presence of a Mo^{VI} substituent cation results in the appearance of two one-electron waves located at less negative potentials compared to the W waves of the parent $\alpha_2\text{-P}_2\text{W}_{17}$. The most positive of these waves is easily attributed to the reduction of the Mo^{VI} center and the second one is attributed to the reduction of W^{VI} ^[4b, 8]. Compared to the CV of P_2W_{18} , the first W reduction wave in $\alpha_2\text{-P}_2\text{Mo}^{\text{VI}}\text{W}_{17}$ cathodically shifts about 200 mV but remains mono-electronic. Reminiscence of the redox behavior of the lacunary parent specie, $\alpha_2\text{-P}_2\text{W}_{17}$, observed on the CVs of all the other substituted compounds $\alpha_2\text{-P}_2\text{W}_{17}\text{M}$ (with $\text{M} = \text{V}^{\text{V}}, \text{Mn}^{\text{II}}, \text{Fe}^{\text{III}}, \text{Co}^{\text{II}}, \text{Ni}^{\text{II}}, \text{Cu}^{\text{II}}$ or Zn^{II}), has almost disappeared here. The first W reduction wave has turned single-electronic again and pH-independent, as in the case of P_2W_{18} . However, the following one is a two-electron, pH-dependent wave, whose behavior resembles that of $\alpha_2\text{-P}_2\text{W}_{17}$. In fact, when the first three waves of $\alpha_2\text{-P}_2\text{Mo}^{\text{VI}}\text{W}_{17}$ are compared with those of P_2W_{18} obtained in the same

experimental conditions, a feature stands out: the addition of a Mo^{VI} center leads to a partial regeneration of the behavior of the saturated compound P_2W_{18} . Also, it is important to note that the two species, $\alpha_2\text{-P}_2\text{Mo}^{\text{VI}}\text{W}_{17}$ and P_2W_{18} , have the same charge.

The CVs of the two isomers α_1 and $\alpha_2\text{-P}_2\text{Mo}^{\text{VI}}\text{W}_{17}$ obtained at pH 3.0 show, as expected, that the Mo^{VI} center is easier to reduce in the α_1 position than in the α_2 position (Figure 4.3). The first electron gained by the α_1 isomer partially delocalizes over the belt region of the molecule, while it is trapped in one of the caps in the α_2 isomer. In the following electron transfer step, expected to be the first reduction of the W centers, the α_1 isomer is still easier to reduce than the α_2 isomer (Table 4.1).

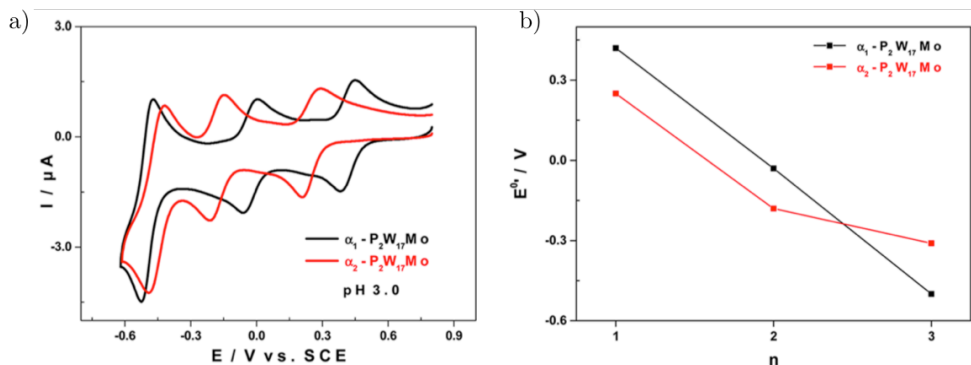


Figure 4.3. (a) CVs of $\alpha_1\text{-[P}_2\text{W}_{17}\text{Mo}^{\text{VI}}\text{O}_{62}]^{6-}$ (black line) and $\alpha_2\text{-[P}_2\text{W}_{17}\text{Mo}^{\text{VI}}\text{O}_{62}]^{6-}$ (red line) in 0.5 M $\text{Na}_2\text{SO}_4 + \text{H}_2\text{SO}_4$, pH = 3.0. Polyoxometalate concentration: 0.5 mM; scan rate: 10 $\text{mV}\cdot\text{s}^{-1}$; working electrode: glassy carbon; reference electrode: SCE. (b) Evolution between the midpoint redox potential values, E^1 , E^2 and E^3 for $\alpha_1\text{-[P}_2\text{W}_{17}\text{Mo}^{\text{VI}}\text{O}_{62}]^{6-}$ (black line) and $\alpha_2\text{-[P}_2\text{W}_{17}\text{Mo}^{\text{VI}}\text{O}_{62}]^{6-}$ (red line).

Interestingly, for this electron transfer, the theoretical calculations for the α_1 and α_2 isomers show that the electron preferentially goes into the belt metal centers of the Wells-Dawson structure^[9]. After this second redox process, and if we concentrate on the belt region of these molecules, which is strongly implicated in electron transfer, we realize that the electron density is higher in the case of the α_1 isomer than in the case of the α_2 isomer. As a consequence, the third reduction wave is found at a more negative potential for isomer α_1 since the belt region is more electron populated (two belt electrons) than in the α_2 isomer (one belt electron) at this stage. Indeed, an inversion in the precedence of the waves occurs, that is, the third wave is observed at a more negative potential for α_1 than for α_2 . This evidence constitutes a

supplementary proof of the fact that the belt region of the Wells-Dawson-type structure is the electron transfer preferential zone when these molecules undergo reduction processes.

Table 4.1. Midpoint redox potential (V *vs.* SCE) values for the first three redox process (E'_1 , E'_2 and E'_3) of α_1 and α_2 - $P_2Mo^VI W_{17}$, at pH 3. In parenthesis, the number of electrons accepted in each reduction process.

	E'_1	E'_2	E'_2
	Mo (1e)	W (1e)	W (2e)
α_1 - P_2MoW_{17}	0.42	-0.03	-0.50
α_2 - P_2MoW_{17}	0.25	-0.18	-0.31
ΔE (α_1 - α_2)	0.17	0.15	-0.19

The electrochemical behavior of the tri-Mo-substituted Wells-Dawson polyoxotungstate, α - $[P_2Mo_3^VI W_{15}O_{62}]^{6-}$, has been described before^[10]. Redox steps associated with the oxidation of the Mo centers in the 3-electron reduced species α - $[P_2W_{15}Mo_3O_{62}]^{9-}$ confirmed that the three electrons remained delocalized in the Mo_3O_{13} cap, which gives rise to three identical Mo^V centers. The same behavior is observed with the tri-vanadium derivative, α - $[P_2V_3^V W_{15}O_{62}]^{9-}$, the three V^V centers being reduced to the +IV oxidation state in two very close successive steps, a two-electron one followed by a single-electron one. The reduction of the V centers takes place at more positive redox potentials.

Finally, whatever the position of the substituted Mo^{VI} (or V^V) cation on the belt or on the cap, and whatever their number (1 or 3), they are always preferentially reduced when compared to the W framework and either for 1 or 3 added electrons, respectively. It is interesting to check if in the cases of α - $[P_2Mo_6^VI W_{12}O_{62}]^{6-}$ and α - $[P_2V_6^V W_{12}O_{62}]^{12-}$, the first 6 added electrons are preferentially transferred and delocalized on the 6 Mo^{VI} or V^V centers.

The CV of α - $[P_2Mo_6^VI W_{12}O_{62}]^{6-}$ at pH 3 begins with three well-defined reversible waves that feature the reduction of Mo centers. The first two-electron wave is largely separated from the two subsequent ones, which are also two-electron. Controlled potential coulometry experiments conducted on a solution of α - $[P_2Mo_6^VI W_{12}O_{62}]^{6-}$ at pH 1 with the potential set at -0.35 V *vs.* SCE (i.e. after the first three waves attributed to the reduction of Mo centers)

consumed an electrical charge corresponding to six moles of electrons per mole of α -[P₂Mo₆^{VI}W₁₂O₆₂]⁶⁻. This confirms the observations and assertions made by Contant et al. who established a direct relation between the number of substituted Mo centers on the Wells-Dawson framework and the number of electrons involved in the first reduction steps attributed to them^[1b]. Furthermore, the comparison with the CV of the lacunary species P₂W₁₂ recorded under the same conditions is in total agreement with the assertion that the first six added electrons are transferred to the six Mo^{VI} centers. The same observation is made with the vanadium-containing analogue α -P₂V₆W₁₂. It may now be established as a general rule that, during the reduction of Mo or V-substituted Wells-Dawson polyoxotungstates, added electrons are first transferred to the Mo or V centers, whatever their number and position. When all of the Mo or V centers are one-electron reduced each, further reduction involves the W framework. Mo and V centers are the initial sites of electron transfer in Wells-Dawson substituted polyoxotungstates. Obviously, it is hard to imagine that these electrons will be trapped in Mo or V orbitals.

4.3 Results and discussion

Some of us recently published a theoretical work showing that DFT calculations including solvent effects are able to reproduce accurately the electrochemical trends for mixed-metal POMs, notably the redox potential differences between compounds^[11]. This firm ground allows us to make use of the DFT to rationalize the present experimental CV data. The main computational results are the REs listed in Table 4.2, which will be referred to the parent compound P₂W₁₈ (RE = -4.234 eV) during the following discussion. It is clear that most REs are more negative than -4.234 eV, indicating the presence of stronger oxidant species, in line with the reduction potentials discussed above. We want to stress that the systems have been modeled in conditions of no protonation, which is not always the most realistic approach. This fact is taken into account in the analysis whenever required. In the present section we make a theoretical analysis of the distribution of the extra electrons among the metal centers and how this is related with electrochemical measurements, making a special emphasis in the different oxidizing power of the α_1 and α_2 isomers of P₂MoW₁₇.

Table 4.2. Computed first and second reduction energies (in eV) for the Wells-Dawson compounds discussed in this chapter. In parenthesis, values with respect to P_2W_{18} (in eV).

	RE₁	RE₂
P_2W_{18}	-4.234 (0.0)	-
$\alpha_2\text{-}P_2W_{17}$	-2.590 (-1.644)	-
$\alpha_1\text{-}P_2MoW_{17}$	-4.594 (+0.360)	-3.767 (-0.467)
$\alpha_2\text{-}P_2MoW_{17}$	-4.426 (+0.192)	-3.586 (-0.648)
$\alpha\text{-}P_2Mo_3W_{15}$	-4.495 (+0.261)	-
$\alpha\text{-}P_2Mo_6W_{12}$	-4.610 (+0.376) (2e) ^a	-
$\alpha_1\text{-}P_2VW_{17}$	-4.673 (+0.439)	-3.298 (-0.936)
$\alpha_2\text{-}P_2VW_{17}$	-4.576 (+0.342)	-3.255 (-0.979)

^a Two-electron process.

4.3.1 Calculations on P_2W_{18} , $\alpha_2\text{-}P_2W_{17}$, $\alpha_2\text{-}P_2Mo_3W_{15}$ and $\alpha\text{-}P_2Mo_6W_{12}$

The plenary P_2W_{18} system is an oxidizing species as strong as, for instance, the Keggin anion, $[PW_{12}O_{40}]^{3-}$, despite carrying a higher negative charge owing to the fact that the charge -6 is distributed over a larger structure. For P_2W_{18} , the first metal electron(s) occupy the belt region, which is more electron attracting than the cap regions. Compared to it, the lacunary $\alpha_2\text{-}P_2W_{17}$ system is more difficult to reduce, with a RE being 1.6 eV less favorable (in non-protonated form) than for P_2W_{18} , a fact arising from the large negative charge of -10 . However, the electrochemical measurement gives a smaller difference between the reduction waves of these two compounds. In the conditions of measurement, $\alpha_2\text{-}P_2W_{17}$ is protonated so its total absolute charge is less negative than -10 , explaining the theoretically predicted value for $\alpha_2\text{-}P_2W_{17}$. Inspection of the molecular orbital occupied by the first incoming electron shows that it is also delocalized over the equatorial (belt) region.

As shown in Table 4.2, $\alpha\text{-}P_2Mo_3W_{15}$ and the mono-substituted $\alpha_2\text{-}P_2MoW_{17}$ compounds have similar REs, the former being 70 meV more negative. The presence of the Mo_3 unit in one of the caps allows for some degree of electron delocalization after reduction and, consequently, a more favorable process than

the extra electron being more localized in a single Mo^{V} site. The CV measurements give a difference of 35 mV at pH 3 between the mentioned compounds. The atomic populations taken from DFT calculations show that each Mo in the cap retains the same amount of the extra electron by topological equivalence, with some participation of the nearest W neighbors.

In $\alpha\text{-P}_2\text{Mo}_6\text{W}_{12}$, the ellipsoidal Mo_6 framework can favor delocalization of extra electron(s) even more than in the above-mentioned $\alpha\text{-P}_2\text{Mo}_3\text{W}_{15}$ system. For the DFT calculations we have taken into consideration the experimental fact that the first reduction wave is a 2e process. To obtain computationally a RE comparable with the position of the first reduction CV wave, a 2e-wave, we computed the 2e-reduced and the oxidized forms and therefore obtained -4.610 eV as the value to be compared with the first midpoint potential of 0.465 V *vs.* SCE. The theoretical value is in good agreement with the measurements since it is the most negative RE of the series, slightly more negative than the RE obtained for the 1e-reduction of $\alpha_1\text{-P}_2\text{MoW}_{17}$. The more advantageous reduction in the hexamolybdate derivative is a consequence of electron delocalization observed in the calculations. DFT results also suggest that the first electrochemically-injected electrons are confined to the four belt molybdenum atoms with the participation of some neighboring belt W centers. We also computed the hypothetical 1e-reduction process ($\alpha\text{-P}_2\text{Mo}_6\text{W}_{15}^{6-} + e \rightarrow \alpha\text{-P}_2\text{Mo}_6\text{W}_{15}^{7-}$), obtaining atomic spin populations of 0.25 electrons per belt-Mo and 0.0 for cap-Mo atoms, and therefore reinforcing the idea that the first electron(s) is (are) delocalized over the belt positions only, leaving the two cap Mo centers fully oxidized. These data put in evidence the importance of delocalization on the electrochemical properties of POMs.

4.3.2 Calculations on α_1 and $\alpha_2\text{-P}_2\text{MoW}_{17}$

First reduction process. The molybdenum mono-substituted Wells-Dawson anions, $\text{P}_2\text{MoW}_{17}$, deserve a detailed analysis since they lead to interesting conclusions. Besides the well-known fact that Wells-Dawson compounds containing Mo are more oxidant than P_2W_{18} , the position of Mo within the structure plays a crucial role in the overall oxidizing power, not only with respect to the first reduction process but also in the second and third ones. In the cap-substituted α_2 isomer there is a *competition* for the first incoming electron between the Mo^{VI} atom, in a polar position, and the belt W atoms. Such competition derives from two opposing facts: (i) chemical: the empty orbitals of Mo^{VI} have lower energy compared to the W^{VI} ones by nature, and

(ii) topological: the empty belt orbitals are lower in energy than the empty cap orbitals. These factors concur in our DFT results showing that the cap-Mo^{VI/V} process is 440 mV more favorable than the belt-W reduction for α_2 -P₂MoW₁₇. Thus, the first metal electron is localized in the cap and it can be concluded that the chemical factor prevails. The other positional isomer of the monosubstituted compound, α_1 -P₂MoW₁₇, behaves similarly although a larger degree of electron delocalization can be observed in the 1e-reduced form based on atomic population analysis. The main difference with respect to the α_2 form is that the chemical and topological factors add up since Mo is situated in the reduction-favorable belt region. This has implications like the degree of localization of the extra electron in the mono-reduced species. For α_2 -P₂MoW₁₇, present calculations show that Mo (cap position) retains about 82% of the extra electron, whereas it decreases to 77% when Mo is in the belt site (α_1 -P₂MoW₁₇). Since electron delocalization usually gives extra stabilization to reduced forms in POMs, the computed 1e-reduction process (P₂MoW₁₇⁶⁻ + e → P₂MoW₁₇⁷⁻) is more favorable by ~170 meV in the α_1 form, reproducing the experimental difference of 170 mV (see Table 4.1). Thermodynamically, the first 1e-reduction process is more favorable for the belt-substituted compound, where the chemical and structural effects add up to favor reduction.

The oxidizing power of α_1/α_2 -P₂MoW₁₇ must also be compared with that of α -P₂Mo₃W₁₅. DFT calculations, in agreement with CV measurements, show that α_1 -P₂MoW₁₇ is a stronger oxidant than α -P₂Mo₃W₁₅ by about 100 mV (see Table 4.2). The advantageous delocalization in the Mo₃ polar group experienced by the metal electron in the 1e-reduced α -P₂Mo₃W₁₅ system cannot be on a par with the extra stabilization produced in the Mo belt position of α_1 -P₂MoW₁₇. The fact that α_2 -P₂MoW₁₇ is slightly less oxidant than α -P₂Mo₃W₁₅, both being cap-substituted compounds, is easily explained by the enhanced electron delocalization occurring in the latter compound.

To end up with the discussion on the first reduction processes, we add a comment on the mono-substituted vanadate, P₂VW₁₇ since it helps rationalizing the previous discussion. The relative shift between the first 1e-wave for α_1 and α_2 -P₂VW₁₇ is $\Delta RE = 97$ meV (measured $\Delta E = 89$ mV). This small difference compared with P₂MoW₁₇ is attributed to the more localized nature of the extra electron in reduced vanadotungstates. In other words, V preserves its nature more than Mo when placed in the Wells-Dawson structure and, therefore, its position (cap or belt) is electrochemically *less relevant*. The

computed atomic spin populations for the 1e-reduced α_1 and α_2 tungstovanadates are ~ 1.0 on the V center, a value to be compared with 0.82 and 0.77 per Mo atom in the homologous molybdate compounds. We can thus establish a difference of about 90 meV as the energy change of belt *vs.* cap metal position, not considering delocalization as an extra factor, which we estimate from the one-electron RE difference for α_1/α_2 -P₂VW₁₇. Consequently, larger differences between Res in cap and belt positions in Mo-substituted anions come from the more delocalized nature of the involved orbitals in the belt region. In other words, the ability of an electron to hop from one center to another, larger in Mo than in V, stabilizes the molecular orbital containing that electron and favors reduction. We infer that the extra stabilization of a belt-localized electron compared to the cap-localized case is intimately related with the different degree of electron delocalization in the belt region.

We carried out a complementary calculation to evaluate further the effect of electron delocalization upon the reduction potential. We compare two systems: α_1 -P₂MoW₁₇ and the hypothetical α -P₂Mo₆W₁₂ model with six neighboring Mo atoms in a single belt ring (W₃:Mo₆:W₆:W₃, see Figure 4.4). Both molecules are equally charged and contain the Mo atoms in the equatorial region, thus any difference in their respective REs must come from the number of Mo atoms in each case. If we consider the first reduction as a 1e-process we find a reduction potential difference of 290 meV in favor of α -P₂Mo₆W₁₂. Such a difference can only be attributed to the effect of the enhanced electron delocalization in α -P₂Mo₆W₁₂. A very similar value of 265 meV was recently computed for the Keggin structure^[11]. As a matter of fact, the energies of the LUMOs of the oxidized form for each compound are progressively deeper in energy as the number of implicated Mo atoms increases, namely, the LUMO for α -P₂W₁₂Mo₆ is 120 meV lower in energy than that of α_1 -P₂MoW₁₇. If we look at the atomic spin populations of the 1e-reduced forms, we find that in α_1 -P₂MoW₁₇ the extra electron is delocalized among the Mo atom and two or three vicinal W atoms. In the case of α -P₂Mo₆W₁₂, 80% of the extra electron is delocalized over the Mo₆ ring, and the other 20% among the other W₆ in the belt. The larger the number of metal centers accepting a fraction of the incoming electron, the more favorable the reduction process is. This phenomenon is applicable when comparing α_2 -P₂MoW₁₇ and α -P₂Mo₃W₁₅, for instance, or α_1 -P₂MoW₁₇ and α -P₂Mo₆W₁₂.

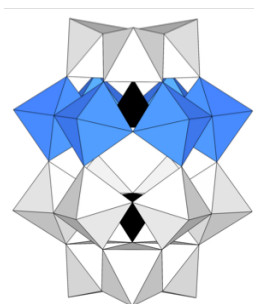


Figure 4.4. Idealized structure of the hypothetical α - $\text{P}_2\text{Mo}_6\text{W}_{12}$ model with six neighboring Mo atoms in a single belt ring. Grey and blue octahedra contain W and Mo atoms in the center, respectively. The black tetrahedra represent the internal PO_4^{3-} units.

Second and third reduction processes. At this point, let us discuss the computational results for the second 1e-reduction process in α_1/α_2 - $\text{P}_2\text{MoW}_{17}$ to complement the CV data. We are especially interested in unraveling the complete electrochemical behavior (first three reduction waves) of α_1 and α_2 - $\text{P}_2\text{MoW}_{17}$, notably the tricky (at least at first sight) relative positions of the second and third waves. Electrochemical data cannot reveal if the second metal electron, supposed to go to the belt region, is mostly localized (Mo^{IV} character) or partially delocalized ($\text{Mo}^{\text{V}}\text{W}_{17}1\text{e}$ character). Having computational evidence for the first 1e-reduction producing Mo^{V} in either isomer, the second electron must go to the fully oxidized W^{VI} belt positions, but at a more negative potential due to the molecular charge increment that the first reduction entails. But what causes the mutual shift of 100 mV of the second wave for each isomer? Why do the second reduction waves not appear at the same potential for both isomers?

In a first step, we computationally reproduced the observed trend. The REs obtained for the $\text{POM}(1\text{e}) + \text{e} \rightarrow \text{POM}(2\text{e})$ process predict that shift to be around 150 meV between the isomers and, thus, we may inspect what is the origin of this phenomenon. We computed the possible solutions for the 2e-reduced systems (Figure 4.5), namely, the unpaired and the paired electron cases represented in Figure 4.6a. Interestingly, at the DFT level, each of these solutions is the most stable for one of the isomers when $M = \text{Mo}$. In α_2 - $\text{P}_2\text{MoW}_{17}$, the unpaired situation is the most stable by 70 meV, indicating that the second electron prefers to delocalize over the W atoms thus avoiding any cap- Mo^{IV} character. On the other hand, the electron-paired solution is 173 meV more stable than the unpaired one in α_1 - $\text{P}_2\text{MoW}_{17}$. In the two cases (α_1 and α_2) the second electron goes to the belt region but in a different manner

and, consequently, with a different energy. The pairing process occurring in α_1 appears as a favorable one, with some Mo^{IV} character as depicted in the scheme, with respect to the non-paired situation in α_2 . In α_1 , the presence of one electron in the belt Mo^{V} does not hinder the second one from occupying the same region, but it actually favors it by e-e pairing. In α_2 , provided that the second electron is forced to go to the belt region, the second reduction is just favored by the lower e-e electrostatic repulsion that, from the present data, appears to be a weaker advantage than e-e pairing. The electron pairing argument is reinforced by the well-known and proved fact that the 2e-reduced P_2W_{18} species is strongly diamagnetic^[12]. The *character* of an electron can be measured by inspection of the molecular orbital it occupies, and also by atomic populations. Both of them coincide in the more delocalized nature of the belt electrons with or without Mo.

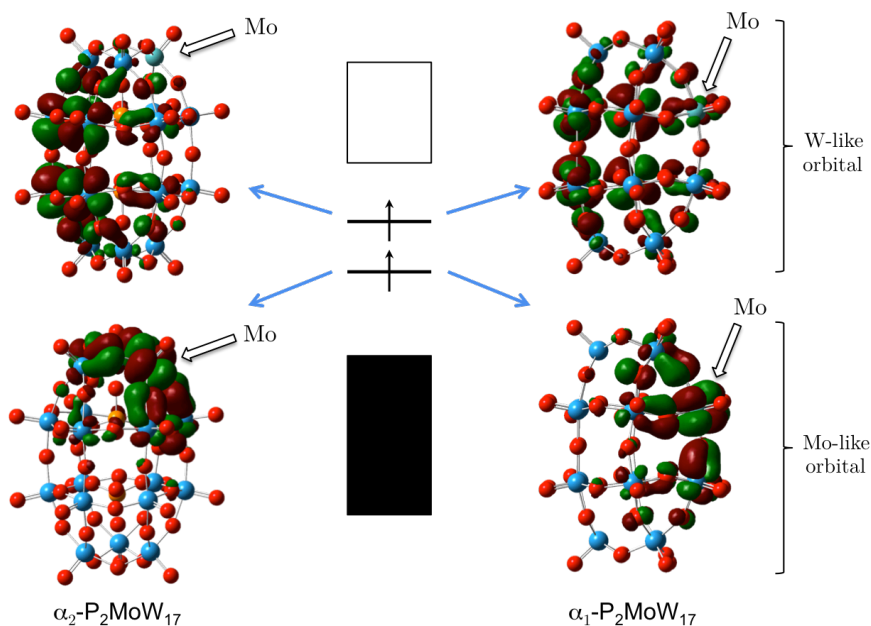


Figure 4.5. Molecular orbital representation for 2e-reduced $\alpha_2\text{-P}_2\text{MoW}_{17}$ (left) and $\alpha_1\text{-P}_2\text{MoW}_{17}$ compounds. Black and white blocks represent filled and empty metal-like and oxygen-like molecular orbitals, respectively.

Present calculations show that, after the second 1e-reduction, the $\alpha_2\text{-P}_2\text{Mo}^{\text{V}}\text{W}_{17}1\text{e}$ situation is the most stable by an energy difference of 70 meV. However, things are different in the α_1 isomer, for which an important Mo^{IV} character is acknowledged. As shown in Table 4.2, the RE difference between the second 1e-processes ($\alpha_1 - \alpha_2$) agrees with the experimental results and

justify them by the different character of the second electron in either isomer in favor of α_1 . Thus, the mentioned facts suggest a possible competition between two factors, namely (i) the unfavorable e-e electrostatic repulsion, and (ii) the favorable electron pairing. Each isomer is characterized by one dominating factor. In α_1 , the first electron already occupies a part of the belt region (Mo^{V} and some W^{V} character of the vicinal atoms). Although the second electron experiences the repulsive presence of the first one, they can pair and thus stabilize the couple (see Figure 4.7, left diagram). On the other hand, the α_2 isomer has the first electron trapped in the cap region, with the belt region free of electron density prior to the second reduction and willing to capture some. This electrostatic advantage with respect to the α_1 isomer prevents electron pairing in the cap region. We may deduce that, as long as the region is sufficiently large for delocalization, the first two electrons will be paired and stabilized. This explanation is schematically depicted in Figure 4.7.

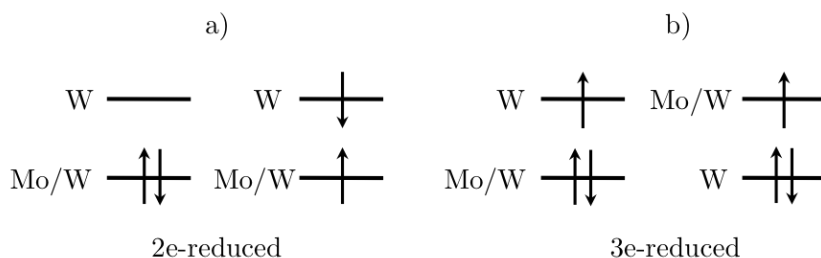


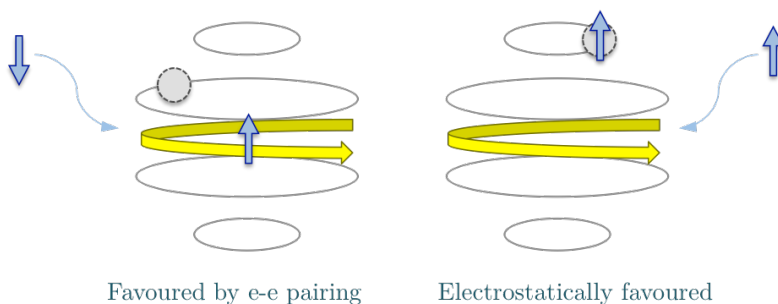
Figure 4.6. Schematic view of the most plausible electron distribution for (a) the two-electron reduced and (b) the three-electron reduced forms of $\text{P}_2\text{MoW}_{17}$. When two electrons occupy the molecular orbital designated Mo/W, some Mo^{IV} character is present, whereas one electron in Mo/W-like orbital implies Mo^{V} .

It must be pointed out that for P_2VW_{17} the present discussion stands, but giving a different final result. Since the first 1e-reduction in the vanadotungstate produces a highly localized V^{IV} electron, the second one has hardly a chance of pairing with it to give V^{III} (see Table 4.2). This would be a too energetic situation compared to the second electron delocalized over some tungstens. Thus, the electrostatic repulsion will be similar irrespective of the position of the initial electron (cap V^{IV} or belt V^{IV}). As a result, the second one-electron waves are much closer between α_1 and α_2 isomers: the computed values differ by 33 meV only. This is an extra evidence of how important delocalization is to electrochemistry.

Finally, the third reduction wave, although it is pH dependent, may be justified using the above arguments. At the stage of 2e-reduced anions, the

situation favors reduction of α_2 at a more positive potential than α_1 since the former isomer contains two unpaired electrons, one in the cap (Mo^{V}) and one in the belt (delocalized W^{V} character). The third electron can pair with one of these, the one in the belt being the most accessible one if we combine the electrostatic and pairing factors. Concerning α_1 , no advantages with respect to α_2 are envisaged since the belt region is highly electron-populated by two paired electrons. Since the third electron is forced to go to the belt, an electron pairing process is not possible any more and a notable electrostatic repulsion will force this process to be less exothermic than for the α_2 partner. The schematic view of the molecular orbital occupations for 3e-reduced anions is shown in Figure 4.6b, where the left-hand situation implies some Mo^{IV} character, whereas the right-hand one corresponds to Mo^{V} .

2nd reduction process:



3rd reduction process:

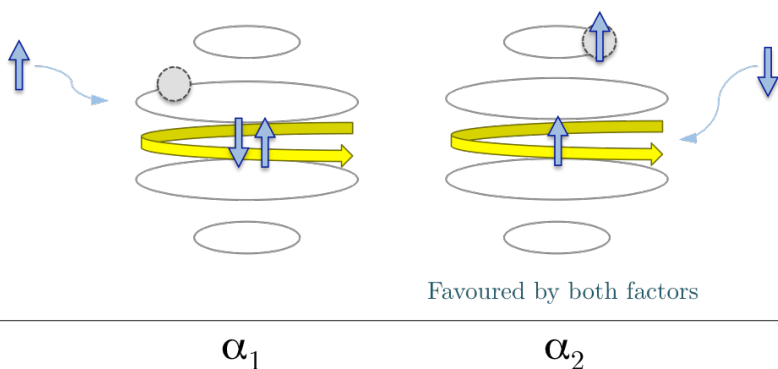


Figure 4.7. Representation of the 2nd and 3rd reduction processes taking place in the α_1 and α_2 - $\text{P}_2\text{MoW}_{17}$ isomers (Mo atoms are represented by grey circles), and the factors favoring them in each case. The four 3:6:6:3 loops of metal atoms in the Wells-Dawson structure are simplified to thin black lines. Black arrows are electrochemically added electrons, and yellow curved arrows represent the delocalization nature of the belt electrons.

4.4 Conclusions

Theoretical evidence has been gathered to explain the relative positions of the first, second and third reduction waves in α_1/α_2 -P₂MW₁₇ isomers with M = Mo or V. After having analyzed the experimental and theoretical data for the cited compounds, some relevant facts arise that may help to rationalize the redox behavior of POMs in general.

The four compounds α_1 and α_2 -[P₂MoW₁₇O₆₂]⁶⁻, α -[P₂Mo₃W₁₅O₆₂]⁶⁻ and α -[P₂Mo₆W₁₂O₆₂]⁶⁻ have been synthesized and characterized by several physico-chemical techniques. Their electrochemical behavior has been compared to that of their homologues containing vanadium, α_2 -[P₂V^VW₁₇O₆₂]⁷⁻, α -[P₂V₃^VW₁₅O₆₂]⁹⁻ and α -[P₂V₆^VW₁₂O₆₂]¹²⁻, and also to that of their parent compounds, that is the saturated species α -[P₂W₁₈O₆₂]⁶⁻ and the lacunary derivative α_2 -[P₂W₁₇O₆₁]¹⁰⁻. This comparative study has allowed, in each case, to identify clearly the redox processes assignable to the Mo^{VI} centers from those attributable to the W^{VI} centers.

The DFT calculations and the experimental observations mentioned above lead to the same conclusions: the Mo^{VI} centers present in the molecules α_1 and α_2 -[P₂MoW₁₇O₆₂]⁶⁻, α -[P₂Mo₃W₁₅O₆₂]⁶⁻ and α -[P₂Mo₆W₁₂O₆₂]⁶⁻, are all reduced first, irrespective of their position or number, and just then the extra electrons are directed towards the W^{VI} centers. We tried to recognize which factors play a role, and which is their relative importance, on the redox potentials of Wells-Dawson anions. DFT calculations carried out on the title compounds have reproduced the general trends of oxidizing power measured by CV. The differences observed between the studied compounds may be assigned to a few chemical or structural factors. Taking P₂W₁₈ as the reference (reduction potential $E = 0.0$ V for convenience), the computed reduction energies of all the Mo-containing compounds are more negative. In the case of α_1 and α_2 -P₂MoW₁₇, the computed reduction potentials are 360 and 192 mV more positive, respectively, than for P₂W₁₈, following the experimental observations. Replacing more W atoms by Mo (up to 3 or 6 adjacent Mo centers) results in a larger degree of delocalization of the extra metallic electron(s) and an enhanced exothermicity of the reduction process (a positive shift of reduction potentials) since the electron-accepting molecular orbitals are more stable as they have contributions from more centers. This assumption allows explaining that the cap-substituted α -P₂Mo₃W₁₅ anion is more oxidant than α_2 -P₂MoW₁₇.

In a similar fashion, the α - $\text{P}_2\text{Mo}_6\text{W}_{12}$ anion is more oxidant than any of the other combinations presented here, notably since two factors add up: the presence of Mo atoms in the belt region, and the synergy of multiple vicinal Mo atoms that boost electron delocalization. The latter goes in favor of an increasing oxidizing power.

The most relevant and general conclusion, which might have a repercussion beyond just redox properties, is the competition of three factors when one or several d metal electrons meet in the Wells-Dawson structure in what concerns stability: (i) the favorable electron delocalization, (ii) the unfavorable e-e electrostatic repulsion, and (iii) the favorable electron pairing. These factors, schematically summarized in Figure 4.7, explain that the second reduction wave occurs at more positive potentials in α_1 than in α_2 - $\text{P}_2\text{MoW}_{17}$, and also why the third electron transfers at a less negative potential in α_2 , reversing the behavior for the first and second waves. In P_2VW_{17} derivatives, the nature of the first d electron is more localized because of the stronger oxidizing character of V^{V} . Thus, the potentials and also the computed REs for the second reduction of either isomer are more similar to each other than for $\text{M} = \text{Mo}$. This may be explained by the lack of electron delocalization in mono-reduced $\text{P}_2\text{V}^{\text{IV}}\text{W}_{17}$ systems.

4.5 Computational details

DFT calculations were performed on a series of compounds using the Gaussian 09 suite of programs^[13]. The geometries of all the structures were optimized in the oxidized and reduced states for the sake of accuracy in the calculation of reduction energies. We applied the B3LYP hybrid functional^[14] with double- ζ quality basis set supplemented with polarization functions (d for oxygen, f for transition metals). For heavy elements, we used the standard double-zeta basis set with LANL pseudopotentials of Hay and Wadt^[15]. The calculations include PCM^[16] to account for the stabilizing effects of an aqueous solution with a dielectric constant $\epsilon = 78.4$. The solute cavity was created using a scaled Van der Waals surface and a grid of 5 points per \AA^2 . The atomic radii correspond to the Universal Force Field parameters. We applied the spin-unrestricted formalism to compute the electron density of open-shell molecules. Atomic spin densities and charges were obtained by means of the Mulliken procedure.

4.6 References

- [1] a) M. Abbessi, R. Contant, R. Thouvenot, G. Hervé, *Inorg. Chem.* **1991**, *30*, 1695; b) R. Contant, M. Abbessi, R. Thouvenot, G. Hervé, *Inorg. Chem.* **2004**, *43*, 3597; c) R. Contant, J.-P. Ciabrini, *J. Inorg. Nucl. Chem.* **1981**, *43*, 1525; d) R. Massart, R. Contant, J. M. Fruchart, J. P. Ciabrini, M. Fournier, *Inorg. Chem.* **1977**, *16*, 2916.
- [2] a) E. Papaconstantinou, M. T. Pope, *Inorg. Chem.* **1967**, *6*, 1152; b) M. T. Pope, E. Papaconstantinou, *Inorg. Chem.* **1967**, *6*, 1147; c) M. T. Pope, G. M. Varga, *Inorg. Chem.* **1966**, *5*, 1249; d) G. M. Varga, E. Papaconstantinou, M. T. Pope, *Inorg. Chem.* **1970**, *9*, 662; e) E. Papaconstantinou, M. T. Pope, *Inorg. Chem.* **1970**, *9*, 667; f) B. Keita, L. Nadjo, *J. Mol. Catal. A: Chem.* **2007**, *262*, 190; g) M. Sadakane, E. Steckhan, *Chem. Rev.* **1998**, *98*, 219; h) I. A. Weinstock, *Chem. Rev.* **1998**, *98*, 113; i) H. Wang, S. Hamanaka, Y. Nishimoto, S. Irle, T. Yokoyama, H. Yoshikawa, K. Awaga, *J. Am. Chem. Soc.* **2012**, *134*, 4918.
- [3] a) C. Sanchez, J. Livage, J. P. Launay, M. Fournier, *J. Am. Chem. Soc.* **1983**, *105*, 6817; b) C. Sanchez, J. Livage, J. P. Launay, M. Fournier, Y. Jeannin, *J. Am. Chem. Soc.* **1982**, *104*, 3194.
- [4] a) J. P. Ciabrini, R. Contant, J. M. Fruchart, *Polyhedron* **1983**, *2*, 1229; b) J. B. Tommasino, R. Contant, J. P. Michaut, J. Roncin, *Polyhedron* **1998**, *17*, 357.
- [5] a) N. Casañ-Pastor, L. C. W. Baker, *J. Am. Chem. Soc.* **1992**, *114*, 10384; b) M. Kozik, N. Casañ-Pastor, C. F. Hammer, L. C. W. Baker, *J. Am. Chem. Soc.* **1988**, *110*, 7697; c) M. Kozik, C. F. Hammer, L. C. W. Baker, *J. Am. Chem. Soc.* **1986**, *108*, 7627.
- [6] a) B. Keita, A. Belhouari, L. Nadjo, R. Contant, *J. Electroanal. Chem.* **1998**, *442*, 49; b) B. Keita, F. Girard, L. Nadjo, R. Contant, J. Canny, M. Richet, *J. Electroanal. Chem.* **1999**, *478*, 76; c) B. Keita, I. M. Mbomekallé, L. Nadjo, R. Contant, *Eur. J. Inorg. Chem.* **2002**, *2002*, 473.
- [7] a) B. Keita, I. M. Mbomekallé, L. Nadjo, P. de Oliveira, A. Ranjbari, R. Contant, *C. R. Chimie* **2005**, *8*, 1057; b) D. McGregor, B. P. Burton-Pye, I. M. Mbomekallé, P. A. Aparicio, S. Romo, X. López, J. M. Poblet, L. C. Francesconi, *Inorg. Chem.* **2012**, *51*, 9017; c) D. McGregor, B. P. Burton-Pye, R. C. Howell, I. M. Mbomekallé, W. W. Lukens, F. Bian, E. Mausolf, F. Poineau, K. R. Czerwinski, L. C. Francesconi, *Inorg. Chem.* **2011**, *50*, 1670.
- [8] B. Keita, *J. Electroanal. Chem.* **1999**, *478*, 76.
- [9] X. López, J. J. Carbó, C. Bo, J. M. Poblet, *Chem. Soc. Rev.* **2012**, *41*, 7537.
- [10] M. Kozik, C. F. Hammer, L. C. W. Baker, *J. Am. Chem. Soc.* **1986**, *108*, 2748.
- [11] P. A. Aparicio, X. López, J. M. Poblet, *J. Mol. Eng. Mater.* **2014**, *2*, 1440004.
- [12] N. Suaud, A. Gaita-Ariño, J. M. Clemente-Juan, E. Coronado, *Chem. Eur. J.* **2004**, *10*, 4041.
- [13] Gaussian 09, Revision A.02, M. J. Frisch, G. W. Trucks, H. B. Schlegel, G. E. Scuseria, M. A. Robb, J. R. Cheeseman, G. Scalmani, V. Barone, B. Mennucci, G. A. Petersson, H. Nakatsuji, M. Caricato, X. Li, H. P. Hratchian, A. F. Izmaylov, J.

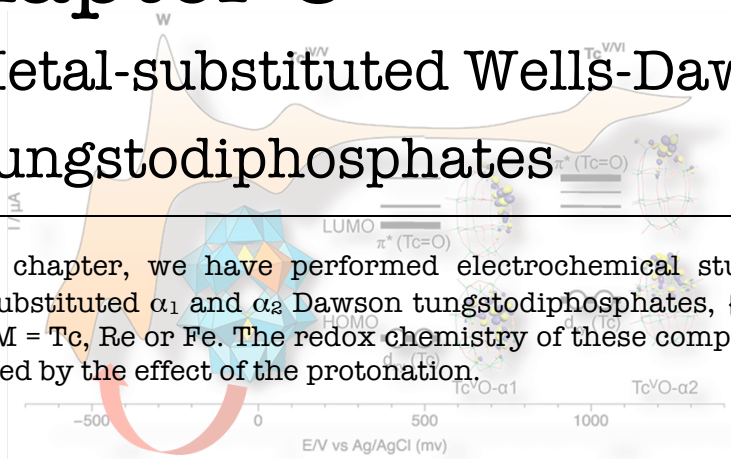
Bloino, G. Zheng, J. L. Sonnenberg, M. Hada, M. Ehara, K. Toyota, R. Fukuda, J. Hasegawa, M. Ishida, T. Nakajima, Y. Honda, O. Kitao, H. Nakai, T. Vreven, J. Montgomery, J. A., J. E. Peralta, F. Ogliaro, M. Bearpark, J. J. Heyd, E. Brothers, K. N. Kudin, V. N. Staroverov, R. Kobayashi, J. Normand, K. Raghavachari, A. Rendell, J. C. Burant, S. S. Iyengar, J. Tomasi, M. Cossi, N. Rega, N. J. Millam, M. Klene, J. E. Knox, J. B. Cross, V. Bakken, C. Adamo, J. Jaramillo, R. Gomperts, R. E. Stratmann, O. Yazyev, A. J. Austin, R. Cammi, C. Pomelli, J. W. Ochterski, R. L. Martin, K. Morokuma, V. G. Zakrzewski, G. A. Voth, P. Salvador, J. J. Dannenberg, S. Dapprich, A. D. Daniels, Ö. Farkas, J. B. Foresman, J. V. Ortiz, J. Cioslowski, D. J. Fox, Gaussian, Inc., Wallingford CT, 2009.

- [14] a) C. T. Lee, W. T. Yang, R. G. Parr, *Phys. Rev. B* **1988**, *37*, 785; b) P. J. Stephens, F. J. Devlin, C. F. Chabalowski, M. J. Frisch, *J. Phys. Chem.* **1994**, *98*, 11623.
- [15] P. J. Hay, W. R. Wadt, *J. Chem. Phys.* **1985**, *82*, 270.
- [16] S. Miertus, E. Scrocco, J. Tomasi, *Chem. Phys.* **1981**, *55*, 117.

Chapter 5

Metal-substituted Wells-Dawson Tungstodiphosphates

In this chapter, we have performed electrochemical studies on the mono-substituted α_1 and α_2 Dawson tungstodiphosphates, $\{P_2MW_{17}O_{62}\}$, where $M = Tc, Re$ or Fe . The redox chemistry of these compounds can be explained by the effect of the protonation.



Related publications:

D. McGregor, B. P. Burton-Pye, I. M. Mbomekallé, P. A. Aparicio, S. Romo, X. López, J. M. Poblet, L. C. Francesconi, *Inorg. Chem.* **2012**, *51*, 9017.

N. Vilà, P. A. Aparicio, F. Sécheresse, J. M. Poblet, X. López, I. M. Mbomekallé, *Inorg. Chem.* **2012**, *51*, 6129.

5.1 Introduction and objectives

The applications of Wells-Dawson compounds as redox or acid catalysts have been deeply studied^[1]. Moreover, many efforts have been dedicated to study the electrochemistry of these compounds. The ability to accept and release electrons can be controlled by applying an external potential. Electrochemical studies showed that Wells-Dawson anions are reduced through two-electron steps without degradation of the structure. The process depends on the pH of the solution since the reduction is usually accompanied by protonation. The reduction process performed in acidic media shifts the redox waves to more negative potentials and split the two-electron waves into two one-electron waves^[1a]. In addition Prof. M. T. Pope demonstrated that Wells-Dawson polyoxoanions can accept up to six electrons both in neutral or acidic media^[2]. According to his spectroscopic studies, the reduction of these compounds takes place in one of the twelve equatorial metal atoms of the belt region.

Removal of one W=O unit in the α -[P₂W₁₈O₆₂]⁶⁻ compound gives rise to the lacunary derivatives α_1 and α_2 -[P₂W₁₇O₆₁]¹⁰⁻, depending if the removal of the metal takes place in the belt or in the cap region. The resulting vacancies provide excellent binding sites for metal atoms and have different electronic properties^[3] (Figure 5.1). These distinct features can be exploited to probe both the coordination and the redox characteristics of metals incorporated into the binding sites.

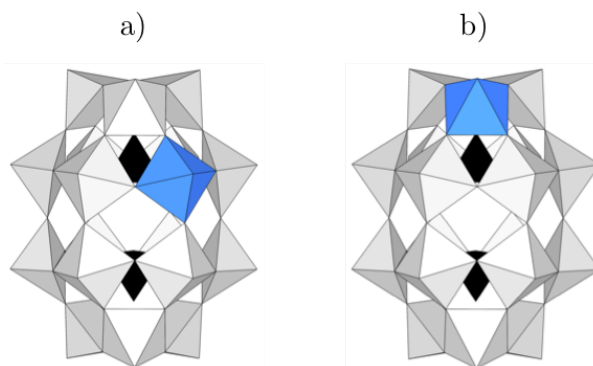


Figure 5.1. Polyhedral representation of (a) α_1 and (b) α_2 -{P₂MW₁₇O₆₂} anions. Grey octahedra represent WO₆ groups, blue octahedra represent MO₆ groups and black tetrahedra represent the internal anions.

Our objective is to provide a more profound theoretical view on the redox properties and the relative stability of the α_1 and α_2 mono-substituted Dawson tungstodiphosphates, $\{P_2MW_{17}O_{62}\}$, where $M = Tc, Re$ or Fe . We have studied the Tc and Re compounds jointly due to their similar properties and oxidation states, from IV to VII (Point 5.2). On the other hand, the Fe structures have different oxidation states (II and III) and it is obtained experimentally only with an aqua terminal group (Point 5.3). DFT calculations give a complete and sufficiently accurate theoretical view of the molecular properties at a reasonable cost, providing valuable data such as the relative stability of compounds, the oxidation states, etc.^[4]. We also want to explain how the redox properties of the isomers depend on protonation. The molecular orbital analysis helps understanding the electrochemical behavior observed in the experimental studies.

5.2 Tc and Re compounds

5.2.1 Experimental background

The isotope ^{99}Tc (half-life = $2.1 \cdot 10^5$ years) is a major byproduct in the nuclear fuel cycle and constitutes ~6% of the fission yield. It is also found in radioactive waste tanks from defense activities of the 1940s and 1950s. In some cases, because of tank leakage, it is found in the environment (in water, soils and fuel reprocessing centers). Regardless of the source, separation and storage of the long-lived ^{99}Tc in an appropriate and stable waste-form is an important issue that needs to be addressed.

^{99}Tc possesses extensive redox chemistry with compounds found in oxidation states of -1 to +7. ^{99}Tc is often found in its highest oxidation state Tc(VII), where it exists primarily as the TcO_4^- anion. This anion is the most stable form of Tc under basic conditions and is extremely mobile within the environment. Most waste sequestration and immobilization strategies involve reduction of TcO_4^- to Tc(IV) in the form of $TcO_2 \cdot nH_2O$ that is relative immobile. To formulate robust and manageable waste remediation strategies it is important to understand the fundamental factors that influence the redox characteristics and stability of Tc within potential storage materials. Considering metal oxide solid-state materials as potential storage matrixes for Tc, we want to examine polyoxometalates as models for trapping agents.

On the other hand, Re (the 3rd row congener of Tc) is widely used as a non-radioactive surrogate for Tc because it possesses similar atomic radii, the same number of d electrons available for bonding and a similarly wide range of oxidation states. However, there are subtle but distinct differences between the reactivity, stability and redox behavior of Tc and Re complexes^[5]. These differences can impact the efficacy of Re as a true chemical surrogate for Tc. Examining both Tc and Re in tandem presents the opportunity to identify the similarities and differences of these elements.

The group of Prof. L. Francesconi (Hunter College of the City University of New York) has studied the electrochemical behavior of α_1 and $\{\alpha_2\text{-MP}_2\text{W}_{17}\text{O}_{62}\}$, where M is Tc or Re. The cyclic voltammetry is a powerful method that can be used to identify the α_1 and α_2 isomers, as Nadjjo and co-workers reported^[6]. With the aim to probe the effect of protonation on the Tc(V) and Re(V) in the α_1 and α_2 frameworks, they performed an electrochemical study as a function of pH comparing the $[\alpha_1\text{-Tc}^{\text{V}}\text{OP}_2\text{W}_{17}\text{O}_{61}]^{5-}$ ($\alpha_1\text{-Tc}^{\text{V}}\text{O}$), $[\alpha_2\text{-Tc}^{\text{V}}\text{OP}_2\text{W}_{17}\text{O}_{61}]^{5-}$ ($\alpha_2\text{-Tc}^{\text{V}}\text{O}$), $[\alpha_1\text{-Re}^{\text{V}}\text{OP}_2\text{W}_{17}\text{O}_{61}]^{5-}$ ($\alpha_1\text{-Re}^{\text{V}}\text{O}$) and $[\alpha_2\text{-Re}^{\text{V}}\text{OP}_2\text{W}_{17}\text{O}_{61}]^{5-}$ ($\alpha_2\text{-Re}^{\text{V}}\text{O}$) complexes to the free α_1 and α_2 ligands. A summary of the reduction potentials as a function of pH for the different compounds can be found in Figure 5.2.

There are two reversible processes attributed to tungsten reduction/oxidation within the α_1 and α_2 POMs. They studied the electrochemical behavior of the α_1 and α_2 lacunaries in the first place. Specifically, these waves can be accredited to two successive two-electron redox couples. The reduction is favored to α_1 at lower pH values. For the first reduction, the shift toward more negative potentials, with increasing pH, is more pronounced in the α_2 than in the α_1 ligand. However, the second reduction in α_1 always occurs at a more negative potential than the corresponding reduction in α_2 , under all available pH conditions. At pH values of 0 and 1, the first tungsten reduction waves for α_1 occur at more negative values than those for α_2 . At pH = 3 these reduction waves are similar (+5 mV difference) and at pH values of 5 and 7 the first tungsten reduction of the α_1 ligand occurs at a more positive potential than that of α_2 . The experimental results indicate that at pH values below 3, the α_2 ligand is more easily reduced than the α_1 ligand, meanwhile at pH values of 3 and above the reduction of the α_1 is more easily achieved than the corresponding reduction for the α_2 ligand.

A comparison of the cyclic voltammetry of α_1 -Tc^VO to the free α_1 ligand shows that the two reductions are attributed to the two one-electron Tc^{IV}/Tc^V and Tc^V/Tc^{VI} redox processes. The redox waves assigned to the Tc^V/Tc^{VI} process are observed to remain consistently impervious to changes in pH. The shift observed for the Tc^V/Tc^{IV} reduction couples toward more negative reduction potentials with increasing pH means that the reduction of Tc^V to Tc^{IV} in the α_1 vacancy is more easily achieved in acidic medium. The ease of reduction at low pH can be attributed to an increase in the number of protons, because they can stabilize the Tc-O⁻ ion that forms upon reduction.

For the α_2 -Tc^VO, the one-electron Tc^V/Tc^{VI} redox process occurs at positive potential and in the negative potential region they observed two reductions that correspond to the Tc^V/Tc^{IV} and Tc^{IV}/Tc^{III} redox processes, by comparison to the free α_2 ligand. The reduction and oxidation waves for the Tc^V/Tc^{VI} couple remain largely unaffected by changes in pH, while the redox couples in the negative potential region show a general shift toward more negative potential values with increasing pH. The trend of more negative reduction potential with increasing pH for the Tc metal center within the α_2 ligand means that the reduction of Tc in the α_2 vacancy is more easily achieved in acidic medium. The ease of reduction at low pH may once again be attributed to an increase of the number of protons. This behavior corroborates what has been found in the literature. For example, Ortega *et. al.*^[7] have observed a similar trend for {SiReW₁₁O₄₀}. In both cases the metal substituted into the lacunary POM showed a shift in reduction potentials for both the M^V/M^{IV} and M^{IV}/M^{III} redox processes toward more negative values with increasing pH.

The comparison between α_1 -Tc^VO and α_2 -Tc^VO reveals that the Tc^V/Tc^{IV} redox couple in α_1 isomer occurs at a more positive potential by ~150 mV at all possible pH values. This means that, independently of protonation effects, Tc in the α_1 vacancy is always more easily reduced than in the α_2 vacancy. Therefore, the first reduction takes place at the equatorial position and transition metal substituted into the belt site will be more readily reduced than those substituted in the cap.

An equivalent electrochemical study was carried out for the Re compounds. The comparison of the α_1 -Re^VO and the α_1 ligand reveal that the two reversible redox processes have been attributed to the Re^V/Re^{IV} and Re^{IV}/Re^{III} couples. As observed with α_1 -Tc^VO, both the reduction and oxidation waves for the Re^V/Re^{VI} couple remains largely unaffected by changes in pH, as the

$\text{Re}^{\text{VI}}/\text{Re}^{\text{VII}}$ redox couple. They observed the general trend of more negative reduction potentials with increasing pH for the Re metal center within the α_1 ligand, which means that the reduction of Re in the α_1 vacancy is more easily achieved in acidic medium.

A comparison of $\alpha_2\text{-Re}^{\text{VO}}$ with the free α_2 ligand shows that the redox couples in the positive potential region are attributed to the two one-electron $\text{Re}^{\text{V}}/\text{Re}^{\text{VI}}$ and $\text{Re}^{\text{VI}}/\text{Re}^{\text{VII}}$ processes. There is a shift of all redox couples present in the negative potential region toward more negative potential values as the pH increases. The potentials for the $\text{Re}^{\text{V}}/\text{Re}^{\text{VI}}$ and $\text{Re}^{\text{VI}}/\text{Re}^{\text{VII}}$ redox processes are found to be unchanged with pH.

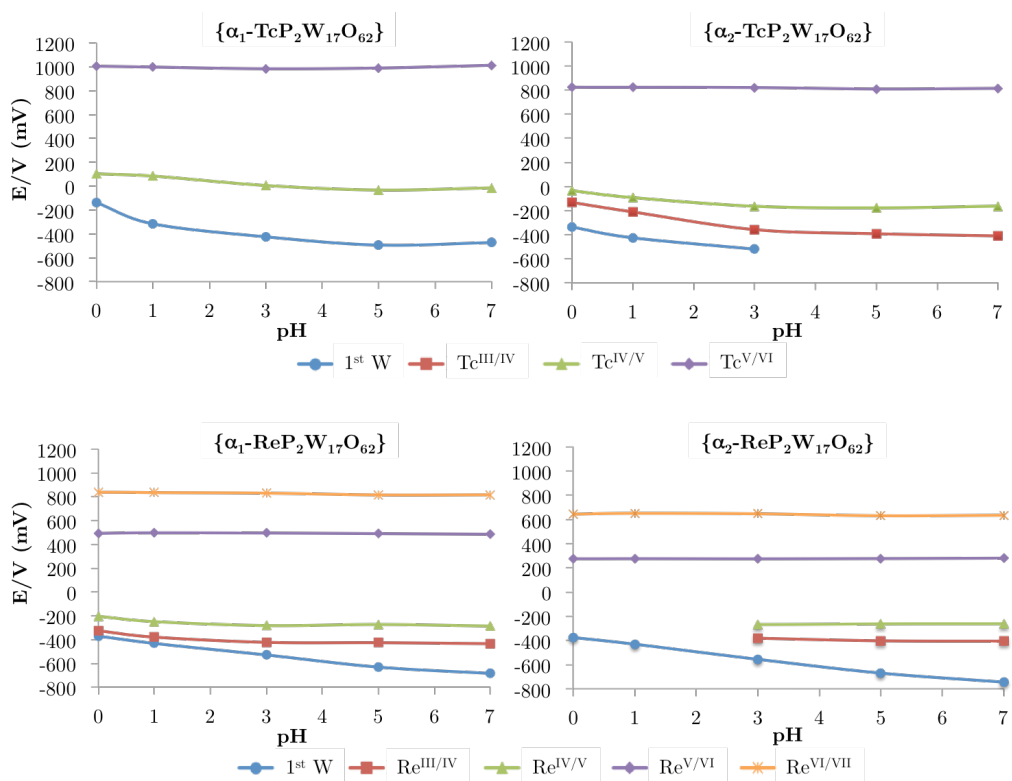


Figure 5.2. Representation of the reduction potentials E/V vs. Ag/AgCl reference electrode of 10^{-3} M α_1 and $\alpha_2\text{-MP}_2\text{W}_{17}\text{O}_{62}$ ($M = \text{Tc}$ or Re) as a function of pH.

A stability study was also performed to evaluate the free energy (ΔG) associated with the $\text{Re}^{\text{V}}/\text{Re}^{\text{IV}}$ reduction reaction for the $\alpha_1\text{-Re}^{\text{VO}}$ and $\alpha_2\text{-Re}^{\text{VO}}$ complexes at different pHs. The ΔG is calculated as: $\Delta G = -nFE$, where n is the charge per one electron, F is the Faraday constant (96500 C mol^{-1}) and E is the potential for the $\text{Re}^{\text{V}}/\text{Re}^{\text{IV}}$ reduction reaction (E_c in V).

The increasingly positive free energy with increasing pH shows that the $\text{Re}^{\text{V}}/\text{Re}^{\text{IV}}$ reduction is easier to achieve in acidic medium. The free energy requirement associated with the reduction of Re in the $\alpha_2\text{-Re}^{\text{VO}}$ complex is greater than in the $\alpha_1\text{-Re}^{\text{VO}}$ at pH 0 and 1. This fact supports the observation of more easy reduction for transition metals substituted in the α_1 POM vacancy. Above pH 1, the free energy requirement for the $\alpha_1\text{-Re}^{\text{VO}}$ becomes slightly greater than that of $\alpha_2\text{-Re}^{\text{VO}}$, which can point to a structural change within the Re-O^- center upon $\text{Re}^{\text{V}}/\text{Re}^{\text{IV}}$ reduction.

A study of the HOMO-LUMO energy gap for the $\alpha_1\text{-Re}^{\text{VO}}$ and $\alpha_2\text{-Re}^{\text{VO}}$ complexes was done. They have found an increase in the size of the energy gap with increasing pH, but at higher values the size of this gap remains constant. The HOMO-LUMO energy gap is consistently larger in the $\alpha_1\text{-Re}^{\text{VO}}$ than in $\alpha_2\text{-Re}^{\text{VO}}$ complex. The Re compounds behave differently under acidic and basic conditions. This can be attributed to the different solvent environments, which likely lead to the formation of protonated species under acidic conditions.

5.2.2 Results and discussion

For a deeper understanding of the above phenomena, DFT calculations for oxidation states from M^{IV} to M^{VII} ($\text{M} = \text{Tc}, \text{Re}$) have been carried out. In each case we have analyzed the structural parameters, energies and electron densities to determine their behavior versus the experimental data. In the first place we studied the monovacant α_1 and $\alpha_2\text{-[P}_2\text{W}_{17}\text{O}_{61}]^{10-}$ compounds. Then the fully oxidized d^0 structures, the α_1 and $\alpha_2\text{-[P}_2\text{W}_{17}\text{O}_{61}\text{M}^{\text{VII}}\text{O}]^{5-}$, and finally the reduced d^1 to d^3 complexes.

The electronic structure of the $[\text{P}_2\text{W}_{18}\text{O}_{62}]^{6-}$ anion has been previously reported^[8] and consists of two well separated molecular orbital sets or bands. The occupied one being associated to the oxo ligands with a highest occupied molecular orbital at -6.73 eV and a set of empty molecular orbitals of $d_{xy}(\text{W})$ nature starting at -4.55 eV (2.18 eV above in energy at DFT/BP86 level). In the case of Dawson compounds, the first unoccupied $d_{xy}(\text{W})$ orbitals are delocalized over the belt region, being the cap $d_{xy}(\text{W})$ orbitals higher in energy, a fact caused by differences in the local geometry of the different regions. This means that the first reduction in a Dawson anion always takes place at the equatorial position, and transition metals substituted into the belt position (α_1) will be more readily reduced than those substituted in the cap (α_2). The

mono-substituted $\{P_2MW_{17}O_{62}\}$ anion is formed upon removal of one $[W^{VI}O]^{4+}$ unit to give the lacunary $[P_2W_{17}O_{61}]^{10-}$ structure, and then with the addition of $[MO]^{n+}$ unit. In their optimized geometries, the computed energy difference between α_1 and α_2 lacunary anions is $\Delta E(\alpha_2-\alpha_1) = -5.7 \text{ kcal mol}^{-1}$, thus the α_2 isomer is more stable. This difference is significant and arises from the different geometry and electronic structure of the vacancies in each isomer.

The orientation of the closest internal tetrahedron $[PO_4]^{3-}$ with respect to the cavity generated by the removal of a $[W^{VI}O]^{4+}$ fragment determines the relative stability of the isomers^[9]. In the $[\alpha_1-P_2W_{17}O_{61}]^{10-}$ compound, one of the internal oxygens remains bound to P and one W atom, whereas in α_2 it is bonded to P and two W atoms. So it is expected that the former destabilize more the system favoring the stability of α_2 . The introduction of a $[Tc^{VII}O]^{5+}$ unit in either monovacant isomer stabilizes them differently, being α_2 more stable than α_1 by $3.7 \text{ kcal mol}^{-1}$. The greater nucleophilicity of the α_1 vacancy explains the reduction of the energy difference between both isomers. The most important set of molecular orbitals are the highest occupied oxo-like and the lowest unoccupied metal-like orbitals, those involved in the redox chemistry. Even if the oxidation state VII is not the most stable for Tc and Re, it is worth showing the sequence of molecular orbitals when no valence electrons are accommodated in the metal ions (Figure 5.3). The LUMO in both isomers is a d_{xy} orbital localized on the substituting metal atom, with some anti-bonding interaction from the surrounding bridging oxo sites. These compounds will gain electrons readily due to the low energy of this d orbital, so the Dawson anions containing Tc^{VII} or Re^{VII} are much stronger oxidizing agents than $\{P_2W_{18}O_{62}\}$. We can observe that the orbital energies associated to Tc are quite different in each isomer. The first electron added to the fully oxidized $[P_2W_{17}O_{61}Tc^{VII}O]^{5-}$ anion occupy the $d_{xy}(Tc)$ orbital, which is found at different energy in each isomer. The information obtained from the molecular orbitals analysis is in agreement with the experimental data.

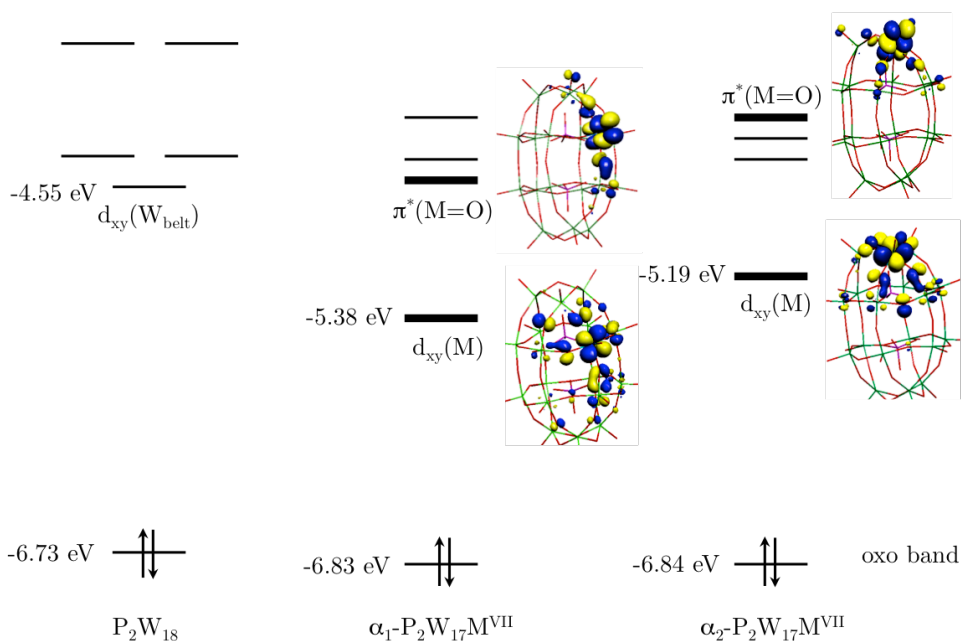


Figure 5.3. Molecular orbital representation of the electronic changes observed upon metal substitution from P_2W_{18} to α_1 and $\alpha_2-P_2W_{17}Tc^{VII}$. Thick lines represent orbitals of mainly Tc character. Absolute energies of the complexes are in solution.

The redox data obtained by theoretical calculations for $M = Tc$ and Re is summarized in the Table 5.1. The reduction process of Tc^{VII} to Tc^{VI} has the energy of -5.41 and -5.18 eV for α_1 and α_2 isomers respectively. The high exothermicity of these processes reinforces the idea that $[P_2W_{17}O_{61}Tc^{VII}O]^{5-}$ anion is much oxidizing to be stable. For the Re compounds, the Re^{VII}/Re^{VI} process are -4.91 eV for the α_1 and -4.62 eV for the α_2 isomer. The trend is equivalent to the Tc complexes, but ~ 0.5 eV less negative values arising from the higher LUMO caused by the more diffuse character of Re valence orbitals. After the first reduction, α_1 and $[\alpha_2-P_2W_{17}O_{61}Tc^{VI}O]^{6-}$ anions have similar energies ($\Delta E(\alpha_2-\alpha_1) = 0.5 \text{ kcal mol}^{-1}$). The second reduction, from Tc^{VI} to Tc^V , gives reduction energy of -4.92 eV for α_1 and -4.74 eV for α_2 . The reduction of α_1 is still more favorable. After the second reduction, the α_1 isomer becomes more stable than α_2 by $4.7 \text{ kcal mol}^{-1}$. This trend also occurs in the Re structures with $\Delta E(\alpha_2-\alpha_1) = -8.8 \text{ kcal mol}^{-1}$ for Re^V . These compounds show little geometrical changes from Tc^{VII} to Tc^V , remaining quite limited to the region of the $Tc-O-W$ bridging oxygens, which elongate from 2.41 to 2.50 Å. The nature of the orbital that is occupied, formally nonbonding $d_{xy}(Tc)$ orbital with some antibonding contribution of the $p(O)$ orbital, explains this fact. The

distance between Tc and terminal O has not changed appreciably. The two-electron reduced form $[\alpha_1\text{-P}_2\text{W}_{17}\text{O}_{61}\text{Tc}^{\text{VO}}]^{7-}$ is more stable than α_2 isomer. The DFT molecular orbitals and the α_1/α_2 relative energies show that the lowest $d_{xy}(\text{Tc})$ level is 2-fold occupied, lying below in energy in α_1 .

Table 5.1. Reduction energies (in eV) of the nonprotonated α_1 and $\alpha_2\text{-P}_2\text{W}_{17}\text{M}$ species (M = Tc and Re).

Reduction Process	Tc			Re		
	α_1	α_2	$\Delta\text{RE}(\alpha_2 - \alpha_1)$	α_1	α_2	$\Delta\text{RE}(\alpha_2 - \alpha_1)$
VII/VI ^a	-5.41	-5.18	0.23	-4.91	-4.62	0.29
VI/V	-4.92	-4.74	0.18	-4.62	-4.38	0.24

^a This process does not take place in Tc derivatives.

Further reduction of the structures implies some important structural changes. An elongation in the Tc and terminal O bond from 1.69 to 1.75 Å occurs after addition of the third metal electron. Calculations show that this third electron occupies the $d(\text{Tc})\text{-p}(\text{O})$ antibonding orbital in the α_1 isomer, a fact agrees with the experimental data. In the case of the α_2 isomer, an orbital of the same nature is found higher in energy, actually embedded into the W band.

Understanding the reduction process M^{V} to M^{IV} is less intuitive. That reduction would take place in the W centers in general, ruling out the formation of M^{IV} . Focusing the discussion in the Re compounds, the DFT calculations indicate that the $\text{Re}^{\text{V}}/\text{Re}^{\text{IV}}$ reduction process might need protonation in the terminal $\text{Re}=\text{O}$ oxygen. This possibility was reported by Pope and coworkers^[7]. Without protonation, DFT calculations show that the one-electron reduction of α_1 and $[\alpha_2\text{-P}_2\text{W}_{17}\text{O}_{62}\text{Re}^{\text{V}}]^{7-}$ produce an extra electron delocalized over some W atoms. This apparently does not coincide with the experimental assignation of that reduction process. The analysis based on molecular orbital energies shows that the antibonding $\pi^*(\text{Re}=\text{O})$ orbital is too high in energy in the non-protonated form, thus inaccessible to the extra electron forbidding the Re^{IV} form in favor of the one-electron reduced compound (Figure 5.4).

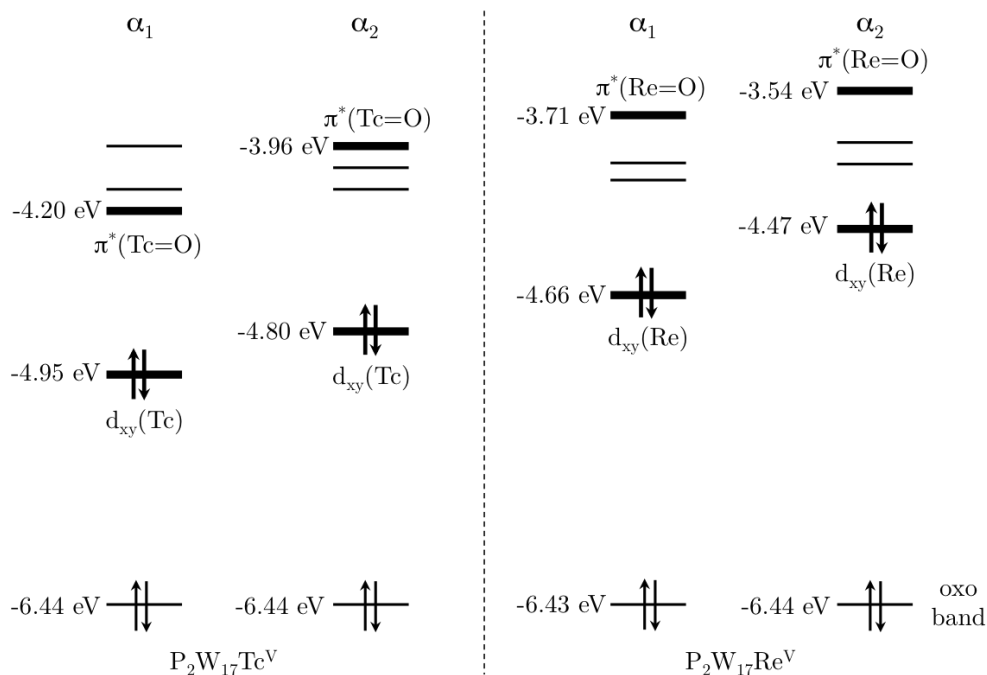


Figure 5.4. Sequence of the doubly occupied highest occupied and the first unoccupied metal-like MOs for the non-protonated α_1 and α_2 - $\text{P}_2\text{W}_{17}\text{M}^{\text{V}}$ ($\text{M} = \text{Tc}$ and Re) species. Thick lines represent orbitals of mainly Tc (respectively Re) character.

In conditions of protonation in the terminal oxygen the Re–O(H) bond weakens, the Re–O distance is enlarged and, thus, the $\pi^*(\text{Re}=\text{O})$ orbital stabilizes (Figure 5.5). The stabilization of this orbital upon reduction and protonation was computed to be 1.1 eV for Tc, and 1.2 eV for Re compounds, and leaves it below the first unoccupied W-like molecular orbital. This allows the extra electron to occupy it and, therefore, the Re^{IV} state can be achieved. Protonation at any other plausible site does not entail so much energy change of an orbital and can by no means favor Re^{IV} . The atomic spin populations calculated for the α_1 - $\text{P}_2\text{W}_{17}\text{Re}^{\text{IV}}$ and α_1 - $\text{P}_2\text{W}_{17}\text{Tc}^{\text{IV}}$ complexes are 0.92 and 0.94 at Re and Tc, respectively, indicating that the third metallic electron is fully localized. So, if even at moderately acid or neutral pH, some portion of the molecules has the terminal Re=O site protonated, these can get reduced preferentially (in Re) making in full agreement calculations and experimental data.

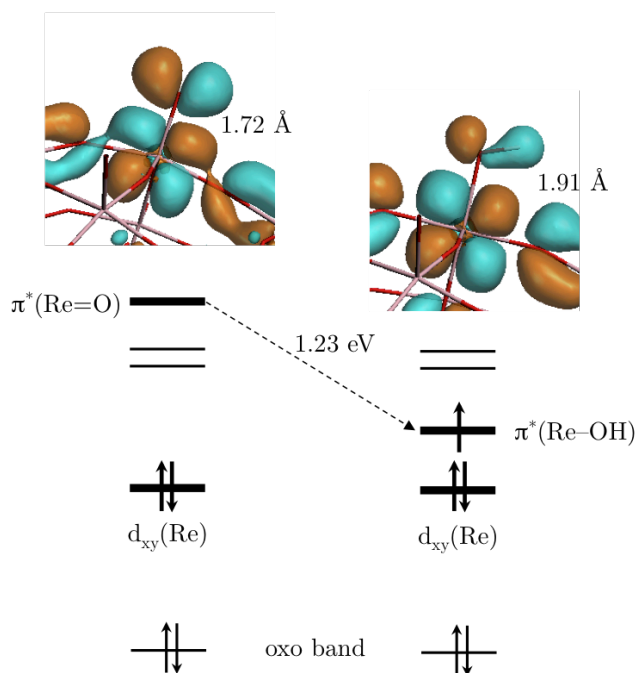


Figure 5.5. Evolution of the molecular orbitals upon reduction and protonation at the terminal oxygen site Re=O of α_1 - $P_2W_{17}Re^V$. The Re-O distances in both states are shown as well as the $\pi^*(\text{Re-O})$ orbital involved in the reduction process.

5.2.3 Conclusions

DFT calculations help to interpret the redox data collected for the α_1 and α_2 - $[P_2W_{17}O_{61}MO]$ ($M = \text{Tc}$ and Re). The Tc derivatives are stronger oxidizing agents than their Re homologues since the extra electrons occupy lower orbitals in the former compounds. Independently of the metal atom, the α_1 isomer is more oxidant than α_2 for the same reason. Calculations show that the first Tc-like orbital is very low in energy and cannot be completely depopulated. This fact explains why the maximum oxidation state for this atom is VI, whereas in the Re case an oxidation state of VII is justified by higher d orbitals. Concerning reduction of the $[P_2W_{17}O_{61}M^V O]$ systems, protonation plays an important role. The M^V/M^{IV} reduction process goes in parallel with protonation. The Tc and Re orbitals populated in this process are $\pi^*(M=O)$, which are too high in energy in non-protonated form. The $[P_2W_{17}O_{61}M^{IV} O]$ anions are formed together with enlargement of terminal $M=O$ distances, that is, addition of a proton on the terminal oxygen.

5.3 Fe compounds

5.3.1 Experimental background

Dr. I. M. Mbomekallé (Institut Lavoisier, Université de Versailles) has studied the electrochemistry of α_1 and $\{\alpha_2\text{-Fe}(\text{OH}_2)\text{P}_2\text{W}_{17}\text{O}_{61}\}$ complexes. Keita *et al.*^[10] conducted a previous study on both compounds in aqueous solution showing that at very low pH values, the first redox process attributed to $\text{Fe}^{3+}/\text{Fe}^{2+}$ reduction and the following one attributed to the reduction of the W framework merged into a single three-electron wave for the α_1 isomer. Under the same experimental conditions, the waves remain separated for the α_2 isomer, that is, a first one-electron wave followed by a second two-electron wave. Another remarkable observation is that, throughout the pH domain explored in the study (0.16-3.00), the $\text{Fe}^{3+}/\text{Fe}^{2+}$ reduction is easier in the case of the α_2 isomer than in the case of the α_1 . This result seems to contradict the electrochemical behavior observed with other metal-substituted Dawson-type tungstodiphosphates, in which the reduction of the substituted metal is always easier for the α_1 isomer than for the α_2 isomer, at the pH where the species are stable^[11]. Some experimental studies were done in order to explain the different electrochemical behavior of the isomers^[3a], but not from a computational point of view.

To carry out a rigorous study based on the pH and electrolyte influence on Fe^{3+} and W redox waves, they proceed under experimental conditions where both waves can be observed separately, that is, the splitting between Fe^{3+} and first W waves is complete. This situation is observed for α_2 isomer in the whole pH domain explored (0.5-8.0), while for α_1 isomer is only observed starting at $\text{pH} > 3$. An important constraint will be the election of the electrolyte that should cover a pH domain where its buffer power remains non-negligible.

The experimental data show that at low pH values ($\text{pH} \leq 5$), the reduction of the Fe center in the α_2 position is easier than in the α_1 position. This behavior is related to the influence of protonation. Moreover, at higher pH values ($\text{pH} \geq 6$) or in an organic medium, when protonation effect become negligible, the normal trend is recovered, i.e., the reduction of the Fe center in the α_2 position becomes easier than in the α_1 position as expected (Figure 5.6).

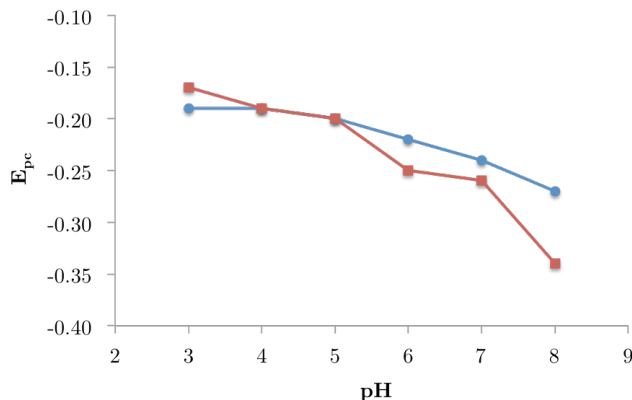


Figure 5.6. Evolution of peak reduction potential values, E_{pc} ($\text{Fe}^{3+}/\text{Fe}^{2+}$), as function of pH for α_1 (blue circles) and $\{\alpha_2\text{-Fe}(\text{OH}_2)\text{P}_2\text{W}_{17}\text{O}_{61}\}$ (red squares) compounds. CVs are recorded at a scan of 10 mVs^{-1} on a glassy carbon-working electrode. Potentials are quoted against the SCE reference electrode.

5.3.2 Results and discussion

Density functional based calculations have been performed to help explaining the relative stability and redox potentials of the iron-substituted Dawson anions $\alpha_1\text{-}[\text{Fe}(\text{OH}_2)\text{P}_2\text{W}_{17}\text{O}_{61}]^{7-}$ and $\alpha_2\text{-}[\text{Fe}(\text{OH}_2)\text{P}_2\text{W}_{17}\text{O}_{61}]^{7-}$, hereafter $\alpha_1\text{-Fe}(\text{OH}_2)\text{W}_{17}$ and $\alpha_1\text{-Fe}(\text{OH}_2)\text{W}_{17}$ respectively, and their dependence with protonation. The acidity of the solution has revealed determinant in the evolution of the redox properties of both isomers. Since we are not capable of explicitly imposing a given pH value to our standard DFT calculations, we have generated a number of differently protonated model structures derived from the parent $\{\text{P}_2\text{W}_{17}\text{FeO}_{62}\}$ that are assumed to be dominant at different pH values. Namely, at neutral pH, the deprotonated $[\text{FeOP}_2\text{W}_{17}\text{O}_{61}]$ structure could be predominant. However, this is not expected regarding the experimental evidences that rule out the stability of these molecules^[3a]. Another likely structure at neutral pH is the mono-protonated one, $[\text{Fe}(\text{OH})\text{P}_2\text{W}_{17}\text{O}_{61}]$. The next protonation step will occur when acidity increases to pH 5, obtaining $[\text{Fe}(\text{OH}_2)\text{P}_2\text{W}_{17}\text{O}_{61}]$. Finally, at even lower pH, another two structures could be formed. The first one is the structure with no terminal atom on the Fe site $[\text{FeP}_2\text{W}_{17}\text{O}_{61}]$ and the second one is the structure with a water molecule linked to the iron atom and a protonated bridging oxygen, $[\text{HFe}(\text{OH}_2)\text{P}_2\text{W}_{17}\text{O}_{61}]$.

We have obtained fully optimized structures for this set of systems with Fe^{2+} and Fe^{3+} , and evaluated the reduction free energy for both isomers, ΔG_1 and

ΔG_2 . We have also extracted the reduction free energy differences ($-\Delta\Delta G_{2-1} = -\Delta G_2 + \Delta G_1$) between both isomers to compare them with the experimental data ($\Delta E_{1/2}^o$) (Table 5.2). When the monoprotonated $\text{Fe}^{\text{III}}(\text{OH})$ species are considered, the reduction occurs more easily for $\alpha_1\text{-Fe}(\text{OH}_2)\text{W}_{17}$, that is, its reduction energy is more negative than for $\alpha_2\text{-Fe}(\text{OH}_2)\text{W}_{17}$ by 17 meV, in good agreement with the experimental half-wave potentials ($\Delta E_{1/2}^o = +30$ mV). The trend is inverted by adding the second proton to the iron-substituted species (simulated moderately acidic pH), when $-\Delta\Delta G_{2-1} = 47$ meV. Under conditions of further protonation (pH 1), this trend is more notable and $-\Delta\Delta G_{2-1}$ rises to 68 or 90 meV, depending on the model, in favor of $\alpha_2\text{-Fe}(\text{OH}_2)\text{W}_{17}$. Our calculations reproduce the trend observed in the experiments.

We would like to point out that three different species, $[\text{Fe}(\text{OH}_2)\text{P}_2\text{W}_{17}\text{O}_{61}]$, $[\text{FeP}_2\text{W}_{17}\text{O}_{61}]$ and $[\text{HFe}(\text{OH}_2)\text{P}_2\text{W}_{17}\text{O}_{61}]$ can be formed as the acidity increases. There are not either experimental or theoretical evidences that suggest which one is the predominant, or if a mix of them coexist in solution. Nevertheless, all of them show the same redox behavior in good agreement with the experimental data.

Table 5.2. Computed reduction free energies for differently protonated forms of isomers $\alpha_1\text{-Fe}(\text{OH}_2)\text{W}_{17}$ and $\alpha_2\text{-Fe}(\text{OH}_2)\text{W}_{17}$ (ΔG_1 and ΔG_2 respectively, in eV), reduction energy differences ($-\Delta\Delta G_{2-1}$), and experimental data ($\Delta E_{1/2}^o$, in V).

	ΔG_1	ΔG_2	$-\Delta\Delta G_{2-1}$	$\Delta E_{1/2}^o$ (<i>exp.</i>)
$[\text{Fe}(\text{OH})\text{P}_2\text{W}_{17}\text{O}_{61}]^{8-}$	-4.017	-4.000	-0.017	-0.030
$[\text{Fe}(\text{OH}_2)\text{P}_2\text{W}_{17}\text{O}_{61}]^{7-}$	-4.592	-4.639	+0.047	+0.080
$[\text{FeP}_2\text{W}_{17}\text{O}_{61}]^{7-}$	-4.746	-4.814	+0.068	-
$[\text{HFe}(\text{OH}_2)\text{P}_2\text{W}_{17}\text{O}_{61}]^{6-}$	-4.853	-4.943	+0.090	-

The uncommon feature that isomers $\alpha_1\text{-Fe}(\text{OH}_2)\text{W}_{17}$ and $\alpha_2\text{-Fe}(\text{OH}_2)\text{W}_{17}$ reverse the ordering of their first reduction potentials at pH 6 deserves further insight. From the electrochemical experiments we observed that the first 1e-reduction takes at the Fe center irrespective of the isomer and the pH, in detriment of the formation of the blue species, $\text{P}_2\text{W}_{17}\text{Fe}^{3+} \rightarrow [\text{P}_2\text{W}_{17}\text{Fe}^{3+} 1e]$, a process that takes place at more negative potentials. So, the delocalized d_{xy} -like molecular orbital of W character appearing at higher energies, also of

nonbonding nature, can be ruled out of the competition towards the first incoming electron. From our DFT results, the orbitals of the oxidized forms of $\alpha_1\text{-Fe}(\text{OH}_2)\text{W}_{17}$ and $\alpha_1\text{-Fe}(\text{OH}_2)\text{W}_{17}$ ready to accept an extra electron are, in principle, the formally nonbonding $d_{xy}(\text{Fe})$ (perpendicular to the terminal oxygen) and the antibonding $\pi^*(\text{Fe-O})$, which is oriented towards the terminal oxygen. The energy of the latter orbital strongly depends on the Fe-O(terminal) mutual interaction, which, in addition, is changing with pH. In both Fe^{2+} isomers, the d_{xy} orbital is more stable than the π^* orbital under conditions of poor protonation ($\text{FeOP}_2\text{W}_{17}\text{O}_{61}$ and $\text{Fe}(\text{OH})\text{P}_2\text{W}_{17}\text{O}_{61}$ structures) while the inversion occurs for $[\text{FeP}_2\text{W}_{17}\text{O}_{61}]$ and $[\text{Fe}(\text{OH}_2)\text{P}_2\text{W}_{17}\text{O}_{61}]$ molecules, assumed to be the predominant species at low pH. This is not so evident for both isomers of the Fe^{3+} form, where the orbital reversal occurs for the α_2 isomer only. This particular behavior depending on pH is not observed in other metal-substituted Dawson-type tungstodiphosphates, such as $\text{P}_2\text{W}_{17}\text{M}$ with $\text{M} = \text{V}$ or Mo ^[11a, 11b, 11d, 11e, 12].

We demonstrate below that the antibonding Fe-O(terminal) interaction changes depending on the pH conditions, namely the protonation state of the system, and governs the inversion of the order in reduction potentials observed around pH 5 for $\alpha_1\text{-Fe}(\text{OH}_2)\text{W}_{17}$ and $\alpha_2\text{-Fe}(\text{OH}_2)\text{W}_{17}$. As expected, the computed Fe-O(terminal) distance increases with the number of protons attached to the terminal oxygen. In conditions of no protonation at Fe-O, the computed distance is $d(\text{Fe-O}) \sim 1.66\text{-}1.76 \text{ \AA}$ depending on the isomeric form, with the $\pi^*(\text{Fe-O})$ orbital lying at high energies with respect to the $d_{xy}(\text{Fe})$ one due to its marked antibonding nature. The general evolution of the $\pi^*(\text{Fe-O})$ orbital from neutral to acidic pH is depicted in Figure 5.7, showing the differences in the molecular orbital sequence for the mono and diprotonated forms of $\alpha_1\text{-Fe}(\text{OH}_2)\text{W}_{17}$ and $\alpha_2\text{-Fe}(\text{OH}_2)\text{W}_{17}$. For the monoprotonated species, $\text{Fe}^{\text{III}}(\text{OH})$, the Fe-O distance increases to $\sim 1.87 \text{ \AA}$ and the $\pi^*(\text{Fe-O})$ is stabilized due to the lower participation of the 2p-O(terminal) orbital, but still remains located above the $d_{xy}\text{-Fe}$ orbital. Finally, when the apical group is doubly protonated, $\text{Fe}^{\text{III}}(\text{OH}_2)$, the Fe-O distance becomes very long (2.08 \AA) and the $\pi^*(\text{Fe-O})$ orbital turns into ‘pure’ $d_{xz}\text{-Fe}$ orbital, more stable than the formally nonbonding $d_{xy}(\text{Fe})$ orbital when an extra electron is added.

The more favorable reduction of $\alpha_2\text{-Fe}(\text{OH}_2)\text{W}_{17}$ at $\text{pH} \leq 5$ compared to $\alpha_1\text{-Fe}(\text{OH}_2)\text{W}_{17}$ can be explained by (i) the dominant role of the $\pi^*(\text{Fe-OH}_2)$ orbital in the reduction process, and (ii) the different orientation of this orbital

in either isomeric form with respect to the bridging oxygen atoms surrounding the iron center. The right hand part of Figure 5.7 shows that the orientation of the π^* orbital in $\alpha_1\text{-Fe(OH}_2\text{)W}_{17}$ coincides with the direction of two Fe-O(bridging) bonds, therefore conferring a stronger antibonding character than the homologous orbital in $\alpha_2\text{-Fe(OH}_2\text{)W}_{17}$. In the latter case, the π^* orbital bisects the Fe-O(bridging) bonds, making the 3d(Fe)-2p(O) interaction weaker. Thus, electron reduction takes place in a higher π^* orbital in $\alpha_1\text{-Fe(OH}_2\text{)W}_{17}$ isomer than in $\alpha_2\text{-Fe(OH}_2\text{)W}_{17}$, and makes the reduction of the latter compound more favorable at sufficiently acidic pH.

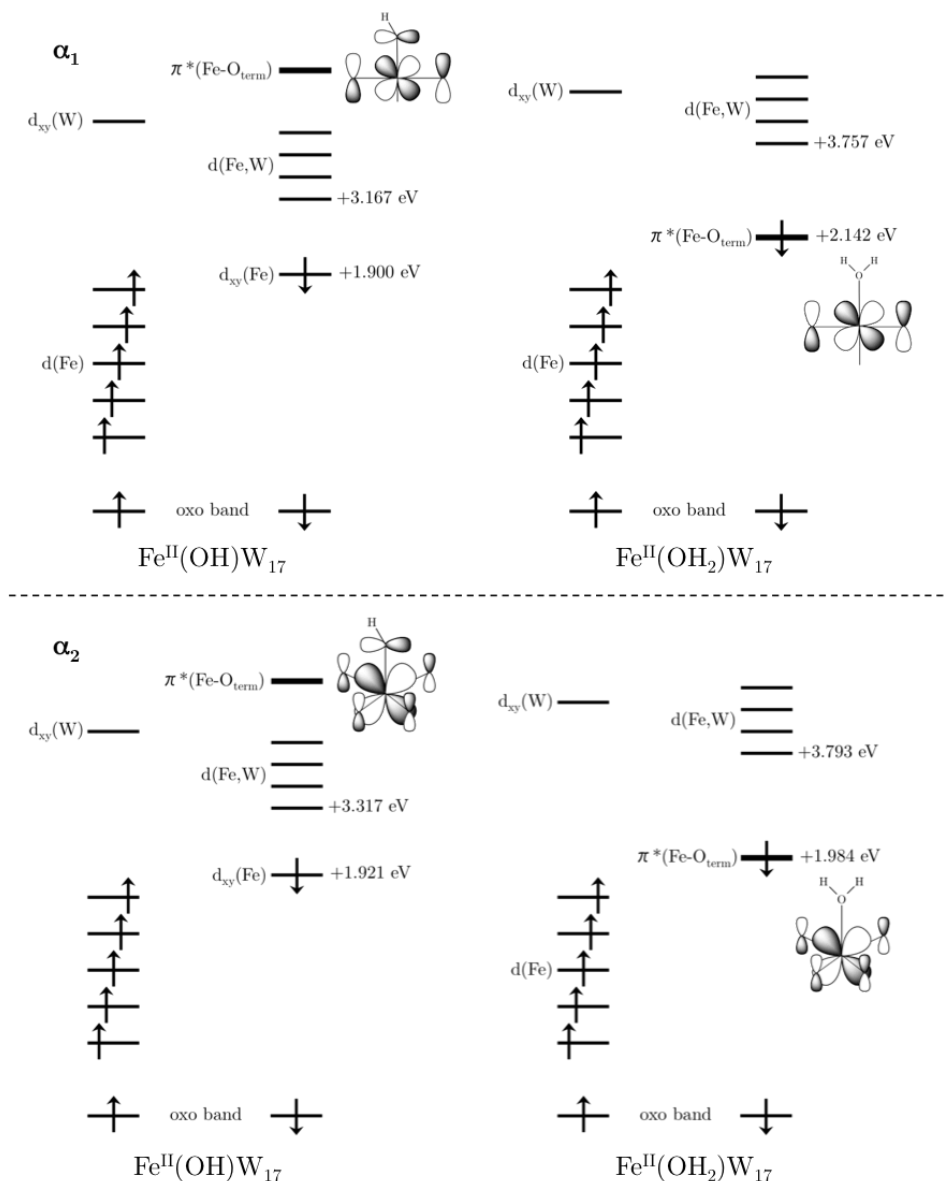


Figure 5.7. Computed frontier orbitals for the Fe^{II}(OH)W₁₇ and Fe^{II}(OH₂)W₁₇ forms of α_1 and α_2 isomers. The character (oxo, Fe, W) of the orbitals and their relative energies (in eV, *vs.* the highest orbital of the oxo band) are shown for the relevant molecular orbitals. Spin-up and spin-down orbitals are separated in two columns for each compound.

A quantitative approach by atomic spin population analysis confirms the above statements. The computed change in spin density of O(terminal) as going from Fe-OH to Fe-OH₂ is remarkable: 0.36 to 0.06 for both α_1 and α_2 forms of P₂W₁₇Fe^{III}. This indicates the decreasing participation of the terminal oxygen in the $\pi^*(\text{Fe-O})$ orbital. For the reduced P₂W₁₇Fe^{II} compounds, the

spin density changes from 0.16 to 0.02 on average for both isomers. The smaller spin density values in the case of reduced forms arise from the longer Fe-O(terminal) distances produced by the population of the $\pi^*(\text{Fe-O})$ orbital.

In summary, protonation on the terminal Fe-O site gradually stabilizes the π^* orbital with respect to the d_{xy} one leading to an inversion of the d_{xy} and π^* ($d_{xz}\text{-Fe}$) orbital energies when the apical group of iron is water. Calculations have revealed that this occurs in both isomeric forms (Figure 5.8).

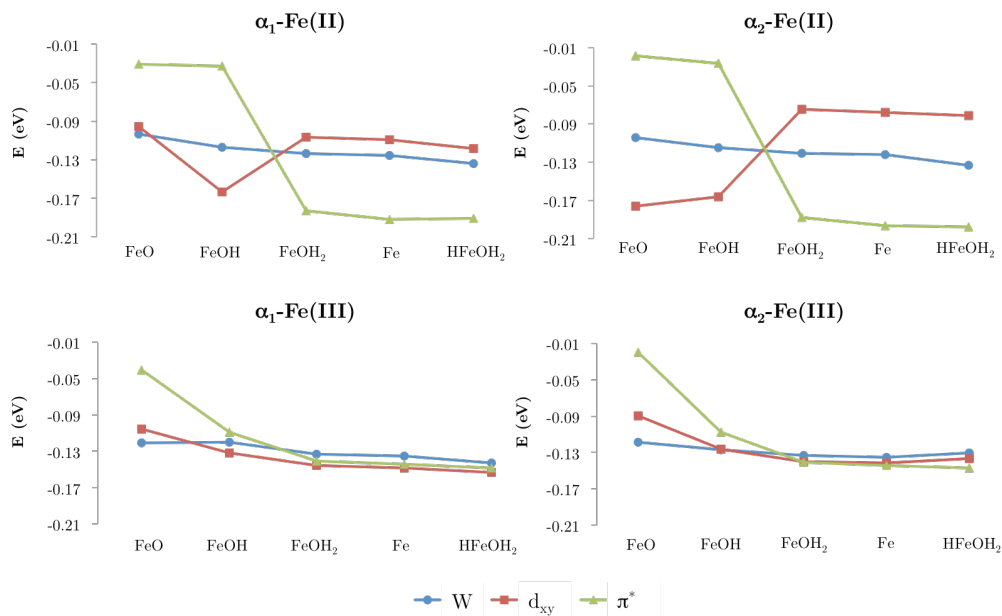


Figure 5.8. Energies (in eV) of W orbital, d_{xy} and π^* Fe orbitals for $[\text{FeOP}_2\text{W}_{17}\text{O}_{61}]$ (FeO), $[\text{Fe}(\text{OH})\text{P}_2\text{W}_{17}\text{O}_{61}]$ (FeOH), $[\text{Fe}(\text{OH})_2\text{P}_2\text{W}_{17}\text{O}_{61}]$ (FeOH₂), $[\text{FeP}_2\text{W}_{17}\text{O}_{61}]$ (Fe) and $[\text{HFe}(\text{OH})_2\text{P}_2\text{W}_{17}\text{O}_{61}]$ (HFeOH₂) molecules, respectively.

5.3.3 Conclusions

A computational study of both α_1 and α_2 - $[\text{Fe}(\text{OH})_2\text{P}_2\text{W}_{17}\text{O}_{61}]$ isomers were done in order to explain their main electrochemical behavior. We were able to reproduce and interpret the experimental results according to the different molecular orbital energies. We have also evidenced the influence of the protonation state of the Fe derivative on the relative reduction potentials of both isomers. At pH values close to 6, reduction energies are more favorable to α_1 , while the opposite trend is observed at low pH values due to the double protonation at the terminal Fe-O site. In both Fe^{II} isomers, the d_{xy} orbital is more stable than the π^* orbital for $[\text{Fe}(\text{OH})\text{P}_2\text{W}_{17}\text{O}_{61}]$, assumed to be

dominant at neutral pH, while the inversion occurs for $[\text{Fe}(\text{OH}_2)\text{P}_2\text{W}_{17}\text{O}_{61}]$ and $[\text{FeP}_2\text{W}_{17}\text{O}_{61}]$, the principal species at low pH.

5.4 Concluding remarks

We have performed a thorough theoretical study supporting the electrochemical data on the α_1 and α_2 mono-substituted Dawson tungstodiphosphates, $\{\text{P}_2\text{MW}_{17}\text{O}_{62}\}$, where $\text{M} = \text{Tc}, \text{Re}$ and Fe . In the Tc and Re compounds, both metal atoms are reduced more easily in the α_1 isomer than in the α_2 counterpart. Tc derivatives are always more readily reduced than their Re homologues. On the other hand, in the Fe compounds the reduction of the metal atom in the α_2 position is easier than in the α_1 position. This behavior can be explained by the influence of the protonation, which plays a crucial role in the electrochemistry of these compounds.

5.5 Computational details

5.5.1 Tc and Re compounds

The theoretical calculations for the Tc and Re structures were done using the DFT as implemented in the ADF 2009.01 program^[13]. Calculations are characterized by GGA, using the $X\alpha$ model with Becke's corrections^[14] for exchange, and the VWN parameterization with Perdew's corrections^[15] for correlation (BP86 functional). The electrons are described by Slater-type functions. Basis sets are of TZP quality for all valence electrons, whereas internal or core electrons (oxygen: 1s, phosphorus: 1s-2p, technetium: 1s-3d, tungsten and rhenium: 1s-4f) were kept frozen and described by single Slater functions with scalar relativistic corrections via ZORA, with core potentials generated using the DIRAC program^[13]. We applied the spin-unrestricted formalism to electronically open-shell species. All the calculations include COSMO^[16] to account for the solvent effects of water ($\epsilon = 78.4$). The ionic radii for the atoms that actually define the size of the solvent cavity were chosen to be 1.20 Å for hydrogen, 0.74 Å for metals and 1.52 Å for oxygen.

As has been reported previously, this methodology must be applied to obtain reliable orbital energies and comparable total energies of differently charged anions^[17]. For the present case, we calculated the energies for the following process: $\text{POM}(\text{ox})_{\text{aq}} + e^-_{\text{gas}} \rightarrow \text{POM}(\text{red})_{\text{aq}}$ or $\text{POM}(\text{ox})_{\text{aq}} + \text{H}_3\text{O}^+_{\text{aq}} + e^-_{\text{gas}} \rightarrow$

HPOM(red)_{aq} + H₂O_{aq}, where ‘gas’ and ‘aq’ stand for species in gas phase or in aqueous solution, respectively. The free electron is considered as in the gas phase since its energy can be taken as zero^[18].

5.5.2 Fe compounds

DFT calculations for the Fe compounds have been carried out with the GAUSSIAN 09 suite of programs^[19]. All the structures were optimized in the oxidized and reduced states for the accuracy of the reduction energies. Our calculations are performed using the B3LYP hybrid functional^[20] with the 6-31G basis set for H and O atoms and the standard 2-double-zeta basis set with LANL pseudopotentials^[21] (LANL2DZ) for W, Fe and P atoms. All the calculations include PCM^[22] to account for the solvent effects of water ($\epsilon = 78.4$). We applied the spin-unrestricted formalism to electronically open-shell molecules. Atomic spin populations and charges were obtained by means of the Mulliken procedure.

5.6 References

- [1] a) E. Papaconstantinou, *Chem. Soc. Rev.* **1989**, *18*, 1; b) T. McCormac, B. Fabre, G. Bidan, *J. Electroanal. Chem.* **1997**, *425*, 49; c) T. McCormac, B. Fabre, G. Bidan, *J. Electroanal. Chem.* **1997**, *427*, 155; d) W. Song, X. Wang, Y. Liu, J. Liu, H. Xu, *J. Electroanal. Chem.* **1999**, *476*, 85; e) R. Carlisle Chambers, C. L. Hill, *Inorg. Chem.* **1991**, *30*, 2776; f) L. A. Combs-Walker, C. L. Hill, *J. Am. Chem. Soc.* **1992**, *114*, 938.
- [2] M. T. Pope, *Heteropoly and Isopoly Oxometalates*, Springer-Verlag, Berlin, 1983.
- [3] a) R. Contant, M. Abbessi, J. Canny, A. Belhouari, B. Keita, L. Nadjo, *Inorg. Chem.* **1997**, *36*, 4961; b) R. Contant, M. Richet, Y. W. Lu, B. Keita, L. Nadjo, *Eur. J. Inorg. Chem.* **2002**, 2587; c) D. McGregor, B. P. Burton-Pye, R. C. Howell, I. M. Mbomekallé, W. W. Lukens, F. Bian, E. Mausolf, F. Poineau, K. R. Czerwinski, L. C. Francesconi, *Inorg. Chem.* **2011**, *50*, 1670.
- [4] a) X. López, P. Miró, J. J. Carbó, A. Rodríguez-Forteza, C. Bo, J. M. Poblet, *Theor. Chem. Acc.* **2011**, *128*, 393; b) J. M. Poblet, X. López, C. Bo, *Chem. Soc. Rev.* **2003**, *32*, 297.
- [5] a) E. Deutsch, K. Libson, J. L. Vanderheyden, *The Inorganic Chemistry of Technetium and Rhenium as Relevant to Nuclear Medicine*, Vol. 3, Cortina International, Verona, 1990; b) K. Libson, L. Helm, A. Roodt, C. Cutler, A. E. Merbach, J. C. Sullivan, E. Deutsch, *Kinetics and Mechanism of Ligand Substitution on Analogous Technetium(V) and Rhenium(V) Complexes*, 3rd ed., Cortina International, Verona, 1989; c) K. Libson, M. Woods, J. C. Sullivan, J. W. Watkins II, R. C. Elder, E. Deutsch, *Inorg. Chem.* **1988**, *27*, 999; d) J. L. Vanderheyden, M. J. Heeg, E. Deutsch, *Inorg. Chem.* **1985**, *24*, 1666.
- [6] B. Keita, F. Girard, L. Nadjo, R. Contant, J. Canny, M. Richet, *J. Electroanal. Chem.* **1999**, *478*, 76.
- [7] F. Ortega, M. T. Pope, *Inorg. Chem.* **1984**, *23*, 3292.
- [8] a) B. Keita, B. Levy, L. Nadjo, R. Contant, *New. J. Chem.* **2002**, *26*, 1314; b) X. López, C. Bo, J. M. Poblet, *Inorg. Chem.* **2003**, *42*, 2634.
- [9] J. P. Ciabrini, R. Contant, *J. Chem. Res. (M)* **1993**, 2720.
- [10] B. Keita, A. Belhouari, L. Nadjo, R. Contant, *J. Electroanal. Chem.* **1998**, *442*, 49.
- [11] a) R. Acerete, S. P. Harmalker, C. F. Hammer, M. T. Pope, L. C. W. Baker, *Chem. Commun.* **1979**, 777; b) J. P. Ciabrini, R. Contant, J. M. Fruchart, *Polyhedron* **1983**, *2*, 1229; c) S. P. Harmalker, M. A. Leparulo, M. T. Pope, *J. Am. Chem. Soc.* **1983**, *105*, 4286; d) M. Abbessi, R. Contant, R. Thouvenot, G. Hervé, *Inorg. Chem.* **1991**, *30*, 1695; e) B. Keita, I. M. Mbomekallé, L. Nadjo, P. de Oliveira, A. Ranjbari, R. Contant, *C. R. Chimie* **2005**, *8*, 1057.
- [12] S. P. Harmalker, M. A. Leparulo, M. T. Pope, *J. Am. Chem. Soc.* **1983**, *105*, 4286.
- [13] ADF2009.01, SCM, Vrije Universiteit, Amsterdam, The Netherlands, <http://www.scm.com>, 2009.

- [14] a) A. D. Becke, *J. Chem. Phys.* **1986**, *84*, 4524; b) A. D. Becke, *Phys. Rev. A* **1988**, *38*, 3098.
- [15] a) J. P. Perdew, *Phys. Rev. B* **1986**, *33*, 8822; b) J. P. Perdew, *Phys. Rev. B* **1986**, *34*, 7406.
- [16] a) A. Klamt, G. Schüürmann, *J. Chem. Soc., Perkin Trans. 2* **1993**, 799; b) C. C. Pye, T. Ziegler, *Theor. Chem. Acc.* **1999**, *101*, 396.
- [17] X. López, C. Bo, J. M. Poblet, *J. Am. Chem. Soc.* **2002**, *124*, 12574.
- [18] a) A. Lewis, J. A. Bumpus, D. G. Truhlar, C. J. Cramer, *J. Chem. Educ.* **2004**, *81*, 596; b) A. Lewis, J. A. Bumpus, D. G. Truhlar, C. J. Cramer, *J. Chem. Educ.* **2007**, *84*, 934.
- [19] Gaussian 09, Revision A.02, M. J. Frisch, G. W. Trucks, H. B. Schlegel, G. E. Scuseria, M. A. Robb, J. R. Cheeseman, G. Scalmani, V. Barone, B. Mennucci, G. A. Petersson, H. Nakatsuji, M. Caricato, X. Li, H. P. Hratchian, A. F. Izmaylov, J. Bloino, G. Zheng, J. L. Sonnenberg, M. Hada, M. Ehara, K. Toyota, R. Fukuda, J. Hasegawa, M. Ishida, T. Nakajima, Y. Honda, O. Kitao, H. Nakai, T. Vreven, J. Montgomery, J. A., J. E. Peralta, F. Ogliaro, M. Bearpark, J. J. Heyd, E. Brothers, K. N. Kudin, V. N. Staroverov, R. Kobayashi, J. Normand, K. Raghavachari, A. Rendell, J. C. Burant, S. S. Iyengar, J. Tomasi, M. Cossi, N. Rega, N. J. Millam, M. Klene, J. E. Knox, J. B. Cross, V. Bakken, C. Adamo, J. Jaramillo, R. Gomperts, R. E. Stratmann, O. Yazyev, A. J. Austin, R. Cammi, C. Pomelli, J. W. Ochterski, R. L. Martin, K. Morokuma, V. G. Zakrzewski, G. A. Voth, P. Salvador, J. J. Dannenberg, S. Dapprich, A. D. Daniels, Ö. Farkas, J. B. Foresman, J. V. Ortiz, J. Cioslowski, D. J. Fox, Gaussian, Inc., Wallingford CT, 2009.
- [20] C. T. Lee, W. T. Yang, R. G. Parr, *Phys. Rev. B* **1988**, *37*, 785.
- [21] P. J. Hay, W. R. Wadt, *J. Chem. Phys.* **1985**, *82*, 270.
- [22] S. Miertus, E. Scrocco, J. Tomasi, *Chem. Phys.* **1981**, *55*, 117.

Chapter 6

Mixed d Metal-Iron Containing Wells-Dawson Sandwich-type Complexes



In this chapter, we aim to study the electrochemical behavior of mixed d metal-iron containing Wells-Dawson sandwich-type complexes $[\text{Fe}_2(\text{OH}_2)_2\text{M}_2\text{X}_4\text{W}_{30}\text{O}_{112}]^{n-}$ and $[\text{M}_2(\text{OH}_2)_2\text{Fe}_2\text{X}_4\text{W}_{30}\text{O}_{112}]^{n-}$ (with $\text{M} = \text{Cr}^{\text{III}}$, Mn^{III} , Mn^{II} , Co^{II} , Ni^{II} , Cu^{II} or Zn^{II} , $\text{X} = \text{P}^{\text{V}}$ or As^{V} and $n = 12$ or 14). The data suggest that the most stable isomers are those with internally-located Fe^{III} centers, $[(\text{M}(\text{OH}_2)_2\text{Fe}_2)]$. Consequently, their reduction is more difficult than externally-located Fe^{III} , $[(\text{Fe}(\text{OH}_2)_2\text{M}_2)]$.

Related publications:

F. Doungmene, P. A. Aparicio, J. Ntienoue, C. S. Ayingone Mezui, P. de Oliveira, X. López, I. M. Mbomekallé, *Electrochim. Acta* **2014**, *125*, 674.

6.1 Introduction and objectives

A versatile and attracting subclass of polyoxometalates is constituted by sandwich-type POMs (STPs). They are based on Keggin-like ($[\text{XW}_9\text{O}_{33}]^{n-}$, $[\text{XW}_9\text{O}_{34}]^{n-}$ and $[\text{XW}_{10}\text{O}_{36}]^{n-}$, $\text{X} = \text{As}^{\text{V}}$, P^{V} , Si^{IV} , etc) or Wells-Dawson-like ($[\text{X}_2\text{W}_{15}\text{O}_{56}]^{12-}$, $\text{X} = \text{As}^{\text{V}}$ or P^{V}) fragments that incorporate metal oxide clusters in the so-called equatorial region^[1]. Such clusters usually contain two, three or four metal centers, the latter two being the most common situations^[2]. Irrespective of the constitutive fragments, the equatorial region features the same connectivity and properties when the metal oxide cluster contains the same number of metal centers^[2u]. The main differences observed between STPs based on the Keggin or the Wells-Dawson architecture are the overall molecular charge and size. The physicochemical properties of this subclass of molecules are still under investigation by virtue of their versatility and potential applications in different fields such as catalysis^[2o], molecular magnetism^[2d], etc^[3].

For the Keggin STPs, the first synthesized complexes were the $[(\text{MOH}_2)_2\text{M}_2(\text{PW}_9\text{O}_{34})_2]^{10-}$ ($\text{M} = \text{Co}^{\text{II}}$, Cu^{II} , Zn^{II}) anions^[2g]. The Co^{II} derivative is also one of the most studied complexes because of its potential application as water oxidation catalyst^[4]. The first characterized mixed-valence transition metal compound was $[(\text{MnOH}_2)_2\text{Mn}_2(\text{PW}_9\text{O}_{34})_2]^{n-}$, reported by Pope and coworkers^[5], where the Mn atoms have a mixture of +II and +III oxidation states. This compound exhibits magnetic properties and has been a model system for the study of electron exchange interactions within the internal cluster^[6]. Another well-studied structure and the first Keggin-derived STP containing just trivalent transition metal ions in the equatorial region is $[(\text{FeOH}_2)_2\text{Fe}_2(\text{PW}_9\text{O}_{34})_2]$, a system studied by Romo *et al.*^[7], by means of DFT calculations. This compound is able to catalyze the oxidation of internal alkenes with H_2O_2 , but it is an inefficient catalyst for primary alkenes. Depending on the nature of the transition metal atoms constituting the equatorial region, these systems may feature magnetic properties^[2c, 2d, 8]. The first example of a mixed-metal sandwich-type complex described by Wasfi *et al.*^[2i] in 1987 proceeded by a one pot synthesis and contained two different d metal centers in its central cluster. Later on, Reinoso *et al.* have described the first heterometallic 3d-4f derivatives based on the B- α - $[\text{GeW}_9\text{O}_{34}]^{10-}$, that

contained either $[\{\text{Ce}^{\text{III}}(\text{H}_2\text{O})_2\}_2\text{Mn}^{\text{III}}_2]$ or $[\{\text{Ce}^{\text{III}}(\text{OAc})\}\text{Cu}^{\text{II}}_3(\text{H}_2\text{O})]$ as central clusters^[9].

As for the Keggin-based STPs, the first synthesized Wells-Dawson-based complexes were the $[(\text{MOH}_2)_2\text{M}_2(\text{P}_2\text{W}_{15}\text{O}_{56})_2]^{16-}$ ($\text{M} = \text{Co}^{\text{II}}, \text{Cu}^{\text{II}}, \text{Zn}^{\text{II}}$) anions^[2f]. The first compound with trivalent metal cations was $[(\text{FeOH}_2)_2\text{Fe}_2(\text{P}_2\text{W}_{15}\text{O}_{56})_2]^{12-}$, synthesized and characterized by Hill and co-workers^[20]. Sometimes one or two transition metal atoms can be substituted by alkali atoms such as Na^+ . Other structures have also been synthesized, like the following complexes: $[(\text{NaOH}_2)_2\text{Fe}_2(\text{X}_2\text{W}_{15}\text{O}_{56})_2]^{16-}$ and $[(\text{NaOH}_2)(\text{FeOH}_2)\text{Fe}_2(\text{X}_2\text{W}_{15}\text{O}_{56})_2]^{14-}$, where $\text{X} = \text{As}^{\text{V}}$ or $\text{P}^{\text{V}[2z]}$; $[(\text{NaOH}_2)_2\text{Cu}_2(\text{X}_2\text{W}_{15}\text{O}_{56})_2]^{18-}$, where $\text{X} = \text{As}^{\text{V}}$ or $\text{P}^{\text{V}[10]}$; $[\text{Na}_2(\text{H}_2\text{O})_2\text{M}_2(\text{As}_2\text{W}_{15}\text{O}_{56})_2]^{18-}$ with $\text{M} = \text{Ni}^{\text{II}}, \text{Mn}^{\text{II}}$ and $\text{Mn}^{\text{III}[11]}$; $[\text{Na}_2(\text{H}_2\text{O})_2\text{Co}_2(\text{P}_2\text{W}_{15}\text{O}_{56})_2]^{18-}$ and $[(\text{NaOH}_2)(\text{MOH}_2)\text{M}_2(\text{P}_2\text{W}_{15}\text{O}_{56})_2]^{17-}$, where $\text{M} = \text{Co}^{\text{II}}$ and $\text{Mn}^{\text{II}[2aa, 12]}$. Substitution of the Na^+ ions by a different metallic center has led to a new class of STPs, the mixed metal complexes: $[\text{Ni}_2(\text{H}_2\text{O})_2\text{Fe}_2(\text{P}_2\text{W}_{15}\text{O}_{56})_2]^{14-}$, $[\text{Zn}_2(\text{H}_2\text{O})_2\text{Fe}_2(\text{X}_2\text{W}_{15}\text{O}_{56})_2]^{14-}$ with $\text{X} = \text{As}^{\text{V}}$ or P^{V} and $[\text{Na}_2(\text{H}_2\text{O})_2\text{Mn}_2(\text{As}_2\text{W}_{15}\text{O}_{56})_2]^{[2n, 2u, 2x, 11]}$.

In this chapter we present an innovative study on the electrochemical behavior of mixed d metal-iron containing Wells-Dawson sandwich-type complexes $[\text{Fe}_2(\text{OH}_2)_2\text{M}_2\text{X}_4\text{W}_{30}\text{O}_{112}]^{n-}$ and $[\text{M}_2(\text{OH}_2)_2\text{Fe}_2\text{X}_4\text{W}_{30}\text{O}_{112}]^{n-}$ (with $\text{M} = \text{Cr}^{\text{III}}, \text{Mn}^{\text{III}}, \text{Mn}^{\text{II}}, \text{Co}^{\text{II}}, \text{Ni}^{\text{II}}, \text{Cu}^{\text{II}}$ or Zn^{II} , $\text{X} = \text{P}^{\text{V}}$ or As^{V} and $n = 12$ or 14), hereafter $[\text{Fe}_2(\text{OH}_2)_2\text{M}_2]$ and $[\text{M}_2(\text{OH}_2)_2\text{Fe}_2]$, respectively. A representation of these compounds can be found in Figure 6.1. These complexes have a four-center equatorial metal cluster constituted of two Fe atoms and two atoms of another metal. The Fe^{III} centers are either in the external position, $[\text{Fe}_2(\text{OH}_2)_2\text{M}_2]$, or in the internal position, $[\text{M}_2(\text{OH}_2)_2\text{Fe}_2]$. Experimental methods (cyclic voltammetry and controlled potential coulometry) and theoretical calculations (DFT) allowed us to determine and analyze the redox potential values associated with the reduction of the Fe^{III} centers in these species. The influence of the position of Fe^{III} centers, the nature of the metal center M and the electron density distribution in the tetranuclear cluster (either $[\text{Fe}_2(\text{OH}_2)_2\text{M}_2]$ or $[\text{M}_2(\text{OH}_2)_2\text{Fe}_2]$) have been studied and rationalized in order to account for the observed behaviors.

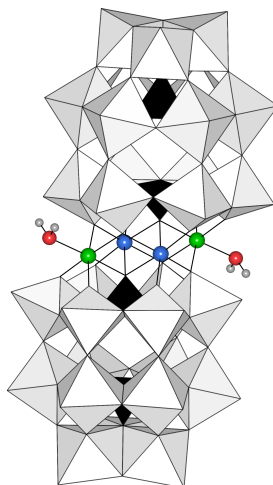


Figure 6.1. Wells-Dawson-based sandwich-type structure, with the cluster of four metal atoms and two water molecules between two $[X_2W_{15}O_{56}]$ fragments (polyhedral view). Ball and stick representation: O in red, H in grey, external metal positions in green, internal metal positions in blue.

6.2 Experimental background

Dr. I. M. Mbomekallé (Institut Lavoisier, Université de Versailles) has carried out electrochemical measurements on the mixed d metal-iron containing Wells-Dawson sandwich-type complexes $[Fe_2(OH_2)_2M_2]$ and $[M_2(OH_2)_2Fe_2]$ (with $M = Cr^{III}, Mn^{II}, Mn^{III}, Fe^{III}, Co^{II}, Ni^{II}, Cu^{II}$ or Zn^{II}). These were carried out solely with $[As_2W_{18}O_{62}]^{6-}$ derivatives. The species containing P as central heteroatom have not been studied experimentally. In fact, the influence of the nature of the heteroatom (As or P) on the electrochemical response is the same for all the clusters such as $[Fe_2(OH_2)_2M_2]$ or $[M_2(OH_2)_2Fe_2]$, namely a slight cathodic shift ($\Delta E < 0.020$ V) of the redox waves when As is replaced by P. This behavior has been already described in several papers^[2x, 13]. The selected STPs were tested in two different media, where both compounds are stable enough: pH 6.0, where the influence of protonation is less obvious, and pH 3.0, where protonation has a greater effect on the redox behavior of these molecules. The peak potentials associated with the reduction of the Fe^{III} centers depend on the nature and on the position of the M cations in the central cluster. The cathodic peak potential values associated with the Fe^{III} centers, $E_{pc}(Fe_1)$ and $E_{pc}(Fe_2)$, obtained by *cyclic voltammetry* (CV), are compiled in Table 6.1.

Table 6.1. Cathodic peak potentials (E_{pc} vs. SCE, in V) for the first and second single-electron reduction step of Fe^{III} centers, either pH 6 or pH 3.

pH 6					
	$E_{pc}(\text{Fe}_1)$	$E_{pc}(\text{Fe}_2)$		$E_{pc}(\text{Fe}_1)$	$E_{pc}(\text{Fe}_2)$
$[(\text{NaOH}_2)_2\text{Fe}_2]$	-0.220	-0.330	-	-	-
$[(\text{ZnOH}_2)_2\text{Fe}_2]$	-0.150	-0.270	$[(\text{FeOH}_2)_2\text{Zn}_2]$	-0.180	-0.280
$[(\text{CuOH}_2)_2\text{Fe}_2]$	-0.130 ^a		$[(\text{FeOH}_2)_2\text{Cu}_2]$	-0.130 ^a	
$[(\text{NiOH}_2)_2\text{Fe}_2]$	-0.200	-0.310	$[(\text{FeOH}_2)_2\text{Ni}_2]$	0.000	-0.100
$[(\text{CoOH}_2)_2\text{Fe}_2]$	-0.090	-0.220	$[(\text{FeOH}_2)_2\text{Co}_2]$	-0.090	-0.260
$[(\text{MnOH}_2)_2\text{Fe}_2]$	-0.160	-0.280	$[(\text{FeOH}_2)_2\text{Mn}_2]$	-0.160	-0.270
$[(\text{Mn}^{\text{III}}\text{OH}_2)_2\text{Fe}_2]^c$	-	-	$[(\text{FeOH}_2)_2\text{Mn}^{\text{III}}_2]$	-0.150	-0.270
$[(\text{Cr}^{\text{III}}\text{OH}_2)_2\text{Fe}_2]^c$	-	-	$[(\text{FeOH}_2)_2\text{Cr}^{\text{III}}_2]$	-0.290 ^b	
pH 3					
	$E_{pc}(\text{Fe}_1)$	$E_{pc}(\text{Fe}_2)$		$E_{pc}(\text{Fe}_1)$	$E_{pc}(\text{Fe}_2)$
$[(\text{NaOH}_2)_2\text{Fe}_2]$	-0.090	-0.200	-	-	-
$[(\text{ZnOH}_2)_2\text{Fe}_2]$	-0.080	-0.190	$[(\text{FeOH}_2)_2\text{Zn}_2]$	-0.070	-0.190
$[(\text{CuOH}_2)_2\text{Fe}_2]$	-0.130 ^a		$[(\text{FeOH}_2)_2\text{Cu}_2]$	-0.120 ^a	
$[(\text{NiOH}_2)_2\text{Fe}_2]$	-0.060	-0.090	$[(\text{FeOH}_2)_2\text{Ni}_2]$	0.006 ^b	
$[(\text{CoOH}_2)_2\text{Fe}_2]$	-0.090 ^b		$[(\text{FeOH}_2)_2\text{Co}_2]$	-0.090	-0.200
$[(\text{MnOH}_2)_2\text{Fe}_2]$	-0.080	-0.200	$[(\text{FeOH}_2)_2\text{Mn}_2]$	-0.080	-0.200
$[(\text{Mn}^{\text{III}}\text{OH}_2)_2\text{Fe}_2]^c$	-	-	$[(\text{FeOH}_2)_2\text{Mn}^{\text{III}}_2]$	-0.100	-0.200
$[(\text{Cr}^{\text{III}}\text{OH}_2)_2\text{Fe}_2]^c$	-	-	$[(\text{FeOH}_2)_2\text{Cr}^{\text{III}}_2]$	-0.100	-0.330

^a The two single-electron steps corresponding to the Fe^{III}/Fe^{II} reduction merge into a single wave which appears as a shoulder on the following wave that concerns the reduction of the Cu^{II} centers. ^b The two single-electron steps corresponding to the reduction of the two Fe^{III} centers merge into a single two-electron wave. ^c This compounds have not been isolated so far.

Two different situations have been envisaged: (i) the compound $[(\text{NaOH}_2)_2\text{Fe}_2]$ is the original structure characterized by a central metallic cluster, in which

the two Fe^{III} centers are internally located. The two external Na ions are then selectively replaced by two metallic M centers and a new cluster is obtained, $[(\text{MOH}_2)_2\text{Fe}_2]$. (ii) In structure $[(\text{NaOH}_2)_2\text{M}_2]$, the Fe^{III} centers will take the place of the two Na ions and will be found in an external position. In short, the two situations allow to study the behavior of Fe^{III} centers found in two different coordination spheres, located either internally or externally, and in an environment influenced by the electronic configuration of the neighboring metallic center, either a sodium ion or a metal cation M.

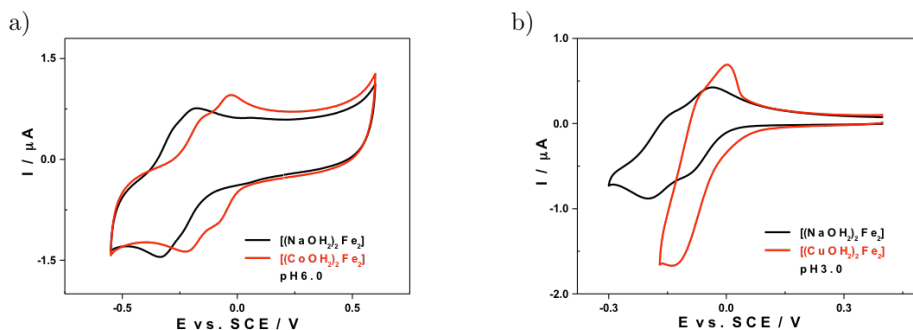


Figure 6.2. Comparison of the CVs obtained with $[(\text{NaOH})_2\text{Fe}_2]$ (black line) and with (a) $[(\text{CoOH})_2\text{Fe}_2]$ or (b) $[(\text{CuOH})_2\text{Fe}_2]$ (red line) in 1.0 M $\text{LiCH}_3\text{COO} + \text{CH}_3\text{COOH}$, at pH 3 and 6 respectively. The potential range is restricted to the Fe^{III} centers. POM concentration: 0.2 M, working electrode: glassy carbon, reference electrode: SCE, auxiliary electrode: platinum, scan rate: 10 mVs^{-1} .

In the first case, when two sodium ions are replaced by two d-type metal cations (M^{II}), the global negative charge decreases from -16 to -14, and the Fe^{III} center reduction becomes easier (Figure 6.2a). At pH 6, when going from $[(\text{NaOH})_2\text{Fe}_2]$ to $[(\text{CoOH})_2\text{Fe}_2]$, a maximum anodic shift of 0.130 V is observed for this family of compounds. In the case of $[(\text{NiOH})_2\text{Fe}_2]$, a species iso-electronic of the previous one, the shift is just 0.020 V. If we consider the series of compounds substituted by divalent d-type cations, the cathodic peak potentials for the reduction of the Fe^{III} centers, $E_{\text{pc}}(\text{Fe}_1)$, follow the order: $E_{\text{pc}}(\text{Fe}_1)_{\text{Ni}} < E_{\text{pc}}(\text{Fe}_1)_{\text{Mn}} < E_{\text{pc}}(\text{Fe}_1)_{\text{Zn}} < E_{\text{pc}}(\text{Fe}_1)_{\text{Cu}} < E_{\text{pc}}(\text{Fe}_1)_{\text{Co}}$. Since all these species have the same global charge, parameters other than the charge have to be taken into account in order to explain the observed behavior. All the divalent cations considered above have rather different electronic configurations as far as their valence d layers are concerned, as well as different acid/base properties in aqueous solution. The vicinity of metal centers M having differently filled d orbitals will directly influence the

electronic density of the Fe^{III} centers and therefore their tendency to accept supplementary electrons.

The influence on $E_{\text{pc}}(\text{Fe}_1)$ observed at pH 3.0, where the protonation effect cannot be ignored, is very different when compared to the one previously reported for pH 6. By and large, when the pH decreases from 6 to 3, the reduction peak potentials $E_{\text{pc}}(\text{Fe}_1)$ are anodically shifted, meaning that at a higher H^+ concentration (pH 3), electron transfer becomes easier. In fact, the Fe^{III} center reduction in the present species is concomitant to protonation. The influence of the acid/base properties of the different complexes becomes predominant in this medium, and the most basic species will more easily and rapidly accept an extra electron. It has been found that the $[(\text{NiOH}_2)_2\text{Fe}_2]$ compound becomes the cluster that will be reduced most easily. On the contrary, $[(\text{CoOH}_2)_2\text{Fe}_2]$, which seems to be more difficult to reduce ($E_{\text{pc}}(\text{Fe}_1) = -0.090$ V), takes up two electrons in a single step. The behavior of $[(\text{CuOH}_2)_2\text{Fe}_2]$ is more peculiar, its cathodic peak potential at -0.130 V corresponding to the simultaneous reduction of the Fe^{III} and the Cu^{II} centers (Figure 6.2b). The protonation influence is too strong at pH 3 and does not allow a neat comparison between the Fe^{III} reduction potential as a function of the associated metal center M within the cluster $[(\text{MOH}_2)_2\text{Fe}_2]$.

At pH 6.0, the observed trend in the reduction peak potentials, $E_{\text{pc}}(\text{Fe}_1)$, matches the theoretical calculation predictions in just two single cases: (i) when Cu^{II} centers are associated with the Fe^{III} centers, the first electron is exchanged at the same potential value (see Table 6.1) and is taken up by the Fe^{III} centers, irrespective of their relative positions, either externally or internally located. (ii) The presence of Ni^{II} centers, which are not electroactive in the potential range used in the present work, strongly influences the electrochemical behavior of the Fe^{III} centers found in the same STP. In fact, externally located Fe^{III} centers are much easier to reduce than internally located ones, both at pH 6 and at pH 3.

The influence of the Fe^{III} centers location within the STP on their reduction peak potential values is more pronounced at pH 6 ($\{E_{\text{pc}}(\text{Fe}_{\text{ext}}) - E_{\text{pc}}(\text{Fe}_{\text{int}})\}_{\text{pH}6} = 0.200$ V and $\{E_{\text{pc}}(\text{Fe}_{\text{ext}}) - E_{\text{pc}}(\text{Fe}_{\text{int}})\}_{\text{pH}3} = 0.066$ V), a medium in which the protonation effect is limited and cannot account for the observed results on their own. Neither do electronic properties suffice to explain this behavior.

For the other metal centers M studied (Mn^{II} , Co^{II} and Zn^{II}), the experimental results disagree with the theoretical calculations, which foresee that externally

located Fe^{III} should be easier to reduce than internally located ones. For example, when Zn^{II} and Fe^{III} centers are combined in the same STP, an inversion of the predicted trend is observed at pH 6, with internally located Fe^{III} centers being easier to reduce than externally-located ones ($\{E_{\text{pc}}(\text{Fe}_{\text{ext}}) - E_{\text{pc}}(\text{Fe}_{\text{int}})\}_{\text{pH}6} = 0.030 \text{ V}$). As far as the Mn^{II} and the Co^{II} centers are concerned, when associated with Fe^{III} centers in STPs, the reduction potentials of the latter are one and the same for both locations, a fact observed both at pH 6 and at pH 3. Last but not least, the study of STPs possessing both Fe^{III} and Zn^{II} centers at pH 3, a medium where protonation is important, revealed that the reduction of externally located Fe^{III} centers is favored, since their protonation is more accessible.

6.3 Results and discussion

Complementing the electrochemical measurements, DFT calculations have been carried out on the mentioned compounds. We computed total molecular energies for the oxidized and 1e-reduced molecules to obtain the relative stabilities of each pair of isomers and the 1e-REs, listed in Table 6.2.

The relative stability of the two positional isomers show, with the sole exception of $\text{M} = \text{Cr}^{\text{III}}$, and not considering protonation, that the DFT-optimized structures with internal Fe^{III} are more stable. For Zn^{II} , Cu^{II} , Ni^{II} , Co^{II} and Mn^{II} the energy difference between both oxidized isomers is $\Delta E_{\text{ox}} = 12 \text{ kcal mol}^{-1}$ on average, decreasing to $\Delta E_{\text{red}} = 7\text{--}8 \text{ kcal mol}^{-1}$ for the monoreduced species ($\text{X} = \text{P}$ or As). Of course, the second reduction makes both isomeric forms even closer in energy. For Mn^{III} , $\Delta E_{\text{ox}} = 24 \text{ kcal mol}^{-1}$, notably larger than for $\text{M} = \text{Co-Zn}$. We can thus consider that, in general, $\text{M}_2\text{Fe}^{\text{III}}_2$ is the dominant and most stable species in oxidized form from a thermodynamic point of view. The fact that $\Delta E_{\text{ox}} > \Delta E_{\text{red}}$ is the computational proof that the $[(\text{Fe}^{\text{III}}\text{OH}_2)_2\text{M}_2]$ form is naturally more oxidant (more exothermic REs) than $[(\text{MOH}_2)_2\text{Fe}^{\text{III}}_2]$, not considering protonation effects. We will see below that the case of $\text{M} = \text{Ni}$ is the expected one from calculations and not an exception within the family of studied systems.

Table 6.2. Computed energy differences between the $[(\text{MOH}_2)_2\text{Fe}_2]$ and $[(\text{FeOH}_2)_2\text{M}_2]$ isomers (ΔE_{ox} and ΔE_{red}), 1e-reduction energies (REs) and their difference (ΔRE) for X = As compounds (in eV).

	Initial charge	ΔE_{ox}	ΔE_{red}	RE	$\Delta\text{RE}^{\text{a}}$
$[(\text{FeOH}_2)_2\text{Zn}_2]$	14-			-4.233	
$[(\text{ZnOH}_2)_2\text{Fe}_2]$	14-	-0.508	-0.191	-3.917	0.316
$[(\text{FeOH}_2)_2\text{Cu}_2]$	14-			-4.127	
$[(\text{CuOH}_2)_2\text{Fe}_2]$	14-	-0.576	-0.604	-4.155	-0.027
$[(\text{FeOH}_2)_2\text{Ni}_2]$	14-			-4.196	
$[(\text{NiOH}_2)_2\text{Fe}_2]$	14-	-0.395	-0.243	-4.044	0.152
$[(\text{FeOH}_2)_2\text{Co}_2]^{\text{b}}$	14-			-4.217	
$[(\text{CoOH}_2)_2\text{Fe}_2]^{\text{b}}$	14-	-0.349	-0.260	-3.893	0.325
$[(\text{FeOH}_2)_2\text{Mn}_2]$	14-			-4.251	
$[(\text{MnOH}_2)_2\text{Fe}_2]$	14-	-0.603	-0.330	-3.977	0.273
$[(\text{FeOH}_2)_2\text{Mn}^{\text{III}}_2]$	12-			-4.777	
$[(\text{Mn}^{\text{III}}\text{OH}_2)_2\text{Fe}_2]$	12-	-1.03	-0.475	-4.225	0.553
$[(\text{FeOH}_2)_2\text{Cr}^{\text{III}}_2]$	12-			-4.517	
$[(\text{Cr}^{\text{III}}\text{OH}_2)_2\text{Fe}_2]$	12-	+0.303	+0.637	-4.183	0.334

^a $\Delta\text{RE} = \text{RE}\{[(\text{MOH}_2)_2\text{Fe}_2]\} - \text{RE}\{[(\text{FeOH}_2)_2\text{M}_2]\}$. ^b Values computed for X = P derivatives.

In line with electrochemical measurements, DFT data reproduce the cathodic shift of 5-20 meV observed when As is replaced by P. Also, among the studied structures, those with higher negative charge present less negative reduction energies, as shown in Table 6.2 (X = As). The range of reduction energies for the 14- charged species is -3.89 to -4.25 eV. For the 12- charged species, the values are comprised between -4.18 and -4.78 eV, that is, 0.3 to 0.5 eV more negative. These are quite exothermic though common values in POMs despite dealing with highly negatively charged molecules. It must be taken into consideration that, if protonation was accounted for in the calculations, these

reduction energies would be even more negative due to the concomitant decrease in the initial negative molecular charge.

The two rightmost columns of Table 6.2 list the REs for each system, and the difference between pairs of isomers (Δ RE), respectively, showing that the most exothermic (favorable) REs always correspond to $[(\text{Fe}^{\text{III}}\text{OH}_2)_2\text{M}_2]$ isomers, thus they are more oxidizing than $[(\text{MOH}_2)_2\text{Fe}^{\text{III}}_2]$. The Δ RE differences for each M are not easy to rationalize although they all oscillate around a mean value of 0.3 eV. We discussed in the experimental section that the case with $\text{M} = \text{Ni}$ presented a somewhat exceptional behavior, even though it is clear from the computational data that all the systems except $\text{M} = \text{Cu}$ behave the same way: without protonation, the systems with external Fe atoms are stronger oxidants.

A possible competition for the incoming electron(s) depends on the nature and position of the metal atoms in the equatorial region. How is the incoming electron shared within the equatorial cluster? To know from calculations where it is located, the oxidation state of the relevant metal atoms has to be monitored by analyzing their atomic spin populations (ASPs, Table 6.3) in the oxidized and reduced forms. These ASPs have a direct correspondence with the number of excess ($\alpha - \beta$) electrons in the valence d shell of metal atoms shown in Figure 6.3. Since we deal with M^{n+} ions in a pseudo-octahedral ligand field, their valence d orbitals ideally split into the two sets represented, accommodating 3 (Cr^{III}) to 10 (Zn^{II}) electrons. We consider that each metal atom is in its high spin configuration owing to the weak ligand field exerted by the oxo groups and the terminal water ligand. Consequently, only d^3 (Cr^{III}) and d^4 (Mn^{III}) based compounds are allowed to accept a new spin-up electron. However, if Fe^{III} (a d^5 atom) accepts an electron, it will enter as spin-down to give the d^6 configuration, thus cancelling out part of the initial spin-up density.

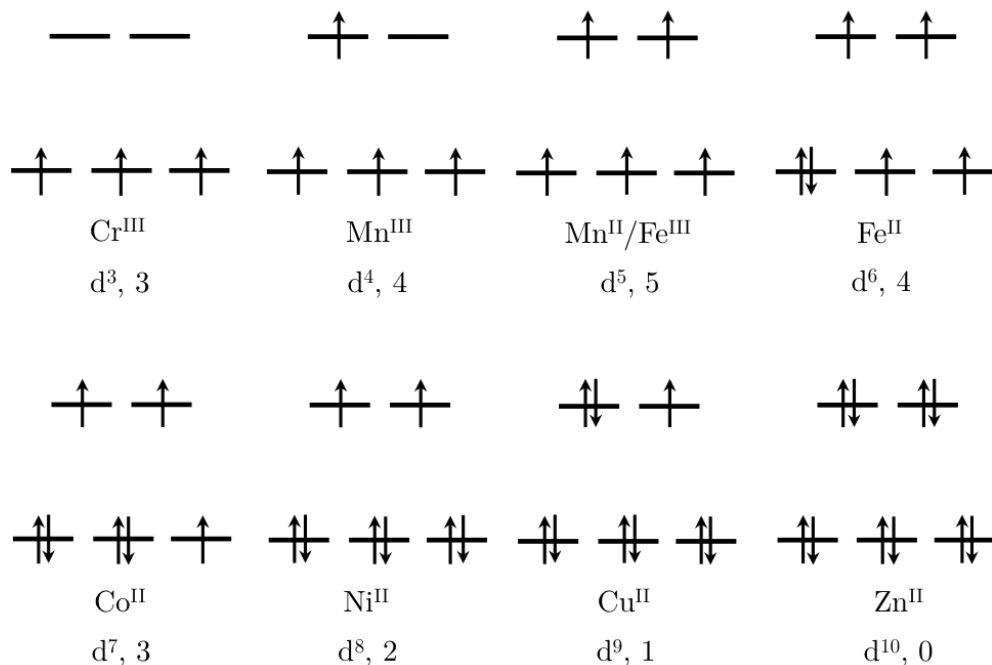


Figure 6.3. Electronic configurations deriving from a weak octahedral field for first row transition metals. The number of $\alpha - \beta$ electrons is shown.

In the computed 1e-reduced compounds it must be considered that the extra electron formally splits between, at least, two metal centers by reasons of molecular symmetry. In addition to this, electron polarization to the neighboring oxygens make the ASP variations small from the oxidized to the reduced states as can be observed in the ASPs of metal ions listed in Table 6.3 (note that the values are smaller than the *formal* ones) except for $M = \text{Mn}^{\text{III}}$, no matter if Fe^{III} is in the internal or external position. This is an important observation since it helps understanding that the process taking place is $\text{Fe}^{\text{III}} + e \rightarrow \text{Fe}^{\text{II}}$ in all cases but for $M = \text{Mn}^{\text{III}}$.

Table 6.3. Atomic spin populations (ASPs) for the equatorial metal atoms^a in the oxidized and reduced forms.

External Fe		Internal Fe					
		Oxidized	Reduced				
[(FeOH ₂) ₂ Zn ₂]	Zn	0.001	-0.005	[(ZnOH ₂) ₂ Fe ₂]	Fe	4.122	3.986
	Fe	4.127	3.999		Zn	-0.005	-0.006
[(FeOH ₂) ₂ Cu ₂]	Cu	0.700	0.678	[(CuOH ₂) ₂ Fe ₂]	Fe	4.137	4.044
	Fe	4.129	4.009		Cu	0.652	0.570
[(FeOH ₂) ₂ Ni ₂]	Ni	1.704	1.699	[(NiOH ₂) ₂ Fe ₂]	Fe	4.126	3.996
	Fe	4.137	4.005		Ni	1.699	1.695
[(FeOH ₂) ₂ Co ₂]	Co	2.714	2.744	[(CoOH ₂) ₂ Fe ₂]	Fe	4.127	3.992
	Fe	4.122	3.994		Co	2.719	2.715
[(FeOH ₂) ₂ Mn ₂]	Mn	4.786	4.783	[(MnOH ₂) ₂ Fe ₂]	Fe	4.114	3.974
	Fe	4.110	3.985		Mn	4.807	4.805
[(FeOH ₂) ₂ Mn ^{III} ₂]	Mn	3.760	4.365	[(Mn ^{III} OH ₂) ₂ Fe ₂]	Fe	4.119	4.115
	Fe	4.106	4.107		Mn	3.901	4.378
[(FeOH ₂) ₂ Cr ^{III} ₂]	Cr	2.941	2.938	[(Cr ^{III} OH ₂) ₂ Fe ₂]	Fe	4.110	3.978
	Fe	4.138	4.007		Cr	2.982	2.969

^aThe initial oxidation state of Fe is +III, and unless otherwise indicated, that of the other elements is +II.

The molecular orbital representation in Figure 6.4 evidences that the molecular orbital accepting the extra electron during the reduction process belongs to the Fe atoms in both isomers, as illustrated in the data presented above. Following the *general* trend obtained by DFT calculations for M^{II}-Fe^{III}

mixtures, Fe^{III} centers are reduced irrespective of what position they occupy in the equatorial cluster. The higher oxidation state of Fe^{III} compared with its M^{II} partners is determinant to this issue: no M^{II} ion from the first period of transition metals will achieve the M^{I} state before Fe^{III} is reduced to Fe^{II} .

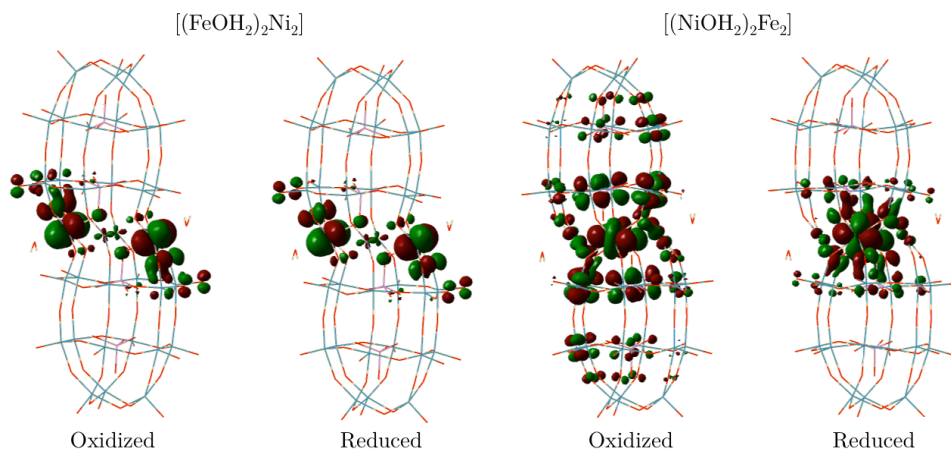


Figure 6.4. Fe-like molecular orbitals of $[(\text{FeOH}_2)_2\text{Ni}_2]$, with external-Fe atoms, and $[(\text{NiOH}_2)_2\text{Fe}_2]$, with internal-Fe atoms, before (oxidized) and after (reduced) accepting the extra electron.

Although it was not possible to be fully characterized by electrochemistry, DFT calculations show that both isomers of the Mn^{III} -containing STPs are firstly reduced in the Mn^{III} centers to reach the Mn^{II} state. This is shown in Table 6.3 by an increase of the net spin density on the high spin Mn atoms, indicating that the $\text{Mn}^{\text{III}} \rightarrow \text{Mn}^{\text{II}}$ process takes place. It is expected that Mn^{III} reduces before Fe^{III} owing to the more favorable $d^4 \rightarrow d^5$ process (Mn) in front of $d^5 \rightarrow d^6$ (Fe). The structure with internal Mn^{III} atoms is more easily reduced by 0.55 eV. After both Mn^{III} atoms are reduced, Fe^{III} atoms gain electrons. Figure 6.5 shows a scheme of the molecular orbitals involved in the reduction processes for an entering spin-up or spin-down electron.

All in all, the Fe-Cu case is the one presenting the most exceptional behavior within the group of divalent M atoms since both isomers are reduced at very similar energies (27 and 18 meV difference only for X = As and P, respectively). Interestingly, the $[\text{Cu}(\text{OH}_2)_2\text{Fe}_2]$ isomer is largely more stable than its external-Fe counterpart by -0.576 eV, inline with the other members of the family. Its specific quality is that an incoming electron cannot distinguish between the two isomers and *see* them as equally oxidising, so the isomerism is electrochemically irrelevant. As a proof of concept, Table 6.3

shows a net decrease in ASPs for both Fe and Cu atoms when going from the oxidized to the reduced form, more clearly for the $[(\text{CuOH}_2)_2\text{Fe}_2]$ isomer. The incoming electron is *shared* between the four equatorial metal atoms, indicating an equal electronegativity in Cu^{II} and Fe^{III} and explaining the experimental and theoretical redox behavior of this pair of isomers.

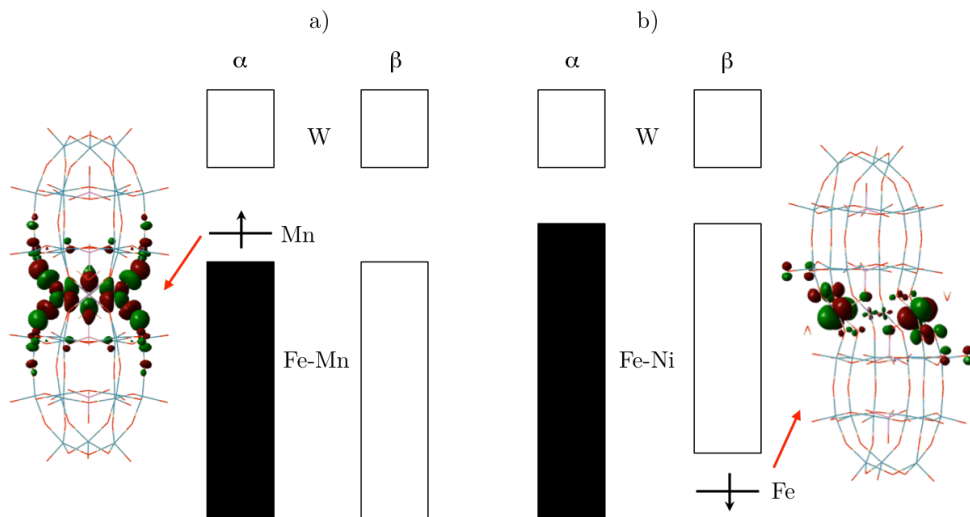


Figure 6.5. Two examples of mono-reduction with the incoming electron (arrow) having either (a) an α spin, case of $\text{Fe}_2\text{Mn}^{\text{III}}_2$, or (b) a β spin, case of Fe_2Ni_2 and others. Black and white blocks represent filled and empty metal-like molecular orbitals, respectively.

6.4 Conclusions

We have carried out an innovative study on the electrochemical behavior of mixed d metal-iron containing Wells-Dawson sandwich-type complexes $[\text{Fe}_2(\text{OH}_2)_2\text{M}_2\text{X}_4\text{W}_{30}\text{O}_{112}]^{14-}$ and $[\text{M}_2(\text{OH}_2)_2\text{Fe}_2\text{X}_4\text{W}_{30}\text{O}_{112}]^{14-}$ (with $\text{M} = \text{Cr}^{\text{III}}, \text{Mn}^{\text{II}}, \text{Mn}^{\text{III}}, \text{Co}^{\text{II}}, \text{Ni}^{\text{II}}, \text{Cu}^{\text{II}}$ or Zn^{II} and $\text{X} = \text{P}^{\text{V}}$ or As^{V}). This study combined experimental methods (cyclic voltammetry and controlled potential coulometry) with theoretical calculations and allowed us to determine redox potential values associated with the reduction of the Fe^{III} centers in these species. In most of the cases, the reduction of the two Fe^{III} centers takes place in two successive single-electron steps, each electron being delocalized over the two centers. DFT calculation led to a compilation of molecular energies associated with the one-electron oxidized and reduced forms of all the compounds in the family. It seems that the most stable isomers are those where Fe^{III} centers are internally-located, $[(\text{MOH}_2)_2\text{Fe}_2]$. Consequently, their

reduction is more difficult than those having externally-located Fe^{III} isomers, $[(\text{FeOH}_2)_2\text{M}_2]$. Some experimental results revealed a few exceptions to this rule, which have not been rationalized yet. In summary, in the majority of the cases studied, we were able to rationalize the redox behavior and the electron distribution within the valence shell orbitals of these compounds, which opens the way to improved prediction capabilities of their electrochemical and magnetic properties.

6.5 Computational details

Density functional theory calculations have been carried out using the Gaussian 09 suite of programs^[14]. The geometries of all the structures were fully optimized in conditions of no protonation and their energies obtained within the constraints of the C_{2h} symmetry point group. Reduction energies (REs) were computed as purely electronic $E_{\text{red}} - E_{\text{ox}}$ energy differences. We applied the B3LYP hybrid functional^[15] and double- ζ + polarization basis sets: 6-31G(d,p), for H and O atoms and Hay-Wadt with LANL pseudopotentials^[16] (LANL2DZ) for metal atoms. The calculations include PCM^[17] to account for the solvent effects of water ($\epsilon = 78.4$), which is essential for a correct description of REs. The solute cavity was created using a scaled van der Waals surface with atomic radii corresponding to the Universal Force Field parameters, with a grids of ~ 5 points per \AA^2 . We applied the spin-unrestricted formalism to electronically open-shell molecules. Atomic spin populations (ASPs) were obtained by means of the Mulliken formula.

6.6 References

- [1] a) M. T. Pope, *Heteropoly and Isopoly Oxometalates*, Springer-Verlag, Berlin, 1983; b) D.-L. Long, R. Tsunashima, L. Cronin, *Angew. Chem., Int. Ed.* **2010**, *49*, 1736.
- [2] a) L.-H. Bi, R.-D. Huang, J. Peng, E.-B. Wang, Y.-H. Wang, C.-W. Hu, *J. Chem. Soc., Dalton Trans.* **2001**, 121; b) L.-H. Bi, E.-B. Wang, J. Peng, R.-D. Huang, L. Xu, C.-W. Hu, *Inorg. Chem.* **2000**, *39*, 671; c) N. Casañ-Pastor, J. Bas-Serra, E. Coronado, G. Pourroy, L. C. W. Baker, *J. Am. Chem. Soc.* **1992**, *114*, 10380; d) J. M. Clemente-Juan, E. Coronado, J. R. Galán-Mascarós, C. J. Gómez-García, *Inorg. Chem.* **1999**, *38*, 55; e) H. T. Evans, C. M. Tourne, G. F. Tourne, T. J. R. Weakley, *J. Chem. Soc., Dalton Trans.* **1986**, 2699; f) R. G. Finke, M. Droege, *Inorg. Chem.* **1983**, *22*, 1006; g) R. G. Finke, M. Droege, J. R. Hutchinson, O. Gansow, *J. Am. Chem. Soc.* **1981**, *103*, 1587; h) R. G. Finke, M. W. Droege, P. J. Domaille, *Inorg. Chem.* **1987**, *26*, 3886; i) C. J. Gómez-García, J. J. Borrás-Almenar, E. Coronado, L. Ouahab, *Inorg. Chem.* **1994**, *33*, 4016; j) C. J. Gomez-García, E. Coronado, P. Gómez-Romero, N. Casañ-Pastor, *Inorg. Chem.* **1993**, *32*, 89; k) C. M. Tourné, G. F. Tourné, F. Zonnevillage, *J. Chem. Soc., Dalton Trans.* **1991**, 143; l) S. H. Wasfi, A. L. Rheingold, G. F. Kokoszka, A. S. Goldstein, *Inorg. Chem.* **1987**, *26*, 2934; m) T. J. R. Weakley, H. T. Evans, J. S. Showell, G. F. Tourne, C. M. Tourne, *J. Chem. Soc., Chem. Commun.* **1973**, 139; n) T. J. R. Weakley, R. G. Finke, *Inorg. Chem.* **1990**, *29*, 1235; o) F. Q. Zhang, Q. Chen, D. C. Duncan, C. Campana, C. L. Hill, *Inorg. Chem.* **1997**, *36*, 4208; p) F. Q. Zhang, Q. Chen, D. C. Duncan, R. J. Lachicotte, C. L. Hill, *Inorg. Chem.* **1997**, *36*, 4381; q) X.-Y. Zhang, C. J. O'Connor, G. B. Jameson, M. T. Pope, *Inorg. Chem.* **1996**, *35*, 30; r) T. M. Anderson, K. I. Hardcastle, N. Okun, C. L. Hill, *Inorg. Chem.* **2001**, *40*, 6418; s) U. Kortz, S. Isber, M. H. Dickman, D. Ravot, *Inorg. Chem.* **2000**, *39*, 2915; t) X. Zhang, T. M. Anderson, Q. Chen, C. L. Hill, *Inorg. Chem.* **2001**, *40*, 418; u) T. M. Anderson, X. Zhang, K. I. Hardcastle, C. L. Hill, *Inorg. Chem.* **2002**, *41*, 2477; v) X. Fang, T. M. Anderson, C. Benelli, C. L. Hill, *Chem. Eur. J.* **2005**, *11*, 712; w) U. Kortz, M. G. Savelieff, B. S. Bassil, B. Keita, L. Nadjo, *Inorg. Chem.* **2002**, *41*, 783; x) I. M. Mbomekallé, R. Cao, K. I. Hardcastle, C. L. Hill, M. Ammam, B. Keita, L. Nadjo, T. M. Anderson, *C. R. Chimie* **2005**, *8*, 1077; y) I. M. Mbomekallé, B. Keita, L. Nadjo, P. Berthet, K. I. Hardcastle, C. L. Hill, T. M. Anderson, *Inorg. Chem.* **2003**, *42*, 1163; z) I. M. Mbomekallé, B. Keita, L. Nadjo, W. A. Neiwert, L. Zhang, K. I. Hardcastle, C. L. Hill, T. M. Anderson, *Eur. J. Inorg. Chem.* **2003**, 3924; aa) L. Ruhlmann, J. Canny, R. Contant, R. Thouvenot, *Inorg. Chem.* **2002**, *41*, 3811; ab) L. Ruhlmann, J. Canny, J. Vaissermann, R. Thouvenot, *Dalton Trans.* **2004**, 794; ac) L. Ruhlmann, L. Nadjo, J. Canny, R. Contant, R. Thouvenot, *Eur. J. Inorg. Chem.* **2002**, *2002*, 975; ad) C. Lydon, C. Busche, H. Miras, A. Delf, D.-L. Long, L. Yellowlees, L. Cronin, *Angew. Chem., Int. Ed.* **2012**, *51*, 2115; ae) C. Ritchie, A. Ferguson, H. Nojiri, H. Miras, Y.-F. Song, D.-L. Long, E. Burkholder, M. Murrie, P. Kögerler, E. Brechin, L. Cronin, *Angew. Chem., Int. Ed.* **2008**, *47*, 5609.
- [3] a) B. Keita, T. Liu, L. Nadjo, *J. Mater. Chem.* **2009**, *19*, 19; b) U. Kortz, A. Müller, J. van Slageren, J. Schnack, N. S. Dalal, M. N. Dressel, *Coord. Chem. Rev.* **2009**, 2315; c) D.-L. Long, E. Burkholder, L. Cronin, *Chem. Soc. Rev.* **2007**, *36*, 105.

- [4] a) J. J. Stracke, R. G. Finke, *J. Am. Chem. Soc.* **2011**, *133*, 14872; b) Q. Yin, J. M. Tan, C. Besson, Y. V. Geletii, D. G. Musaev, A. E. Kuznetsov, Z. Luo, K. I. Hardcastle, C. L. Hill, *Science* **2010**, *328*, 342.
- [5] X.-Y. Zhang, G. B. Jameson, C. J. O'Connor, M. T. Pope, *Polyhedron* **1996**, *15*, 917.
- [6] C. J. Gómez-García, E. Coronado, P. Gómez-Romero, N. Casañ-Pastor, *Inorg. Chem.* **1993**, *32*, 3378.
- [7] S. Romo, J. Fernández, J. Maestre, B. Keita, L. Nadjo, C. de Graaf, J. M. Poblet, *Inorg. Chem.* **2007**, *46*, 4022.
- [8] J. M. Clemente-Juan, E. Coronado, A. Gaita-Ariño, C. Giménez-Saiz, H.-U. Güdel, A. Sieber, R. Bircher, H. Mutka, *Inorg. Chem.* **2005**, *44*, 3389.
- [9] a) S. Reinoso, J. Galán-Mascarós, *Inorg. Chem.* **2010**, *49*, 377; b) S. Reinoso, J. R. Galán-Mascarós, L. Lezama, *Inorg. Chem.* **2011**, *50*, 9587.
- [10] T. M. Anderson, X. Fang, I. M. Mbomekallé, B. Keita, L. Nadjo, K. I. Hardcastle, A. Farsidjani, C. L. Hill, *J. Clust. Sci.* **2006**, *17*, 183.
- [11] a) M. Lebrini, I. M. Mbomekallé, A. Dolbecq, J. Marrot, P. Berthet, J. Ntienoue, F. Sécheresse, J. Vigneron, A. Etcheberry, *Inorg. Chem.* **2011**, *50*, 6437; b) I. M. Mbomekallé, P. Mialane, A. Dolbecq, J. Marrot, F. Sécheresse, P. Berthet, B. Keita, L. Nadjo, *Eur. J. Inorg. Chem.* **2009**, *34*, 5194.
- [12] L. Ruhlmann, C. Costa-Coquelard, J. Canny, R. Thouvenot, *J. Electroanal. Chem.* **2007**, *603*, 260.
- [13] a) B. Keita, I. M. Mbomekallé, L. Nadjo, *Electrochem. Commun.* **2003**, *5*, 830; b) B. Keita, I. M. Mbomekallé, L. Nadjo, R. Contant, *Eur. J. Inorg. Chem.* **2002**, *2002*, 473.
- [14] Gaussian 09, Revision A.02, M. J. Frisch, G. W. Trucks, H. B. Schlegel, G. E. Scuseria, M. A. Robb, J. R. Cheeseman, G. Scalmani, V. Barone, B. Mennucci, G. A. Petersson, H. Nakatsuji, M. Caricato, X. Li, H. P. Hratchian, A. F. Izmaylov, J. Bloino, G. Zheng, J. L. Sonnenberg, M. Hada, M. Ehara, K. Toyota, R. Fukuda, J. Hasegawa, M. Ishida, T. Nakajima, Y. Honda, O. Kitao, H. Nakai, T. Vreven, J. Montgomery, J. A., J. E. Peralta, F. Ogliaro, M. Bearpark, J. J. Heyd, E. Brothers, K. N. Kudin, V. N. Staroverov, R. Kobayashi, J. Normand, K. Raghavachari, A. Rendell, J. C. Burant, S. S. Iyengar, J. Tomasi, M. Cossi, N. Rega, N. J. Millam, M. Klene, J. E. Knox, J. B. Cross, V. Bakken, C. Adamo, J. Jaramillo, R. Gomperts, R. E. Stratmann, O. Yazyev, A. J. Austin, R. Cammi, C. Pomelli, J. W. Ochterski, R. L. Martin, K. Morokuma, V. G. Zakrzewski, G. A. Voth, P. Salvador, J. J. Dannenberg, S. Dapprich, A. D. Daniels, Ö. Farkas, J. B. Foresman, J. V. Ortiz, J. Cioslowski, D. J. Fox, Gaussian, Inc., Wallingford CT, 2009.
- [15] C. T. Lee, W. T. Yang, R. G. Parr, *Phys. Rev. B* **1988**, *37*, 785.
- [16] P. J. Hay, W. R. Wadt, *J. Chem. Phys.* **1985**, *82*, 270.
- [17] S. Miertus, E. Scrocco, J. Tomasi, *Chem. Phys.* **1981**, *55*, 117.

Chapter 7

ϵ -Keggin Polyoxomolybdate

Capped with Lanthanide Groups

In this chapter, we aim to study the relative stability and structural characterization of ϵ -Keggin polyoxomolybdates. These compounds can only be obtained in reduced form and capped with four stabilizing positively charged groups. In the present study, lanthanide cations play this role.

Related publication:

H. El Moll, B. Nohra, P. Mialane, J. Marrot, N. Dupré, B. Riflade, M. Malacria, S. Thorimber, B. Hasenknopf, E. Lacôte, P. A. Aparicio, X. López, J. M. Poblet, A. Dolbecq, *Chem. Eur. J.* **2011**, *17*, 14129.

7.1 Introduction and objectives

The structure and properties of Keggin polyoxometalates can be finely tuned at the molecular level^[1] according to different methodologies. Our strategy is based on the substitution of one Mo or W atom by another transition metal or lanthanide ion. Another usual way adds metal cations or complexes to the surface of the $\{XM_{12}O_{40}\}$ framework as capping groups.

Keggin polyoxotungstates can lead to the so-called lacunary or vacant POMs by removal of one or several WO_6 polyhedra, and their reactivity with various electrophilic groups has led to numerous derivatives. On the other hand, vacant polyoxomolybdates are far less stable but the reactivity of the plenary $\{XMo_{12}O_{40}\}$ forms is still quite rich. Indeed, they can be easily reduced and have been studied as building units of higher nuclearity assemblies by aggregation with electrophilic entities^[2]. Some groups have shown, some time ago, that it is possible to isolate a POM with four lanthanum cations capping an $\{\epsilon\text{-}PMo_{12}O_{40}\}$ framework^[3], an isomer of the $\{\alpha\text{-}PMo_{12}O_{40}\}$ Keggin structure resulting from successive 60° rotations of the four M_3O_{13} units around the 3-fold axes of the molecule. Halide salts of the eight-electron-reduced POM $[\epsilon\text{-}PMo^V_8Mo^{VI}_4O_{36}(OH)_4\{La(H_2O)_4\}_4]^{5+}$ (Figure 7.1) have been thus structurally characterized.

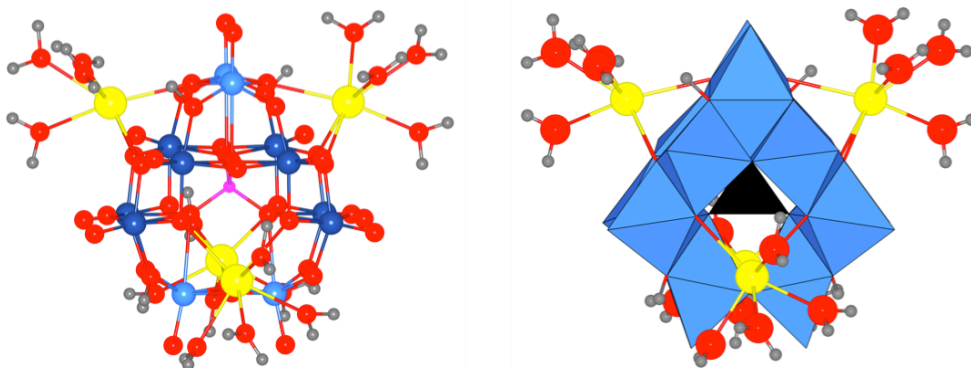


Figure 7.1. Ball and stick (left) and polyhedral with the capping groups in ball and stick (right) representation of $[\epsilon\text{-}PMo^V_8Mo^{VI}_4O_{36}(OH)_4\{La(H_2O)_4\}_4]^{5+}$. Color scheme: La in yellow, O in red, P in pink, H in grey, Mo^{VI} in light blue and Mo^V in dark blue.

It should be noted that similar structural types have also been reported with 3d or 4d capping cations, such as $Mo^{VI[4]}$, $Ni^{II[5]}$, $Co^{II[6]}$ or $Zn^{II[7]}$ ions. Their structures and behaviors in aqueous solution have been deeply investigated.

DFT studies driven on polyoxometalates have largely proven to give valuable information regarding structure, relative stability, electronic properties, etc.^[8]. In the present work we deal with rather intricate structures from the geometrical point of view due to the presence of a large number of labile ligands (H₂O, Cl). The main goals of this section are (i) to reproduce the geometrical features of $[\epsilon\text{-PMo}^{\text{V}}_8\text{Mo}^{\text{VI}}_4\text{O}_{36}(\text{OH})_4\{\text{La}(\text{H}_2\text{O})_4\}_4]\text{Cl}_5$ and $[\epsilon\text{-PMo}^{\text{V}}_8\text{Mo}^{\text{VI}}_4\text{O}_{36}(\text{OH})_4\{\text{La}(\text{H}_2\text{O})_4\}_4]\text{Cl}_4^+$, hereafter $\epsilon\text{-La}_4$ and $\epsilon\text{-La}_4^+$ respectively, such as the positions of the chlorine atoms, which appear to be disordered in the X-ray characterization, (ii) to obtain and rationalize the distribution of the eight metal electrons over the $\{\epsilon\text{-PMo}_{12}\text{O}_{40}\}$ framework, and (iii) to get a qualitatively correct trend of stabilities from the calculations driven on lanthanide-containing $\{\epsilon\text{-PMo}_{12}\text{O}_{40}\}$ compounds.

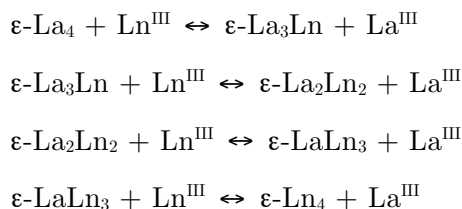
7.2 Experimental background

The group of Prof. Dolbecq (Institut Lavoisier, Université de Versailles) has studied the $[\epsilon\text{-PMo}^{\text{V}}_8\text{Mo}^{\text{VI}}_4\text{O}_{36}(\text{OH})_4\{\text{Ln}(\text{H}_2\text{O})_4\}_4]^{5+}$ (Ln = La, Ce, Nd, Sm) polyoxocations ($\epsilon\text{-Ln}_4$). They have synthesized them at room temperature as water-soluble chlorine salts. These types of structures have revealed to be good building units for the assembly of extended frameworks. The inclusion of rare earth cations is likely to bring catalytic properties, as previously described for mono-substituted polyoxotungstates^[9]. In our joint study, our group and Dolbecq's have analyzed the properties of the molybdate counterpart.

The ³¹P-NMR studies have allowed a comparison of the affinity of the reduced $\{\epsilon\text{-PMo}_{12}\text{O}_{40}\}$ core towards cationic groups, showing that the La^{III} ions are the preferred ones in contrast with rare earths heavier than Eu^{III}, which do not attach to the ϵ -Keggin anion surface. They also performed valence bond calculations with an examination of the Mo-Mo distances confirming the presence of 8 Mo^V and 4 Mo^{VI} ions in the $\epsilon\text{-Sm}_4$ compound, and showing that four bridging oxygen atoms are protonated. This structural determination has not been possible in $\epsilon\text{-Ce}_4$ because of the disorder induced by the cubic crystal packing. These Ln ions are bound to the POM core via Ln-O bonds with three bridging oxygen atoms. The counterions of the cationic species are chlorine anions. In all cases, but some differences can be observed between them. In $\epsilon\text{-Ce}_4$ the five chlorine atoms are disordered and have been located with partial occupancy factors on a position close to the Ce ions at a distance of 2.73 Å, slightly longer than the Ce-OH₂ distance of 2.5 Å. For $\epsilon\text{-La}_4$, they found a

similar situation, while in ϵ -Sm₄ the chlorine atoms are not bound to the Sm ions. Only two of the five chlorine atoms have been located occupying vacant spaces between the POMs with Cl-O distances around 3.2 Å.

In the Versailles group the rare earth exchange in ϵ -Ln₄ species has also been studied. When CeCl₃ is added to a solution of ϵ -La₄, increasingly substituted species can be formed: ϵ -La₃Ce, ϵ -La₂Ce₂, ϵ -LaCe₃ and ϵ -Ce₄. ϵ -La₄, initially present, disappears when sufficient equivalents of CeCl₃ are added. A similar experiment was performed with ϵ -Ce₄ as the starting reactant, to which increasing amounts of LaCl₃ were added. At variance with the previous case, ϵ -La₃Ce and ϵ -La₄ were the only species observed. The comparison of both experiments indicates that ϵ -La₄ is more stable than ϵ -Ce₄. To compare the relative stability of ϵ -Ln₄ POMs, they added LnCl₃ (Ln = Ce, Nd, Sm and Eu) to a solution of ϵ -La₄, leading to a mixture of ϵ -La₄, ϵ -La₃Ln, ϵ -La₂Ln₂, ϵ -LaLn₃ and ϵ -Ln₄ complexes, according to the following scheme:



Finally they studied the relative stability constants of each molecule. This study shows that La^{III} is the rare earth cation with the highest affinity for the ϵ -Keggin surface and that there is no exchange with rare earth cations with ionic radii smaller than Eu^{III}.

7.3 Rotational isomers and electronic structure of Keggin polyoxoanions

The Keggin ion possesses five geometrical isomers, proposed by Baker and Figgis^[10], designated by the prefixes α , β , γ , δ and ϵ , resulting from successive 60° rotations of the M₃O₁₃ edge-sharing units about 3-fold symmetry axes of the α isomer (Figure 7.2). Among the isomers, the ϵ form presents unique electronic and geometric features. It has been observed when {XMo₁₂O₄₀} is fully (i.e. contains 12 Mo^V ions) or partially (i.e. contains 8 Mo^V and 4 Mo^{VI} ions) reduced. As mentioned above, these ϵ structures have never been observed “naked”, that is, without positive groups attached to the surface, probably because of its high negative charge. DFT calculations confirm that

the fully oxidized naked ϵ isomer is very unstable ($+45.6 \text{ kcal mol}^{-1}$) with respect to α due to the presence of six pair-wise short $\text{Mo}^{\text{VI}}\text{-Mo}^{\text{VI}}$ contacts^[3, 11] computed to be $d_{\text{Mo-Mo}} = 2.99 \text{ \AA}$. These destabilizing interactions appear after the second Mo_3 rotation.

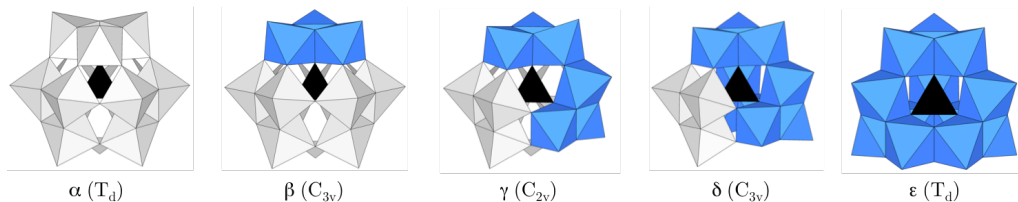


Figure 7.2. Polyhedral representation of the five rotational isomers of the Keggin anion. Each rotated M_3O_{13} unit is colored blue. The internal black tetrahedra contain the heteroatom.

The most common isomers, α and β , do not present any of these Mo-Mo close contacts so they are the most stable forms of the series. The γ form presents one of such close contacts, its energy being $+10.4 \text{ kcal mol}^{-1}$ higher than the α isomer. The δ isomer, with three Mo-Mo contacts, has $E_{\text{rel}} = +25.2 \text{ kcal mol}^{-1}$. Thus, each Mo-Mo close contact present in the oxidized structure causes a destabilization of approximately $8\text{--}10 \text{ kcal mol}^{-1}$, considering the idealized maximal symmetry of the compounds. It is well known that polyoxomolybdates may present a significant Pfeiffer effect^[12], a structural distortion recently analyzed by theoretical methods and attributed to a second order Jahn-Teller effect^[13]. However, the $\{\text{PMo}_{12}\text{O}_{40}\}$ Keggin anion is poorly distorted and its energy is very close (computed $0.8 \text{ kcal mol}^{-1}$) to the undistorted one. The homologous polyoxotungstates behave similarly in the α - ϵ series^[14], although featuring a somewhat larger average destabilization per W-W contact (Table 7.1).

Previously reported DFT calculations on Keggin isomers showed the determinant role of bonding Mo orbitals in the stabilization of the ϵ form^[15]. Let us take the optimized structures of the oxidized $\{\alpha\text{-PMo}_{12}\text{O}_{40}\}$ and $\{\epsilon\text{-PMo}_{12}\text{O}_{40}\}$ anions and their sequence of molecular orbitals (MOs). Even if the lowest unoccupied MO is found at a similar energy in α and ϵ isomers, the nature of the lowest empty MOs varies from isomer to isomer. In the α isomer they are formally nonbonding combinations of d_{xy} molybdenum orbitals and reduction of this compound produces no appreciable structural changes. On the other hand, the first six empty MOs in the ϵ isomer have Mo-Mo bonding character leading to notable geometrical changes upon reduction.

Table 7.1. Relative energies of oxidized and eight-electron-reduced (in parentheses) anions computed, and LUMO energies for the five Baker-Figgis isomers of the Keggin anion.

Isomer (no. of rotated triads)	M–M close contacts	[PMo ₁₂ O ₄₀] ³⁻		[PW ₁₂ O ₄₀] ³⁻
		Rel. Energy ^a	<i>E</i> (LUMO) ^b	Rel. Energy ^a
α	0	0.0 (0.0)	-4.98	0.0 (0.0)
β (1)	0	+5.4	-5.12	+4.6
γ (2)	1	+10.4	-5.09	+13.9
δ (3)	3	+25.2	-5.03	+30.7
ϵ (4)	6	+45.6 (-5.0)	-4.89	+55.9 (+11.2)
		This work		Ref.[14]

^a In kcal mol⁻¹. ^b In eV.

Our results show that Mo–Mo close contacts shorten from 2.99 Å in the fully oxidized form to 2.83 Å in the 8-electron reduced naked [ϵ -PMo₁₂O₄₀]¹¹⁻ anion. At this stage, the ϵ isomer becomes *more stable* than the α isomer by about 5.0 kcal mol⁻¹ but, in practice, such high negative charge must be compensated by counterions attached to the POM surface, such as [ML_{*n*}]^{*q+*} cationic units. We want to stress that the eight-fold reduced homologous tungstate, [ϵ -PW₁₂O₄₀]¹¹⁻, is still 11.2 kcal mol⁻¹ higher in energy than its eight-electron reduced α counterpart. The situation with localized electrons in W–W bonding MOs is less advantageous than in molybdates, as illustrated by Rohmer *et al.* for the 2-electron reduced { γ -SiW₁₂O₄₀}^[16], another isomer featuring a close W–W contact. In this molecule, the metal electrons delocalize over the rest of the molecule via d_{xy}(W) orbitals with nonbonding character rather than in the bonding W–W molecular orbitals. These are evidences that may explain why ϵ -Keggin tungstates are unknown.

In fully oxidized form, the electronic configuration of Mo is d⁰ (Mo^{VI}), so that allows them to accept electrons. The electronic structure of many POMs could be viewed as a set of occupied orbitals belonging to oxygen atoms (oxo band) and a set of unoccupied orbitals with d-metal nature (Figure 7.3), that can accept extra electrons. In polyoxomolybdates, the HOMO is 95% composed of p-oxygen orbitals and the LUMO has predominant Mo character, about 65%.

In the tungsten counterpart these values are 95% and 75%, respectively. The HOMO-LUMO gap for the symmetrical (T_d) $\{\alpha\text{-PMo}_{12}\text{O}_{40}\}$ is 1.99 eV but for the $\alpha\text{-PW}_{12}\text{O}_{40}$ the value is 2.73 eV. In $\{\epsilon\text{-PMo}_{12}\text{O}_{40}\}$ the HOMO-LUMO gap is 1.69 eV, whereas in $\{\epsilon\text{-PW}_{12}\text{O}_{40}\}$ it is close to 2.0 eV.

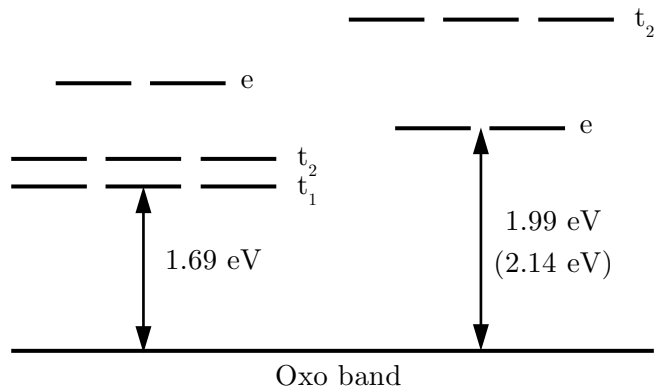


Figure 7.3. MO scheme for the fully oxidized ϵ (left) and α Keggin molybdate (right). In parentheses the value for the distorted structure.

7.4 Structural characterization of $\epsilon\text{-La}_4$ and $\epsilon\text{-La}_3\text{Gd}$

Finding energy minima for the structures discussed in the present work is a difficult task at any computational level. The reason is the flat potential energy surfaces around energy minima for the present structures (Figure 7.4). The origin can be found in the large number of external aqua groups stabilizing the capping Ln^{III} ions and their high mobility around their equilibrium positions. DFT geometry optimizations were carried out with the standard *tight* convergence thresholds, allowing the optimization algorithm to explore a large portion of the potential energy surface until a flat region of low energy is reached (although not a real minimum from the point of view of the convergence parameters used). For the purpose of the present computational study, the structures obtained are of enough quality (Table 7.2). This strategy gives better results and more stable structures than just lowering the thresholds to looser values to assure convergence. In our view, it is a more realistic scenario the one in which labile ligands are always fluctuating around a given average position.

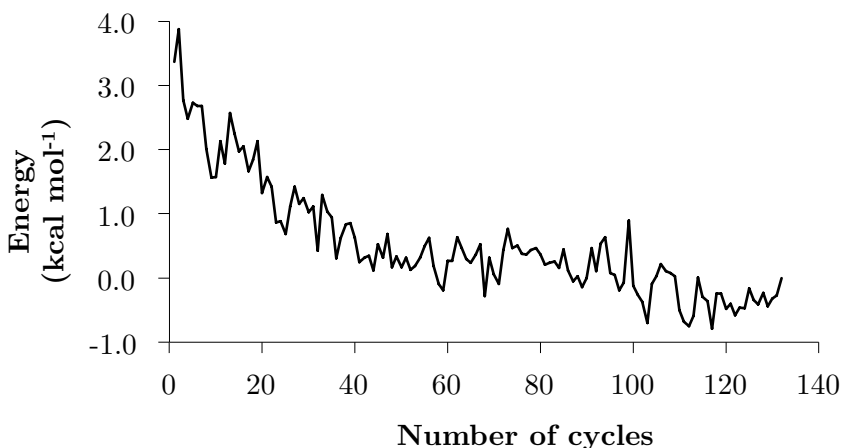


Figure 7.4. Energy oscillations during the geometry optimization procedure of ϵ -La₄⁺.

In the X-ray characterization of the ϵ -La₄ system, one of the five Cl positions could not be fully determined, suggesting that it is not covalently linked to any La^{III} ion. Thus, a molecule with four chlorine atoms must be almost equal in what concerns the main geometrical parameters, so the first system tackled by DFT is [ϵ -PMo₁₂O₃₆(OH)₄{La(H₂O)₄Cl}₄]⁺, ϵ -La₄⁺, a monocationic model compound with four chlorine atoms of the experimentally observed neutral compound. For the optimization of this system, the initial positions of aqua and Cl ligands were deduced from X-ray data, so with some disorder. A 130-cycle geometry optimization run with standard convergence parameters led the molecule to a *flat* region of the potential surface with energy oscillations smaller than 1 kcal mol⁻¹. This is a tiny value over the total energy of the molecule and we consider any of the structures comprised in this energy range a stable form of the compound.

The analysis of the geometry allows us to confirm that the structure makes sense and resembles much that of ϵ -La₄. It should be stressed that present calculations fully reproduce the typical electron distribution of eight metal electrons expected in the { ϵ -PMo₁₂O₄₀} Keggin cluster. In fact, the ϵ -La₄ structure presents disorder due to the cubic symmetry, and the Mo-Mo distances cannot be resolved precisely. DFT calculations allow distinguishing the eight Mo^V ions from the four Mo^{VI} ions, and all the Mo-Mo distances are in accordance to what is expected for four short and two long Mo-Mo contacts. Short ones (2.618 Å) correspond to two bonded Mo^V atoms, whereas long ones (3.191 Å) are characteristic of non-bonded Mo^{VI} atoms, in full agreement with

previously reported X-ray short (2.60 Å) and long (3.10 Å) Mo-Mo distances for the reduced $\{\epsilon\text{-PMo}_{12}\text{O}_{40}\}$ compound^[1]. A list of relevant computed interatomic distances is shown in Table 7.2.

Table 7.2. Selected averaged DFT *vs.* X-ray geometrical parameters for $\epsilon\text{-La}$, in Å. The DFT parameters for the monocationic species $\epsilon\text{-La}^+$ are included for comparison.

	DFT		X-ray
	d ($\epsilon\text{-La}^+$)	d ($\epsilon\text{-La}$)	d ($\epsilon\text{-La}$)
Mo ^{VI} -Mo ^{VI} (2x)	3.191	3.183	3.10 (ref.[1])
Mo ^V -Mo ^V (4x)	2.618	2.618	2.60 (ref.[1])
La-Cl	2.848	2.823	2.795
La-O _{POM} (short)	2.514	2.479	-
La-O _{POM} (long)	2.652	2.613	-
La-O _{POM} (average)	2.518	2.524	2.550
La-O _w (equatorial)	2.594	2.611	2.591
La-O _w (apical)	2.591	2.606	2.745

The MOs composition and occupation for this structure explain the mentioned geometrical parameters. The highest four occupied orbitals are of Mo-Mo bonding nature, whereas the two lowest unoccupied ones are of the same nature but with a poorer overlap due to the longer Mo-Mo distance (Figure 7.5). From population analysis (multipole derived charges) it arises that eight Mo centers carry a positive charge notably smaller than the other four (2.0 *vs.* 2.5), in accordance to the molecular orbital occupations.

Present DFT calculations allow clarifying some structural issues that the X-ray data could not determine. The computed La-O_{POM} distances can be classified into short (2.514 Å) and long (2.652 Å), its average being 2.518 Å, very close to the experimental 2.55 Å. The monocationic $\epsilon\text{-La}_4^+$ structure contains several hydrogen bonds between water hydrogens and bridging oxygens of the POM framework that stabilize the water ligands within the structure.

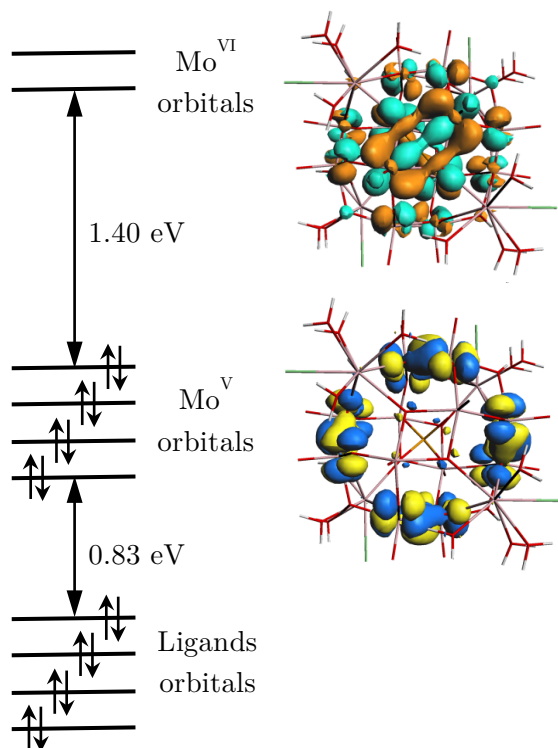


Figure 7.5. Molecular orbital diagram obtained from DFT calculations, with four doubly occupied Mo-Mo bonding orbitals, and two empty Mo-Mo orbitals, along with a 3D representation of each one.

For the neutral compound, ϵ -La₄, we carried out equivalent calculations. The starting geometry corresponds to the final one obtained for ϵ -La₄⁺ by DFT optimization, with an additional chlorine atom. Since there is no clear experimental clue of the position of the fifth chlorine atom, we put it at bonding distance from one of the four La^{III} ions, with a plausible distribution of the other ligands linked to the same La atom. After 200 optimization cycles without reaching full convergence but having achieved a flat potential energy region (Figure 7.6), one of the five Cl⁻ ions of the structure was found far from its initial position, just close to three water molecules and stabilized by hydrogen bonds (Figure 7.7).

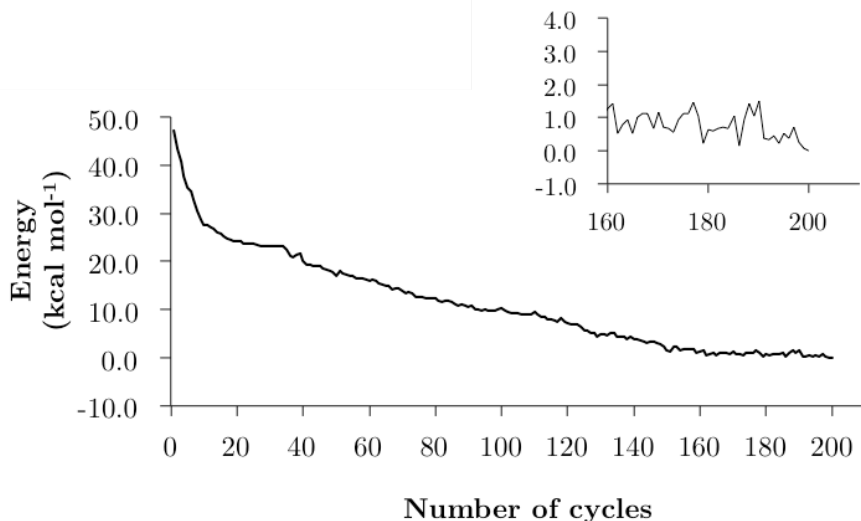


Figure 7.6. Energy oscillations during the geometry optimization procedure of ϵ -La₄. Inlay shows the energy oscillations for the last 40 cycles.

This confirms the X-ray observations in the sense that one chlorine position cannot be resolved. It actually remains in the surroundings of the POM structure without being strongly bound to it and, therefore, rather mobile, whereas the other four Cl atoms remain linked to La ions. Table 7.2 summarizes computed and X-ray interatomic distances for the neutral compound. The other important features of the system, as the Mo-Mo distances, are well reproduced also in this calculation.

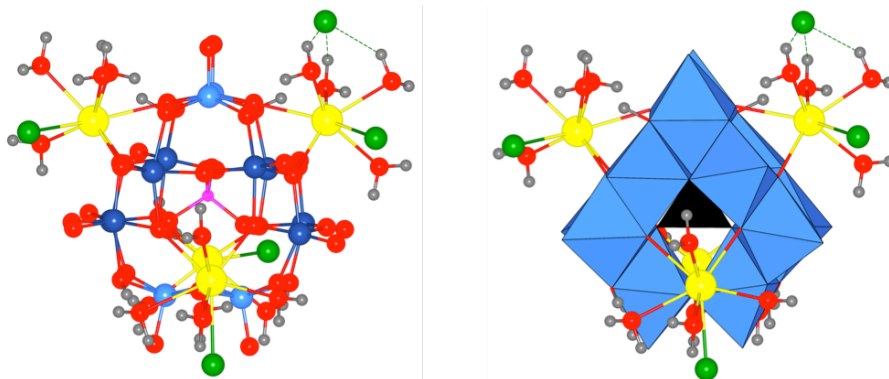


Figure 7.7. Ball and stick (left) and polyhedral with the capping groups in ball and stick (right) representation of $[\epsilon\text{-PMo}^{\text{V}}_8\text{Mo}^{\text{VI}}_4\text{O}_{36}(\text{OH})_4\{\text{La}(\text{H}_2\text{O})_4\}_4\text{Cl}_5]$. Color scheme: La in yellow, O in red, P in pink, H in grey, Cl in green, Mo^{VI} in light blue and Mo^V in dark blue. The “free” Cl atom is stabilized by long weak interactions (dashed lines).

The DFT calculations have completely determined the existence of eight bonding (localized) metal electrons. Also, the protons bound to μ -O sites of the structure (-OH groups) and the positions of chlorines obtained are in very good agreement with previous experimental characterizations.

Now we analyze some structural features of another lanthanide derivative of the $\{\epsilon\text{-PMo}_{12}\text{O}_{40}\}$ anion. The experimental data collected for compounds with Ln = La, Ce, Nd, Sm and Eu show that the stability of the Ln tetracapped ϵ -Keggin molecules decreases from left to right in the period, a fact tentatively attributed to the size of the Ln^{III} atom. To learn more on this, we study the replacement of La^{III} by Gd^{III} and check the geometrical features. Use of this model structure is justified by the electronic configuration of Ln^{III} cations. The Gd^{III} ion has a half-filled f valence shell (f^7), much easier to handle computationally than cations with otherwise-filled valence shells, like f^{1-6} (Sm features a f^5 configuration). In addition, Gd^{III} can be considered similar enough to Sm^{III} for a stability test *versus* La^{III}. So, our *model* structure contains three La atoms and one Gd (ϵ -La₃Gd) and its experimental counterpart is the ϵ -Sm₄ compound. Substitution of four La by four Gd atoms is much too involved from the theoretical point of view since four Gd atoms would carry 28 unpaired electrons. Thus, we consider that one La to Gd substitution suffices to study local geometry changes. Another feature of our model compound is that it contains three chlorine ligands (one per La atom), which confers a total charge of 2+.

It is interesting not only to describe the final geometry obtained upon optimization but also the starting point. Our first geometry for the ϵ -La₃Gd derivative contained one Gd ion coordinated by six ligands: (H₂O)₅ + Cl⁻, although we expected it to be coordinated by five. The inclusion of the chlorine atom in the coordination sphere of Gd allows us to observe if, during the optimization process, Gd gets rid of it or, on the contrary, an aqua ligand is released. The first geometry of this calculation features $d(\text{Gd-Cl}) = 2.82 \text{ \AA}$ and $d(\text{Gd-O}_w) = 2.56/2.61 \text{ \AA}$. After a few geometry steps, these turned into $d(\text{Gd-Cl}) = 3.03 \text{ \AA}$ and $d(\text{Gd-O}_w) = 2.47 \text{ \AA}$ (averaged), confirming that the chlorine ion tends to leave the Gd coordination sphere, whereas the five water ligands not only remain bound but strengthen their interaction with Gd. Other geometrical parameters that confirm the quality of the DFT results obtained with the ϵ -La₃Gd model are shown in Table 7.3 in comparison with the X-ray analysis for ϵ -Sm₄, which in turn is not affected by disorder. The chlorine

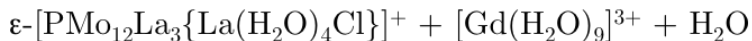
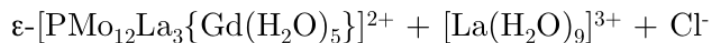
atoms necessary to compensate the positive charge have not been considered since they lie in undetermined positions far from the Ln environment.

Table 7.3. Selected DFT geometrical parameters related to the Gd region in the model compound ϵ -La₃Gd and the X-ray data for the experimental reference, the ϵ -Sm₄ molecule. Distances are in Å.

	DFT	X-ray
	d(ϵ -La ₃ Gd)	d(ϵ -Sm ₄)
Ln-O _{POM}	2.315	2.374
Ln-O _{POM}	2.373	2.391
Ln-O _{POM}	2.517	2.508
Ln-O _w (equatorial)	2.453	2.455
Ln-O _w (apical)	2.507	2.522

7.5 Relative stability of ϵ -La₄ and ϵ -La₃Gd

The model compound ϵ -La₃Gd allows us examining the relative energy with respect to ϵ -La₄. We have demonstrated above that Gd satisfactorily plays the role of Sm in what concerns the structure of capped Keggin systems, while being much easier to handle at the DFT level. In order to quantify the relative stability of the two systems, we propose the following reaction:



Comparison of molecules with different chemical composition can be studied by means of reaction energies that fulfill conservation of matter, and not directly by comparing computed absolute energies of these molecules. The *free* Ln^{III} ions in solution have been coordinated to nine aqua ligands and their geometries fully optimized, following the typical coordination numbers of Ln^{III} ions^[17]. The chlorine anion has been considered without explicit water

molecules around (just the solvent effects introduced by the COSMO) since it is a quite soft ion, the coordination sphere of which is too labile to be precisely determined or modeled. The energy of the process, ΔE_r , determines the relative stability of the La-POM and Gd-POM linkages, respectively.

Our calculations reveal that $\Delta E_r = -22$ kcal mol⁻¹ in favor of the ϵ -La₄ form, a rather large reaction energy indicating a strongly disfavored exchange process in the direction La to Gd, in agreement with the fact that the La to Eu exchange is not observed experimentally. It must be pointed out that two La-replacements would cost ~ 45 kcal mol⁻¹, three replacements ~ 66 kcal mol⁻¹, until a value of the order of ~ 90 kcal mol⁻¹ for the replacement of all four La ions. We also expect that ΔE_r would be smaller for ions situated to the left of Gd in the periodic table, like Ce, Nd or Sm.

7.6 Conclusions

Theoretical calculations have been performed in order to provide a deeper insight into the geometries and reactivity of the systems studied. The $\{\epsilon\text{-PMo}_{12}\text{O}_{40}\}$ isomer has the need to gain electrons arising from the Mo^{VI}-Mo^{VI} bonding character of the lowest empty orbitals (LUMO). Successive reductions of these orbitals compensate the high energy of the fully oxidized ϵ isomer by (i) reducing the electrostatic repulsion in Mo-Mo contacts, and (ii) filling bonding molecular orbitals. Comparison with tungstate counterparts show that these are not likely to be obtained as ϵ isomers. Calculations driven on La- and Gd-containing derivatives of the ϵ -Keggin anion give complementary information on the structure and relative stability of such compounds. DFT geometries agree very well with X-ray data, giving some extra information in case of disorder (ϵ -La₄ structure). We have also proven that the La compound is much more stable than the Gd one in solution, a behavior that resembles that of Eu, confirming that the smaller Ln ions are not stable in the surface of the $\{\epsilon\text{-PMo}_{12}\text{O}_{40}\}$ molecule.

7.7 Computational details

To carry out the DFT calculations we have used the ADF2009.01 suite of programs^[18]. Our calculations are characterized by GGA functionals, applying the X α model with Becke's corrections^[19] for describing exchange, and the VWN parameterization with Perdew's corrections^[20] for correlation (BP86).

The electrons were described by Slater-type functions with basis sets of TZP quality for valence electrons. *Core* electrons were kept frozen and described by single Slater functions (core shells by atom: O: 1s; P, Cl: 1s-2p; Mo: 1s-3d; La, Gd: 1s-4d) with core potentials generated using the DIRAC program^[18], and scalar relativistic corrections included by means of ZORA^[21]. All the calculations include COSMO^[22] to take into account the effects of the solvent (water) and the counterions ($\epsilon = 78.4$). The solvent cavities surrounding the molecules were created using the solvent-excluding method with fine tesserae. The ionic radii for the atoms that actually define the size of the solvent cavity were chosen to be 0.74 Å for molybdenum, 1.30 Å for lanthanum, 1.19 Å for gadolinium, 1.20 Å for hydrogen, 1.70 Å for chlorine and 1.52 Å for oxygen. We applied the spin-unrestricted formalism to electronically open shell species.

7.8 References

- [1] A. Dolbecq, P. Mialane, L. Lisnard, J. Marrot, F. Sécheresse, *Chem. Eur. J.* **2003**, *9*, 2914.
- [2] a) A. Dolbecq, E. Cadot, F. Secheresse, *Chem. Commun.* **1998**, 2293; b) A. Müller, E. Beckmann, H. Bögge, M. Schmidtman, A. Dress, *Angew. Chem., Int. Ed.* **2002**, *41*, 1162.
- [3] P. Mialane, A. Dolbecq, L. Lisnard, A. Mallard, J. Marrot, F. Sécheresse, *Angew. Chem., Int. Ed.* **2002**, *41*, 2398.
- [4] a) M. I. Khan, Q. Chen, J. Salta, C. J. O'Connor, J. Zubieta, *Inorg. Chem.* **1996**, *35*, 1880; b) M. I. Khan, A. Müller, S. Dillinger, H. Bögge, Q. Chen, J. Zubieta, *Angew. Chem., Int. Ed. Engl.* **1993**, *32*, 1780; c) T. Yamase, E. Ishikawa, *Bull. Chem. Soc. Jpn.* **2008**, *81*, 983.
- [5] a) X.-B. Cui, S.-T. Zheng, G.-Y. Yang, *Z. Anorg. Allg. Chem.* **2005**, *631*, 642; b) A. Müller, C. Beugholt, P. Kögerler, H. Bögge, S. Bud'ko, M. Luban, *Inorg. Chem.* **2000**, *39*, 5176; c) W. Wang, L. Xu, G. Gao, L. Liu, X. Liu, *CrystEngComm* **2009**, *11*, 2488.
- [6] H.-H. Yu, X.-B. Cui, J.-W. Cui, L. Kong, W.-J. Duan, J.-Q. Xu, T.-G. Wang, *Dalton Trans.* **2008**, 195.
- [7] a) C. Lei, J.-G. Mao, Y.-Q. Sun, J.-L. Song, *Inorg. Chem.* **2004**, *43*, 1964; b) L. M. Rodriguez Albelo, A. R. Ruiz-Salvador, D. W. Lewis, A. Gomez, P. Mialane, J. Marrot, A. Dolbecq, A. Sampieri, C. Mellot-Draznieks, *Phys. Chem. Chem. Phys.* **2010**, *12*, 8632; c) L. M. Rodriguez-Albelo, A. R. Ruiz-Salvador, A. Sampieri, D. W. Lewis, A. Gómez, B. Nohra, P. Mialane, J. Marrot, F. Sécheresse, C. Mellot-Draznieks, R. Ngo Biboum, B. Keita, L. Nadjo, A. Dolbecq, *J. Am. Chem. Soc.* **2009**, *131*, 16078.
- [8] a) J. M. Maestre, X. López, C. Bo, J. M. Poblet, N. Casañ-Pastor, *J. Am. Chem. Soc.* **2001**, *123*, 3749; b) F. Q. Zhang, W. Guan, Y. T. Zhang, M. T. Xu, J. Li, Z. M. Su, *Inorg. Chem.* **2010**, *49*, 5472.
- [9] J.-P. Wang, J.-W. Zhao, X.-Y. Duan, J.-Y. Niu, *Cryst. Growth Des.* **2006**, *6*, 507.
- [10] L. C. W. Baker, J. S. Figgis, *J. Am. Chem. Soc.* **1970**, *92*, 3794.
- [11] D. L. Kepert, *Inorg. Chem.* **1969**, *8*, 1556.
- [12] J. F. Garvery, M. T. Pope, *Inorg. Chem.* **1978**, *17*, 1115.
- [13] L. Yan, X. López, J. J. Carbó, R. T. Sniatynsky, D. D. Duncan, J. M. Poblet, *J. Am. Chem. Soc.* **2008**, *130*, 8223.
- [14] X. López, J. M. Poblet, *Inorg. Chem.* **2004**, *43*, 6863.
- [15] F. Q. Zhang, X. M. Zhang, H. S. Wu, Y. W. Li, H. Jiao, *J. Phys. Chem. A* **2007**, *111*, 1683.
- [16] M. M. Rohmer, M. Bénard, *Chem. Soc. Rev.* **2001**, *30*, 340.
- [17] T. Yaita, H. Narita, S. Suzuki, S. Tachimori, H. Motohashi, H. Shiwaku, *J. Radioan. and Nuc. Chem.* **1999**, *239*, 371.

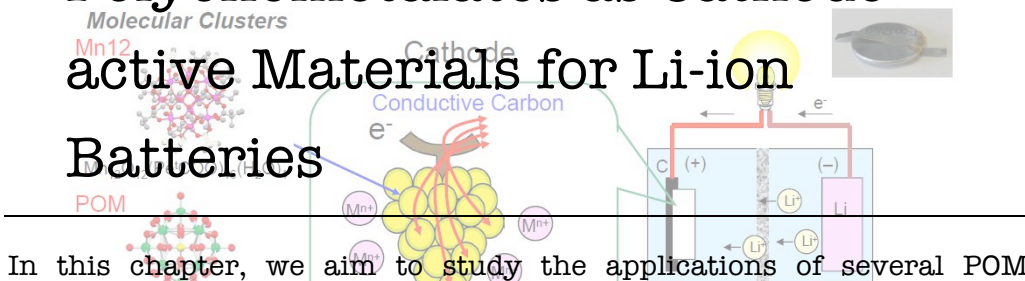
- [18] ADF2009.01, SCM, Vrije Universiteit, Amsterdam, The Netherlands, <http://www.scm.com>, 2009.
- [19] a) A. D. Becke, *J. Chem. Phys.* **1986**, *84*, 4524; b) A. D. Becke, *Phys. Rev. A* **1988**, *38*, 3098.
- [20] a) J. P. Perdew, *Phys. Rev. B* **1986**, *33*, 8822; b) J. P. Perdew, *Phys. Rev. B* **1986**, *34*, 7406.
- [21] a) E. van Lenthe, E. J. Baerends, J. G. Snijders, *J. Chem. Phys.* **1993**, *99*, 4597; b) E. van Lenthe, E. J. Baerends, J. G. Snijders, *J. Chem. Phys.* **1994**, *101*, 9783; c) E. van Lenthe, A. E. Ehlers, E. J. Baerends, *J. Chem. Phys.* **1999**, *110*, 8943.
- [22] a) A. Klamt, G. Schüürmann, *J. Chem. Soc., Perkin Trans. 2* **1993**, 799; b) A. Klamt, *J. Chem. Phys.* **1995**, *102-103*, 2224; c) J. Andzelm, C. Kölmel, A. Klamt, *J. Chem. Phys.* **1995**, *103*, 9312; d) C. C. Pye, T. Ziegler, *Theor. Chem. Acc.* **1999**, *101*, 396.

Chapter 8

Polyoxometalates as Cathode-

active Materials for Li-ion

Batteries



In this chapter, we aim to study the applications of several POM compounds (Keggin, Wells-Dawson, Preyssler and Vanadates) as cathode-active materials for rechargeable Li-ion batteries, from both experimental and theoretical points of view. This work is a joint collaboration between the groups of Prof. Irle and Assist. Prof. Yoshikawa at Nagoya University, and our group.

8.1 Introduction and objectives

The improvement of high-performance rechargeable batteries is one of the most important global issues to solve the increasing environmental and energy concerns^[1]. The *lithium ion batteries* (LIBs) are widely used in portable electronic devices, such as laptops and mobile phones, due to their high energy densities^[2]. However, the practical battery capacity of the LIBs is limited to less than 50% of the theoretically possible value of the cathode-active material. In addition, the charging/discharging rate of the LIBs is slow. These drawbacks have motivated many researchers to develop alternative cathode-active materials for new rechargeable batteries with higher capacities and charging/discharging rates^[3].

Redox active molecular materials are good candidates for high-performance cathode active materials. Recently, the collaborative research of Prof. Irle, Assist. Prof. Yoshikawa, and Prof. Awaga in Nagoya University has developed molecular cluster batteries^[4] (MCBs, Figure 8.1), in which the cathode is made of polynuclear metal complexes and the anode is lithium. It is expected that MCBs show high capacity and a quick charging/discharging due to multi-electron redox reactions of the molecular clusters^[5] and quick lithium diffusion, respectively. A few years ago, Awaga and co-workers prepared an MCB using the Mn₁₂ cluster ([Mn₁₂O₁₂(CH₃COO)₁₆(H₂O)₄]^[4d], which is well-known as a single molecular magnet^[6]. They found an extremely high discharging capacity of over 200 A h kg⁻¹, which was larger than those of the LIBs (150 A h kg⁻¹). They carried out X-ray absorption fine structure (XAFS) analyses of the cathode materials in the Mn₁₂ MCBs to elucidate the solid-state electrochemical reactions in these batteries, because this spectroscopy is a powerful technique to determine the time evolution of both the local environment and oxidation state of the metal ions^[7]. This study revealed a super-reduction from [Mn₁₂]⁰ to [Mn₁₂]⁸⁻ in the discharging process, which contributed to the overall high capacity. More recently, they performed *in operando* Mo K-edge XAFS measurements on the MCBs of a Keggin-type POM, TBA₃[PMo₁₂O₄₀] (TBA = [N(CH₂CH₂CH₂CH₃)₄]⁺), and it was found a 24-electron reduction in the discharging processes, which resulted in a high capacity of the POM-MCBs^[8].

To make a high performance rechargeable battery using POMs, it is important to develop a POM model structure that can be studied both by experimental

8.2 Results and discussion

In the present work, several POM compounds have been synthesized in order to examine their application as cathode-active materials in Li-ion batteries. The list of tested compounds can be found in Table 8.1. Additionally, a theoretical study has been performed to complement and rationalize the experimental results. The results present in this chapter are preliminary and further investigation will be done to fully understand all the experimental evidences.

Table 8.1. List of compounds tested as cathode-active materials in Li-ion batteries.

Polyoxometalates
$\text{H}_3\text{PMo}_{12}\text{O}_{40}$
$\text{H}_3\text{PW}_{12}\text{O}_{40}$
$(\text{Me}_4\text{N})_4(\text{S}_2\text{Mo}_{18}\text{O}_{62})$
$(\text{NH}_4)_6\text{P}_2\text{Mo}_{18}\text{O}_{62} \cdot 12\text{H}_2\text{O}$
$\text{K}_{12.5}\text{Na}_{1.5}[\text{NaP}_5\text{W}_{30}\text{O}_{110}] \cdot 5\text{H}_2\text{O}$
$[\text{Na}_2(\text{H}_2\text{O})_8]_2\text{H}_2[\text{V}_{10}\text{O}_{28}] \cdot 4\text{H}_2\text{O}$
$\text{K}_4\text{Li}_2[\text{V}_{10}\text{O}_{28}] \cdot 10\text{H}_2\text{O}$
$(\text{CN}_3\text{H}_6)_8\text{H}(\text{PV}_{14}\text{O}_{42}) \cdot 7\text{H}_2\text{O}$
$(\text{TMA})_3\text{H}_6\text{V}_{15}\text{O}_{42} \cdot 2.5\text{H}_2\text{O}$

8.2.1 Keggin compounds

Despite the fact that the battery performance of Keggin $[\text{PMo}_{12}\text{O}_{40}]^{3-}$ compound has been reported^[8-9], we examined it again to confirm its high capacity. We also measured the battery performance of the W counterpart for comparison. Coin cell batteries were prepared using a POM mass fraction of 10% in the cathode. The charge/discharge curves were measured at a constant load current of 1.0 mA in the voltage range of 1.5-4.2 V. The Mo salt showed a high capacity of ca. $C = 260 \text{ A h kg}^{-1}$ (Figure 8.2) whereas the W analogue showed $C = 140 \text{ A h kg}^{-1}$ (Figure 8.3). It is usual to take the maximum experimental capacity as the highest value obtained during the first discharging process (1D). The capacity of a battery depends directly on the

number of electrons that the cathode material can accept and it is inversely proportional to the molecular mass. Both Keggin-type compounds can accept up to 24 electrons, but the $[\text{PW}_{12}\text{O}_{40}]^{3-}$ salt has a higher molecular mass and therefore a lower capacity. We tested the battery performance for the first 10 charging (C)/discharging (D) cycles and a slight decrease in the battery capacities can be observed.

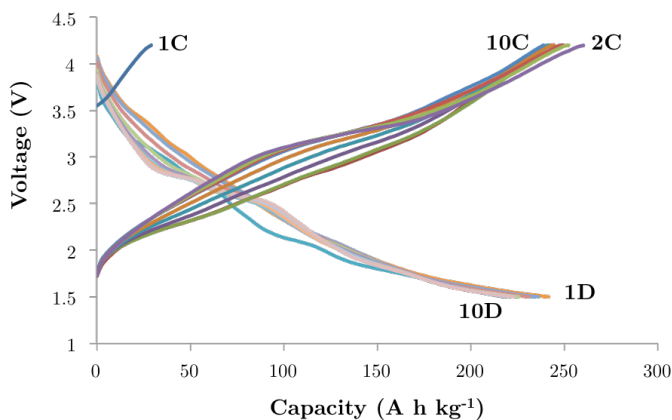


Figure 8.2. The first 10 charging/discharging cycles of $[\text{H}_3\text{PMo}_{12}\text{O}_{40}]$.

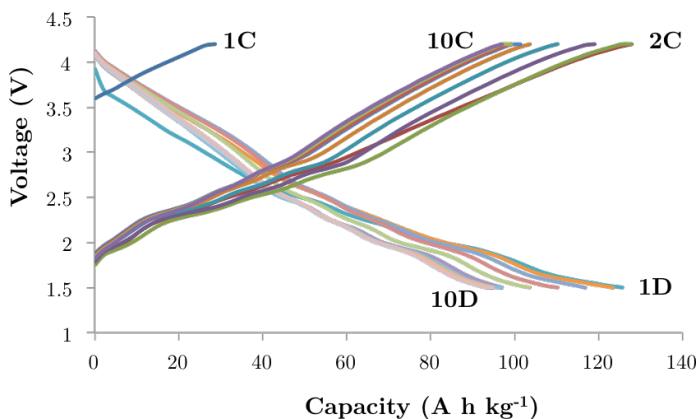


Figure 8.3. The first 10 charging/discharging cycles of $[\text{H}_3\text{PW}_{12}\text{O}_{40}]$.

Theoretical calculations based on DFT were performed to elucidate the location of the extra 24 electrons gained by the Mo Keggin compound^[8, 10]. The starting point was the super-reduced structure obtained by XAFS. It was proven that the Keggin anion formed 4 Mo_3 triads, where each Mo atom is covalently bonded to two other Mo atoms. If each Mo-Mo bond contains two electrons, and in the Keggin structure there are 12 Mo atoms, the total

number of electrons forming Mo-Mo bonds is 24. The driving force for this unusual geometrical and electronic arrangement is a local Jahn–Teller distortion at individual transition-metal octahedral sites. The same study has not been done for the W counterpart because of the low experimental capacity. It was expected a similar behavior, although the W centers do not present local Jahn-Teller distortion.

8.2.2 Wells-Dawson compounds

After the re-examination of the battery performance of Keggin compounds, we have synthesized and tested two different Wells-Dawson salts as cathode-active materials: $(\text{Me}_4\text{N})_4(\text{S}_2\text{Mo}_{18}\text{O}_{62})$ and $(\text{NH}_4)_6\text{P}_2\text{Mo}_{18}\text{O}_{62} \cdot 12\text{H}_2\text{O}$, hereafter S_2Mo_{18} and P_2Mo_{18} respectively. We have chosen Mo derivatives because of the lower molecular mass compared to the W counterparts. The Dawson-type POM has 18 metals atoms in its structure and consequently it can accept up to 36 electrons because, in principle, each Mo^{6+} is reduced to Mo^{4+} . The battery performance of P_2Mo_{18} showed a discharging capacity of ca. 300 A h kg^{-1} (Figure 8.4), which is higher than that of the Mo Keggin-type salt. Following the same trend, the battery performance of S_2Mo_{18} showed a capacity of ca. 370 A h kg^{-1} (Figure 8.5), higher than the capacity of the Mo Keggin POM and the P_2Mo_{18} salt. The capacity decreases as the number of cycles increases (Figure 8.6). In this case, maybe the internal SO_4 groups can be reduced because we observe a higher capacity than the nominal one (313 A h kg^{-1}).

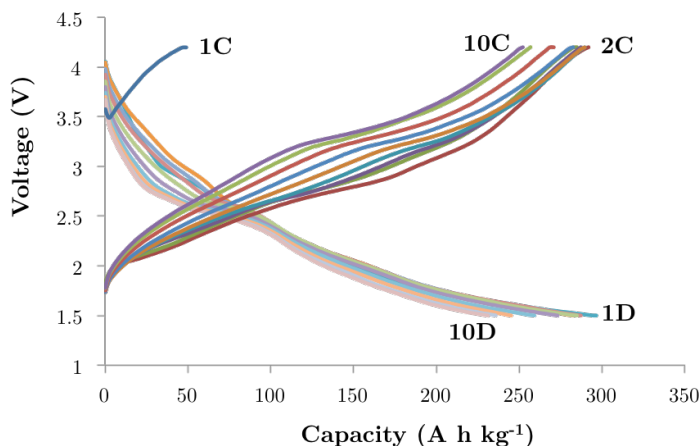


Figure 8.4. The first 10 charging/discharging cycles of $(\text{NH}_4)_6\text{P}_2\text{Mo}_{18}\text{O}_{62} \cdot 12\text{H}_2\text{O}$.

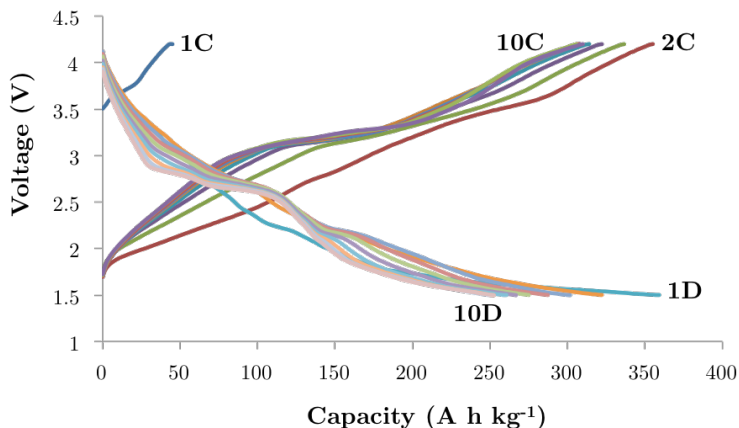


Figure 8.5. The first 10 charging/discharging cycles of $(\text{Me}_4\text{N})_4(\text{S}_2\text{Mo}_{18}\text{O}_{62})$.

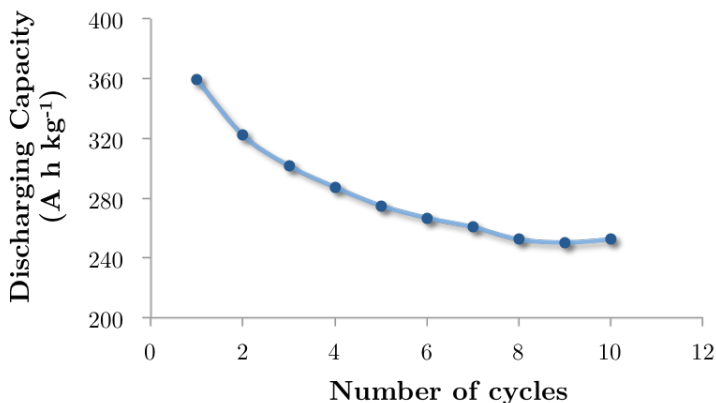


Figure 8.6. The discharging capacity *vs.* the number of cycles of the $(\text{Me}_4\text{N})_4(\text{S}_2\text{Mo}_{18}\text{O}_{62})$ battery performance.

DFT calculations were performed on both Wells-Dawson compounds. As for the case of the Keggin compound, we were looking for the formation of Mo-Mo bonds to locate the extra electrons. In this case, Mo_3 triangles were not found, although some Jahn-Teller distortion was observed in Mo centers. The starting point of optimization in this case is the oxidized structure, so it is very difficult that the geometrical optimization can distort the structure to the super-reduced one. XAFS analysis should be performed in order to elucidate the right starting point, and then we can carry out geometrical optimization expecting the Mo-Mo bonds, where the extra electrons will be located.

8.2.3 Preyssler compound

We have also studied the Preyssler compound $\text{K}_{12.5}\text{Na}_{1.5}[\text{NaP}_5\text{W}_{30}\text{O}_{110}] \cdot 5\text{H}_2\text{O}$, which is one of the largest POMs where all the metals atoms are fully oxidized. The 30 W atoms in its structure can accept up to 60 electrons since each metal atom can be reduced from W^{6+} to W^{4+} . Due to the high molecular mass of the Preyssler salt, the capacity of this compound is 180 A h kg^{-1} (Figure 8.7).

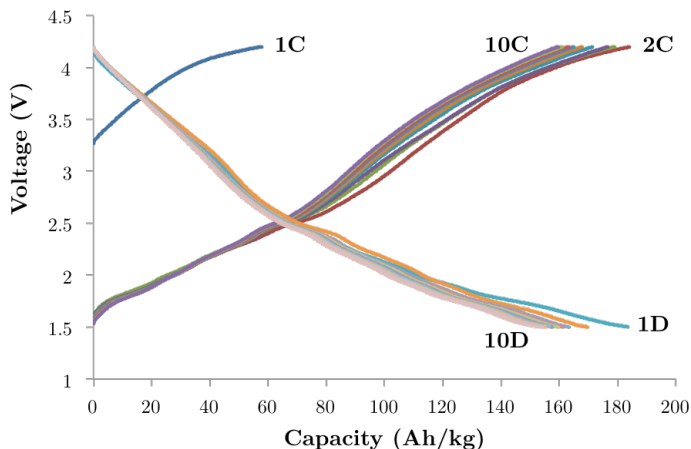


Figure 8.7. The first 10 charging/discharging cycles of $\text{K}_{12.5}\text{Na}_{1.5}[\text{NaP}_5\text{W}_{30}\text{O}_{110}] \cdot 5\text{H}_2\text{O}$.

In this case, the discharging capacity also decreases but not as sharply as in the other compounds (Figure 8.8). The structure of the Preyssler anion is more robust than the other POMs because of the high number of metals atoms. Also, it is well-known that the structures with W atoms are not as *flexible* as Mo-based structures.

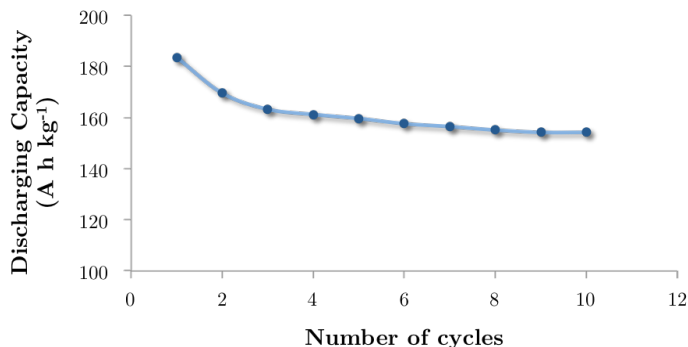


Figure 8.8. The discharging capacity *vs.* the number of cycles of the $\text{K}_{12.5}\text{Na}_{1.5}[\text{NaP}_5\text{W}_{30}\text{O}_{110}] \cdot 5\text{H}_2\text{O}$ battery performance.

We also carried out theoretical calculations on the Preyssler compound. In this case, no W-W bonds were found. The geometrical optimization showed no significant change comparing the starting point with the final structure. In the initial structure the closest W-W distance is 3.37 Å and in the final one is 3.32 Å. The W atoms cannot present local Jahn-Teller distortion.

8.2.4 Vanadate compounds

All these measurements led us to understand and rationalize the behavior of POMs as cathode-active materials. For the achievement of higher capacity in the batteries we tested several vanadates. The V atoms can be formally reduced from V^{5+} to V^{3+} , so each metal atom can accept two electrons, as in the other cases. It is also lighter than Mo and W, so the molecular mass of V-based POMs will be lower. These compounds are very good candidates for acting as cathode-active materials in LIBs.

The first V POM that we tested was the decavanadate. This molecule has been largely studied but it has never been tested as cathode material in a battery. We tested the battery performance of two different decavanadates: $[\text{Na}_2(\text{H}_2\text{O})_8]_2\text{H}_2[\text{V}_{10}\text{O}_{28}] \cdot 4\text{H}_2\text{O}$ and $\text{K}_4\text{Li}_2[\text{V}_{10}\text{O}_{28}] \cdot 10\text{H}_2\text{O}$. The first one has $C = 280 \text{ A h kg}^{-1}$ (Figure 8.9) and the second one $C = 375 \text{ A h kg}^{-1}$, both accepting up to 20 electrons.

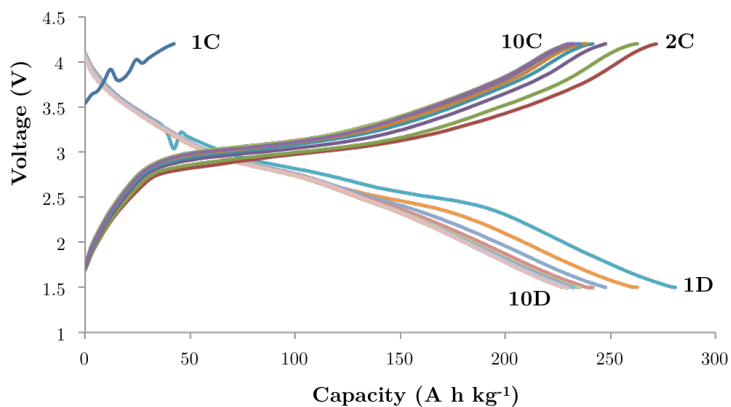


Figure 8.9. The first 10 charging/discharging cycles of $[\text{Na}_2(\text{H}_2\text{O})_8]_2\text{H}_2[\text{V}_{10}\text{O}_{28}] \cdot 4\text{H}_2\text{O}$.

We have also tested $(\text{CN}_3\text{H}_6)_8\text{H}(\text{PV}_{14}\text{O}_{42}) \cdot 7\text{H}_2\text{O}$, hereafter PV_{14} , a Keggin-like structure with two extra VO_2 capping groups. The capacity of PV_{14} is 360 A h kg^{-1} . Although it can accept up to 28 electrons, its capacity is not very high due to its molecular mass. Finally, we also tested the $(\text{TMA})_3\text{H}_6\text{V}_{15}\text{O}_{42} \cdot 2.5\text{H}_2\text{O}$

compound, hereafter V_{15} . It has the same structure as PV_{14} but with V instead of P in the XO_4 internal unit. If we assume that all the V atoms can be reduced from +5 to +3, the V_{15} is able to accept up to 30 electrons. The measured capacity of V_{15} is 450 A h kg^{-1} , the highest one reported for a POM-MCB (Figure 8.10). In this case, though, it is necessary to decrease the voltage from 1.5 to 1.0 V to achieve a value of the capacity close to the nominal one.

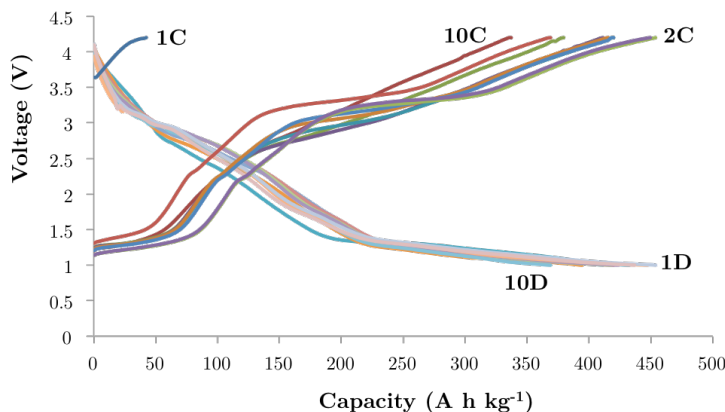


Figure 8.10. The first 10 charging/discharging cycles of $(TMA)_3H_6V_{15}O_{42} \cdot 2.5H_2O$.

Further experimental investigations were carried out to complement the capacity measurements. We performed XAFS analysis of the V_{15} compound to unravel the reduced structure and the valence of the V atoms. Firstly, we measured the V K-edge XANES spectra of the standard samples: $V^{III}_2O_3$, $V^{IV}O_2$ and $V^{V}_2O_5$. The comparison of V_{15} with the standard samples shows a signal very close to the $V^{V}_2O_5$ compound, which means that at the beginning all the V atoms in the V_{15} structure are fully oxidized (Figure 8.11).

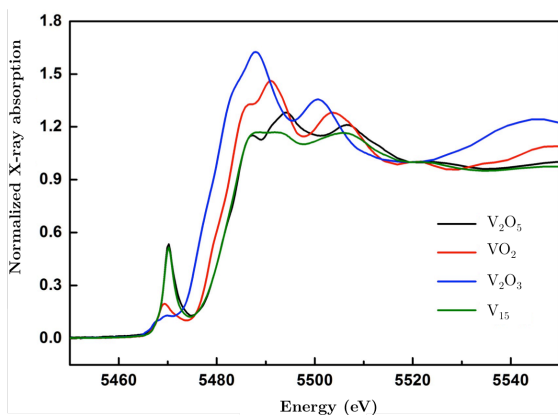


Figure 8.11. V K-edge XANES spectra of the standard samples, V_2O_3 , VO_2 and V_2O_5 , and the V_{15} compound.

Then, we performed XANES spectra of the V_{15} compound during the 1st charging/discharging process. We stopped the cycle at different voltages in order to figure out the valence of the V atoms at each point: 1st charge at 4.2 V and 1st discharge at 3, 2, 1.5 and 1 V. We can observe that the V oxidation state changes from +5 to +4 after the 1st discharging cycle (Figure 8.12). We were not able to observe the reduction from +4 to +3, which indicates that the V atoms in the V_{15} compound cannot accept two electrons in the reduction processes. Taking into account this fact, the high discharging capacity observed for V_{15} must involve a compound other than V_{15} or another process of charge accumulation.

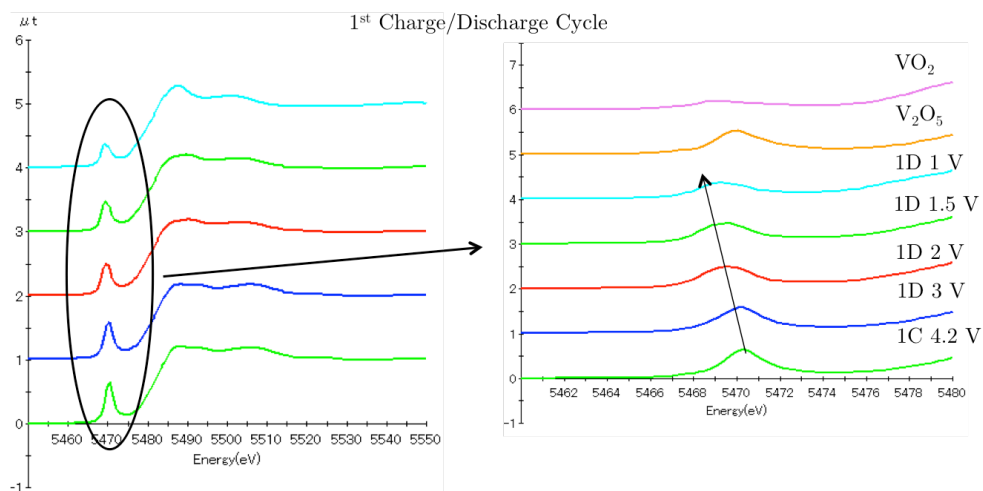


Figure 8.12. V K-edge XANES spectra of V_{15} compound (left) and the comparison with the standard samples (right) during the 1st charging/discharging process.

If we now assume that V_{15} can accept one electron per V atom, the nominal discharging capacity is 240 A h kg^{-1} , very similar to the value of $[H_3PMo_{12}O_{40}]$. The experimental capacity in the range 4.2-1.5 V is 230 A h kg^{-1} , very close to the nominal one. In the case of V_{15} , compared with the Mo Keggin, we can reach the same discharging capacity but only with one electron per metal atom. Another advantage of the V derivatives is the lower mass of the V atoms compared to Mo or W.

Deeper investigation in the electronic structure changes of V atoms in the V_{15} compound was done. In Figure 8.13 we can observe how the V valence changes depending on the applied voltage. During the 1st discharging process, the V valence goes from +4.8 to +4.2 in the range of 4.2-1.5 V (Figure 8.13, left). Achieving the formal oxidation state +4 is only possible decreasing the voltage

to 0.8 V, which means application of an over-potential. In the 2nd charging process, it is not possible to get V^V, the value of the V atoms valence is just ca. +4.6, showing that the reduction/oxidation processes are not completely reversible. This could be associated with the fact that the V₁₅ structure can be partially decomposed after the first cycles. A similar trend was observed in the case of the Mo Keggin compound.

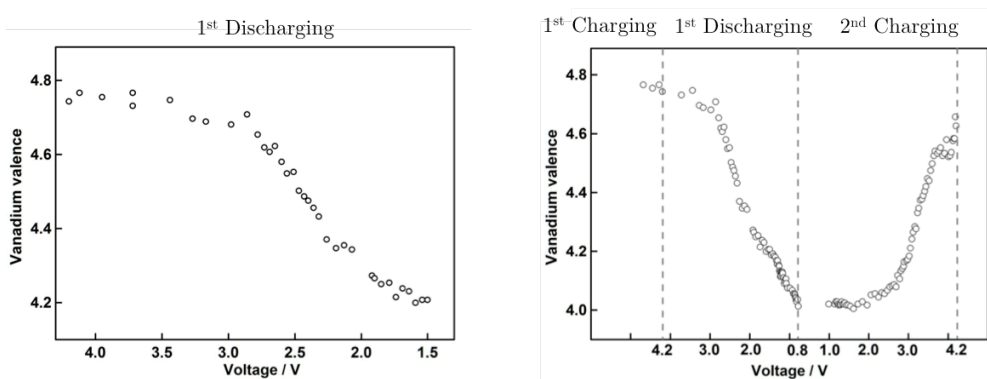


Figure 8.13. *In situ* averaged V valence changes during the 1st discharging process in the range 4.2-1.5 V (left) and the 1st charging/discharging and the 2nd charging process in the range 4.2-0.8 V (right).

The extra capacitance shown by the V₁₅ compound in the range of 1.5-1.0 V might be attributed to the formation of *electrical double layers* (EDLs)^[11] at the electrode interfaces (Figure 8.14). This is the usual energy-storage mechanism used by supercapacitors^[12] to store electrostatic energy.

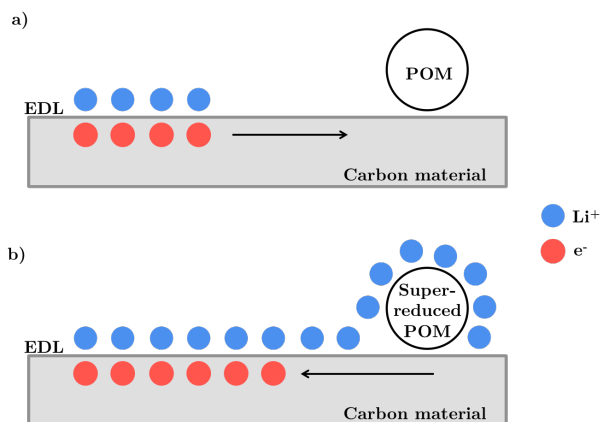


Figure 8.14. Schematic view of the POM in the nanohybrid carbon material and Li⁺ atoms (a) before and (b) after the reduction of the POM. (a) The negative charge of electrons in the EDLs interacts with the POM. (b) The negative charge of the super-reduced POM enhances the EDL formation.

DFT calculations were performed for all vanadate compounds. In this case, as in the Preyssler compound, we found no V-V bonds because the Jahn-Teller distortion is not present in the V centers. In the initial structure the closest V-V distance is 3.02 Å and in the final one is 2.92 Å. Further investigations should be done in order to elucidate the right structure of the super-reduced systems.

8.3 Conclusions

We have synthesized several polyoxometalates and tested their application as cathode-active materials in Li-ion batteries. The results obtained for the Mo Keggin compound are in agreement with the previously reported. We observe that the Wells-Dawson compounds, P_2Mo_{18} and S_2Mo_{18} , show a higher capacity than the Keggin anion. On the other hand, the Preyssler compound shows low capacity due to its high molecular mass. The vanadates are the polyoxometalates showing the highest experimental capacity.

V_{15} is the compound with the highest capacity among all tested vanadates, assuming that each V atom can accept only one electron. XANES analysis shows that the oxidation state of V atoms changes from +5 to +4. As we have mentioned, further investigations should be performed in order to fully understand the behaviour of the V_{15} compound.

8.4 Computational details

We performed density functional theory (DFT) calculations on the super-reduced POMs. All calculations were carried out using the TURBOMOLE program^[13]. We applied the exchange-correlation functional of Becke^[14] and Perdew^[15], named BP86, and the def-SVP standard effective core potentials and basis sets as implemented in the TURBOMOLE program (Li, O and V^[16]; Mo and W^[17]). In order to describe dispersion interactions, the empirical correction proposed by Grimme *et al.*^[18] was also added. The resolution of the identity (RI) method^[19] was introduced to decrease computational costs for all calculations.

8.5 Experimental methodology

All POMs were synthesized according to the methods described in the literature: the Wells-Dawson $(Me_4N)_4(S_2Mo_{18}O_{62})$ ^[20] and

$(\text{NH}_4)_6\text{P}_2\text{Mo}_{18}\text{O}_{62} \cdot 12\text{H}_2\text{O}^{[21]}$, the Preyssler $\text{K}_{12.5}\text{Na}_{1.5}[\text{NaP}_5\text{W}_{30}\text{O}_{110}] \cdot 5\text{H}_2\text{O}^{[22]}$, the decavanadates $\text{Na}_2(\text{H}_2\text{O})_8]_2\text{H}_2[\text{V}_{10}\text{O}_{28}] \cdot 4\text{H}_2\text{O}^{[23]}$ and $\text{K}_4\text{Li}_2[\text{V}_{10}\text{O}_{28}] \cdot 10\text{H}_2\text{O}^{[24]}$, $(\text{CN}_3\text{H}_6)_8\text{H}(\text{PV}_{14}\text{O}_{42}) \cdot 7\text{H}_2\text{O}^{[25]}$ and $(\text{TMA})_3\text{H}_6\text{V}_{15}\text{O}_{42} \cdot 2.5\text{H}_2\text{O}^{[26]}$. The cathode was prepared using a POM, carbon black (Tokai Carbon) and polyvinylidene fluoride (Aldrich). They were mixed at a mass ratio of 10:70:20 respectively, and then the mixture was spread evenly with a thickness of 0.5 mm onto a polypropylene sheet and dried. The anode material was a lithium metal foil with a thickness of 0.2 mm. The cathode, anode and separator (polyolefin film) were placed in a coin-shape cell with an electrolyte, 1 M LiPF_6 , in a mixed solution of ethylene carbonate (EC)/diethyl carbonate (DEC) (1:1, v/v) in an inert atmosphere to assemble the coin cell batteries.

8.6 References

- [1] a) M. Armand, J. M. Tarascon, *Nature* **2008**, *451*, 652; b) J. M. Tarascon, M. Armand, *Nature* **2001**, *414*, 359.
- [2] A. Manthiram, *NATO Sci. Ser. II* **2002**, *61*, 157.
- [3] a) K. Nakahara, K. Oyaizu, H. Nishide, *Chem. Lett.* **2011**, *40*, 222; b) P. J. Nigrey, D. J. MacInnes, D. P. Nairns, A. G. MacDiarmid, A. J. Heeger, *J. Electrochem. Soc.* **1981**, *128*, 1651; c) S. J. Visco, M. Liu, L. C. De Jonghe, *J. Electrochem. Soc.* **1990**, *137*; d) T. L. A. Nguyen, R. Demir-Cakan, T. Devic, M. Morcrette, T. Ahnfeldt, P. Auban-Senzier, N. Stock, A. M. Goncalves, Y. Filinchuk, J. M. Tarascon, G. Fèrey, *Inorg. Chem.* **2010**, *49*, 7135.
- [4] a) N. Kawasaki, H. Wang, R. Nakanishi, S. Hamanaka, R. Kitaura, H. Shinohara, T. Yokoyama, H. Yoshikawa, K. Awaga, *Angew. Chem., Int. Ed.* **2011**, *50*, 3471; b) H. Wang, S. Hamanaka, T. Yokoyama, H. Yoshikawa, K. Awaga, *Chem. Asian J.* **2011**, *6*, 1074; c) H. Yoshikawa, S. Hamanaka, Y. Miyoshi, Y. Kondo, S. Shigematsu, N. Akutagawa, M. Sato, T. Yokoyama, K. Awaga, *Inorg. Chem.* **2009**, *48*, 9057; d) H. Yoshikawa, C. Kazama, K. Awaga, M. Satoh, J. Wada, *Chem. Commun.* **2007**, 3169.
- [5] R. Sessoli, H. L. Tsai, A. R. Schake, S. Wang, J. B. Vincent, K. Folting, D. Gatteschi, G. Christou, D. N. Hendrickson, *J. Am. Chem. Soc.* **1993**, *115*, 1804.
- [6] A. Caneschi, D. Gatteschi, R. Sessoli, A. L. Barra, L. C. Brunel, M. Guillot, *J. Am. Chem. Soc.* **1991**, *113*, 5873.
- [7] A. Braun, S. ShROUT, A. C. Fowlks, B. A. Osaisai, S. Seifert, E. Granlund, J. Cairns, *J. Synchrotron Radiat.* **2003**, *10*, 320.
- [8] H. Wang, S. Hamanaka, Y. Nishimoto, S. Irle, T. Yokoyama, H. Yoshikawa, K. Awaga, *J. Am. Chem. Soc.* **2012**, *134*, 4918.
- [9] a) B. M. Azumi, T. Ishihara, H. Nishiguchi, Y. Takita, *Electrochemistry* **2002**, *70*, 869; b) M. Lira-Cantú, P. Gómez-Romero, *Chem. Mater.* **1998**, *10*, 698.
- [10] Y. Nishimoto, D. Yokogawa, H. Yoshikawa, K. Awaga, S. Irle, *J. Am. Chem. Soc.* **2014**.
- [11] P. Björnbohm, *Electrochem. Commun.* **2007**, *9*, 211.
- [12] G. Wang, L. Zhang, J. Zhang, *Chem. Soc. Rev.* **2012**, *41*, 797.
- [13] TURBOMOLE V6.5 2013, a development by the University of Karlsruhe and Forschungszentrum Karlsruhe GmbH, 1989-2007, TURBOMOLE GmbH, since 2007; available from <http://www.turbomole.com>, 2013.
- [14] A. D. Becke, *Phys. Rev. A* **1988**, *38*, 3098.
- [15] J. P. Perdew, *Phys. Rev. B* **1986**, *33*, 8822.
- [16] A. Schäfer, H. Horn, R. Ahlrichs, *J. Chem. Phys.* **1992**, *97*, 2571.
- [17] K. Eichkorn, F. Weigend, O. Treutler, R. Ahlrichs, *Theor. Chem. Acc.* **1997**, *97*, 119.
- [18] S. Grimme, *J. Comput. Chem.* **2006**, *27*, 1787.

- [19] W. Kutzelnigg, W. Klopper, *J. Chem. Phys.* **1991**, *94*, 1985.
- [20] T. Hori, S. Himeno, *Chem. Lett.* **1987**, *16*, 53.
- [21] H. Wu, *J. Biol. Chem.* **1920**, *43*, 189.
- [22] M. H. Alizadeh, S. P. Harmalker, Y. Jeannin, J. Martin-Frere, M. T. Pope, *J. Am. Chem. Soc.* **1985**, *107*, 2662.
- [23] G. Z. Kaziev, A. V. Oreshkina, S. H. Quinones, A. F. Stepnova, V. E. Zavodnik, A. Ita, D. A. Alekseev, *Russ. J. Coord. Chem.* **2010**, *36*, 887.
- [24] Y. Lü, Y. Feng, *Chin. J. Chem.* **2010**, *28*, 2404.
- [25] R. Kato, A. Kobayashi, Y. Sasaki, *Inorg. Chem.* **1982**, *21*, 240.
- [26] D. Hou, K. S. Hagen, C. L. Hill, *J. Chem. Soc., Chem. Commun.* **1993**, 426.

Chapter 9

Concluding Remarks

In this chapter we want to summarize the most important achievements presented in the thesis. The main goals of this work have been modeling the redox properties of polyoxometalates, focusing in the description of the few electronic effects that govern electron distribution and reduction energies. The effect of localization/delocalization has been rationalized in different types of polyoxometalates. The electronic repulsion and pairing are two of the most important factors governing the electrochemistry of polyoxometalates.

A brief, chapter-by-chapter summary of the major achievements can be enumerated:

Chapter 2: Ability of DFT Calculations to Describe Redox Potentials and Electron (De)Localization

In this chapter we searched for the best functional to estimate the reduction energies and the localization/delocalization of the extra electrons in redox processes. To test the different functionals we take both isomers of the mono-substituted Wells-Dawson anion $[\text{P}_2\text{MoW}_{17}\text{O}_{62}]^{7-}$ as model compounds. We found that the B3LYP hybrid functional gives the best results in comparison to the electrochemical data, giving electron-localized solutions when expected, even in clusters containing different sites or regions with similar electron affinity.

Chapter 3: Tungsten Redox Waves in Keggin Compounds: Effect of Localized *versus* Delocalized Charges

We have studied some relevant aspects related to the redox chemistry of mono-substituted Keggin derivatives. DFT calculations showed that the oxidizing power of these systems do not decrease in a *uniform* way with the addition of negative charge. Three different cases were analyzed: internal charge effect (heteroatom replacement), external localized charge effect (addenda replacement) and external delocalized charge effect (presence of one *blue* electron). It arises that the nature of the unitary charge increment affects differently the reduction energy, the mildest change occurring upon variations in the internal position, and the strongest, the presence of a delocalized electron. In between, replacement of a metal atom in an external position by another one with different oxidation states.

Chapter 4: Effect of Electron (De)Localization and Pairing in the Electrochemistry of Wells-Dawson Mo/W-derivatives

The most relevant and general conclusion is the competition of three factors in what concerns stability, when one or several metal electrons meet in the Wells-Dawson structure: (i) the favorable electron delocalization, (ii) the unfavorable e-e electrostatic repulsion, and (iii) the favorable electron pairing. DFT calculations carried out on Wells-Dawson Mo/W-derivatives have reproduced the general trends of oxidizing power.

Chapter 5: Metal-substituted Wells-Dawson Tungstodiphosphates

The redox chemistry of some systems can be explained by the effect of protonation. This is the case of the mono-substituted Wells-Dawson anions with Fe, Tc and Re. Tc derivatives are stronger oxidizing agents than their Re homologues since the extra electrons occupy lower orbitals in the former compounds. We have also evidenced the influence of the protonation state of the Fe derivative on the relative reduction potentials of both isomers. At pH values close to 6, reduction energies are more favorable to α_1 , while the opposite trend is observed at low pH.

Chapter 6: Mixed d Metal-Iron containing Wells-Dawson Sandwich-type Complexes

We have studied on the electrochemical behavior of mixed d metal-iron containing Wells-Dawson sandwich-type complexes. In most of the cases, the reduction of the two Fe^{III} centers takes place in two successive single-electron steps, each electron being delocalized over the two centers. DFT calculations led to a compilation of molecular energies associated with the one-electron oxidized and reduced forms of all the compounds in the family. It seems that the most stable isomers are those where Fe^{III} centers are internally-located. Consequently, their reduction is more difficult than those having externally-located Fe^{III} isomers.

Chapter 7: ϵ -Keggin Polyoxomolybdates Capped with Lanthanide Groups

Calculations driven on La and Gd-containing derivatives of the ϵ -Keggin anion give complementary information on the structure and relative stability of such compounds. DFT geometries agree very well with X-ray data, giving some extra information in case of disorder. The $\{\epsilon\text{-PMo}_{12}\text{O}_{40}\}$ isomer is able to gain eight metal electrons arising from the $\text{Mo}^{\text{VI}}\text{-Mo}^{\text{VI}}$ bonding character of LUMO, forming then four $\text{Mo}^{\text{V}}\text{-Mo}^{\text{V}}$ bonds. We have also proven that the La compound is much more stable than the Gd one in solution, a behavior that resembles that of Eu, confirming that the smaller Ln ions are not stable in the surface of the $\{\epsilon\text{-PMo}_{12}\text{O}_{40}\}$ molecule.

Chapter 8: Polyoxometalates as Cathode-Active Materials for Li-ion Batteries

We have synthesized several polyoxometalates and tested their application as cathode-active materials in Li-ion batteries. The results obtained for the Mo Keggin compound are in agreement with previously reported data. We observe that Wells-Dawson compounds, P_2Mo_{18} and S_2Mo_{18} , show a higher electrical capacity than the Keggin anion. On the other hand, Preyssler compound has a low capacity due to its high molecular mass. Vanadates are the polyoxometalates showing the highest experimental capacity per extra electron. The V_{15} is the compound with the highest capacity among all tested vanadates. XANES analysis shows that the valence of the V atoms changes from +5 to +4. As we have commented above, further investigations should be performed in order to fully understand the behaviour of the V_{15} compound.

List of publications

Related to the thesis:

[1]. **Lanthanide Polyoxocationic Complexes: Experimental and Theoretical Stability Studies and Lewis Acid Catalysis**

H. El Moll, B. Nohra, P. Mialane, J. Marrot, N. Dupré, B. Riflade, M. Malacria, S. Thorimbert, B. Hasenknopf, E. Lacôte, P. A. Aparicio, X. López, J. M. Poblet, A. Dolbecq, *Chem. Eur. J.* **2011**, 17, 50, 14129

[2]. **Electrochemical Behaviour of α_1/α_2 -[Fe(H₂O)P₂W₁₇O₆₁]⁷⁻ Isomers in Solution: Experimental and DFT Studies**

N. Vilà, P. A. Aparicio, F. Sécheresse, J. M. Poblet, X. López, I. M. Mbomekallé, *Inorg. Chem.* **2012**, 51, 11, 6129

[3]. **⁹⁹Tc and Re Incorporated into Metal Oxide Polyoxometalates: Oxidation State Stability Elucidated by Electrochemistry and Theory**

D. McGregor, B. P. Burton-Pye, I. M. Mbomekallé, P. A. Aparicio, S. Romo, X. López, J. M. Poblet, L. C. Francesconi, *Inorg. Chem.* **2012**, 51, 16, 9017

[4]. **Tungsten Redox Waves in [XMW₁₁O₄₀]ⁿ⁻ (X = P, Si, Al and M = W, Mo, V, Nb, Ti) Keggin Compounds – Effect of Localized/Delocalized Charges**

P. A. Aparicio, J. M. Poblet, X. López, *Eur. J. Inorg. Chem.* **2013**, 1910.

[5]. **Ability of DFT Calculations to Correctly Describe Redox Potentials and Electron (De)Localization in Polyoxometalates**

P. A. Aparicio, X. López, J. M. Poblet, *J. Mol. Eng. Mater.* **2014**, 2, 1440004

[6]. **Electrochemical Behavior of Mixed d Metal-Iron Containing Wells-Dawson Sandwich-Type Complexes:** $[(\text{FeOH}_2)_2\text{M}_2(\text{X}_2\text{W}_{15}\text{O}_{56})_2]^{n-}$ and $[(\text{MOH}_2)_2\text{Fe}_2(\text{X}_2\text{W}_{15}\text{O}_{56})_2]^{n-}$ (M = Cr^{III}, Mn^{III}, Mn^{II}, Co^{II}, Ni^{II}, Cu^{II}, Zn^{II}, X = As or P and n = 12 or 14)

F. Doungmene, P. A. Aparicio, J. Ntienoue, C. S. Ayingone Mezui, P. de Oliveira, X. López, I. M. Mbomekallé, *Electrochim. Acta* **2014**, 125, 674.

[7]. **Effect of Electron (De)localization and Pairing in the Electrochemistry of Polyoxometalates. Study of Wells-Dawson Molybdotungstophosphate Derivatives**

P. Loïc, P. A. Aparicio, P. de Oliveira, A. L. Teillout, J. M. Poblet, X. López, I. M. Mbomekallé, *Inorg. Chem.* **2014**, 53, 5941.

Not related to the thesis:

[1]. **A Modular Synthetic Device to Calibrate Promoters**

D. Gamermann, A. Montagud, P. A. Aparicio, E. Navarro, J. Triana, F. R. Villatoro, J. F. Urchueguía, P. Fernández de Córdoba, *J. Bio. Sys.* **2012**, 20, 1, 37

[2]. **Modular Molecules: Site-Selective Metal Substitution, Photoreduction and Chirality in Polyoxometalate Hybrids**

M. Vonci, F. Akhlaghi Bagherjeri, P. D. Hall, R. W. Gable, Y. Liu, J. Zhang, M. Field, M. B. Taylor, J. Du Plessis, G. Bryant, M. Riley, L. Sorace, P. A. Aparicio, X. López, J. M. Poblet, C. Ritchie, C. Boskovic, *Chem. Eur. J.* **2014**, *Accepted*.

Acknowledgements

In the final section of the book I would like to thank all the people that has been with me during this *journey*. Most parts are written in Spanish for the better understanding of the people involved.

Aunque esta parte de la tesis debería ser la más fácil, lo cierto es que me está costando mucho saber bien que escribir. Creo que lo más justo es empezar por agradecer a mis directores de tesis, Xavier López y Josep Maria Poblet, quienes me dieron la oportunidad de hacer el doctorado en su grupo sin prácticamente conocerme. También me gustaría agradecer al resto de *jefes* del grupo su ayuda durante estos años: Toni, Coen, Jordi, Rosa, Mar y Anna. También quiero nombrar a los informáticos del grupo: Jose, Elisenda y Moisés, sin vosotros no podríamos haber lanzado ni un cálculo.

Para mis compañeros del grupo sólo tengo palabras de agradecimiento. A los de antes, los veteranos cuando llegué aquel septiembre de 2010: Álex, Alberto, Zhara, Laia, Mireia, Eva y Yanick. Gracias por todos los buenos momentos que pudimos compartir. A Sonia, gracias por tu amistad tanto dentro como fuera de la universidad y aunque eras un poco agresiva (todos saben que nos pegabas), nunca te olvidaré. Gracias por resolver todas mis dudas con el ADF, lo explicas mejor que el manual. Jess, fuiste mi primera compañera de despacho (201), sin duda el mejor, y no olvidaré todo lo que me has ayudado durante estos años. Eres una luchadora y una de las que más se ha dejado la piel haciendo la tesis, por eso sé que en el futuro te irá genial. Por cierto, echaré de menos que me preguntes qué me pasa. Pablito, gracias por cuidarme el piso mientras estuve de estancia. Ha sido un placer compartir estos años contigo, eres una buenísima persona pero te falla ser del Madrid. Como a Marc, con quien compartí el primer año de sufrimiento en el máster, los fines de semana en la universidad haciendo programación y estudiando para los exámenes, y pidiendo pizzas para coger fuerzas. Gian, empezaste a la vez que yo y creo que el hecho de ser los dos de fuera nos unió mucho. Posiblemente seas una de las personas más transparentes, buenas y locas que he tenido el placer de conocer. Aunque es un poco difícil mantener catorce (infinitas) conversaciones en paralelo contigo, siempre tendrás un sofá para quedarte en mi casa. Magda, nunca pierdas la capacidad de sorprenderte y recuerda que siempre nos quedará París. Nunca olvidaré tu *dulzura* y *buen humor* antes del café y tus “ay sí!!”, pero sobre todo tu compañerismo y alegría (a partir de las 11). Sergi, menos mal que has estado durante estos años para poner algo de

Acknowledgements

estilo en el grupo. Acuérdate de tus compañeros de despacho cuando montes una empresa de éxito. Gerard, digno heredero de Xavi, nos has amenizado horas y horas con tus bromas y monólogos sobre todo tipo de temas. Ten presente quien iba a tus conciertos cuando tu grupo sea famoso a nivel mundial y te hagas una estrella del pop-rock. Laura, recuerda que tanto deporte no es sano y que *running is life, running is life*. Ximo, compatriota de tierras alicantinas, tienes la barba y el pelazo más envidiado del grupo y del ICIQ. Ha sido un placer compartir estos años y algún que otro congreso contigo (Lanzarote fue un festival!!). Diego, aunque has sido uno de los últimos en llegar, te has integrado perfectamente en nuestro grupo. Se nota que tienes muy buen fondo y espero que te vaya muy bien, como científico y como Dj. Al resto sólo me queda desearos suerte para el futuro: Pedro, Mariano, Pep, Murillo y Zhonling Lang.

Por último me queda agradecer a dos personas que han sido pilares imprescindibles durante mis años en Tarragona. A Xavi, mi primo, gracias por tu amistad. No olvidaré nuestro humor particular, que nadie más entiende, pero que a nosotros nos hace llorar de risa. A Núria, no voy a decir nada que no sepas ya. Te aprecio mucho como compañera de grupo, pero sobretodo como amiga. Tu amistad es una de las cosas más importantes que me llevo de estos años en el grupo. Gracias por tu ayuda, prometo leer más tus notas. Gracias por todo!!

También me gustaría mencionar a gente de otros grupos como son Miriam e Idoia. Gracias por tantos días de cenas, fiestas y conciertillos. Nunca perdáis vuestra sonrisa.

A mis compañeros del máster diabólico: Melchor, Marc, Arnau, Oriol, Jordi, Laia, Carlos (química computacional, nena!!), Fernando, Ángel, etc.; gracias por un año inolvidable de cuántica, fortran, tardes en la *Ovella Negra* y risas, muchas risas.

No quiero dejar pasar esta oportunidad para agradecer también a los profesores Estanislao Silla e Iñaki Tuñón por dejarme dar mis primeros pasos en la investigación en su grupo de la Universidad de Valencia. También a Javier, quien me ayudo durante mi primer verano con ellos, y a Violeta, quien me echó más de una mano durante los meses que hice el trabajo final de carrera. Ya que he mencionado mis años de estudiante, no puedo dejar de agradecer a profesores como Enrique Ortí, con quien descubrí la Química

Física por primera vez, y Manuela Merchán, quien me enseñó Química Cuántica e hizo que el Szabo fuera nuestro libro de cabecera favorito.

Me gustaría mencionar la suerte que tuve de formar parte del proyecto iGEM Valencia 2007. Gracias a los profesores P. Fernández de Córdoba, A. Ferrando, J. Urchueguía y A. Jaramillo pude aprender los fundamentos de la Biología Molecular y la Ingeniería Genética. Gracias también a mis compañeros Arnau, Emilio, Javi, Raúl, Hicela y Olga, entre todos formamos un grupo intrínsecamente multidisciplinar. Además, tener la oportunidad de pasar unos días en el MIT presentando nuestro proyecto es algo que no olvidaré jamás.

I'm very grateful to Prof. Stephan Irlé for giving me the opportunity to work in his Quantum Chemistry Group at Nagoya University (Japan) during 5 months. I also want to thank to Assist. Prof. Hirofumi Yoshikawa and Prof. Kunio Awaga for letting me work at their lab. In this stay I was learning both new theoretical and experimental techniques. Thanks to Nishimoto-San and Yamada-San for all their help and discussions about the project. I would like to thank all the members of both groups for their support and advice during my stay. Thanks to the *Japan Society for the Promotion of Science* (JSPS) for the short-term fellowship.

I have to say that I was very lucky during my stay in Nagoya because all the nice people that I met. Daniel, gracias por tu amistad, nunca olvidaré nuestros paseos por el Aeon Mall, los cafés y visitas al centro de la ciudad. Michele, contigo formamos un gran grupo, *Los Espartanos*, entre cuyos logros siempre quedará la conquista del monte Fuji. Simone, Alkmini, Asuka and Rei thanks for your friendship and for all the dinners and trips that we did together. Thanks to Eriko, my favorite waitress, and Miku, a good friend who showed me one of the best places in Nagoya. Arigato gozaimashita!! Mi estancia en Japón fue un punto de inflexión en muchos sentidos...dejé muchas cosas detrás de mi, algunas buenas y otras no tanto...pero fue una experiencia que no olvidaré jamás.

Ahora le toca el turno a mis amigos de siempre, los que han estado a mi lado ayudándome y apoyándome durante estos años. Carl, qué te voy a decir...si no fuera por ti nunca habría sido capaz de empezar esta tesis (literalmente). Fuiste el primero en apoyarme a la hora de buscar becas y proyectos para empezar un doctorado, aunque fuera en química. Sin tu confianza nada de esto hubiera sido posible. El resto pues ya lo sabes...qué te voy a decir. Y a tus padres, mis tíos Manolo y María José, sólo les diré que gracias por hacerme

Acknowledgements

sentir como de la familia durante tantos años. Para mi vuestra casa es un hogar. Alberto, que sepas que das mucha rabia...siempre diciendo lo que no queremos oír y encima teniendo razón...eres como nuestro Pepito Grillo. Tampoco te voy a decir nada que ya no sepas. Aquí estamos un día más, un quimi-consejo más, otra etapa más que superamos juntos...y las que nos quedan!! Pabl y Ann, Lara e Isaac (los sobrinos!!) me siento muy afortunado de formar parte de vuestra familia. Su, somos amigos desde hace mucho tiempo y espero que no cambie pase lo que pase. A Paúl y Esteban, juntos formamos el trío calavera y los tres mosqueteros del billar durante los años de instituto. Gracias por vuestro apoyo y amistad, sin vosotros nada seria lo mismo. A Erich, pienso en todas las cosas que te podrían definir y hay una que destaca sobre el resto, eres el amigo que todo el mundo debería tener. Nunca olvidaré el verano de 2010 con nuestras tardes de café y tiendas de música. A Vicent, mi gemelo y *brother*, empezamos siendo amigos de biblioteca y barandilla (nuestro templo) y hemos acabado siendo familia. A Miguel, el guarro, muchas gracias por tu amistad durante estos años, por dejarme un hueco en tu casa cada vez que tenía que ir a Barcelona, gracias también a tu hermano Toni (*Au revoir*). A los dos sucios, Vicent y Miguel, sólo os diré una cosa más: lo que la suciedad ha unido nada puede separar (**OS3**).

Me gustaría agradecer al grupo de fisiquillos con los que compartí mis años de universidad: Rica, Javi (Alicante), Javi (Aragorn), Fons, Avelino, etc. Gracias por recordarme constantemente que la química viene de la física. A Rica y Fons, con los que la amistad siguió tiempo después de haber terminado la carrera, espero que podamos compartir cosas juntos en el futuro.

A mi amigo Pablo, Don Apolinar, nos conocimos en primero de primaria y desde entonces hemos sido muy buenos amigos. Ya sabes que te admiro mucho y que creo que eres una de las personas más valientes que conozco.

Finalmente quiero agradecer a mi familia por todo su apoyo durante estos años. A mi padre y Maribel, Carlos y Pilar, Pili, Vicky y Miguel. A mi madre y Alfonso. A mis hermanas Ana y Laura, de quien estoy muy orgulloso y admiro por haber luchado y conseguido su sueño. A mis tíos Arturo y Lola, mis primos Arturo y Marina. A mi tío Luis. A mi abuela Paquita, quien hacía la mejor paella del mundo. A mis abuelos Luis y Amparo, quienes tienen gran parte de culpa de que hoy en día sea como soy y a los que nunca podré agradecer suficientemente todo lo que hicieron por mi. Muchas gracias a todos!!

Hasta aquí la última parte de mi tesis. Al final he escrito más de lo que pensaba. He querido aprovechar los agradecimientos para decir todas esas cosas que muchas veces no decimos y que aunque damos por sabidas, creo que es importante recordar.

Un abrazo a todos!!

Y como dice la canción:

This is the end, my only friend, the end.

The Doors.

From the beginning of the degree until I become a postdoc, there are several thoughts that I would like to share with you.

Never forget the basic things:

In this house we obey the laws of thermodynamics.

Homer J. Simpson.

About starting a career in research:

Don't tell me what I can't do.

John Locke.

Talking with experimentalists:

If the facts don't fit the theory, change the facts.

Albert Einstein.

After finishing the PhD thesis:

Remember "PhD" is not the end, but only a transition.

Metropolis Pt. 2, Dream Theater.

About being a postdoc:

I refuse to join any club that would have me for a member.

Groucho Marx.

